DEVELOPMENT AND CHARACTERIZATION OF TUNABLE HYDROGEL NANOPARTICLE ASSEMBLIES

A Dissertation
Presented to
The Academic Faculty

by

Shalini Saxena

In Partial Fulfillment
of the Requirements for the Degree
Doctor of Philosophy in the
School of Materials Science and Engineering

Georgia Institute of Technology
August 2015

DEVELOPMENT AND CHARACTERIZATION OF TUNABLE HYDROGEL NANOPARTICLE ASSEMBLIES

Approved by:

Dr. L. Andrew Lyon, Advisor
Schmid School of Science and Technology
Chapman University

Dr. Valeria Milam
School of Materials Science and Eng.
Georgia Institute of Technology

Dr. Haskell Beckham
School of Materials Science and Eng.
Georgia Institute of Technology

Dr. Paul Russo
School of Materials Science and Eng.
Georgia Institute of Technology

Dr. David Bucknall
School of Materials Science and Eng.
Georgia Institute of Technology

Date Approved: May 4th, 2015

For my parents – thank you for always believing in me.

ACKNOWLEDGEMENTS

First, I would like to acknowledge that I would not be here without the support of my parents, Sharmila and Virendra, and my sisters, Roheeni and Pooja Saxena. Ever since I was a child my parents have encouraged my curiosity about the world around me, which has ultimately led me to develop a lifelong love of learning. From a young age they encouraged me to challenge myself by teaching me that the best things in life require hard work. Over the years they have supported my many dreams; instilled me with a remarkable work ethic; nurtured my intuitive and adventurous nature; and taught me how to believe in myself. In particular, I would like to thank my mother for the many sacrifices she has made to nurture and direct me. There have been countless occasions when I wanted to branch out from the traditional educational system, but she has managed to help me stay on a straight and narrow path all these years. I would also like to thank my father for providing me with not only a solid traditional educational background, but also strong foundation as an artist; this background has produced a well of creativity in me that overflows into my research as a scientist. As the youngest of three daughters, I have also learned a great deal about life from my sisters, who have served as inspiring role-models to me over the years. Not only did they help me learn how to cooperate and handle conflict with others, they have also shown me the value of independence and have helped me develop an innate sense of self-confidence in my decisions and actions. Though the three of us have ventured down different paths in our lives and now live hundreds of miles apart, I know that I can always count on them.

Additionally, I would like to thank my fellow lab mates in the Lyon Group, as they have had a large impact on my time as a graduate student. Though the Lyon Group has changed dramatically during my time at Georgia Tech, we have all shared this journey together. When I joined the Lyon Lab I was welcomed by a group of individuals who were ready and willing to help me become a self-sufficient researcher. In particular, I would like to thank Dr. Jeff Gaulding, who was my first mentor in the lab; he has tremendously impacted my research interests by teaching me how to fabricate both composite microparticles and microgel films. I would also like to thank Dr. Mark Spears, Dr. Hiro Yoshida, and Dr. Ashely Brown, three lab members who I worked closely with on collaborative research projects. Finally, I would like to thank Ms. Caroline Hansen who has been a supportive friend to me over the years. She has become someone I can talk to about my research or life in general and she always provides me with realistic and useful feedback.

Due to the interdisciplinary nature of my research, I would like to thank the many collaborators I have worked with. I would especially like to thank Dr. Todd McDevitt and Denise Sullivan who I have worked closely with over the duration of my PhD solving challenging stem cell engineering problems. I would also like to thank Dr. Andres Garcia, Dr. Alberto Fernandez-Nieves, Dr. Breedveld, Dr. Lam, and Dr. Barker, who I have either worked with or have provided me with access to their labs. Finally, I would like to thank Dr. Anh Nguyen, Dr. Miguel A.P. Fernandez, Dr. Elaissa Harding, Dr. Sri Charan Yarlagga and John Hyatt for their help on a variety of projects.

I would also like to thank my friends who have provided me with an invaluable support network. In particular, I would like to thank Erin Sullivan, a fellow MSE Georgia

Tech graduate student I met in my first year, who has become a lifelong friend. I would also like to thank Alessandra, Mollie, Kaiyi, Holly, Sadie, Kyle, Rob, and Ming, who, I am sure, have heard far too many stories about my graduate student experience over the years, but have always encouraged me to chase my dreams and pursue new opportunities. Finally, I would like to thank Adam who has been a great friend and has been very supportive in my final year of my PhD.

In addition, I would like to thank my academic advisor, Haskell Beckham, who has advised me throughout my graduate career and has also served on my PhD committee. As a first year graduate student, the conversations we had and the advice he provided me largely influenced my decision to join Dr. Lyon's Group. And last, but not least, I would like to thank my thesis advisor, Dr. Andrew Lyon. I came to Georgia Tech as a young adult, fresh out of college, and full of enthusiasm for science. My journey as a graduate student has not been without bumps and unexpected turns, but Dr. Lyon has always provided me with the help I needed to navigate difficult situations. His guidance over the years has helped me develop critical research, communication, and interpersonal skills that have enabled me to become a competent and confident young scientist, able to effectively collaborate with others. He has helped me balance my research interests with strict deadlines, which has resulted in the development of a cohesive dissertation.

TABLE OF CONTENTS

LIST OF TABLES

LIST OF FIGURES

LIST OF SCHEMES

LIST OF SYMBOLS AND ABBREVIATIONS

N-isoproprylacrylamide	NIPAm
Poly(*N*-isoproprylacrylamide)	pNIPAm
N-isoproprylmethacrylamide	NIPMAm
Poly*(N*-isoproprylmethacrylamide)	pNIPMAm
N,N'-methylenebis(acrylamide)	BIS
Acrylic Acid	AAc
Sodium Dodecyl Sulfate	SDS
Ammonium Persulfate	APS
1-ethyl-2-[2-dimethylaminopropyl]carbodiimide hydrochloride	EDC
N-hydroxysuccinimide	NHS
4-Aminobenzophenone	AB
Ethanol	EtOH
Dimethylsulfoxide	DMSO
Polystyrene	PS
Phosphate Buffer Saline	PBS
Poly(diallyldimethylammonium chloride)	PDADMAC
Poly(ethylene glycol)	PEG
Polyethylenimine	PEI
N,O-dimethacryloyl hydroxylamine	DMHA
3-aminopropyltrimethoxysilane	APTMS
(1,2-dihydroxyethylene)bisacrylamide	DHEA
Aminopropyl methacrylate	APMA
2-(N-morpholino)ethanesulfonic acid	MES
Polydimethylsiloxane	PDMS
Small interfering RNA	siRNA
Multi-Angle Light Scattering	MALS
Atomic Force Microscopy	AFM
Scanning Electron Microscopy	SEM
Raspberry-Like Particles	RLPs
Raspberry-Like Patchy Particles	RLPPs
Layer by Layer	LbL
Effective Volume Fraction	φ_{eff}

SUMMARY

Hydrogels are physically or chemically cross-linked hydrophilic polymer networks. Discrete hydrogel nanoparticles, microgels, are tunable constructs that can be used as building blocks to assemble complex, functional material systems. Microgels properties such as network structure, overall architecture, size, stiffness, and responsivity can be finely tuned based on the chemical composition and synthesis conditions. These dispersions exhibit low polydispersity, which is beneficial for development of modular assemblies with uniform properties and behavior. Microgels with complex architectures have been synthesized including core-shell, or even hollow, architectures. They have also been synthesized to respond to stimuli such as temperature, pH, oxidative conditions, and light. Microgels exhibit unique properties that fundamentally distinguish them from both bulk hydrogels and hard colloids. Due to their size, they respond on faster time scales than hydrogels and are often able to maintain that fast response when assembled. Microgels are also soft materials having a low Young's moduli on the order of tens to hundreds of kilopascals. Because of their inherent softness, microgels exhibit rich phase behavior that cannot be predicted by hard sphere colloidal theory. Over the last decade research on microgel systems has grown as they have been demonstrated to be a powerful tool for the development of functional materials, particularly for biomedical applications.

This dissertation describes investigations into hydrogel nanoparticle assemblies, with the aim of expanding their utility as drug delivery systems and as biological interfaces; these assemblies are specifically designed with the intent to either direct, inhibit, or promote cellular proliferation. In particular, this work focuses on

understanding innovative and enabling routes to fabricate two-dimensional and three-dimensional microgel assemblies, as well as composite polymeric assemblies. **Chapter 1** serves to introduce microgels and describe the fabrication and properties of microgel assemblies. This chapter describes a great deal of research that has been generated by the Lyon Group, which has added to the growing body of literature demonstrating the importance of microgel properties in the design of specialized biomaterials. This chapter also includes key examples from the literature that highlight the diverse range of applications for which microgels are well-suited.

Chapter 2 investigates the parameter space for a technique developed in the Lyon Group that enables the deposition of microgel films onto colloidal substrates. This chapter specifically details the influence of microgel network structure and stiffness on a three-dimensional coating process, which can be extended to other coating processes. **Chapter 3** builds upon this study to investigate the deposition of microgel films from binary microgel dispersions onto colloidal substrates in order to demonstrate the utility of the modular handle that tunable microgels present. This chapter also bridges the development of films on colloidal substrates to the development of films on macroscopic substrates. **Chapter 4** details the ability to scale up this fabrication process in order to produce useful quantities of material for applications studies targeted at investigating the use of these constructs as drug delivery vehicles for sensitive biological systems.

Chapter 5 explores a fabrication of microgel films on macroscopic, planar substrates using a well-established film buildup method. This chapter also details the mechanical properties of these microgel films and reveals a facile method for the modulation of film mechanical properties. Studies in this chapter interrogate the use of

these films as a biological interface, revealing the importance of microgel mechanics in the development of these constructs. **Chapter 6** details an innovative film fabrication technique that can be extended to fabricate two-dimensional and three-dimensional constructs with lateral and perpendicular patterning of polymeric building blocks. This technique enables the fabrication of a variety of polymer constructs with unique architectures and mechanical properties not previously realized in the Lyon Group, while simultaneously providing a fast route to the development of previously established films. In addition, this chapter investigates the use of these films as a biological interface, demonstrating that this method is a facile route to the fabrication of well-designed experimental tools to interrogate fundamental cellular behavior. This chapter also demonstrates that this method can be used to develop macroscopic gels with incorporated cells, which can be used for biomedical applications. Building upon these studies, **Chapter 7** explores the use of microgel films prepared using this technique as a biomedical device designed to augment blood clotting.

Finally, **Chapter 8** provides an additional perspective on each of the preceding chapters and suggests future investigations that could be pursued. The work in this dissertation serves to demonstrate the utility of the development of biomaterial systems from tunable colloidal building blocks. Furthermore, this work highlights the added benefits of using microgels as modular building blocks in conjunction with or in comparison to other polymeric building blocks for the development of material systems with hierarchical ordering. This work highlights the utility of these constructs for development of drug delivery systems and biological interfaces with the aim of easing the accessibility and fabrication of such constructs for further experimental investigation.

CHAPTER 1

INTRODUCTION

Adapted with permission from:
Saxena, S., Hanson, C.E., Lyon, L.A. Microgel Mechanics in Biomaterial Design. In *Accounts of Chemical Research.* **2014**, *47*(8), 2426-2434

1.1. Biomaterial Design Considerations

The field of biomaterials has grown concurrently with advances in polymer chemistry, applying new technology to biological applications such as drug delivery, wound healing, and tissue scaffolds.[1] In the beginning, biomaterials were defined as materials, other than foods or drugs, composed of biologically derived components such as amino acids.[2] However, as the field of synthetic polymers has grown, the definition of a biomaterial has expanded to include many of these polymers that are either used for medical applications or are derived from bio-renewable components. As of now, both natural and synthetic, organic and inorganic biomaterials have been explored for a myriad of applications, medical and otherwise; such technological advancement has been beneficial for developing new tools and devices. However, when specifically considering biomaterials used for biomedical applications, growth in this area has also lead to unforeseen challenges such as negative biological responses and unexpected material behavior; materials properties themselves have also been known to influence biological outcomes through control over factors such as drug release rates of drugs or even biocompatibility.[3]

Biocompatability is an obvious yet challenging hurdle for any biomaterial, where the material must not only be nontoxic and avoid foreign body reactions, but

depending on the specific application, might also need to be nonfouling, promote cell infiltration, proliferation, and/or differentiation.[4-5] An ideal biomaterial might be expected to promote regenerative biological pathways for reconstructive healing and degrade over a timescale relevant for tissue regeneration.[5] Honing biologically integrative properties such as amphiphilicity, functional group identity/density, charge density, size, shape, and biodegradability offer routes to enhance the biocompatibility of polymeric materials.[6-10]

Although several of these areas have been heavily investigated for many years, only recently have researchers tailored mechanical properties to mimic the target system's mechanics as a method to enhance a material's integration into a mammalian host.[11] By mimicking elasticity ranges of biological tissues (~0.5 kPa for soft tissue (e.g. brain), ~10 kPa for moderate tissue (e.g. muscle), and >30 kPa for hard tissue (e.g. bone)) in a biomaterial, one can influence cellular response to that material, which can then prolong circulation times for drug delivery vehicles or facilitate cell proliferation on tissue scaffolds.[11-12] Importantly, substrate stiffness has been shown to influence cellular adhesion, cytoskeletal formation, and the differentiation of stem cells.[13, 12]

1.2. Hydrogels

Hydrogels have been used for a variety of biomedical applications such as drug delivery, implant coatings, tissue-engineering scaffolds, micro-arrays, and sensors.[14] Hydrogels are hydrated polymer networks that are held together through either physical or chemical cross-links and have been fabricated from both natural and synthetic polymers. Physically cross-linked hydrogels have been fabricated by

leveraging a variety of forces including micellar packing, crystallizing segments, and polymer entanglements; exploration of chemically cross-linked hydrogels has also found that hydrogen bonding, ionic bonding, and covalent bonding can be used to stabilize these macro assemblies.[15] Many hydrogels have mechanical properties somewhat matched to natural tissues, which can enhance biological interactions and improve integration when used as a biomaterial construct.[16-18]

1.3. Tunable Hydrogel Nanoparticles

1.3.1. Microgels

While macroscopic hydrogels are appropriate for some biological applications, there are numerous applications wherein nano- to micrometer length-scales are important.[19-20] Microgels are similar to hydrogels in that they comprise a solvent swollen polymer network. However, microgels are colloidal particles with dimensions ranging from 10's of nm to many microns, enabling their interfacing with cellular and subcellular domains.[6] Characteristics such as responsivity, charge, amphiphilicity, degradability, segment density, porosity, size, and softness can be tuned by selecting specific synthetic conditions, monomers, and monomer ratios.

Depending on their chemical composition, microgels can be stimuli-responsive and have been designed to respond to stimuli such as light, pH, ionic strength, temperature, and the presence of macromolecules.[21] Microgels have the added advantage of responding on faster time scales than bulk hydrogels due to their smaller sizes. In addition, they are often able to maintain this fast responsivity even when assembled into larger constructs. Thermo-responsive microgels composed of poly(*N*-isopropylacrylamide) (pNIPAm) have been the most widely studied in the

field. PNIPAm exhibits a volume phase transition temperature (VPTT) at 32 °C where it transitions from a swollen gel to a collapsed globule state.[21] This transition is governed by a shift from favorable polymer-solvent interactions to favorable polymer-polymer interactions, which could also be described as a shift from a hydrophilic state to a hydrophobic state of the polymer. This collapse of the gel is entropically driven by the release of water molecules structured around the backbone and the side chains; these molecules gain freedom as the polymer backbone begins to interact with itself and they are released into solution. In addition, poly(*N*-isopropylmethacrylamide) (pNIPMAm) based microgels have been used in the field; they exhibit a transition temperature of approximately 41 °C.[21] The presence of the methyl group stiffens the backbone, resulting in the necessity for a higher energy input to induce a collapse.

1.3.2. Microgel Synthesis

Numerous methods can be used to synthesize microgels including emulsion polymerization, self-assembly, and free-radical polymerizations. In this investigation, all microgels were synthesized via free-radical polymerization (**Scheme 1.1**). In this method, the monomer, co-monomer, cross-linker, and surfactant are dissolved in an aqueous solution, heated to 70 °C, and purged with nitrogen. This reaction must occur above the lower critical solution temperature (LCST) of the parent polymer to avoid the formation of a bulk hydrogel. Above the LCST, the parent polymer exists as hydrophobic, insoluble polymer globule, allowing for nucleation and growth of insoluble polymer particles.

To begin the reaction an initiator such as ammonium persulfate (APS) is dissolved in an aqueous solution and added. This reagent undergoes thermal

decomposition, forming two reactive radicals, which initiate the polymerization. An oligoradical forms and grows until it reaches a critical chain length (~10 monomer units), at which point it undergoes an entropically driven collapse. These insoluble particles are termed "precursor particles" and serve as nucleation sites for further chain growth and aggregation. A stable particle is typically formed when the surface is sufficiently hydrophilic to inhibit further polymer chain growth. After 4-6 h the temperature is then decreased to room temperature, resulting in the formation of hydrophilic microgels. This reaction allows for a high degree of synthetic control and results in a relatively monodisperse population of microgels.

Scheme 1.1. Precipitation polymerization is used to form microgels.

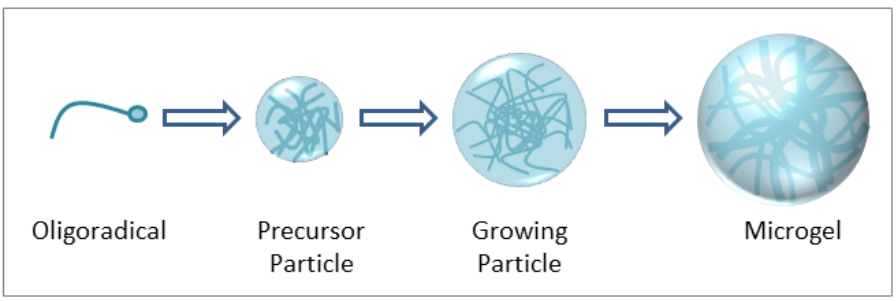

1.3.3. Facile Routes to Tune Microgel Characteristics

Fundamental studies of microgels originally focused on understanding the relationship between chemical composition and stimuli (e.g. temperature, pH, ionic strength, and light)[21] triggered swelling and deswelling responses of poly(*N*-isopropylacrylamide) (pNIPAm) or poly(*N*-isopropylmethacrylamide) (pNIPMAm) microgels.

1.3.3.1. Synthetic Control of Polymer Network Density

Adjusting cross-linker concentration is perhaps the most straightforward way to modulate microgel stiffness. Increasing cross-linker content increases polymer (segment) density and subsequently decreases network flexibility. Chain confinement results in an increase in particle density, smaller particle size, and decreased swelling. In addition, reactivity ratios between the monomers and cross-linkers present another path to modulate polymer density. Saunders *et al.* validated a "core/shell" polymer density structure in pNIPAm microgels cross-linked with either 1% or 10 mol-% *N,N'*-methylenebis(acrylamide) (BIS) using small angle neutron scattering.[22] The cross-linker BIS has a higher reactivity than the monomer NIPAm resulting in a highly cross-linked core. Because less cross-linker is available towards the end of the reaction, the microgel periphery consists of a low segment density shell with highly flexible polymer chains.

The Lyon Group has also explored how polymer distribution in microgels impacts downstream properties, such as erosion in studies related to the clearance of drug delivery vehicles. Microgels consisting of either pNIPAm or pNIPMAm were synthesized with 10 mol-% of degradable cross-linker (1,2-dihydroxyethylene)bisacrylamide (DHEA).[23] Microgel degradation was initiated with periodate and monitored via multi-angle light scattering (MALS). Degradation of pNIPAm-based microgels produced a nonlinear mass decay beginning at the periphery, with erosion terminating with a remnant particle of branched, presumably core-localized polymer chains (**Figure 1.1**). A chain transfer mechanism is suggested to cause such branching through hydrogen abstraction via either the α-carbon on the

amide functionality in the polymer backbone or the tertiary carbon of the isopropyl group, resulting in non-degradable cross-links in the microgels.[24]

In contrast, degradation of pNIPMAm showed a slight increase in size at the onset followed by complete decay of the polymer. Such behavior is indicative of a homogenous polymer network, where initial cross-link scission affords concomitant network swelling; sizeable mass loss occurs only when the network connectivity is decreased enough to liberate soluble chains. The difference in network density between pNIPAm and pNIPMAm is explained by their reactivity ratios with cross-linker. The monomer NIPMAm and cross-linker have similar reactivity ratios resulting in a homogenous network with higher overall network density. As a result, microgels made from pNIPMAm are noticeably stiffer than pNIPAm microgels, which have a soft periphery of loosely cross-linked chains. Thus, we see that even the selection of the main monomer itself contributes to the large changes in the mechanical properties of individual microgels, their network topology, and pathway of erosion.

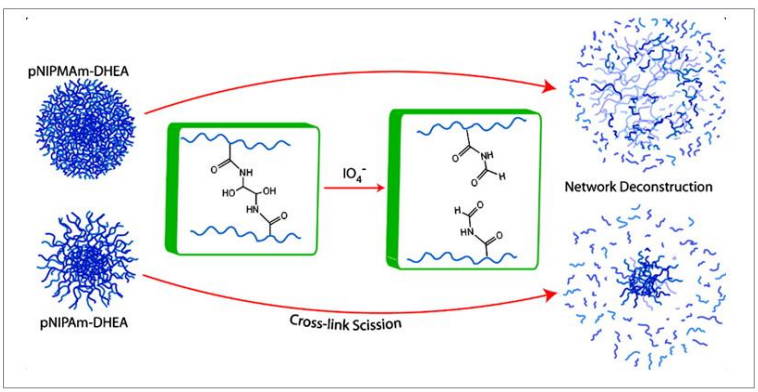

Figure 1.1. (Top) Erosion of pNIPMAm-DHEA microgels and (bottom) erosion of pNIPAm-DHEA microgels Adapted with permission from Ref. 23. Copyright 2011, American Chemical Society.

In a subsequent investigation, microgel degradation was monitored with atomic force Microscopy (AFM) in serum at 37 °C, mimicking a biological environment. AFM was used to resolve initial particle swelling and mass loss events.[25] PNIPMAm microgels with 2 mol-% acrylic acid (AAc) were cross-linked with 2 mol-% *N,O*-dimethacryloyl hydroxylamine (DMHA), which is susceptible to base hydrolysis at pH > 5. Microgels were eroded under swollen and collapsed conditions to compare effects of swelling (**Figure 1.2**). Under deswollen conditions, a decrease in height by 14% was seen, while microgels imaged under hydrated conditions showed an initial increase in height during erosion. These results corroborate that initial height increase of pNIPMAm is due to swelling caused by initial cross-link scission, even though mass is simultaneously being lost (as shown via imaging under deswollen conditions).

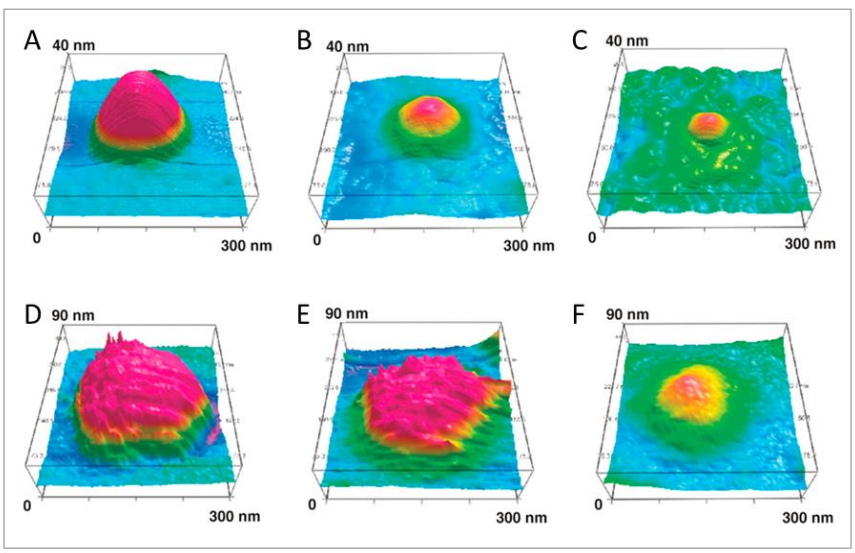

Figure 1.2. Three-dimensional renderings of AFM images obtained from a single microgel during erosion under deswollen (A-C) or swollen (D-F) conditions at 0 (A,

D), 24 (B, E), and 434 hours (C, F). Adapted with permission from Ref. 25 Copyright 2011, American Chemical Society.

Another important parameter to consider in drug delivery is the ability to load solute within the carrier. For microgels, it is easy to see the correlation between mesh size and loading ability. Protein loading, and how it correlates with microgel charge, was recently evaluated in the Lyon Group using cytochrome C (cyt C), a positively charged protein.[26] Microgels were composed of pNIPAm, BIS (2 mol-%), and AAc in varied amounts (10, 20, and 30 mol-%) to impart anionic charges in the microgel, facilitating cyt C uptake through Coulombic interactions. MALS revealed the 30 mol-% AAc microgel loaded significantly more protein per available AAc site than either the 20 mol-% or 10 mol-% acid particles – 0.13 compared to 0.05 and 0.01, respectively.

The drastic increase in loading ability of the 30 mol-% AAc microgels is attributed to a more porous internal polymer network. The greater amount of internal charge present in the 30 mol-% AAc microgel leads to a higher internal osmotic pressure. Subsequently, a lower segment density is established during synthesis, allowing more cyt C to penetrate further into the microgel. No statistically meaningful difference in binding constants was observed, suggesting that multivalent interactions between AAc and cyt C was not a major factor in increased loading. Charged comonomer concentration consequently functions as an important factor for tailoring porosity and subsequent macromolecule loading.

1.3.3.2. Synthetic Control through Exotic Architectures

Previously, the Lyon Group developed methods for the synthesis of well-defined core/shell microgels, which were envisioned to have potential as drug carriers.[27] These microgels have different chemical compositions in the core and shell, allowing for multiple characteristics to be employed such as two VPTTs (e.g. ~31 °C for pNIPAm and ~45 °C for pNIPMAm) or specific localization of charge and functional groups.[27-28] Core/shell microgels are also of fundamental interest because they exhibit a phenomenon known as core compression, where the shell physically compresses the core.[29] Core compression occurs because the shell synthesis occurs above the core VPTT. When the solution is cooled to room temperature, the core cannot fully swell due to the presence of the surrounding shell, which essentially acts to "shrink wrap" the core.

The Lyon Group further investigated core/shell structures by means of controlled shell degradation.[30] Microgels consisting of a non-degradable pNIPAm-BIS (2 mol-%) core and a pNIPMAm shell of varying DMHA cross-linker concentration (2 mol-% and 4 mol-%) were studied. The core/shell particles had roughly the same diameter as the cores alone (measured by MALS), which is an expected result of core compression.[29] Particle deformability was studied with AFM through footprint and height measurements after deposition onto glass. As shown in **Figure 1.3**, the cores exhibited a deposited height of 7 ± 1 nm, while core/shell microgels exhibited heights of 32 ± 5 nm and 30 ± 3 nm for 2% and 4 mol-% cross-linker concentrations, respectively. The greater particle stiffness seen in the core/shell microgels is attributed to the added connectivity and rigidity imparted by the pNIPMAm shell, as well as the added polymer mass.

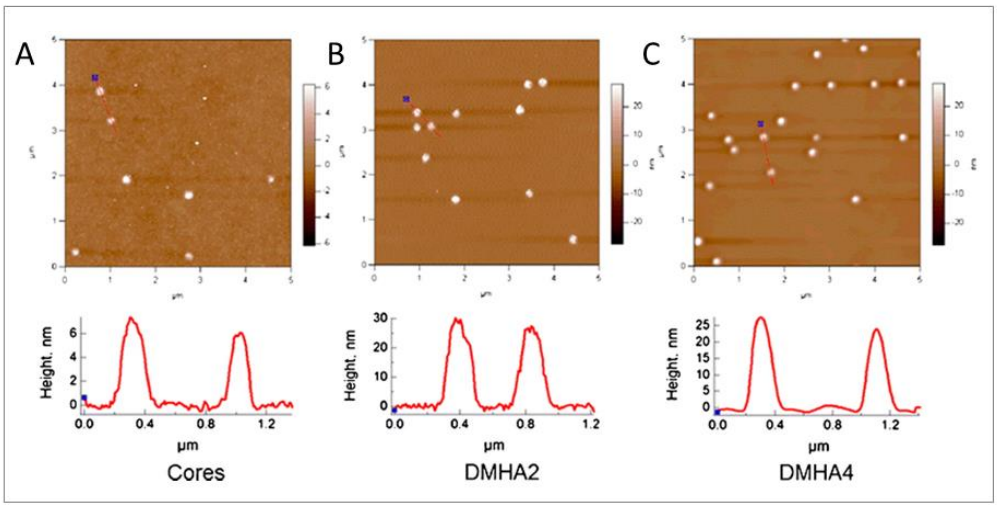

Figure 1.3. AFM (height) images and height line traces of (A) core particles, (B) 2 mol-% DMHA core/shell particles, and (C) 4 mol-% DMHA core/shell particles. Adapted with permission from Ref. 30. Copyright 2013, Springer.

Particle diameter after shell degradation was characterized using asymmetrical flow field-flow fractionation coupled to MALS, which resolved an increase in radius of ~3 nm and ~4 nm for both 2 mol-% and 4 mol-% DMHA shells, respectively. Microgel size increases are likely due to core compression alleviation – removal of shell cross-linker and shell density allows the core to approach its full swelling capacity. Spreading of the 2 mol-% DMHA particle increased by 94 ± 28 nm and height decreased by 20 nm, while the 4 mol-% DMHA particle's spreading increased by 13 ± 27 nm and height decreased by 8 nm (**Figure 1.4**). The observation that 4 mol-% DMHA microgel changes were smaller than those observed in the 2 mol-% DMHA case is likely associated with incomplete erosion of the shell in the 4 mol-% case. Nonetheless, it is clear deformability and porosity increased as a result of shell

degradation for both core/shell constructs, further illustrating how spatial control in core/shell microgels is an effective approach to both chemical and mechanical tuning.

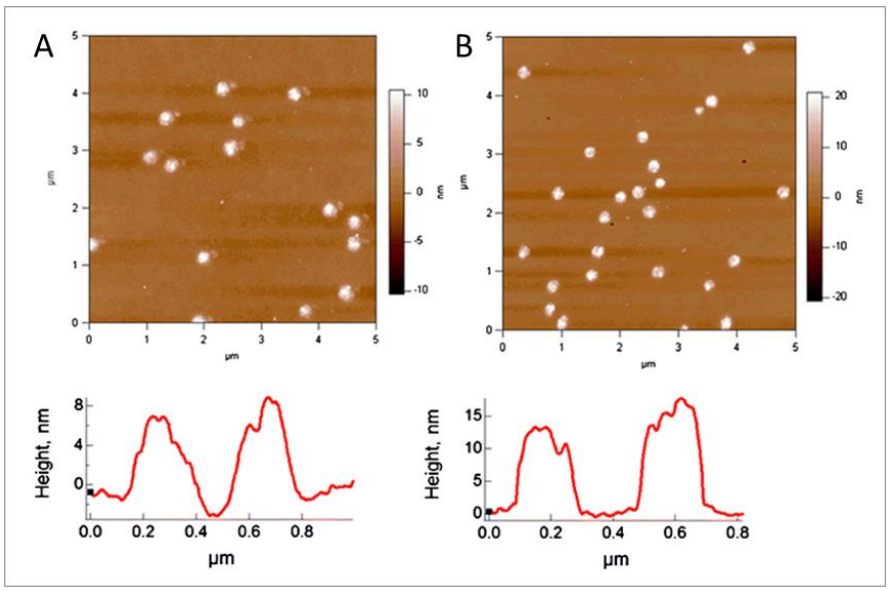

Figure 1.4. AFM (height) images and height line traces of 2 mol-% DMHA (a) and 4 mol-% DMHA (b) following 1 month of erosion in pH 7.4 buffer at 37 °C. Adapted with permission from Ref. 30. Copyright 2013, Springer.

The Lyon Group has also explored the development of hollow microgels for use as multifunctional nanoreactors, encapsulation and delivery vehicles, and for protection of sensitive catalysts. Hollow pNIPAm microgels were synthesized from core-shell nanoparticles through oxidation of the particle core, which was cross-linked by DHEA to produce a degradable core.[31] Polymer segments were removed via centrifugation leaving only the non-degradable BIS containing pNIPAm microgel shell. Building upon this investigation, we have demonstrated the ability to synthesize microgels with nanoscale, thermoresponsive inclusions, a construct inspired by complex biological systems such as the eukaryotic cell.[32] Synthesis of such constructs

was possible by taking advantage of the phase separation of a dilute pNIPAm solution above the LCST to yield a dispersion of colloidally stable polymer aggregates.

1.3.4. Microgels Interacting with Physiologically Relevant Environments

1.3.4.1. Microgel Bio-conjugation Influences Physiological Processes

Microgels can also be conjugated with biomolecules post-synthesis to enhance cellular responses or for targeted delivery. Previously, the Lyon Group has demonstrated the ability to synthesize core/shell nanogels with the surface localized, 12 amino acid peptide (YSAYPDSVPMMS or YSA).[33] This peptide mimics the ligand ephrin-A1, which binds to erythropoietin-producing hepatocellular (Eph) A2 receptor. By taking advantage of this specific ligand-receptor binding motif targeted delivery of small interfering RNA (siRNA) encapsulated within the nanogels to ovarian carcinoma cell lines exhibiting overexpression of Eph2A receptors. Core/shell microgels were synthesized with a pNIPAm/BIS core and a pNIPAm/BIS shell that also contained aminopropyl methacrylate (APMA). In order to enable bio-conjugation of the peptide, functionalized nanogels with maleimide through the EDC coupling of ε-maleimidocaproic acid (EMCA) to the primary amines present in the shell of the nanoparticle due to the inclusion of APMA. Using maleimide coupling, the YSA peptides were then conjugated to the cysteine residue on the C-terminal end of the peptides. *In vitro* studies demonstrated efficient loading and release up to 40% siRNA. *In vitro* targeting studies were also used to establish efficacy through uptake of nanogels by two ovarian cancer cell lines, Hey and BG-1. These studies demonstrated that core/shell nanogels conjugated to YSA peptide exhibited high uptake by cell lines and that siRNA was efficiently delivered within cell lines.

1.3.4.2. Microgel Mechanical Properties Influence Physiological Processes

When using microgels for biological applications, the influence of mechanics on various cellular and physiological processes must be considered. In discriminatory biological environments in particular, microgel mechanics can be highly influential. Banquy *et al*. previously investigated the influence of the elasticity of hydrogel nanoparticles on cellular uptake and intracellular fate in murine macrophages.[34] Nanoparticle elasticity was controlled by varying cross-linker concentration during emulsion polymerization. Using AFM, the Young's modulus for all nanoparticles was determined; values ranged from 18 ± 4 kPa (1.7 mol-% cross-linker) to 39 ± 43 kPa (15 mol-% cross-linker). Investigation of the uptake mechanisms was performed by treating cells with endocytic and metabolic inhibitors prior to incubation with the nanoparticles. The investigators determined that softer nanoparticles, with the lowest Young's modulus (18 ± 4 kPa) were internalized almost exclusively by macropinocytosis. In contrast, more elastic nanoparticles, with slightly higher Young's moduli (35 ± 10 kPa and 136 ± 39 kPa), were internalized via clathrin-and/or caveolae-mediated entry routes. Finally, the stiffest nanoparticles, with the highest Young's modulus (211 ± 43), were internalized mainly by a clathrin-mediated endocytosis. Here it is clear that when it comes to cellular uptake, the relevant mechanism is highly dependent on microgel softness.

1.3.5. Physiologically Relevant Constraints on Microgels

Renal filtration is another biological process that is constrained by a material's mechanical properties, requiring passage of nanoparticles through roughly 8 nm diameter pores under a pressure differential of 40-80 Torr.[35-36] For many rigid nanoparticles, this clearance mechanism provides strict size limitations. In contrast,

deformable nanoparticles could potentially overcome these size restrictions, which might result in delivery vehicles that can be eliminated via normal excretion pathways, thereby limiting the amount of nanocarrier hepatic and renal deposition and retention. To investigate this, we have studied microgel deformation by translocation through cylindrical pores under biologically relevant pressure differentials in order to mimic renal filtration (**Scheme 1.2**).[37]

Scheme 1.2. Filtration method for evaluating microgel pore translocation.

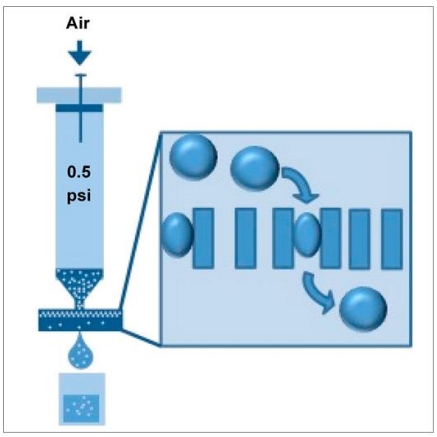

Track-etch membranes were used to model endothelial pores present in the renal system. The microgels were composed of pNIPAm, AAc (10 mol-%), 4-acrylamidofluorescein (0.02 mol-%), and either 1 mol-% BIS (R_H ~ 570 nm at pH 7.4) or 3 mol-% BIS (R_H ~ 433 at pH 7.4). Investigation of translocation of microgels and rigid polystyrene (PS) spheres of similar size indicated that at pH 7.4, PS spheres exhibited jamming in the pores. In contrast, the deformable microgels did not jam appreciably, and passed through pores under modest applied pressure. Furthermore, increasing the microgel cross-linker content to 3 mol-% BIS did not inhibit translocation, even when the pore openings were more than tenfold smaller than microgel diameter.

This concept was further investigated using resistive pulse sensing with 25-50 μm-thick glass nanopore membranes (GNMs) prepared to contain a single conical pore with orifice radii ranging from 200-700 nm.[38] Pressure-driven microgel translocation was monitored, measuring the change in ion current as microgels (dispersed in an electrolyte solution) passed through the pore. Microgels (R_H ~ 570 nm) were composed of pNIPAm, AAc (10 mol-%), and BIS (1 mol-%).

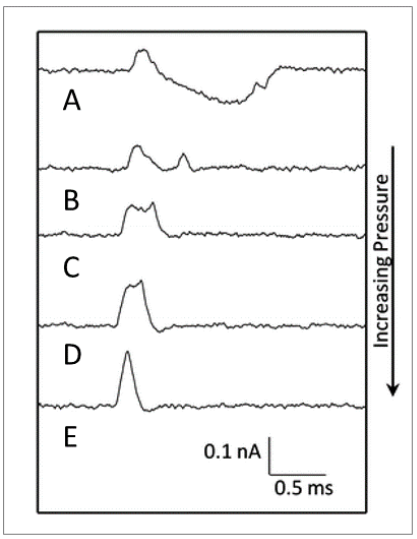

Figure 1.5. Expanded *i-t* traces of individual microgel (R_H ~ 570 nm) translocations through a GNM. Traces represent translocation events through a 302 nm radius pore at applied pressures of (A) -70, (B) -80, (C) -100, (D) - 120 and (E) -150 mmHg. Reproduced from Ref. 38 with permission from The Royal Society of Chemistry.

When microgels had a diameter smaller than the pore size, a single current peak was observed where the current increased due to the highly charged anionic microgel displacing pore electrolyte during passage. In contrast, when the microgels had a diameter larger than the pore, a more complex peak pattern consisting of multiple current transients was observed. These larger microgels must deform in order to translocate, resulting in an expulsion of electrolyte solution and a subsequent

decrease in current from the peak maximum associated with the initial bath electrolyte displacement. After the microgel passes through the narrowest portion of the pore, the electrolyte solution is reabsorbed, the microgel passes out of the sensing zone, and the current returns to baseline. At higher applied pressures, the single current peak returns, as the two transients seem to collapse into one, suggesting that the microgel deforms and passes through the pore with minimal volume change, indicating the translocation rate is faster than the effective deswelling rate (**Figure 1.5)**. In these studies, a minimum nanopore-to-microgel radius ratio of ~ 0.4 for translocation was observed, which suggests a theoretical limit imposed by the compressibility of the microgel and Coulombic repulsion between the microgels and the pore walls. This theoretical limit is largely determined by the properties of the microgel, such as internal density of charged groups, chain flexibility, and strength of the solvent-polymer interactions. These properties can be tuned to adjust microgel mechanics in order to control response to the surrounding (mechanical) environment.

1.4. Microgel Assemblies

1.4.1. Microgel Assemblies Explored Within This Dissertation

As shown in **Scheme 1.3,** there are four types of microgel assemblies investigated within this thesis: (1) packed microgel dispersions (colloidal fluids, crystals, glasses) (2) microgels interacting with colloidal substrates (monolayers), (3) electrostatically cross-linked polyelectrolyte microgel assemblies (multilayers and gels), and (4) covalently cross-linked microgel assemblies (multilayers and gels). Microgels exhibit rich phase behavior which has been heavily investigated in the past. The influence of packed microgel dispersions on composite assembly fabrication will

be discussed in **Chapter 2** and **Chapter 3**. Influence of the properties of these assemblies on drug delivery applications will be discussed in **Chapter 4**. Development and applications of electrostatically and covalently cross-linked polyelectrolyte microgel assemblies will be compared and contrasted in **Chapter 5, Chapter 6,** and **Chapter 7**.

Scheme 1.3. Types of microgel assemblies explored in this dissertation.

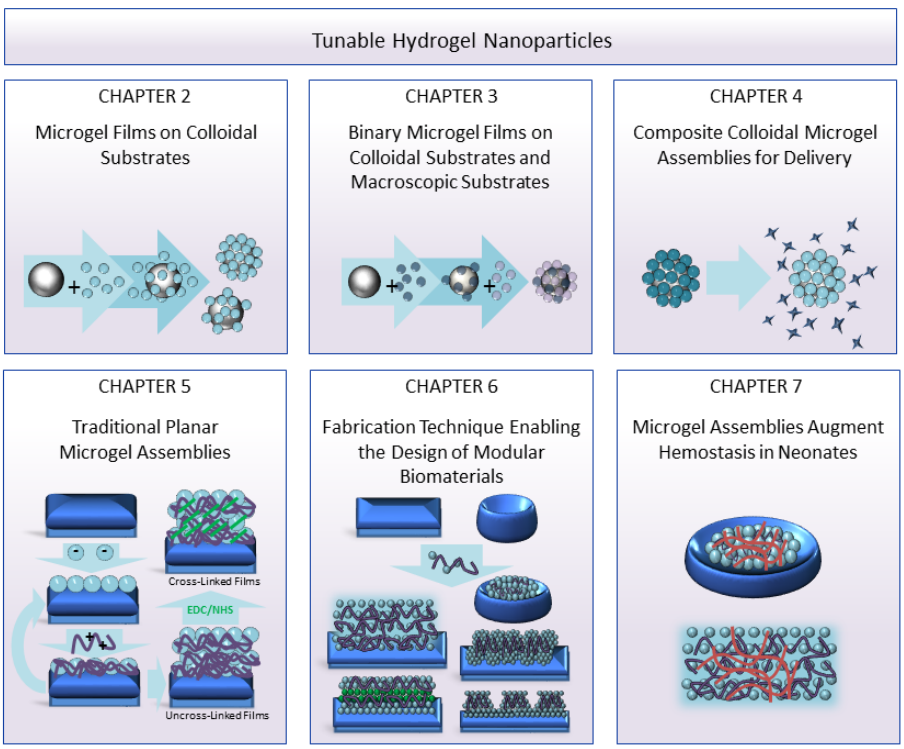

1.4.2. Tunable Microgel Assemblies

For two-dimensional and three-dimensional assemblies of microgels, the softness of the matrix can be adjusted through covalent or non-covalent inter-microgel cross-linking.[19] For example, Jia *et al.* used a hyaluronic acid for *in situ* construction of a microgel network to repair damaged canine vocal folds.[19] The investigators

compared the viscoelastic range of microgel networks with and without covalent inter-microgel cross-linking to the viscoelasticity of undamaged canine vocal chords. Full recovery of the entire viscoelastic range (and presumably the ultimate function) was only achieved in the network containing a significant level of inter-microgel cross-linking.

Not only do external cross-links provide an additional handle to modify biomaterial mechanics, they allow for microgel solutions to be physically gelled *in situ* after injection to the target site. Such an option is attractive from a logistical perspective because it is less invasive than the surgical implantation typically required for macroscopic hydrogel scaffolds.[19, 39] Saunders *et al.* utilized the *in situ* gelling methodology to introduce load bearing scaffolds into damaged intervertebral discs (IVDs) as an alternative to traditional, high-risk spinal implantation surgery for IVD repair.[39-40] A solution of poly(methyl methacrylate-*co*-methacrylic acid-*co*-ethyleneglycol dimethacrylate) microgels functionalized with glycidyl methacrylate was injected into the tissue free space of damaged bovine IVDs. A pH-triggered fluid-to-gel transition was utilized to gel the microgel solution *in vitro* while covalent inter-microgel cross-links were formed via free radical chemistry. The investigators showed that the microgel network restored mechanical properties of IVDs to ranges observed in undamaged IVDs and showed little cytotoxicity toward human nucleus pulposus cells, making the doubly cross-linked microgel approach viable for IVD repair.

1.4.3. Layer-by-Layer Film Assembly

Microgel films can be assembled using a variety of passive and active monolayer deposition techniques, including spin-coating[41-42] and centrifugal deposition.[43] In these methods, substrate surface charge must be opposite that of the microgel charge enabling bonding via Coulombic charge interactions. Building upon this monolayer foundation, microgel multilayers may be produced using the Layer-by-Layer technique (LbL). The LbL method was popularized by Descher *et al*. to produce films consisting of two complementary linear polymer components of opposite electrostatic charge where each layer is applied in an alternating manner using either passive or active deposition method.[44]

This method was first adapted by the Lyon Group to form microgel films in 2003.[45] Since then, the Lyon Group has heavily investigated intricacies of the film buildup process. In 2009, the Lyon Group demonstrated the ability to build microgel films through active deposition of the microgel layer by centrifugation, enabling a faster fabrication method.[43] Typically, amine-functionalized glass are used as the substrate and anionic microgels are deposited via centrifugation followed by passive adsorption of a linear polycation such as poly(diallyldimethylammonium chloride) (PDADMAC) or a branched polycation such as poly(ethylenimine) (PEI).

1.4.4. Properties of Microgel Assemblies

1.4.4.1. Microgel Assembly Responsivity

Such films are typically both thermoresponsive, due to the base monomers, and pH responsive, due to the addition of an acidic comonomer to provide the required electrical charge, during microgel synthesis. The Lyon Group has previously

demonstrated the ability to tune microgel assemblies by combining varied microgel building blocks. For example, the Lyon Group demonstrated the ability to finely-tune the deswelling temperatures of microgel films within physiologically relevant ranges by preparing films with varying ratios of pNIPAm and pNIPMAm microgels.[46] Microgel film behavior is often complex; interactions between the microgels and the polycation lead to unusual and unexpected behaviors, not simply described by an addition of the properties of the two components. For example, studies demonstrate that the pH responsivity of films is dependent on both particle swelling and polyelectrolyte complexation.[47] Additionally, these polyelectrolyte microgel films exhibit intriguing autonomic self-healing properties when damaged in the dry state and subsequently exposed to moisture.[48]

1.4.4.2. Mechanical Properties of Microgel Assemblies

Moving beyond individual particles, the Lyon Group has interrogated the mechanical properties of self-healing polyelectrolyte multilayer microgel films on multiple scales using a variety of techniques. Recently, the Lyon Group investigated microgel film self-healing to gain more insight into the mechanism of film damage and to understand what drives restoration of film integrity.[49] Films were assembled using a Layer-by-Layer (LbL) approach from microgels containing pNIPAm, AAc (10 mol-%), and BIS (2 mol-%) and the linear polycation PDADMAC on elastomeric poly(dimethylsiloxane) (PDMS) substrates. Dried films were subjected to linear strains between 0% and 30%. These studies reveal that an undamaged film stretched to a strain of 30% then relaxed forms a parallel wrinkled pattern on its surface.

However, if the film is then hydrated the wrinkles disappear and the original film integrity is restored, demonstrating that these films can self-heal.

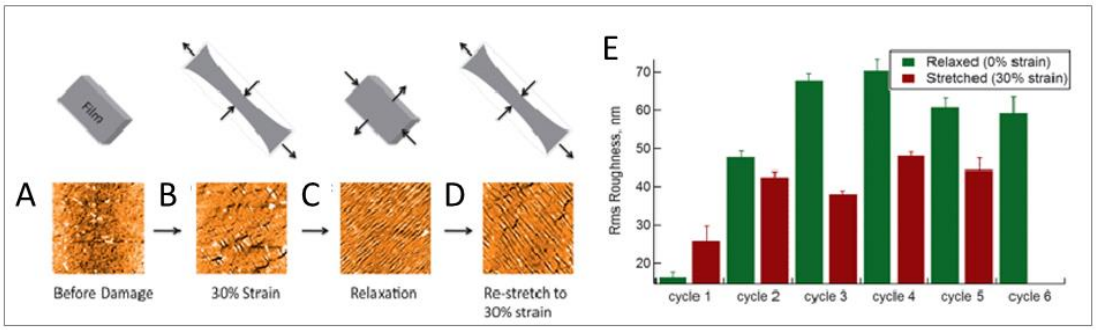

Figure 1.6. AFM (height) images of microgel multilayer films shown (A) before cycling at 0% strain, (B) at 30% strain, (C) when the film is relaxed back to 0% strain, and finally (D) when the film is re-stretched to 30% strain. (E) The pattern of roughness persists throughout multiple cycles. All AFM images are 40 μm x 40 μm. Adapted from Ref. 49 with permission from The Royal Society of Chemistry.

For an undamaged film that is initially stretched to a strain of 30% and is then relaxed (**Figures 1.6A-1.6C**), the resulting wrinkles lie orthogonal to the stretching axis, which suggests a buckling behavior following plastic deformation of the microgel film. If the same film is re-stretched to 30% strain in the same direction (**Figure 1.6D**), the wrinkles appear to reorient themselves orthogonal to the original pattern (parallel to the direction of strain). This directional change results from elongation and compression forces experienced by the film during stretching on the elastomeric PDMS substrate. During the initial stretching period, the PDMS substrate elongates along the stretching axis and compresses along the perpendicular axis. If we assume the entire film must also undergo some degree of deformation during the initial stretching event, the in-plane film axis perpendicular to the initial stretching

axis is under compression during a second stretching event. This compression creates a new wrinkling pattern perpendicular to the stretching axis. Upon relaxation of the stress, the effective surface area of the substrate is reduced, inducing wrinkling of the film that occurs because of the elasticity mismatch between the film and the underlying PDMS substrate.

Because individual microgels are connected via non-covalent (Coulombic) interactions between PDADMAC and AAc sites, these weak bonds can be sacrificed in favor of an altered ion pairing structure. This allows for an increase in film dimension along the stretching axis to dissipate the stress and prevent failure. Because there is a mismatch in elasticity between the multilayer and the PDMS substrate, the disrupted interactions cannot recover at the same rate as the PDMS, resulting in wrinkling of the elongated film. During hydration, the polymer and ion mobility that occurs allows restoration of the smooth, low-energy confirmation.

In this complex structure, polymer chain flexibility and particle deformability allow for self-healing to occur under hydrating conditions. Such softness has given microgel films an additional application in the area of non-adhereing coatings. Previously, Yamato *et al.* demonstrated the ability to harvest keratinocytes on culture dishes grafted with thermoresponsive pNIPAm hydrogels.[50] Keratinocytes proliferated and formed multilayers at 37 °C on grafted surfaces and the non-grafted culture dishes. By lowering the temperature to 20 °C, these multilayered keratinocyte sheets detached from grafted surfaces completely leaving no remnants. Building upon this investigation, Schmidt *et al.* demonstrated the ability to use pNIPAm-BIS (6 mol-% cross-linker) microgel films cross-linked with (PEI) for thermally controlled

detachment of adsorbed fibroblasts.[51] After a 48 h incubation at 37 °C in cell culture medium, fibroblasts were observed to adhere and spread well. After cooling to 20 °C, the cells exhibited a round morphology (effectively detached) and were removed from the surface with gentle washing. Successive cycles of spreading/rounding were also observed, indicating a reversible behavior. Cell detachment from microgel coatings may be attributed to increased hydration of the polymer, reducing attractive van der Waals interactions and increasing repulsive osmotic interactions. Ellipsometry and AFM measurements indicated that upon crossing the VPTT the water content changed from 90 wt-% to less than 30 wt-% and the elastic modulus of the microgels increased by an order of magnitude. At 37 °C, the water content was 70 wt-% and the modulus was in the range of several hundred kPa, making the substrate more suitable for cell adhesion.

1.4.5. Applications of Microgel Assemblies

Microgel assemblies have been extensively explored for use in drug delivery applications. Due to their thermoresponsivity, microgel thin films have been used for triggered release of insulin.[52] The Lyon Group demonstrated that thermal cycling can be used to direct pulsatile and extended release of insulin over many cycles. Similarly, the Lyon Group demonstrated the ability to encapsulate and release the chemotherapeutic drug doxorubicin based on changes in temperature.[41] Microgel films have also been explored in the context of non-fouling implant coatings to reduce inflammatory response. The Lyon Group studied the use of pNIPAm microgels cross-linked with poly(ethylene glycol) diacrylate (PEGDA) coatings on clinically relevant polymeric materials to significantly reduce *in vitro* fibrinogen adsorption and human

monocyte/macrophage adhesion and spreading.[53] Development of microgel films as a biological interface to inhibit physiological responses is further investigated in **Chapter 5**.

1.5. Tapping into Microgel Potential for Applications

Microgels offer a bottom-up and multi-scale route by which chemical and mechanical properties can be tailored on the individual level from particle synthesis or in assemblies through functionalization and inter-microgel cross-links. The ease of synthesizing microgels to display a wide range of chemical and mechanical properties on the particle level and in assemblies affords microgel-based materials real potential in a variety of biomedical applications. This dissertation describes new routes to fabricate tunable microgel-based materials for the next generation of regenerative medicine, wound healing, and other biomedical tools, as a new frontier for microgel-related research.

1.6. References

1. Deshayes, S.; Kasko, A. M., Polymeric biomaterials with engineered degradation. *J. Polym. Sci. A Polym. Chem.* **2013**, *51* (17), 3531-3566.

2. Peppas, N. A.; Langer, R., New challenges in biomaterials. *Science.* **1994**, *263* (5154), 1715-1720.

3. Langer, R.; Tirrell, D. A., Designing materials for biology and medicine. *Nature.* **2004**, *428* (6982), 487-492.

4. Galperin, A.; Long, T. J.; Ratner, B. D., Degradable, thermo-sensitive poly(N-isopropyl acrylamide)-based scaffolds with controlled porosity for tissue engineering applications. *Biomacromolecules.* **2010**, *11* (10), 2583-2592.

5. Bryers, J. D.; Giachelli, C. M.; Ratner, B. D., Engineering biomaterials to integrate and heal: The biocompatibility paradigm shifts. *Biotechnol. Bioeng.* **2012**, *109* (8), 1898-1911.

6. Saunders, B. R.; Laajam, N.; Daly, E.; Teow, S.; Hu, X.; Stepto, R., Microgels: From responsive polymer colloids to biomaterials. *Adv. Colloid Inter.* **2009**, *147-148*, 251-62.

7. Wang, Y.-X.; Robertson, J.; Spillman, W., Jr.; Claus, R., Effects of the chemical structure and the surface properties of polymeric biomaterials on their biocompatibility. *Pharm. Res.* **2004**, *21* (8), 1362-1373.

8. Champion, J.; Walker, A.; Mitragotri, S., Role of particle size in phagocytosis of polymeric microspheres. *Pharm. Res.* **2008**, *25* (8), 1815-1821.

9. Champion, J. A.; Katare, Y. K.; Mitragotri, S., Particle shape: A new design parameter for micro- and nanoscale drug delivery carriers. *J. Control. Release.* **2007,** *121* (1–2), 3-9.

10. Drummond, D. C.; Meyer, O.; Hong, K.; Kirpotin, D. B.; Papahadjopoulos, D., Optimizing liposomes for delivery of chemotherapeutic agents to solid tumors. *Pharmacol. Rev.* **1999**, *51* (4), 691-744.

11. Mitragotri, S.; Lahann, J., Physical approaches to biomaterial design. *Nat. Mater.* **2009**, *8* (1), 15-23.

12. Rehfeldt, F.; Engler, A. J.; Eckhardt, A.; Ahmed, F.; Discher, D. E., Cell responses to the mechanochemical microenvironment—implications for regenerative medicine and drug delivery. *Adv. Drug Deliv. Rev.* **2007**, *59* (13), 1329-1339.

13. Discher, D. E.; Janmey, P.; Wang, Y. L., Tissue cells feel and respond to the stiffness of their substrate. *Science.* **2005**, *310* (5751), 1139-1143.

14. Peppas, N. A.; Hilt, J. Z.; Khademhosseini, A.; Langer, R., Hydrogels in biology and medicine: from molecular principles to bionanotechnology. *Adv. Mater.* **2006**, *18* (11), 1345-1360.

15. Hennink, W. E.; van Nostrum, C. F., Novel crosslinking methods to design hydrogels. *Adv. Drug Del. Rev.* **2002**, *54* (1), 13-36.

16. Bae, K. H.; Wang, L.-S.; Kurisawa, M., Injectable biodegradable hydrogels: progress and challenges. *J. Mater. Chem. B* **2013**, *1* (40), 5371-5388.

17. Tibbitt, M. W.; Anseth, K. S., Hydrogels as extracellular matrix mimics for 3D cell culture. *Biotechnol. Bioeng.* **2009**, *103* (4), 655-663.

18. Kharkar, P. M.; Kiick, K. L.; Kloxin, A. M., Designing degradable hydrogels for orthogonal control of cell microenvironments. *Chem. Soc. Rev.* **2013**, *42* (17), 7335-7372.

19. Jia, X.; Yeo, Y.; Clifton, R. J.; Jiao, T.; Kohane, D. S.; Kobler, J. B.; Zeitels, S. M.; Langer, R., Hyaluronic acid-based microgels and microgel networks for vocal fold regeneration. *Biomacromolecules.* **2006**, *7* (12), 3336-3344.

20. Dai, Z.; Ngai, T., Microgel particles: The structure-property relationships and their biomedical applications. *J. Polym. Sci. A Polym. Chem.* **2013**, *51* (14), 2995-3003.

21. Hendrickson, G. R.; Smith, M. H.; South, A. B.; Lyon, L. A., Design of multiresponsive hydrogel particles and assemblies. *Adv. Funct. Mater.* **2010**, *20* (11), 1697-1712.

22. Saunders, B. R., On the structure of poly(N-isopropylacrylamide) microgel particles. *Langmuir.* **2004**, *20* (10), 3925-3932.

23. Smith, M. H.; Herman, E. S.; Lyon, L. A., Network deconstruction reveals network structure in responsive microgels. *J. Phys. Chem. B.* **2011**, *115* (14), 3761-3764.

24. Gao, J.; Frisken, B. J., Cross-linker-free *N*-isopropylacrylamide gel nanospheres. *Langmuir.* **2003,** *19* (13), 5212-5216.

25. South, A. B.; Lyon, L. A., Direct observation of microgel erosion via in-liquid atomic force microscopy. *Chem. Mater.* **2010,** *22* (10), 3300-3306.

26. Smith, M. H.; Lyon, L. A., Tunable encapsulation of proteins within charged microgels. *Macromolecules.* **2011,** *44* (20), 8154-8160.

27. Jones, C. D.; Lyon, L. A., Synthesis and characterization of multiresponsive core−shell microgels. *Macromolecules.* **2000,** *33* (22), 8301-8306.

28. Berndt, I.; Richtering, W., Doubly temperature sensitive core−shell microgels. *Macromolecules.* **2003,** *36* (23), 8780-8785.

29. Jones, C. D.; Lyon, L. A., Shell-restricted swelling and core compression in poly(*N*-isopropylacrylamide) Core−Shell Microgels. *Macromolecules* **2003,** *36* (6), 1988-1993.

30. Gaulding, J.; South, A.; Lyon, L. A., Hydrolytically degradable shells on thermoresponsive microgels. *Colloid Polym. Sci.* **2013,** *291* (1), 99-107.

31. Nayak, S.; Gan, D. J.; Serpe, M. J.; Lyon, L. A., Hollow thermoresponsive microgels. *Small* **2005,** *1* (4), 416-421.

32. Hu, X. B.; Tong, Z.; Lyon, L. A., One-pot synthesis of microcapsules with nanoscale Inclusions. *Macromolecular Rapid Communications* **2011,** *32* (18), 1461-1466.

33. Blackburn, W. H.; Dickerson, E. B.; Smith, M. H.; McDonald, J. F.; Lyon, L. A., Peptide-functionalized nanogels for targeted siRNA delivery. *Bioconjugate Chem.* **2009,** *20* (5), 960-968.

34. Banquy, X.; Suarez, F.; Argaw, A.; Rabanel, J.-M.; Grutter, P.; Bouchard, J.-F.; Hildgen, P.; Giasson, S., Effect of mechanical properties of hydrogel nanoparticles on macrophage cell uptake. *Soft Matter* **2009,** *5* (20), 3984-3991.

35. Deen, W. M.; Lazzara, M. J.; Myers, B. D., Structural determinants of glomerular permeability. *Am. J. Physiol. Renal Physiol.* **2001,** *281* (4), F579-F596.

36. Lau, C.; Sudbury, I.; Thomson, M.; Howard, P. L.; Magil, A. B.; Cupples, W. A., Salt-resistant blood pressure and salt-sensitive renal autoregulation in chronic streptozotocin diabetes. *Am. J. Physiol. Regul. Integr. Comp. Physiol.* **2009,** *296* (6), R1761-70.

37. Hendrickson, G. R.; Lyon, L. A., Microgel translocation through pores under confinement. *Angew. Chem. Int. Ed.* **2010,** *49* (12), 2193-2197.

38. Holden, D. A.; Hendrickson, G. R.; Lan, W.-J.; Lyon, L. A.; White, H. S., Electrical signature of the deformation and dehydration of microgels during translocation through nanopores. *Soft Matter.* **2011,** *7* (18), 8035-8040.

39. Saunders, J. M.; Tong, T.; Le Maitre, C. L.; Freemont, T. J.; Saunders, B. R., A study of pH-responsive microgel dispersions: from fluid-to-gel transitions to mechanical property restoration for load-bearing tissue. *Soft Matter.* **2007,** *3* (4), 486-494.

40. Milani, A. H.; Freemont, A. J.; Hoyland, J. A.; Adlam, D. J.; Saunders, B. R., Injectable doubly cross-linked microgels for improving the mechanical properties of degenerated intervertebral discs. *Biomacromolecules.* **2012,** *13* (9), 2793-2801.

41. Serpe, M. J.; Yarmey, K. A.; Nolan, C. M.; Lyon, L. A., Doxorubicin uptake and release from microgel thin films. *Biomacromolecules.* **2005,** *6* (1), 408-413.

42. Schmidt, S.; Motschmann, H.; Hellweg, T.; von Klitzing, R., Thermoresponsive surfaces by spin-coating of PNIPAM-co-PAA microgels: A combined AFM and ellipsometry study. *Polymer.* **2008,** *49* (3), 749-756.

43. South, A. B.; Whitmire, R. E.; Garcia, A. J.; Lyon, L. A., Centrifugal deposition of microgels for the rapid assembly of nonfouling thin films. *ACS Applied Materials & Interfaces.* **2009,** *1* (12), 2747-2754.

44. Decher, G., Fuzzy nanoassemblies: toward layered polymeric multicomposites. *Science.* **1997,** *277* (5330), 1232-1237.

45. Serpe, M. J.; Jones, C. D.; Lyon, L. A., Layer-by-layer deposition of thermoresponsive microgel thin films. *Langmuir.* **2003,** *19* (21), 8759-8764.

46. Clarke, K. C.; Lyon, L. A., Modulation of the deswelling temperature of thermoresponsive microgel films. *Langmuir.* **2013,** *29* (41), 12852-12857.

47. Sorrell, C. D.; Lyon, L. A., Bimodal swelling responses in microgel thin films. *J. Phys. Chem. B.* **2007,** *111* (16), 4060-4066.

48. South, A. B.; Lyon, L. A., Autonomic self-healing of hydrogel thin films. *Angew. Chem. Int. Edit.* **2010,** *49* (4), 767-771.

49. Gaulding, J. C.; Spears, M. W.; Lyon, L. A., Plastic deformation, wrinkling, and recovery in microgel multilayers. *Polym. Chem.* **2013,** *4* (18), 4890-4896.

50. Yamato, M.; Utsumi, M.; Kushida, A.; Konno, C.; Kikuchi, A.; Okano, T., Thermo-responsive culture dishes allow the intact harvest of multilayered keratinocyte sheets without dispase by reducing temperature. *Tissue Eng.* **2001,** *7* (4), 473-480.

51. Schmidt, S.; Zeiser, M.; Hellweg, T.; Duschl, C.; Fery, A.; Möhwald, H., Adhesion and mechanical properties of PNIPAM microgel films and their potential use as switchable cell culture substrates. *Adv. Funct. Mater.* **2010,** *20* (19), 3235-3243.

52. Nolan, C. M.; Serpe, M. J.; Lyon, L. A., Pulsatile release of insulin from Layer-by-Layer assembled microgel thin films. *Macromolecular Symposia*. **2005,** *227*, 285-294.

53. Bridges, A. W.; Singh, N.; Burns, K. L.; Babensee, J. E.; Lyon, L. A.; Garcia, A. J., Reduced acute inflammatory responses to microgel conformal coatings. *Biomaterials.* **2008,** *29* (35), 4605-4615.

CHAPTER 2

MICROGEL FILMS ON COLLOIDAL SUBSTRATES

Portions reproduced from:
442, Saxena, S. and Lyon, L.A. Influence of Microgel Packing on Raspberry-Like Heteroaggregate Assembly. *Journal of Colloid and Interface Science*, 39-48.,

2.1 Introduction

Recently, architectural control of composite nano- and microparticles has gained importance in the development of functional materials. The creation of multi-material colloidal particles (i.e. polymer/polymer,[1] polymer/metal,[2] polymer/mineral,[3] mineral/metal,[4] metal/metal,[5] etc.) can lead to complex properties that are not simple compositional averages of the individual materials, with those properties being tunable to meet specific needs of an application. Previous studies have investigated the use of hybrid colloids for a wide range of purposes such as drug delivery,[6-7] sensing,[8-9] photonics,[10] optoelectronics,[11] coatings,[12] and stabilizers.[13]

Hybrid colloids often involve two distinct materials arranged in a core-shell architecture. A variety of techniques have been explored for the development of such core-shell systems, one of which is heteroaggregation.[14] Heteroaggregates are caused by the aggregation of particles with different compositions and/or sizes in colloidal dispersions and have been investigated for use in manufacturing coatings, separations techniques, as well as pharmaceutical devices and biotechnology.[15] Previous methods to produce core-shell heteroaggregates have often relied on ion-pairing to drive heteroaggregation or require covalent grafting of a shell onto a core particle.[16-19] Such methods result in a construct where the core particle is surrounded by a nanoparticle

shell, which resembles a raspberry and is often termed a raspberry-like particle (RLP). Various parameters can be used to control the heteroaggregation process. For example, ion-pair driven heteroaggregation, which relies on electrostatic interactions between the core-particle and the shell particle, is sensitive to pH, ionic strength, and particle sizes. When stimuli-responsive components are used, this offers additional routes to control the rate of heteroaggregation including hydrogen bonding, temperature, or light.[20-21] Such parameters can even be used to produce reversible heteroaggregation.

Heteroaggregates have been constructed from a variety of materials, such as polystyrene/silicon dioxide,[12] polystyrene/iron oxide,[22] polystyrene/poly(2-vinylpyridine),[23] hydroxypropyl cellulose/silica,[19] alginate/$CaCO_3$,[24] and many others. In addition, soft material components, such as microgels, have been investigated for the development of heteroaggregates including RLPs.[23, 25] Using soft, deformable microgels to assemble atop hard sphere "cores" allows for increased contact area; the microgels are able to spread onto the hard spheres, which improves the mechanical stability of the complex.[25] This is beneficial because assembly of heteroaggregates is limited by both the strength of intra-particle bonds and the contact area between the particles. As an example of such soft/hard heteroaggregates, poly(*N*-isopropylacrylamide) (pNIPAm) microgels have been employed due to interest in their thermosensitivity.[15] PNIPAm microgels have been assembled atop SiO_2 core particles in a number of studies to produce RLPs.[16]

Raspberry-structured microgel heteroaggregates can be used as stand-alone microparticles for applications such as drug delivery or separations in situations

where microgels alone may not be appropriate. In this manner, RLPs open the door for use of microgel-based assemblies in unique systems due to the added functionality of the core particle that can provide size, density, magnetism, or other desirable characteristics without compromising the synthetic control over microgel behavior. In addition, these composite assemblies are unique building blocks due to their unusual raspberry-structured topography, as well as the combination of varied chemical and mechanical properties localized in the core or the shell. Assembly of these microparticles into two-dimensional or three-dimensional constructs offers a facile means to create hierarchically ordered, stable assemblies that can function as a biological interface.

The Lyon Group has previously reported the synthesis of raspberry-structured microgel heteroaggregates by immersing core particles into a densely packed colloidal (microgel) phase to apply a microgel coating.[26] It is hypothesized that this heteroaggregation occurs due to the amphiphilic nature of pNIPAm and pNIPMAm microgels, making interactions with the amphiphilic charged polystyrene core possible, even in the case where components possess charges of the same sign. Using this method, the Lyon Group has shown that ultra violet (UV) irradiation can be used to couple the microgels to carboxylated polystyrene (PS) core particles modified with 4-aminobenzophenone (AB). This covalent coupling via UV irradiation is not necessary for the formation of RLPs, but can be employed to enhance stability of the assembly. This previous study demonstrated the assembly of RLPs using two different microgel compositions (neutral and anionic) and two different core particles (4.5 μm PS and "rough" PS with iron oxide grafted on the surface). This method allows for

versatility in the composition of RLP components, lacking the constraints of ion-pair driven heteroaggregation such as sensitivity to pH and ionic strength. Moreover, since chemical compositional limitations have not yet been discovered for this system, it can be utilized to interrogate fundamental aspects of microgel deformation at a curved interface.

Herein the sensitivity of the colloidal-phase mediated heteroaggregation process to the volume fraction of the microgel phase is explored. The previously described method[26] has been modified to enable the creation of colloidal-phases of known volume fractions (**Scheme 2.1**), thereby obtaining greater control over the packing of microgels around the core particles. Volume fraction is the thermodynamic parameter of interest for colloidal phases.[27] For dispersions of spherical, repulsive hard spheres, the phase diagram predicts a disordered "fluid" phase at sphere volume fractions below 0.49, fluid/crystal coexistence, from 0.49-0.55, and an fcc crystalline phase above 0.55, with the maximal close packing occurring at 0.74. It is also typical to observe a kinetically trapped "glassy" phase with an approximate maximal packing of ~0.64; this glassy phase may coexist with a polycrystalline phase as well. Previous investigations of microgel phase behavior have indicated that microgels behave as hard spheres up to a volume fraction of 0.5.[28] However, above this volume fraction, particle softness begins to influence the phase behavior, leading to a shift in the fluid/crystal phase boundary and a narrowing of the coexistence region.[28] Due to the unique softness of microgels, the parameter volume fraction is often replaced by the effective volume fraction (φ_{eff}) according to Equation (1), where a represents the average distance between the center of two adjacent microgels, σ represents the

microgel hydrodynamic diameter in dilute dispersions, and 0.740 corresponds to the volume fraction for hard sphere closest packing.

$$\varphi_{eff} = 0.740/(a/\sigma)^3 \qquad \text{Equation (1)}$$

The present investigation explores the influence of microgel network structure on deformation at an interface based on microgel monomer and cross-linker content. Investigation of microgel deformation at planar interfaces demonstrates the influence of microgel compositions on microgel rigidity and subsequent microgel spreading, leading to varied topographical features. Visual studies of several RLPs composed of different microgel compositions further elucidate the complex influence microgel structure has on coating efficiency and resulting topography when curved interfaces are introduced to a system. An understanding of these implications could be widely applicable to systems in which microgel deformation occurs on a rigid, curved surface.

Scheme 2.1. Colloidal-phase mediated heteroaggregation.

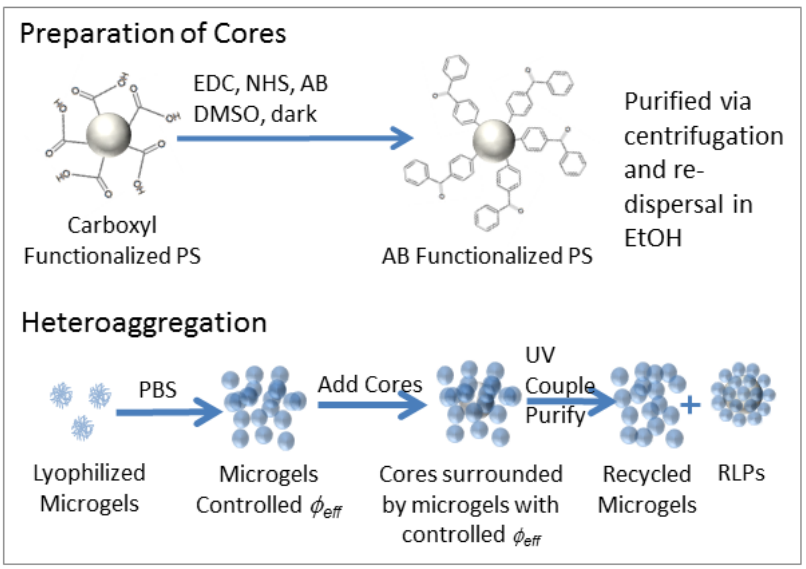

2.2. Experimental

2.2.1. Materials

All reagents were purchased from Sigma-Aldrich (St. Louis, MO) and used as received, unless otherwise noted. Reagents *N,N'*-methylenebis(acrylamide) (BIS), acrylic acid (AAc), sodium dodecyl sulfate (SDS), ammonium persulfate (APS), 1-ethyl-2-[2-dimethylaminopropyl]carbodiimide hydrochloride (EDC), *N*-hydroxysuccinimide (NHS), 4-aminobenzophenone (AB), ethanol (EtOH), dimethylsulfoxide (DMSO), 3-aminopropyltrimethoxysilane (APTMS), sodium phosphate monobasic, formic acid, and 2-(N-morpholino)ethanesulfonic acid (MES) were all used as received. The monomers *N*-isopropylacrylamide (NIPAm) and *N*-isopropylmethacrylamide (NIPMAm) were recrystallized from hexanes (VWR international, West Chester, PA) and dried *in vacuo* prior to use. Carboxyl modified polystyrene (PS) spheres were purchased from Polysciences, Inc. (Warrington, PA).

Deionized water used in all reactions, purifications, and buffer preparations was purified to a resistance of 18 MΩ (Barnstead E-Pure system), and filtered through a 0.2 μm filter to remove particulate matter.

2.2.2. Microgel Synthesis

Microgels were synthesized as previously described using precipitation polymerization.[29] For pNIPAm microgels, the total monomer concentration was 100 mM with molar compositions of 95 mol-% pNIPAm and 5 mol-% BIS (denoted pNIPAm:BIS (95:5)) or 99 mol-% pNIPAm and 1 mol-% BIS (pNIPAm:BIS (99:1)). For samples containing pNIPMAm, the total monomer concentration was 140 mM with molar compositions of either 95 mol-% pNIPMAm and 5 mol-% BIS (denoted pNIPMAm:BIS (95:5)) or 99 mol-% pNIPMAm and 1 mol-% BIS (pNIPMAm:BIS (99:1)). Monomer, cross-linker, and surfactant (SDS) were dissolved in water and filtered to remove any undissolved solids. The solution was placed in a 3-neck round bottom flask equipped with a condenser and mixed with a magnetic stir bar (stir speed 450 RPM) during the entire reaction. The solution was then heated to 70 °C and purged with N_2 for approximately 1 h. Finally, 1 mL of the initiator APS was added with a syringe needle. A total APS concentration of 1 mM was used for all microgels except the 99 mol-% pNIPMAm and 1 mol-% BIS sample, which required an APS concentration of 4 mM for enhanced control over microgel size. The solution was held at ~70 °C overnight, and then cooled to room temperature. The microgel solution was filtered through glass wool, purified via sedimentation, and lyophilized for storage.

2.2.3. Microgel Characterization

Microgel morphological characteristics such as height and spread of individual microgels were determined by passive deposition of dilute solutions of microgels in 10 mM, pH 7.4 phosphate buffer saline (PBS) with a high ionic strength (HIS) of 100 mM NaCl overnight on amine-functionalized silica glass coverslips. These samples were imaged using an MFP-3D Atomic Force Microscope (AFM) system (Asylum Research, Santa Barbara, CA). The parameters associated with 10 microgels were used to determine the average height and spread for each composition. Microgel hydrodynamic radius (R_H) values were determined using a DynaPro Dynamic Light Scattering (DLS) instrument (Wyatt, Technology, Santa Barbara, CA) in high HIS PBS.

2.2.3.1. Characterization of Microgel Swelling via Viscometry

Viscometry studies were conducted to determine the effective volume fraction of the microgels in solution for further understanding of the colloidal phase. For microgels, the volume fraction occupied in a solution is difficult to predict since they are solvent-swollen structures. In such cases, viscometry studies that measure the viscosity of dilute solutions can be used to determine the effective volume fraction.

Viscometry data were obtained using an Ubbelohde viscometer with a viscometer constant of 0.003121 cSt/s at 21 °C. Samples were prepared between 0.05 wt-% and 0.35 wt-% depending on the microgel composition. Five weight fractions were used for each microgel composition and three trials were performed at each weight fraction. The swelling ratio, *k*, was determined by fitting the data to the Einstein-Batchelor equation.[30] The Ubbelohde viscometer provides a residence time of the fluid as it moves within a capillary tube. This residence time (τ) can then be

converted to the dynamic viscosity (μ) using the given viscometer constant (VC), 0.003121 cSt/s through Equation (2).

$$\mu = \tau * VC \qquad \text{Equation (2)}$$

Using the density of the solvent, water, the dynamic viscosity can be converted to the kinematic viscosity (η) using Equation (3).

$$\eta = \mu * \rho_{H2O} \qquad \text{Equation (3)}$$

Using the Einstein-Batchelor expression,[30] the volume fraction can be determined using Equation (4).

$$\eta/\eta_o = 1 + 2.5\varphi + 5.2\ \varphi^2 \qquad \text{Equation (4)}$$

In this expression, η is the kinematic viscosity of the solution, η_o is the kinematic viscosity of the solvent, and φ is the volume fraction of the microgels. This expression is valid for $\varphi < 0.74$. After plotting this data and fitting it to a quadratic expression, the swelling ratio (*k)* can be determined using concentration (*c)*. Using Equation (5), the swelling ratio can then be used to determine the effective volume fraction at any concentration, extrapolating outside of the dilute regime for which the Einstein-Batchelor expression holds. In this manner, the swelling ratio provides insight into the particle swelling behavior.

$$\varphi_{eff} = k * c \qquad \text{Equation (5)}$$

Thus, after determining the swelling ratio for each microgel set, this value can be used to find the effective volume fractions at the concentration used in the experiments.

2.2.4. Preparation of Aminobenzophenone-Functionalized PS Cores

Before heteroaggregation, core particles were conjugated to AB to enable UV coupling of the core particles to the microgels to add stability to the resulting RLPs (**Scheme 2.1**). Carboxylated-PS core particles were functionalized with AB (25 mM) via carbodiimide coupling using EDC (2 mM)/NHS (5 mM) in DMSO for 2 h in the dark on a shaker. PS core particles were purified in EtOH via ten rounds of sedimentation/re-suspension.

2.2.5. Preparation of Raspberry-Like Particles

RLPs were prepared using colloidal-phase mediated heteroaggregation (**Scheme 2.1**). Unless otherwise specified, 5 mg of microgels were dissolved in varied volumes of HIS PBS. AB-functionalized PS core particles were re-suspended in HIS PBS and added to the colloidal phase (0.25% w/v, 50 μL) to produce mixed colloidal dispersions with effective volume fractions between 0.01-0.9. To fabricate RLPs for the investigation of the influence of pH and ionic strength during synthesis, this same process was followed except that all samples were fabricated to have an effective volume fraction of 0.60. To fabricate RLPs for the investigation of the influence of synthesis conditions, 5 mg of microgels were dissolved in 300 μL of various buffers or deionized water. The solutions were homogenized via vortexing after which the samples were exposed to longwave UV rays from a Blak Ray 100 W lamp for 30 min. Samples were purified via sequential sedimentation and re-suspension in EtOH.

2.2.6. Characterization of Raspberry-Like Particles

Microparticles were imaged using a NOVA 200 Focused Ion Beam/ Scanning Electron Microscope system (FEI, Hillsboro, OR) to assess the resulting RLP microgel coverage. Samples were prepared by placing a drop of purified

microparticles dispersed in EtOH on copper tape adhered to a metal stub. After the EtOH evaporated, the samples were coated with gold/palladium for 2-3 min at 25 V using a Hummer V Sputterer (Anatech USA, Union City, CA). Semi-quantitative characterization of the mean diameter of the RLPs was performed using a qNano particle analyzer (iZON, Oxford, United Kingdom) with a 4000 nm pore. Measurements were made in filtered 10 mM formate buffer of pH 3.3 and 10 mM NaCl. Voltage and pressure values were set to optimize the signal to ensure high sensitivity. Controlling the voltage setting ensures that the current is in a range where blockade events can be resolved. Increased pressure is often necessary to ensure that particles translocate at an appropriate rate without clogging the pore. The voltage was set to either 0.16 V for PS core samples and pNIPAm RLP samples or 0.20 V for pNIPMAm samples. The pressure was set to either 10 cm H_2O for PS samples and pNIPAm samples or 15 cm H_2O for pNIPMAm RLP samples. The pore was set to a stretch of 49 mm for all samples. The measurements were calibrated using the provided 4050 nm latex standard. For each sample, three trials were analyzed via qNano.

2.2.7. Statistical Analysis of qNano Translocation Data

Due to the nature of these microparticles and the qNano, large particle aggregates (diameter > 3σ of each sample set) were removed prior to statistical analysis. All statistical analyses for qNano translocation studies were performed with InStat (GraphPad, San Diego CA). Average particle diameter data were statistically analyzed using one-way analysis of variance using the Tukey-Kramer multiple comparisons test at a 95% confidence interval (n = 3000 particles).

2.3. Results and Discussion

2.3.1. Determination of Microgel Structure and Properties

Microgels were prepared using either pNIPAm or pNIPMAm as the main comonomer to determine whether the microgel composition, and hence morphology, influence the heteroaggregation process. Two concentrations (1 mol-% or 5 mol-%) of the cross-linker *N,N'*-methylenebis(acrylamide) (BIS) were used to determine the influence of particle stiffness on the heteroaggregation process. Previous studies in the Lyon Group have revealed that the microgel network structure is dictated by the monomer of choice.[31] PNIPAm particles typically have a heterogeneous cross-linker distribution, resulting in a dense core surrounded by a loose corona of dangling chains. In contrast, pNIPMAm particles have been demonstrated to have a more homogenous network structure with cross-linking uniformly distributed throughout the entire particle domain. Indeed, the differences in particle morphology can be seen via AFM when evaluating the height of free standing microgels that have been passively deposited (**Table 2.1** and **Figure 2.1**).

Table 2.1. Microgel characterization.

Monomer and Cross-linker Molar Ratio		**Spread / nm**	**Height / nm**	**R_H / Nm**	**Swelling Ratio/ mL-mg^{-1}**
pNIPAm:BIS	99:1	986 ± 31	17 ± 1	233 ± 3	24 ± 1
pNIPAm:BIS	95:5	560 ± 24	52 ± 8	254 ± 6	15 ± 1
pNIPMAm:BIS	99:1	935 ± 47	31 ± 2	399 ± 4	21 ± 1
pNIPMAm:BIS	95:5	585 ± 20	98 ± 6	288 ± 3	10 ± 1

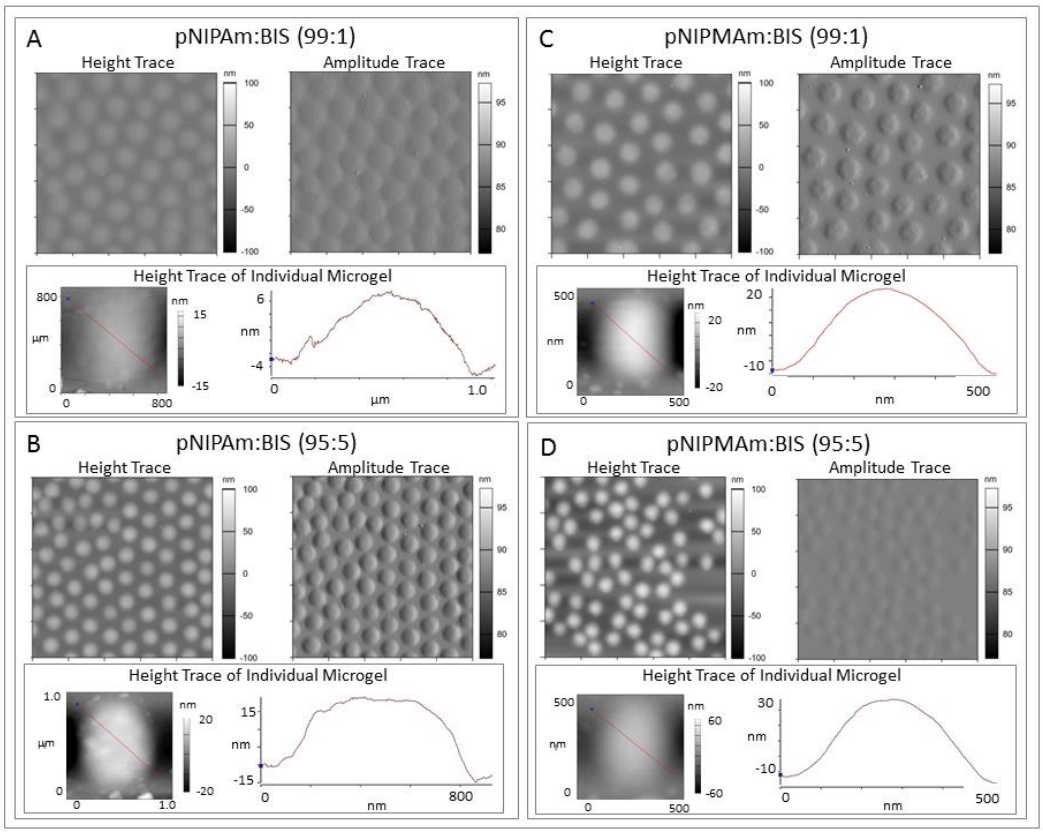

Figure 2.1. Representative AFM images of passively deposited microgel samples (and close-up image of an individual microgel) onto APTMS-functionalized coverslips. The height trace and amplitude trace of all four samples: (A) pNIPAm:BIS (99:1), (B) pNIPAm:BIS (95:5), (C) pNIPMAm:BIS (99:1), and (D) pNIPMAm:BIS (95:5). All images are 5 μm x 5 μm scans unless otherwise specified.

AFM characterization of individual microgels indicates that pNIPAm microgels are more deformable than pNIPMAm microgels, exhibiting significantly smaller heights upon deformation than do the pNIPMAm microgels, which suggests structural dissimilarities. Moreover, pNIPAm microgels also exhibit larger swelling ratios as determined by viscometry compared to their pNIPMAm counterparts, which indicates that the pNIPAm microgels are able to swell to a higher degree than the pNIPMAm microgels; the swelling ratio is a scaling parameter that provides an indication of volume fraction occupied by a swollen particle. Two cross-linker

contents for both pNIPAm and pNIPMAm microgels were also investigated to determine the influence of particle rigidity on this heteroaggregation process. Higher cross-linker contents lead to larger heights determined via AFM and smaller swelling ratios determined via viscometry (**Table 2.1** and **Figure 2.2**).

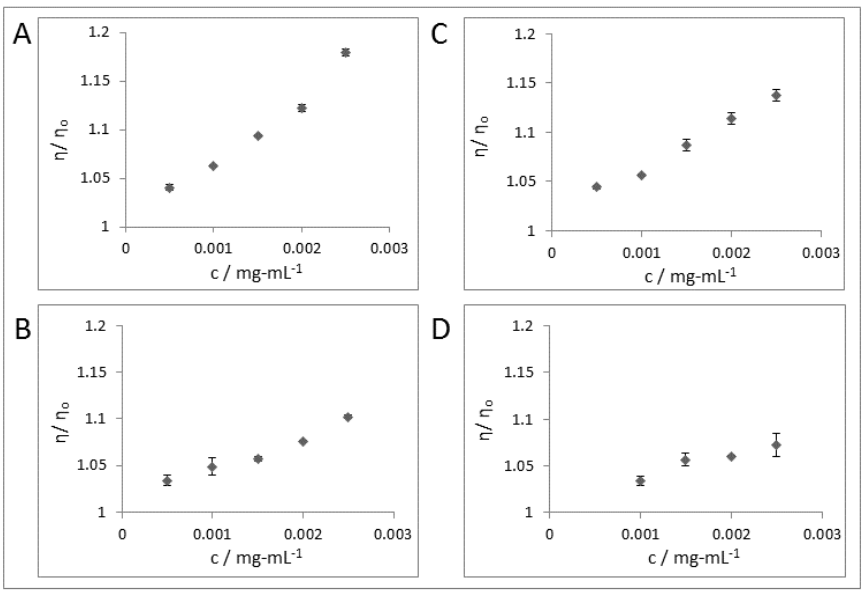

Figure 2.2. Viscometry data for (A) pNIPAm:BIS (99:1), (B) pNIPAm:BIS (95:5), (C) pNIPMAm:BIS (99:1), (C) and pNIPMAm:BIS (95:5). Data points represent the average of three trials. Error bars represent plus or minus one standard deviation of three trials.

2.3.2. Qualitative Evaluation of Raspberry-Like Particle Coverage

Heteroaggregation was evaluated at a range of effective volume fractions to determine the influence on the resulting microgel coverage of the RLP. Analysis of SEM imaging suggests that the ability of microgels to spread is a critical factor in determining the degree of coating success to form an RLP via colloidal-phase mediated heteroaggregation. SEM imaging (**Figure 2.3A**) indicates that the pNIPAm:BIS (99:1) microgels are able to spread and coat the surface at all effective

volume fractions with little variation in the degree of coverage. The pNIPAm:BIS (95:5) microgels similarly are able to spread and cover the surface at all effective volume fractions; however, the coverage is notably patchier at the highest effective volume fraction of 0.8. Thus, the microgel cross-linker content and colloidal phase effective volume fraction appear to have a limited influence on the resulting microgel coverage of the pNIPAm RLPs.

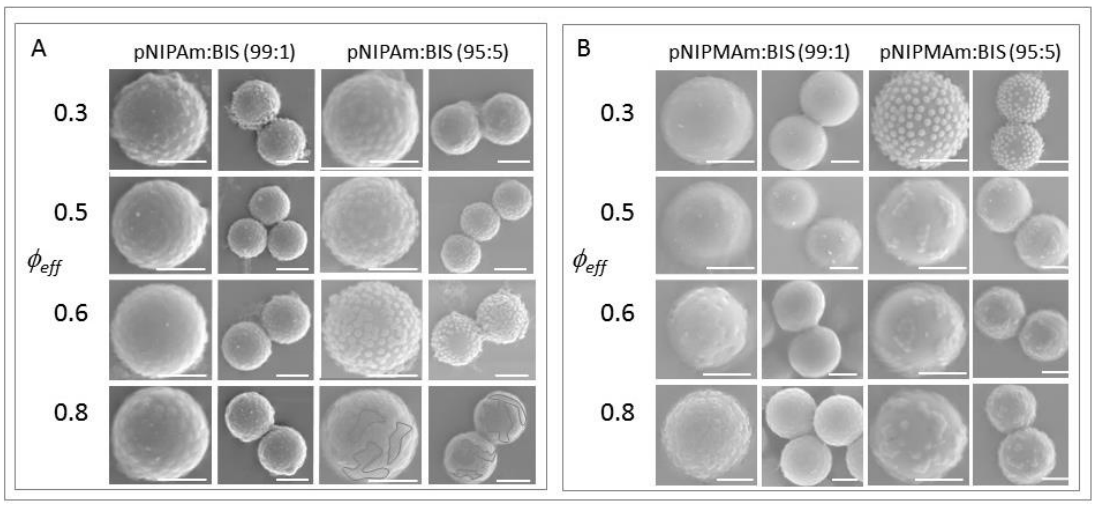

Figure 2.3. Representative SEM images for (A) pNIPAm and (B) pNIPMAm RLPs produced at varying effective volume fractions indicate a high degree of microgel coverage for all samples. Samples are coated with gold/palladium prior to imaging. In the sample at φ = 0.8, areas devoid of microgels are outlined in grey. All scale bars represent 2 μm.

In contrast, SEM imaging of pNIPMAm RLPs (**Figure 2.3B**) suggests that the heteroaggregation process is highly dependent on effective volume fraction when using pNIPMAm microgels. The pNIPMAm:BIS (99:1) microgels are able to coat more effectively at higher effective volume fractions (φ_{eff} = 0.6 and 0.8). However, at effective volume fractions corresponding to the hard sphere fluid (φ_{eff} = 0.3) and

coexistence (φ_{eff} = 0.5) phases, very few microgels can be found on the surface of the resulting RLPs. In contrast, the pNIPMAm:BIS (95:5) microgels are most successful at coating the PS core at the lowest effective volume fraction (φ_{eff} = 0.3) corresponding to the fluid phase. As the effective volume fraction of the colloidal phase is increased, the coating appears to become irregular and less consistent from particle to particle. This irregularity of the microgel coating is likely caused by unfavorable energetics that inhibit deformation of the microgels at the hard PS interface. Here we see not only a strong dependence on effective volume fraction, but also a strong influence of the microgel stiffness. Heteroaggregation was assessed at a larger range of effective volume fractions for all microgels and imaged via SEM (**Figure 2.4**). The appearance of the pNIPAm and pNIPMAm RLPs via SEM imaging are strikingly dissimilar due to different modes of microgel deswelling that occur during drying. The pNIPAm microgels, which are more deformable are capable of undergoing anisotropic deswelling, regardless of cross-linker content. In contrast, pNIPMAm microgels are not as easily deformed and would favor isotropic deswelling particularly when the network is further constrained by a high cross-linker content, as we see in the sample at φ_{eff} = 0.3 (**Figure 2.3**).

This method consistently produces homogeneously coated RLPs when using soft, deformable pNIPAm microgels. In contrast, denser, more rigid pNIPMAm microgels are more sensitive to effective volume fraction of the colloidal phase for successful heteroaggregation. The influence of microgel stiffness on coating coverage and topography seen in characterization studies on planar surfaces is likely magnified upon introduction of a curved interface, which requires increased network

deformation. The influence of microgel stiffness on colloidal-phase mediated heteroaggregation can likely be attributed to the energy required to deform the microgel at the interface of a PS core particle. The loose pNIPAm microgel network allows for facile deformation of the dangling polymer chains of the microgel, enabling these microgels to greatly deform at the PS interface and separate from the colloidal phase. In contrast, the denser, more uniform pNIPMAm microgel network requires a higher energy input to deform the entire microgel network at the PS interface to separate out of the colloidal phase. This deformation process is likely energetically unfavorable, resulting in a more sensitive heteroaggregation process that can be easily disturbed by parameters such as the cross-linker content and the effective volume fraction.

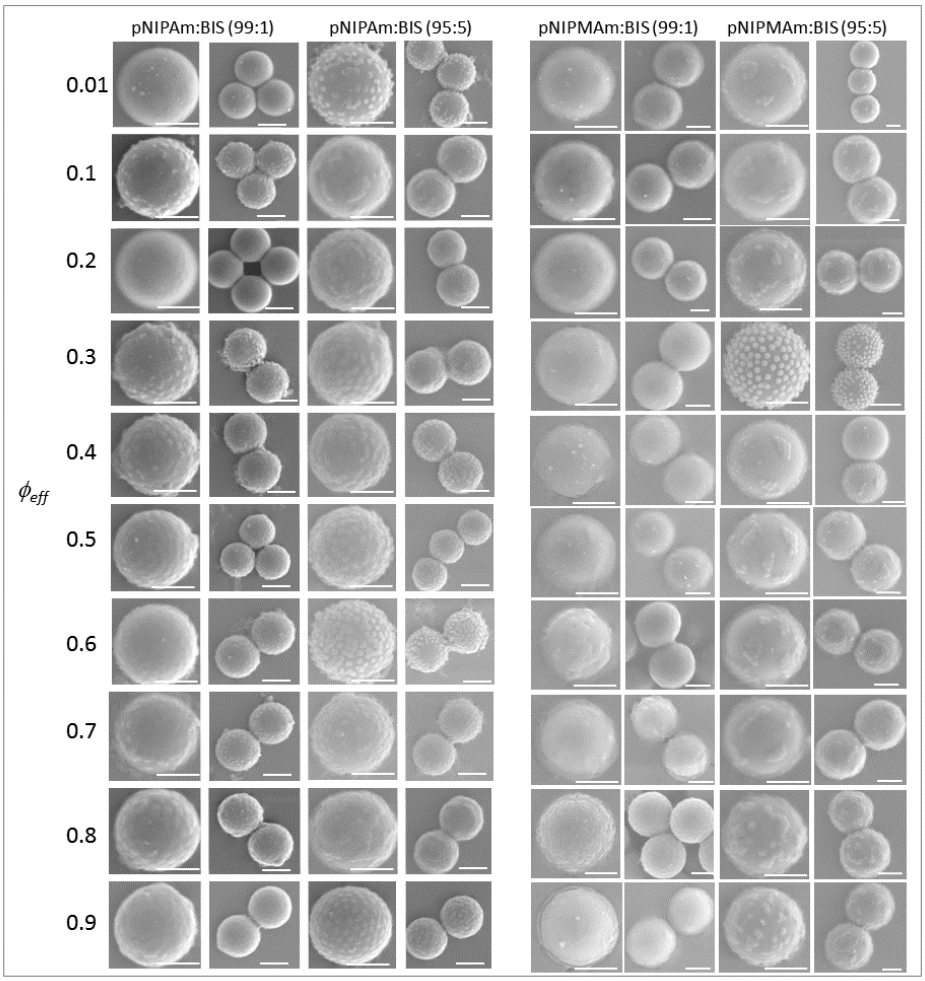

Figure 2.4. Representative SEM images of (A) pNIPAm and (B) pNIPMAm microgel RLPs at varying effective volume fractions. All scale bars represent 2 μm.

The relationship between microgel cross-linker content and effective volume fractions for successful heteroaggregation is not yet well understood. The microgel stiffness could be influencing the structure and fluidity of the colloidal phase during this process. Previous investigators have demonstrated that pNIPAm microgel softness can cause changes in colloidal-phase behavior and cause shifting in the phase boundaries.[29] However, pNIPMAm microgel phase behavior has received markedly less investigation in this context. Such microgels, which show inherent structural

differences, may exhibit widely different phase behavior that is influencing this heteroaggregation process.

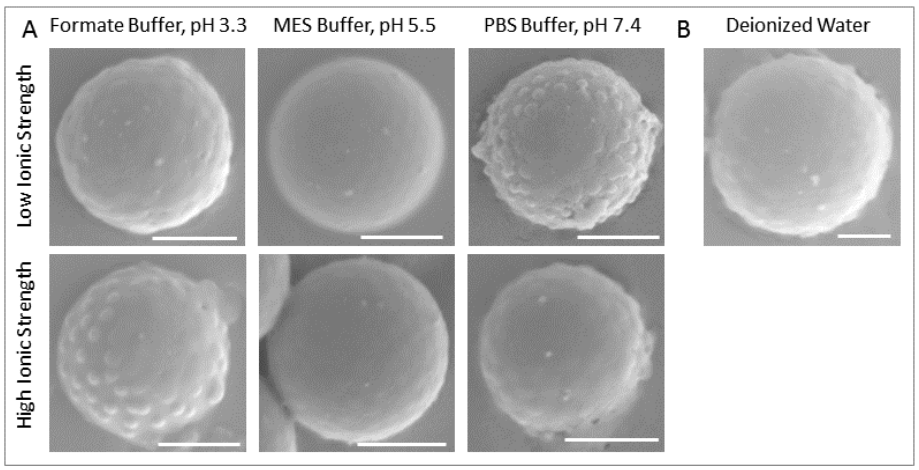

Figure 2.5. Representative SEM images of pNIPAm RLPs fabricated in buffers of (A) varied pH and ionic strength and (B) deionized water. All scale bars represent 2 μm.

After establishing conditions for effective coating using colloidal-phase mediated heteroaggregation, a series of experiments were performed to compare the sensitivity of this technique to the sensitivity of the established ion-pair driven heteroaggregation. Because ion-pair driven heteroaggregation relies on electrostatic-charge interactions, solution conditions such as pH and ionic strength can drastically disturb this process. For comparison, colloidal-phase mediated heteroaggregation was assessed at varied pH and salt concentrations (**Figure 2.5**). SEM imaging of RLPs fabricated at varied synthesis conditions reveals that colloidal-phase mediated heteroaggregation is not influenced by pH or ionic strength; all RLPs were well-coated. Particle size can also influence the success of ion-pair driven

heteroaggregation. Colloidal-phase mediated heteroaggregation studies were performed using microgels with varied sizes to determine the influence of size. In these studies, four additional microgel samples were used (**Table 2.2**). SEM imaging reveals RLPs are well-coated regardless of microgel size, suggesting the size ratio of the two components is not a major contributing factor to the success of this process (**Figure 2.6**). Together, these studies demonstrate that colloidal-phase mediated heteroaggregation has fewer limitations in terms of synthesis conditions, particle sizes, and particle compositions than ion-pair driven heteroaggregation.

Table 2.2. Characterization of additional microgels used in size-dependent studies.

Monomer and Cross-linker Molar Ratio		**R_H / nm**	**Swelling ratio/ mL-mg^{-1*}**
pNIPAm:BIS	99:1	433 ± 12	27 ± 1
pNIPAm:BIS	95:5	380 ± 5	14 ± 3
pNIPAm:BIS	99:1	178 ±2	41 ± 10
pNIPAm:BIS	95:5	197 ± 3	15 ± 5

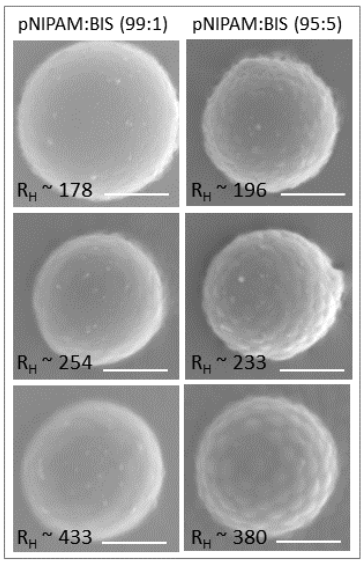

Figure 2.6. Representative SEM images of pNIPAm RLPs fabricated using microgels with varied sizes. All scale bars are 2 μm.

2.3.3. Semi-Quantitative Evaluation of Raspberry-Like Particle Coverage

2.3.3.1. Evaluation of Increase in Particle Diameter

Next, the use of the qNano particle analyzer was investigated as a means for a semi-quantitative, high-throughput technique to analyze the resulting microgel coverage of the RLPs. The qNano particle analyzer relies on tunable resistive pulse sensing. This technique monitors the current flow through an aperture (in this case a pore in an elastomeric sheet), while also allowing for a tunable aperture size via stretching of the pore. Individual particles can be detected while they pass through the pore as a change in the ionic current flow (blockade event). The amplitude of such a blockade, known as the blockade magnitude, is indicative of the particle size. Using this instrument, the mean RLP diameters (**Figure 2.7**) and the size distribution were determined, as inferred from the translocation behavior through a pore of specified size (4000 nm with a 49 mm stretch in all cases for this work). The pNIPAm:BIS (99:1) RLPs exhibit mean diameters that are significantly larger ($p < 0.001$) than the bare PS cores. Additionally, for these samples, RLP mean diameters are significantly different from RLP samples at most other effective volume fractions. However, the comparison of RLP samples at $\varphi_{eff} = 0.6$ and $\varphi_{eff} = 0.8$ shows no significant difference in mean diameter. The pNIPAm:BIS (95:5) RLPs also exhibit significantly larger ($p < 0.001$) mean diameters as compared to the bare PS cores. These mean diameters are also significantly different ($p < 0.001$) as compared to RLPs produced at other effective volume fractions with the exception of the comparison of RLPs produced at $\varphi_{eff} = 0.3$ and $\varphi_{eff} = 0.8$.

The pNIPMAm:BIS (99:1) RLPs exhibit mean RLP diameters that are more similar to the PS cores for two effective volume fractions: 4370 ± 140 nm (φ_{eff} = 0.5) and 4370 ± 80 nm (φ_{eff} = 0.8). RLPs are significantly smaller ($p < 0.001$) for φ_{eff} = 0.3 (4220 ± 60 nm) and significantly larger ($p < 0.001$) for φ_{eff} = 0.6 (4650 ± 30 nm). In addition, RLP samples at different φ_{eff} are significantly different ($p < 0.001$) except for the comparison of samples fabricated at φ_{eff} = 0.5 and φ_{eff} = 0.8. The pNIPMAm:BIS (99:5) RLPs also exhibit varied mean diameters depending on the effective volume fraction. Mean RLP diameters are significantly larger ($p < 0.001$) than the bare PS cores only in the case of φ_{eff} = 0.3 where the mean diameter is 4470 ± 40 nm. Mean RLP diameters are significantly smaller ($p < 0.001$) than the bare PS cores for φ_{eff} = 0.5 (4050 ± 90 nm), φ_{eff} = 0.6 (4220 ± 60 nm), and φ_{eff} = 0.8 (4090 ± 30 nm). Additionally, RLP samples at different φ_{eff} are significantly different ($p < 0.001$) for all comparisons except for RLPs fabricated at φ_{eff} = 0.5 compared to those fabricated at φ_{eff} = 0.8. For the case of both the pNIPMAm microgel RLPs, several RLP samples exhibit mean diameters that are smaller than the PS cores, which could suggest the presence of unpurified microgel aggregates. Overall, for most cases the standard deviations for three trials are relatively small, indicating reproducibility of this assessment technique. However, these data provide little information about the heterogeneity of the resulting RLP populations.

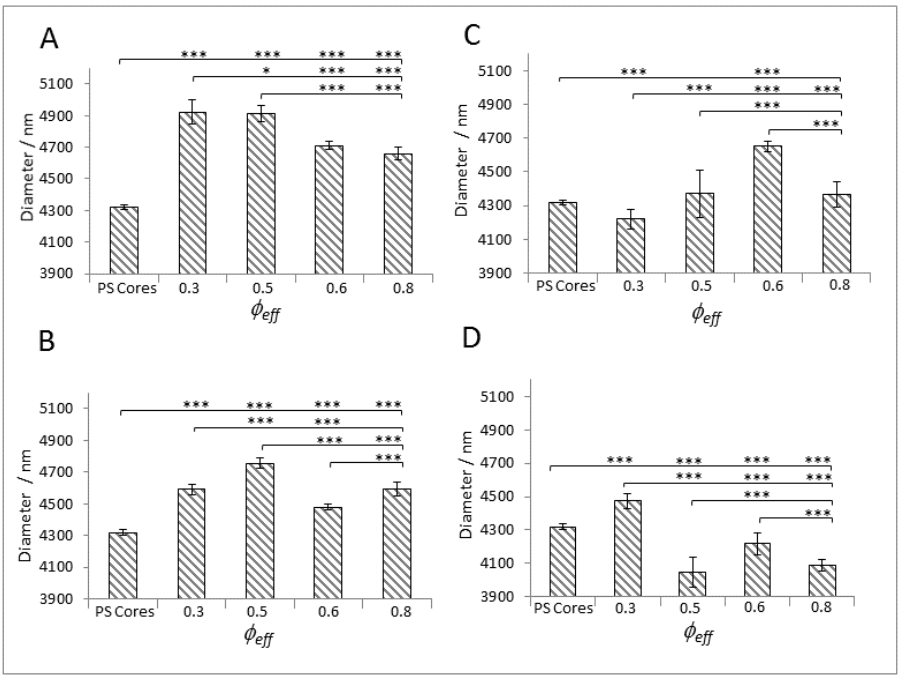

Figure 2.7. qNano particle counter mean RLP diameter for three trials of (A) pNIPAm:BIS (99:1) RLPs, (B) pNIPAm:BIS (95:5) RLPs, (C) pNIPMAm:BIS (99:1) RLPs, and (D) pNIPMAm:BIS (95:5) RLPs. Error bars represent the standard deviation between three trials of 1000 particle blockade events. The p-values are indicates by asterisks where * indicates $p < 0.05$ and *** indicates $p < 0.001$.

2.3.3.2. Evaluation of Particle Diameter Histograms

Particle diameter information was also analyzed in a histogram format for enhanced visualization of the data (**Figure 2.8, Figure 2.9, Figure 2.10,** and **Figure 2.11**). Comparison between RLP samples synthesized with the same microgel population can provide information about the efficiency of the coating process because of the nature of the qNano measurements. The resistive pulse sensing technique is influenced by the degree of microgel coverage for individual RLPs, providing an average particle diameter (**Scheme 2.2**). A particle with low microgel coverage will still have a measured diameter that is larger than the PS core alone because the swollen microgels will cause a slight increase in the magnitude of the

blockade. As the microgel coverage is increased, the blockade magnitude, and particle diameter, will increase until a maximum is reached when the RLP exhibits full microgel coverage. Thus, the largest peak shifts within a given RLP composition suggest the highest coating efficiency while smaller peak shifts suggest lower coating efficiencies. However, such comparisons between RLP populations composed of different microgels would not provide much insight into the coating efficiencies because different microgels have different swelling behaviors. Analysis of the distribution curve width can provide useful information about the homogeneity of the RLP population.

Scheme 2.2. Factors influencing qNano determination of diameter.

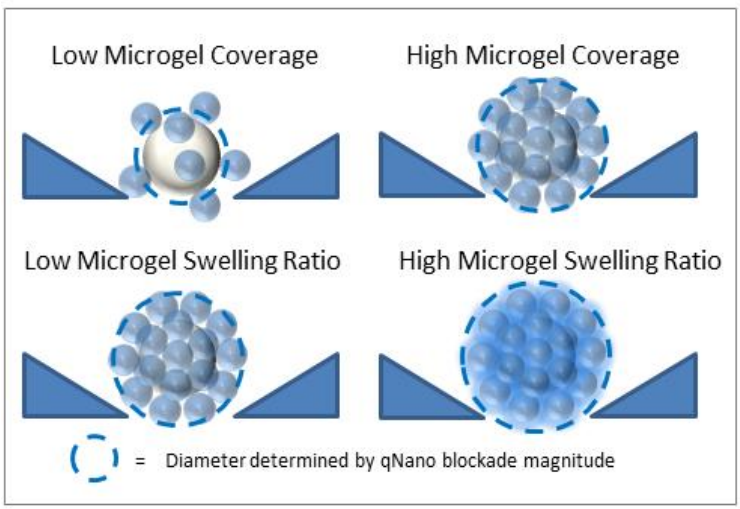

PNIPAm:BIS (99:1) RLPs exhibit a peak shift for all effective volume fractions in comparison to the PS core particles (**Figure 2.8**). For φ_{eff} = 0.3 and 0.5, the RLPs exhibit large peak shifts (~450 nm) with a constant distribution width

(~1500 nm) (**Figure 2.8A** and **Figure 2.8B**). Such a shift in the entire distribution curve indicates that a constant microgel shell thickness has been added to all PS cores, suggesting that the resulting RLP population has a homogenous coating. For the higher values of φ_{eff} = 0.6 and 0.8, the peak shift is less pronounced (~300 nm) with a narrower distribution width (~1300 nm) as compared to the PS cores (~1500 nm). A narrowing of the distribution width provides us with little information on the heterogeneity of the samples. However, it is possible that the narrowing of this distribution curve is caused by multiple populations of RLPs that have different degrees of microgel coatings; for instance, smaller core particles could be fully coated while larger core particles may be partially coated. The RLPs constructed using pNIPAm:BIS (95:5) exhibit a smaller peak shift in all cases (~300 nm), which is likely caused by the greater stiffness (and decreased swelling) of the microgels due to the higher percent of the cross-linker, BIS (**Figure 2.9**). For these samples, the width of the peak is similar to that of the PS cores, suggesting the presence of a homogeneously coated population of RLPs. Tails in the distributions at larger sizes suggest the presence of a small population of RLP aggregates.

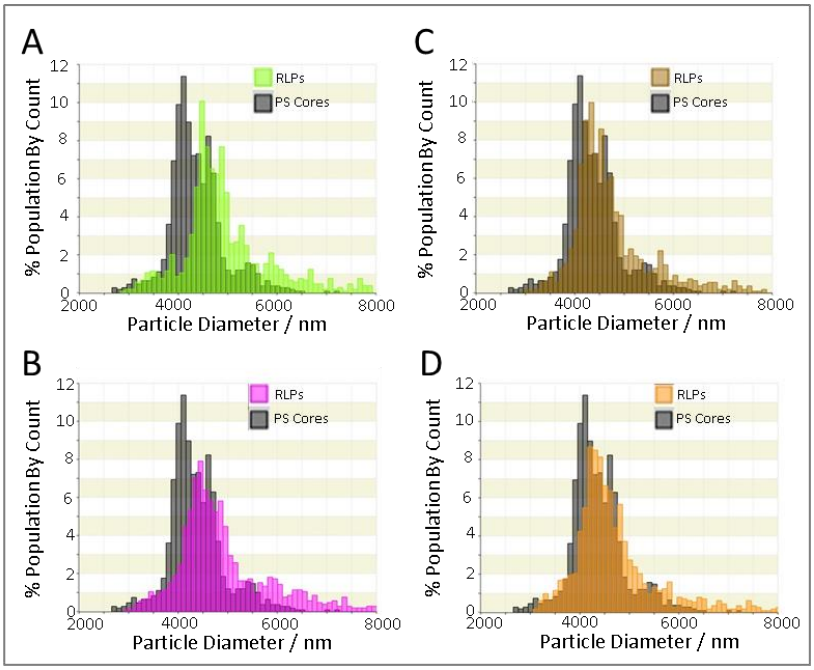

Figure 2.8. qNano particle diameter representative histograms for pNIPAm:BIS (99:1) RLPs at (A) φ_{eff} = 0.3, (B) φ_{eff} = 0.5, (C) φ_{eff} = 0.6, and (D) φ_{eff} = 0.8. RLP and PS Cores data were collected using a 4000 nm pore at an applied stretch of 49 mm, an applied pressure setting of 10 cm H_2O, and a voltage setting of 0.16 V. All samples were calibrated using the provided 4050 nm latex standards.

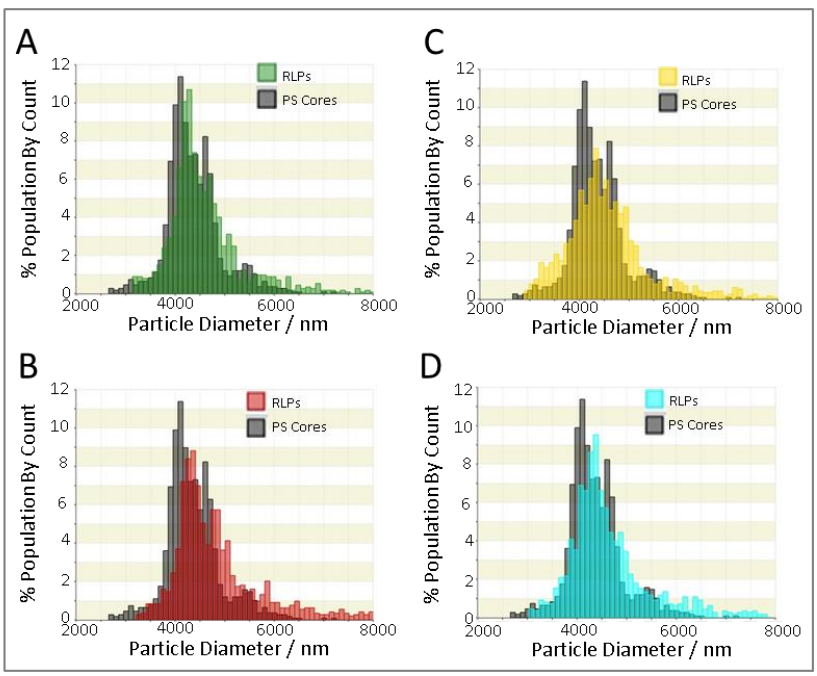

Figure 2.9. qNano particle diameter representative histograms for pNIPAm:BIS (95:5) RLPs at (A) φ_{eff} = 0.3, (B) φ_{eff} = 0.5, (C) φ_{eff} = 0.6, and (D) φ_{eff} = 0.8. RLP and PS Cores data were collected using a 4000 nm pore at an applied stretch of 49 mm, an applied pressure of 10 cm H_2O, and a voltage setting of 0.16 V. All samples were calibrated using the provided 4050 nm latex standards.

The pNIPMAm:BIS (99:1) RLPs exhibit a slight peak shift (~200 nm) at φ_{eff} = 0.3 and 0.5 (**Figure 2.10A** and **Figure 2.10B**). However, the entire distribution curve does not shift with the peak. At φ_{eff} = 0.6 and φ_{eff} = 0.8, these RLPs exhibit larger peak shifts (~325 nm) with little difference in the distribution curve width in comparison to the PS cores, suggesting the presence of homogeneously coated RLPs (**Figure 2.10C** and **Figure 2.10D**). These RLP samples also have a larger population of smaller particles, which are likely caused by microgel aggregates. In contrast, the pNIPMAm:BIS (95:5) RLPs do not exhibit appreciable curve shifts (**Figure 2.11**). These RLP samples also exhibit larger populations of smaller particles, again likely due to the presence of microgel impurities.

For the pNIPMAm:BIS (95:5) sample, although the φ_{eff} = 0.3 sample exhibits a significant increase in mean RLP diameter ($p > 0.001$), the histogram shows little variation between the RLP sample and the PS core sample (**Figure 2.11**). This could be attributed to the denser, more rigid pNIPMAm microgel network structure. Stiffer microgels are limited in their ability to deform, leading to reduced spreading on the core surface. Once coupled to the core, stiffer microgels are also limited in their ability to swell, which directly influences the blockade magnitude measured by the qNano. Microgels that exhibit a higher degree of swelling likely produce a thicker coating in the swollen state (**Scheme 2.2**), causing a larger blockade magnitude that results in a greater difference in mean diameter of the RLP as compared to the bare PS

cores. For microgels that exhibit less swelling, the blockade magnitude is smaller, resulting in a smaller difference in particle mean diameter before and after heteroaggregation. These data suggest a minimum swelling percentage must be achieved by the microgels for a marked peak shift to occur via qNano.

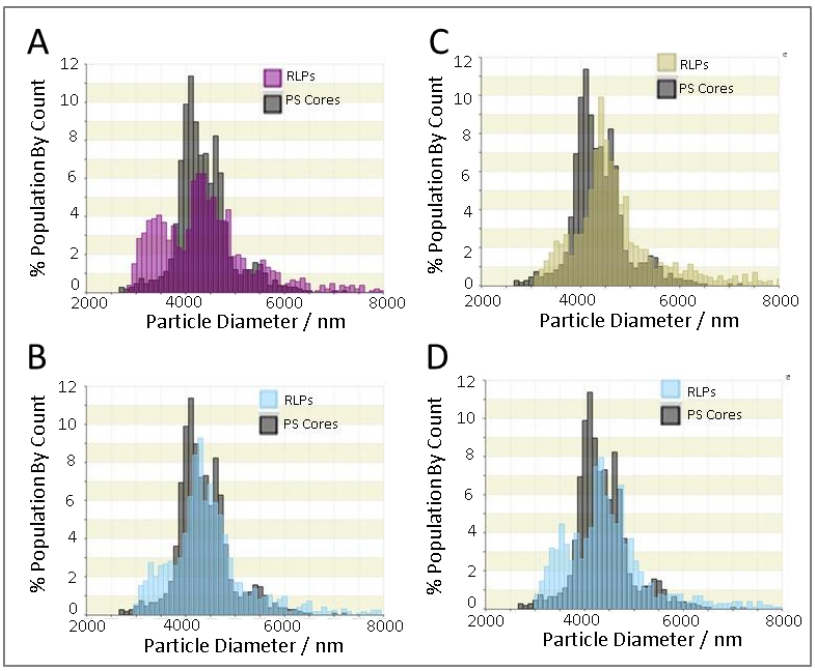

Figure 2.10. qNano particle diameter representative histograms for pNIPMAm:BIS (99:1) RLPs at (A) φ_{eff} = 0.3, (B) φ_{eff} = 0.5, (C) φ_{eff} = 0.6, and (D) φ_{eff} = 0.8. RLP data were collected using a 4000 nm pore at an applied stretch of 49 mm, an applied pressure setting of 15 cm H_2O, and a voltage setting of 0.20 V. PS Cores data were collected using a 4000 nm pore at an applied stretch of 49 mm, an applied pressure setting of 10 cm H_2O, and a voltage setting of 0.16 V. All samples were calibrated using the provided 4050 nm latex standard.

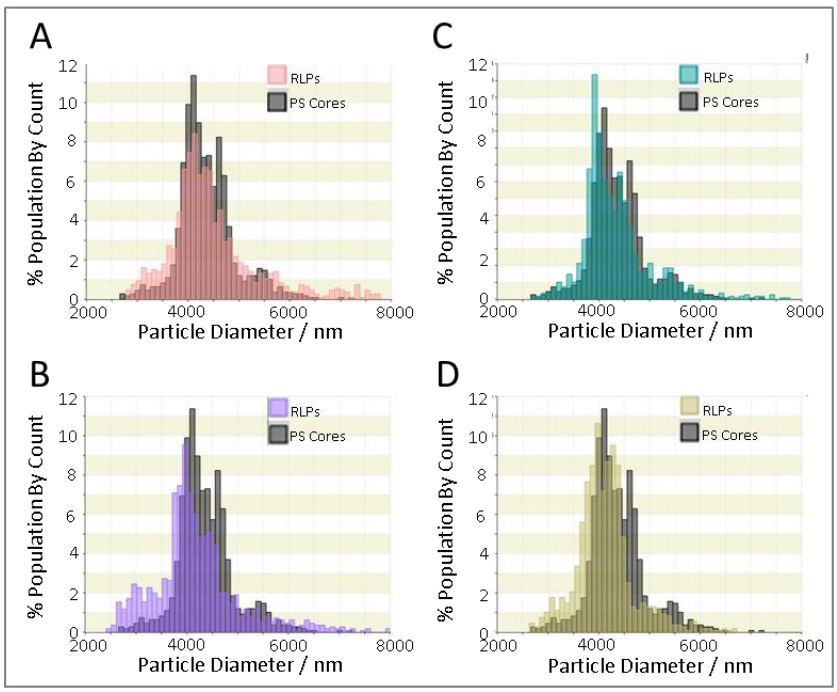

Figure 2.11. qNano particle diameter representative histograms for pNIPMAm:BIS (95:5) RLPs at (A) φ_{eff} = 0.3, (B) φ_{eff} = 0.5, (C) φ_{eff} = 0.6, and (D) φ_{eff} = 0.8. RLP data were collected using a 4000 nm pore at an applied stretch of 49 mm, an applied pressure setting of 15 cm H_2O, and a voltage setting of 0.20 V. PS Cores data were collected using a 4000 nm pore at an applied stretch of 49 mm, an applied pressure setting of 10 cm H_2O, and a voltage setting of 0.16 V. All samples were calibrated using the provided 4050 nm latex standard.

Comparison of the qNano translocation data to the SEM images suggests that the qNano may be an effective, high-throughput analysis tool to determine the presence of a microgel coating on a core particle after heteroaggregation when both the mean diameters of the samples and the histograms are analyzed. For each microgel composition, the RLP mean diameter data aligns with the SEM images, except in the case of pNIPMAm:BIS (99:1) at φ_{eff} = 0.8. In this case, the mean RLP diameter found by the qNano particle translocation analysis indicates that the microgel coverage is limited; yet, SEM images indicate the presence of homogeneously coated RLPs (**Figure 2.3**). Analysis of the qNano histogram (**Figure**

2.10) indicates the presence of a microgel population that remains after purification, leading to a lowered mean diameter; additionally, the peak shift (~325 nm) of the entire distribution curve indicates the presence of a homogeneously coated RLP population. Analysis of both the qNano RLP mean diameter and histograms provide information on several aspects of the RLP population obtained from this heteroaggregation process including reproducibility, coating efficiency, heterogeneity of the microgel coating, and the presence of microgel impurities. However, the use of the qNano is limited in its ability to ascertain information about subtleties in the RLP topography that are more clearly seen via SEM image analysis such as microgel spreading at the interface and spacing of microgels.

Analysis of qNano translocation data suggests that success of this technique in determining RLP microgel coverage is influenced by the ability of the microgels to swell. Indeed pNIPAm:BIS (99:1) microgels, which demonstrate the highest degree of swelling in PBS, as indicated by the largest swelling ratio (24 ± 1), produce RLPs that exhibit the largest peak shifts (~450 nm) (**Figure 2.8**). Furthermore, when the cross-linker content is increased and the pNIPAm:BIS (95:5) microgels are used, the swelling ratio scaling parameter decreases (15 ± 1) as does the peak shift exhibited by the RLPs (~300 nm), even though SEM imaging indicates that both pNIPAm microgels are able to form well-coated RLPs at all effective volume fractions (**Figure 2.3** In this case, the qNano measurements do indicate the presence of a microgel coating that is not as thick as in the case of the pNIPAm:BIS (99:1) RLPs. Since these microgels have very similar hydrodynamic radii (**Table 2.1**), one would expect the resulting coating to have similar thickness and thus a similar peak shift, if microgel

swelling were not influencing the detection. Analysis of pNIPMAm microgel RLPs further supports this conclusion. The pNIPMAm microgels have smaller swelling ratios than the pNIPAm microgel (pNIPMAm:BIS (99:1) ~ 21 ± 1 and pNIPMAm:BIS (95:5) ~ 10 ± 1). Though the pNIPMAm:BIS (99:1) microgels exhibit a peak shift (~325 nm) at $\varphi_{eff} = 0.6$ and $\varphi_{eff} = 0.8$, corresponding to well-coated RLPs via SEM image analysis, it is markedly smaller than those produced by the corresponding pNIPAm:BIS (99:1) RLPs (**Figure 2.8** and **Figure 2.10**). Moreover, RLPs constructed using pNIPMAm:BIS (95:5) microgels do not exhibit an appreciable peak shift even at $\varphi_{eff} = 0.3$ (**Figure 2.11**) where SEM image analysis and qNano mean RLP diameter data confirm the presence of a microgel coating. The lack of a peak shift is likely caused by the inability of these microgels to swell to an appreciable extent due to their greater rigidity as demonstrated by their small swelling ratio (10 ± 1). Taken together, analysis of qNano mean diameter data and histograms of diameters can be used to determine success of RLP coatings. In cases where excess microgel populations exist, purification processes can be modified and success can be analyzed via qNano histograms. Upon elimination or reduction of microgel aggregates, mean diameter data can be used to identify populations of well-coated RLPs. However, it is likely that when microgels of vastly different compositions are used, SEM imaging may be required to qualitatively calibrate initial qNano results.

2.4. Conclusion

The influence of microgel composition and colloidal-phase volume fraction on colloidal-phase mediated heteroaggregation is assessed. Though pNIPAm microgels have a relatively high coating affinity regardless of cross-linker content or colloidal-

phase volume fraction, pNIPMAm microgels are much more sensitive to these parameters. This difference is likely caused by the inherent structural dissimilarities between the two microgel types, which influence the amount of energy required for deformation to occur at the curved PS interface. PNIPAm microgels are easily deformed at an interface, likely requiring little energy input for deformation to occur; as such, they are an ideal candidate for colloidal-phase mediated heteroaggregation with a non-deformable core particle. In contrast, pNIPMAm microgels do not deform as easily as pNIPAm microgels, likely due to unfavorable energetics, resulting in a more sensitive coating process that is further limited upon increased stiffness. These coating behaviors are likely magnified due to the increased deformation that must occur at a curved interface. An understanding of microgel deformation at a curved interface can be widely applicable to other systems such as Pickering emulsions[32-33] and colloidosomes.[34-35]

Gaining insight into the influence that the colloidal-phase volume fraction and the microgel composition have on this heteroaggregation process enables one to use this method to develop a platform of complex stimuli-responsive microparticles with few compositional restraints. Through exploration of the parameter space of colloidal-phase mediated heteroaggregation, critical information about the synthesis conditions that can be used for scale-up of RLP synthesis has been gained. Through comparison of SEM imaging and qNano translocation events, qNano has been demonstrated to be a high-throughput analysis method to gain information regarding the coating efficiency, homogeneity of the population, and purity of samples. Further comparison of qNano data provided as mean diameters versus histograms can even provide insight

into properties of the microgels such as the ability to swell. In this manner, the use of such a high-throughput analysis technique will enable us to develop a platform of RLPs for use in a variety of applications ranging from drug delivery to tissue engineering.

2.5. References

1. Zhang, M. F.; Breiner, T.; Mori, H.; Muller, A. H. E., Amphiphilic cylindrical brushes with poly(acrylic acid) core and poly(n-butyl acrylate) shell and narrow length distribution. *Polymer.* **2003**, *44* (5), 1449-1458.

2. Cong, Y.; Xia, T.; Zou, M.; Li, Z. N.; Peng, B.; Guo, D. Z.; Deng, Z. W., Mussel-inspired polydopamine coating as a versatile platform for synthesizing polysytrene/Ag nanocomposite particles with enhanced antibacterial activities. *J. Mat. Chem. B.* **2014**, *2* (22), 3450-3461.

3. Zhang, S. W.; Zhou, S. X.; Weng, Y. M.; Wu, L. M., Synthesis of SiO2/polystyrene nanocomposite particles via miniemulsion polymerization. *Langmuir.* **2005**, *21* (6), 2124-2128.

4. Caruso, F.; Spasova, M.; Saigueirino-Maceira, V.; Liz-Marzan, L. M., Multilayer assemblies of silica-encapsulated gold nanoparticles on decomposable colliod templates. *Adv. Mater.* **2001**, *13* (14), 1090-1094.

5. Zhou, S. G.; McIlwrath, K.; Jackson, G.; Eichhorn, B., Enhanced CO tolerance for hydrogen activation in Au-Pt dendritic heteroaggregate nanostructures. *J. Am. Chem. Soc.* **2006**, *128* (6), 1780-1781.

6. Park, S.; Park, H. H.; Kim, S. Y.; Kim, S. J.; Woo, K.; Ko, G., Antiviral properties of silver nanoparticles on a magnetic hybrid colloid. *Appl. Environ. Microbiol.* **2014**, *80* (8), 2343-2350.

7. Wu, K. H.; Liu, C. I.; Yang, C. C.; Wang, G. P.; Chao, C. M., Preparation and characterization of aminosilane-modified silicate supported with silver for antibacterial behavior. *Mater. Chem. Phys.* **2011**, *125* (3), 802-806.

8. Zhang, J.; Ma, N.; Tang, F.; Cui, Q.; He, F.; Li, L., pH- and glucose-responsive core-shell hybrid nanoparticles with controllable metal-enhancedd fluorescence effects. *ACS Appl. Mater. Interfaces.* **2012**, *4* (3), 1747-1751.

9. Mansur, A.; Mansur, H.; Gonzalez, J., Enzyme-polymers conjugated to quantum-dots for sensing applications. *Sensors.* **2011**, *11* (10), 9951-72.

10. Ohnuma, A.; Cho, E. C.; Jiang, M.; Ohtani, B.; Xia, Y., Metal-polymer hybrid colloid particles with an eccentric structure. *Langmuir.* **2009**, *25* (24), 13880-7.

11. Perro, A.; Reculusa, S.; Ravaine, S.; Bourgeat-Lami, E. B.; Duguet, E., Design and synthesis of janus micro- and nanoparticles. *J. Mater. Chem.* **2005**, *15* (35), 3745-3760.

12. Qian, Z.; Zhang, Z. C.; Song, L. Y.; Liu, H. R., A novel approach to raspberry-like particles for superhydrophobic materials. *J. Mater. Chem.* **2009**, *19* (9), 1297-1304.

13. Fujii, S.; Yokoyama, Y.; Miyanari, Y.; Shiono, T.; Ito, M.; Yusa, S.; Nakamura, Y., Micrometer-sized gold silica janus particles as particulate emulsifiers. *Langmuir.* **2013**, *29* (18), 5457-5465.

14. Islam, A. M.; Chowdhry, B. Z.; Snowden, M. J., Heteroaggregation in colloidal dispersions. *Adv. Colloid Interface Sci.* **1995**, *62* (2-3), 109-136.

15. Bradley, M.; Lazim, A. M.; Eastoe, J., Stimulus-responsive heteroaggregation of colloidal dispersions: reversible systems and composite materials. *Polymers.* **2011**, *3* (3), 1036-1050.

16. Dechezelles, J. F.; Malik, V.; Crassous, J. J.; Schurtenberger, P., Hybrid raspberry microgels with tunable thermoresponsive behavior. *Soft Matter.* **2013**, *9* (10), 2798-2802.

17. Harley, S.; Thompson, D. W.; Vincent, B., The adsorption of small particles onto larger particles of opposite charge- direct electron microscope studies. *Colloids Surf.* **1992**, *62* (1-2), 163-176.

18. Luckham, P.; Vincent, B.; Hart, C. A.; Tadros, T. F., The controlled focculation of particulate dispersions using small particles of opoosite charge. 1. Sediment volumes and morphology. *Colloids Surf.* **1980**, *1* (3-4), 281-293.

19. Furusawa, K.; Anzai, C., Heterocoagulation behavior of polymer lattices with spherical silica. *Colloids Surf.* **1992**, *63* (1-2), 103-111.

20. Starck, P.; Ducker, W. A., Simple method for controlled association of colloidal-particle mixtures using pH-dependent hydrogen bonding. *Langmuir.* **2009**, *25* (4), 2114-20.

21. Plunkett, K. N.; Mohraz, A.; Haasch, R. T.; Lewis, J. A.; Moore, J. S., Light-regulated electrostatic interactions in colloidal suspensions. *J. Am. Chem. Soc.* **2005**, *127* (42), 14574-14575.

22. Lu, Z. Y.; Qin, Y. Q.; Fang, J. Y.; Sun, J.; Li, J.; Liu, F. Q.; Yang, A. S., Monodisperse magnetizable silica composite particles from heteroaggregate of carboxylic polystyrene latex and FE(3)O(4) nanoparticles. *Nanotechnology*. **2008,** *19* (5), 055602.

23. Snoswell, D. R. E.; Rogers, T. J.; Howe, A. M.; Vincent, B., Controlling porosity within colloidal heteroaggregates. *Langmuir*. **2005,** *21* (24), 11439-45.

24. Liu, H.; Wang, C.; Gao, Q.; Liu, X.; Tong, Z., Fabrication of novel core-shell hybrid alginate hydrogel beads. *Int. J. Pharm.* **2008,** *351* (1), 104-112.

25. Snoswell, D. R. E.; Brill, R. K.; Vincent, B., pH-responsive microrods produced by electric-field-induced aggregation of colloid particles. *Adv. Mater.* **2007,** *19* (11), 1523-1527

26. Gaulding, J. C.; Saxena, S.; Montanari, D. E.; Lyon, L. A., Packed colloidal phases mediate the synthesis of raspberry-structured microgel heteroaggregates. *Acs Macro Lett.* **2013,** *2* (4), 337-340.

27. Smith, R. K.; Lewis, P. A.; Weiss, P. S., Patterning self-assembled monolayers. *Prog. Surf. Sci.* **2004**, *75* (1), 1-68.

28. Senff, H.; Richtering, W., Temperature sensitive microgel suspensions: colloidal phase bheavior and rheology of soft spheres. *J. Chem. Phys.* **1999**, *111* (4), 1705.

29. Hendrickson, G. R.; Smith, M. H.; South, A. B.; Lyon, L. A., Design of multiresponsive hydrogel particles and assemblies. *Adv. Funct. Mater.* **2010**, *20* (11), 1697-1712.

30. Borrega, R.; Cloitre, M.; Betremieux, I.; Ernst, B.; Leibler, L., Concentration dependence of the low-shear viscosity of polyelectrolyte micro-networks: from hard spheres to soft microgels. *Europhysical Lett.* 1999, *47* (6), 729-735.

31. Smith, M. H.; Herman, E. S.; Lyon, L. A., Network deconstruction reveals network structure in responsive microgels. *J. Phys. Chem. B.* **2011,** *115*, 3761-3764.

32. Ramsden,W. Separation of solids in the surface-layers of solutions and „suspensions“ (observations on surface-membranes, bubbles, emulsions and mechanical coagulation.) Preliminary Account. *Proc. R. Soc. London.* **1903**, 72, 156-164.

33. Pickering, S.U. Emulsions. *J. Chem. Soc.* **1907**, 91, 2001-2021.

34. Kim, J.W.; Fernandez-Nieves, A.; Dan, N.; Utada, A.S.; Marquez, M.; Weitz, D.A. Colloidal assembly route of responsive colloidosomes with tunable permeability. *Nano Lett.* **2007**, 7, 2876.

35. Lawrence, D.B.; Cai, T.; Hu, Z.; Marquz, M.; Dinsmore, A.D. Temperature-resposnive semipermeable capsules composed of colloidal microgel spheres. *Langmuir*, **2007**, 23, 395

CHAPTER 3

BINARY MICROGEL FILMS ON COLLOIDAL AND MACROSCOPIC SUBSTRATES

3.1. Introduction

Microgels are colloidal hydrogel nano- or microparticles that have been proposed for a variety of applications including tissue engineering scaffolds,[1-2] drug delivery,[3-4] biomimetic constructs,[5-6] and separations.[7-8] Microgel dispersions exhibit rich phase behavior due to the softness of the individual colloidal particles.[9] In particular, the phase behavior of thermoresponsive poly(*N*-isopropylacrylamide) (pNIPAm) microgels has been investigated in detail, revealing that the softness imparted on these colloids increases the thermodynamic parameter of interest, the effective volume fraction, required for crystallization and narrows the coexistence region in comparison to hard spheres.[10] While the phase behavior of single-component pNIPAm microgel dispersions has been investigated in detail,[11-14] the phase behavior of binary microgel mixtures has received markedly less attention. Though there has been investigation of other hard sphere colloidal mixtures including latex particles,[15-18] it is reasonable to predict that binary microgel dispersions will exhibit unique behavior due to the softness of the building blocks.

Previously, the Lyon Group investigated the behavior of colloidal crystals composed of two microgel components. In one study, colloidal crystal lattices were formed from pNIPAm microgels containing acrylic acid (AAc) (R_H ~ 375 ± 20 nm) and observed that such crystals were able to seamlessly integrate large, "defect

microgels," (R_H ~ 873 ± 66 nm) doped in at 0.1 wt-%.[19] Our lab has also explored how binary microgel dispersions respond at an interface through centrifugal (active) and passive deposition on a planar glass surface.[20] Decreases in microgel footprints were observed during deposition for both passive and active methods, which was an indication of how particle-particle repulsion dictated microgel spreading at solid substrates. However, these studies were not designed to capture colloidal phase behavior in solution.

In the present contribution, the deposition of binary microgel mixtures with defined effective volume fractions (φ_{eff}) onto planar and curved interfaces is explored (**Scheme 3.1**). The influence of microgel stiffness on film formation is investigated using a mixture of pNIPAm microgels containing either 1 mol-% or 5 mol-% *N,N'*-methylenebis(acrylamide) (BIS). The influence of microgel network structure on film formation from a binary mixture is explored using pNIPAm microgels and poly(*N*-isopropylmethacrylamide) (pNIPMAm) microgels both containing 5 mol-% BIS. Understanding of binary microgel mixtures can shed light on development of complex microgel coatings or microparticles, which are of particular interest for biomedical applications, including drug delivery and tissue engineering scaffolds,[21] where sensitive biological systems are highly influenced by mechanical properties,[22-24] topographical features,[25-26] microstructure,[27-28] and spatial/temporal presentation of biomolecules.[29-30]

Scheme 3.1. (A) Behavior of binary concentrated microgel dispersions was evaluated by placing a drop of highly packed microgel dispersions on coverslips. (B) Behavior of binary concentrated microgel dispersions at a curved interface was evaluated by

fabricating raspberry-like patchy particles using colloidal-phase mediated heteroaggregation.

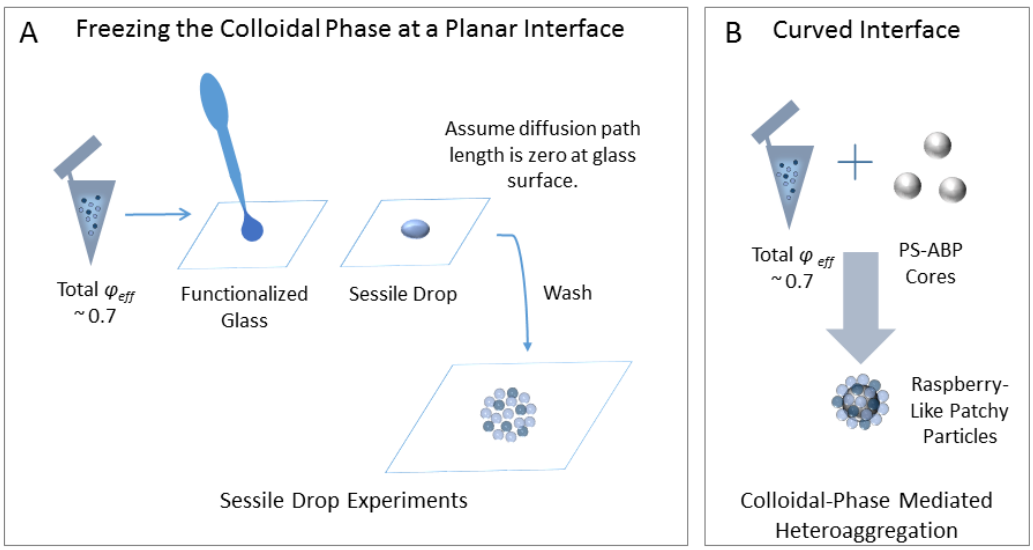

3.2. Experimental

3.2.1. Materials

Materials used in this investigation are described in section **2.2.1**.

3.2.2. Microgel Synthesis

Microgels were synthesized as previously in section described in section **2.2.4** using precipitation polymerization.[31]

3.2.3. Microgel Characterization

Microgel hydrodynamic radius (R_H) values were determined using a DynaPro Dynamic Light Scattering (DLS) instrument (Wyatt, Technology, Santa Barbara, CA) in HIS PBS (**Table 3.1**). Viscometry data were obtained using an Ubbelohde viscometer with a viscometer constant of 0.003121 cSt/s at 21 °C (**Figure 3.1**). Samples were prepared between 0.05 wt-% and 0.25 wt-% depending on the microgel composition. At least four weight fractions were used for each microgel composition and three trials were performed at each weight fraction. The swelling ratio, *k*, was

determined by fitting the data to the Einstein-Batchelor equation as described previously[32] (**Table 3.1**). Microgel stiffness was also characterized using AFM nanoindentation. Samples were prepared by creating highly packed microgel dispersions with an effective volume fraction of 0.7. A single drop of this dispersion was deposited onto an APTMS-functionalized glass coverslip and rinsed to remove excess microgels. Samples were hydrated in HIS PBS and interrogated via AFM using a silicon nitride tip with a spring constant ~0.16 N/m. For each sample, a minimum of three 32 x32 point arrays were collected. Representative images are shown.

3.2.4. Preparation of Aminobenzophenone-Functionalized PS Cores

PS cores were functionalized with AB as previously described in section **2.2.4**.

3.2.5. Single-Step Preparation of Raspberry-Like Patchy Particles

RLPPs were prepared according to colloidal-phase mediated heteroaggregation. For each sample, varied amounts of each microgel sample were dissolved in 400 μL of HIS PBS and were allowed to equilibrate for a minimum of two days. AB-functionalized PS core particles were re-suspended in HIS PBS and added to the colloidal phase (0.25% w/v, 100 μL) to produce mixed colloidal dispersions with effective volume fractions of approximately 0.7.

3.2.6. Preparation of Raspberry-Like Particles

All RLPs were prepared using colloidal-phase mediated heteroaggregation as previously described in section **2.2.5** with a few modifications. For each sample, 5 mg of microgels were dissolved in varied volumes of HIS PBS. AB-functionalized PS core particles were re-suspended in HIS PBS and added to the colloidal phase (0.25%

w/v, 100 μL) to produce mixed colloidal dispersions with effective volume fractions between 0.1-0.6.

3.2.7. Two-Step Preparation of Raspberry-Like Patchy Particles

RLPs were prepared using colloidal-phase mediated heteroaggregation. Dispersions of pNIPMAm:BIS (95:5) and pNIPAm:BIS (95:5) were prepared by suspending microgels in 400 μL of HIS PBS and allowing the particles to solvate for two days. AB-functionalized PS core particles were re-suspended in HIS PBS and added to the pNIPMAm:BIS (95:5) colloidal phase (0.25% w/v, 100 μL) to produce mixed colloidal dispersions with an effective volume fraction of 0.30. The solutions were homogenized via vortex after which the samples were exposed to longwave UV light from a Blak Ray 100 W lamp for 30 min. Samples were purified via sequential sedimentation and re-suspension in EtOH. Single component RLPs were then suspended in 100 μL PBS and added to the pNIPAm:BIS (95:5) colloidal phase to produce mixed colloidal dispersions with an effective volume fraction of 0.49. The solutions were homogenized via vortexing, after which the samples were exposed to longwave UV light from a Blak Ray 100 W lamp for 30 min. Samples were purified via sequential sedimentation and re-suspension in EtOH.

3.2.8. Colloidal Phase Characterization at a Planar Interface

Concentrated microgel dispersions were prepared by weighing out individual microgel components in the dry state and solvating these mixtures in 10 mM, pH 7.4 phosphate buffer saline with 100 mM NaCl (HIS PBS) for a minimum of 4 days on a shaker to establish an equilibrium. These samples were also periodically vortexed to ensure mixing. Glass coverslips were functionalized with 1% APTMS for 2 h.

Coverslips were washed with deionized water and dried with nitrogen. Using a transfer pipette, a single drop of the concentrated microgel dispersion was applied to the surface of the functionalized coverslip. The coverslip was then immediately washed with deionized water to remove excess solution. These samples were imaged using an MFP-3D AFM system (Asylum Research, Santa Barbara, CA).

3.2.9. Characterization of Raspberry-Like Patchy Particles and Raspberry-Like Particles

Microparticles were characterized as previously described in section **2.2.6**.

3.3 Results and Discussion

Previously, the Lyon Group developed a method to produce core-shell microgel heteroaggregates called raspberry-like particles (RLPs) where AB-functionalized PS cores are immersed in a concentrated dispersion of microgels; this dispersion is irradiated with ultra-violet light to covalently bond a microgel shell atop the PS core.[33] This method is more versatile than previous methods because it eliminates the need for electrostatic charge pairing. **Chapter 2** demonstrates that colloidal-phase mediated heteroaggregation is a robust approach using a variety of core and shell components with limited constraints due to synthesis conditions. In addition to being a useful fabrication method, this approach also presents a unique avenue towards the exploration of microgel interactions at a curved interface. As demonstrated in **Chapter 2**, microgel stiffness, microgel network structure, and effective volume fraction of the colloidal phase influence particle interactions at a curved interface.[32] Recently, the Lyon Group has become interested in understanding how binary mixtures of microgels behave at such an interface. The influence of the

mechanical stiffness and network structure of microgels on binary microgel dispersion interfacial behavior is explored. Previous microgel degradation studies in the Lyon Group have revealed that microgel network structure is dictated in some cases by the parent monomer.[34] These studies indicate that microgels composed of pNIPAm exhibit a heterogeneous cross-linker distribution, containing a densely cross-linked core surrounded by a loosely cross-linked periphery. In contrast, microgels composed of pNIPMAm exhibit a more homogeneous cross-linker distribution. In addition, varying cross-linker density has been demonstrated to be another facile route to tune microgel network structure as well as subsequent mechanical properties such as the Young's modulus and bulk modulus.[35-37] Herein, the coating behavior of binary microgel dispersions containing microgels with varied monomer and varied cross-linker content was investigated. A binary mixture of pNIPAm microgels composed of either 1 mol-% or 5 mol-% BIS and another binary mixture composed of 95 mol-% pNIPAm or pNIPMam with 5 mol-% BIS was explored. Microgels were synthesized and characterized (**Table 3.1** and **Figure 3.1**).

Table 3.1. Microgel characterization.

Monomer and Cross-linker	**Molar Ratio**	**R_H / nm**	**Swelling-Ratio/ mL-mg^{-1}**
pNIPAm:BIS	99:1	433 ±12	27 ± 1
pNIPAm:BIS	95:5	380 ± 5	14 ± 1
pNIPMAm:BIS[32]	95:5	288 ±3	10 ± 1

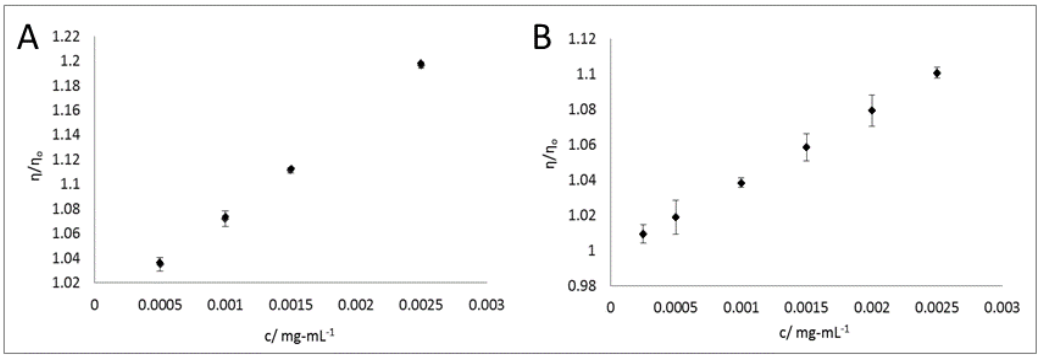

Figure 3.1. Viscometry data for (A) pNIPAm:BIS (99:1) and (B) pNIPAm:BIS (95:5). Viscometry data for pNIPMAm:BIS (95:5) microgels. Data points represent the average of three trials. Error bars represent the standard deviation of three trials.

3.3.1. Investigation of Microgel Coatings on a Planar Substrate

To investigate the microgel arrangement within the colloidal phase, a sessile drop of each highly packed binary microgel dispersion (**Table 3.2**) was deposited onto a glass substrate and immediately washed away the excess solution (**Scheme 3.1**). Binary dispersion compositions were selected based on previous studies of colloidal-phase mediated heteroaggregation using these microgel compositions, which demonstrated that pNIPAm microgels were capable of producing well-coated RLPs at a wide range of effective volume fractions (regardless of cross-linker concentration) while pNIPMAm microgels containing 5-mol-% BIS produced well-coated RLPs over a limited range of effective volume fractions.[32] Due to the high effective colloidal volume fraction, it is assumed that the microgels have very short diffusion paths within the dispersed phase, resulting in a diffusion path-length of almost zero at the glass interface. As a result, the interfacial arrangement of the phase should be frozen at the planar interface. AFM imaging of these experiments revealed that the

ability to coat a planar substrate is influenced by the microgel components (**Figure 3.2**).

Table 3.2. Compositions for binary microgel dispersions.

Label	φ_{eff}	φ_{eff} of Components		
		pNIPAm:BIS (99:1)	pNIPAm:BIS (95:5)	pNIPMAm:BIS (95:5)
A1	0.70	0.14	0.56	0
A2	0.69	0.27	0.42	0
A3	0.69	0.41	0.28	0
A4	0.68	0.54	0.14	0
B1	0.68	0	0.28	0.40
B2	0.70	0	0.35	0.35
B3	0.72	0	0.42	0.30
B4	0.72	0	0.49	0.23

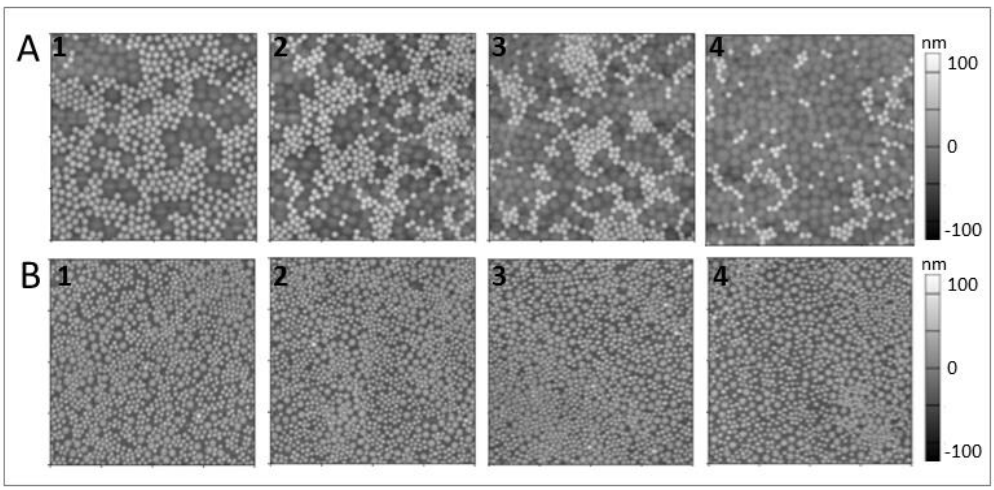

Figure 3.2. AFM images reveal height differences in the surface topography of binary microgel dispersions deposited onto a glass substrate. (A) AFM images of binary microgel dispersions with varied ratios of 1 mol-% and 5 mol-% BIS cross-linked pNIPAm microgels deposited onto a functionalized coverslip. (B) AFM images of binary microgel dispersions with varied ratios of pNIPAm or pNIPMAm microgels containing 5 mol-% BIS deposited onto a functionalized coverslip. Binary microgel

dispersion compositions used for this investigation are listed in **Table 3.2**. Images are 20 μm x 20 μm scans.

For the binary dispersions containing pNIPAm microgels alone, observations reveal that the microgels effectively interact with the substrate and form robust, ordered coatings (**Figure 3.2A**). In these images, the contrast is indicative of topographical height differences; the particles that are brighter correspond to the 5 mol-% BIS microgels and the particles that are darker correspond to the 1 mol-% BIS microgels. As the volume fraction of 5 mol-% BIS pNIPAm microgels is decreased (moving from left to right in **Figure 3.2A**), the surface coverage of these microgels decreases, as well. In all cases, the microgels appear to have a high packing efficiency while also exhibiting some degree of order and phase segregation. For this binary microgel dispersion, the overall composition of the dispersion clearly dictates the composition of the coating.

Next, distinct microgel dispersions were created that contain the same pNIPAm microgels containing 5 mol-% BIS to which a new secondary component, pNIPMAm microgels containing 5 mol-% BIS, was added (**Figure 3.2B**). These pNIPAm/pNIPMAm microgel dispersions contain microgels with different network structures, but similar cross-linker contents. In these images, the pNIPAm microgels appear larger than the pNIPMAm microgels. For these coatings, decreasing the volume fraction of pNIPAm microgels with 5 mol-% BIS (from right to left in **Figure 3.2B**) does not correspond to an obvious decrease in the apparent surface coverage of the microgel. In addition, these coatings exhibit domains of ordered pNIPMAm microgels with little or no order in regards to the pNIPAm microgels. The regions of

the coating rich in pNIPMAm microgels are broken up into smaller ordered domains. What is even more striking is the decreased packing exhibited by the pNIPAm microgels in the pNIPAm/pNIPMAm coatings. Here, pNIPAm microgels disrupt the order of the pNIPMAm regions while also exhibiting a low tendency to form single-component domains. This behavior is dissimilar from the previous experiment where the coating regions rich in pNIPAm microgels containing 5 mol-% BIS exhibit homogenous packing around the softer pNIPAm microgels (**Figure 3.2A**). Fast Fourier transforms of the data also suggest differing degrees of order in the two sets of experiments (**Figure 3.3**). In addition, these data suggest that the overall phase composition does not dictate the composition of the coating that is deposited. Finally, when compared to one another, these sets of experiments suggest that simply changing one component of the microgel dispersion causes the 5 mol-% BIS pNIPAm microgels to become less effective at coating a planar substrate.

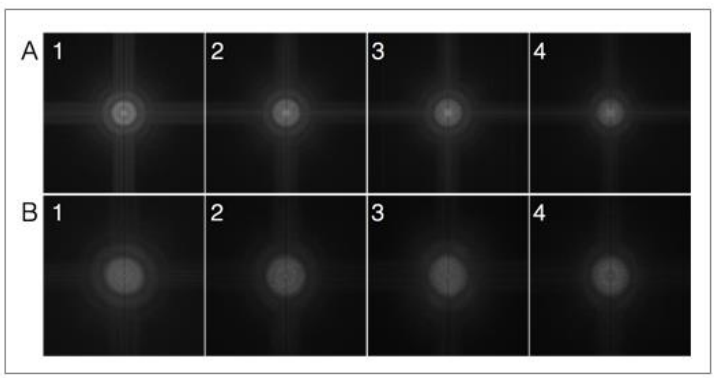

Figure 3.3. Fast Fourier transforms of AFM images of the microgel dispersions listed in **Table 3.2**. Each number corresponds to an AFM image in **Figure 3.2**.

Microgel dispersion composition clearly influences the ability to form ordered coatings. It is surprising that the binary pNIPAm microgel dispersions create ordered coatings with apparent phase segregation at the interface, as the two microgels are chemically very similar. Though the cross-linker, BIS, is more hydrophobic than the pNIPAm, it is likely core-localized due to the mismatched reactivity ratios of pNIPAm and BIS, which should result in the two different microgels (1 mol-% and 5 mol-% BIS) presenting similar surface chemistries. Thus, this difference in chemical composition does not provide an obvious reason for the apparent interfacial phase segregation. Moreover, the apparent lack of interfacial phase segregation in the pNIPAm/pNIPMAm microgel dispersions, where the chemical differences are more significant, would suggest another factor may be influencing the coating process. The decreased coating ability for the pNIPAm/pNIPMAm microgel dispersions, in particular, could be a result of using stiffer microgel particles; as microgel stiffness increases their ability to deform decreases, which could lead to diminished coating ability. Furthermore, recent studies in the Lyon Group have elucidated the importance of microgel mechanical properties in a variety of contexts and we suggest that microgel stiffness may influence the phase behavior observed here for the binary microgel dispersions at an interface.

3.3.2. Investigation of Microgel Mechanical Properties

AFM nanoindentation studies were performed to determine the Young's moduli of the microgels (**Figure 3.4**). These studies revealed that pNIPAm:BIS (99:1) microgels are the softest, with a Young's modulus of <50 kPa. In comparison, the pNIPAm:BIS (95:5) microgels exhibit varying Young's moduli due to the core-

localization of the 5 mol-% BIS, leading to a Young's modulus of ~125 kPa in the core and ~50 kPa in the surrounding shell. Microgels composed of pNIPMAm:BIS (95:5) have a similar Young's modulus around 150 kPa. However, nanoindentation studies of these microgels exhibit more heterogeneity, which could be caused by less efficient microgel packing on the surface of the coverslip, as well as a decreased ability to spread on the surface, resulting in sampling of the underlying substrate. These nanoindentation studies suggest that pNIPAm:BIS (99:1) microgels are a at least three times softer than the pNIPAm:BIS (95:5) and pNIPMAm:BIS (95:5) microgels. These studies also suggest that the pNIPAm:BIS (95:5) and pNIPMAm:BIS (95:5) microgels have mechanical properties that are more similar to each other than to the pNIPAm:BIS (99:1) microgels.

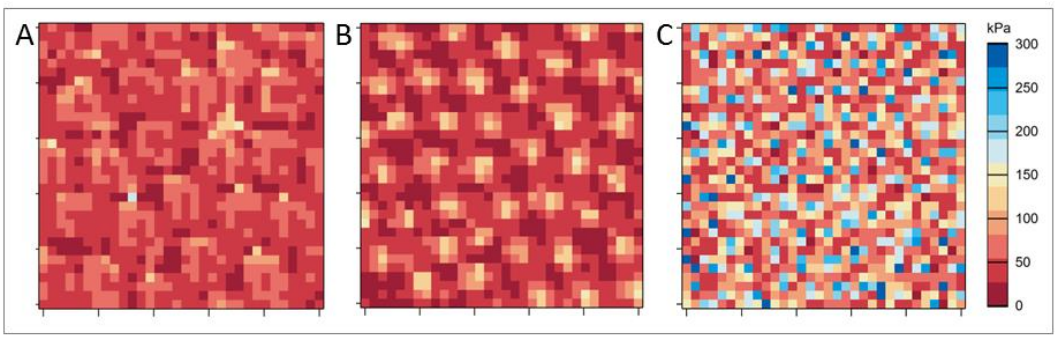

Figure 3.4. The Young's moduli for (A) pNIPAm:BIS (99:1), (B) pNIPAm:BIS (95:5), and (C) pNIPMAm:BIS (95:5) generated in 32 x 32 arrays through AFM nanoindentation studies. Each scan is 5 μm x 5 μm.

3.3.3. Investigation of Microgel Coatings on a Curved Substrate

The behavior of microgel mixtures at a curved interface was next explored through colloidal-phase mediated heteroaggregation with PS beads, resulting in the development of raspberry-like patchy particles (RLPPs), in order to determine

whether interfacial rearrangement of the colloidal phase occurs on the surface of the PS core particles. The difference in degree of ordering and phase segregation at a curved interface can be seen by comparing the likelihood of finding two distinct microgel types sitting next to one another. RLPPs fabricated using the dispersions of pNIPAm microgels with varying BIS contents, results in particles with packed, ordered coatings; phase segregation is also apparent at the PS interface (**Figure 3.5A**). Each microgel type appears to be ordered in large areas, suggesting these microgels prefer to interact with microgels of the same composition. In contrast, when using the pNIPAm/pNIPMAm microgel dispersions to fabricate RLPPs, particles exhibit poor coating and phase segregation is not as obviously present at the PS interface (**Figure 3.5B**). In this case, the likelihood of finding two distinct microgel types sitting next to each other on the PS surface appears to be higher than the coatings produced using the pNIPAm microgel dispersions. These studies reveal that RLPP microgel coverage distribution is consistent with planar experiments, suggesting that interfacial reorganization of the colloidal phase does not occur when a curved interface is introduced into the system.

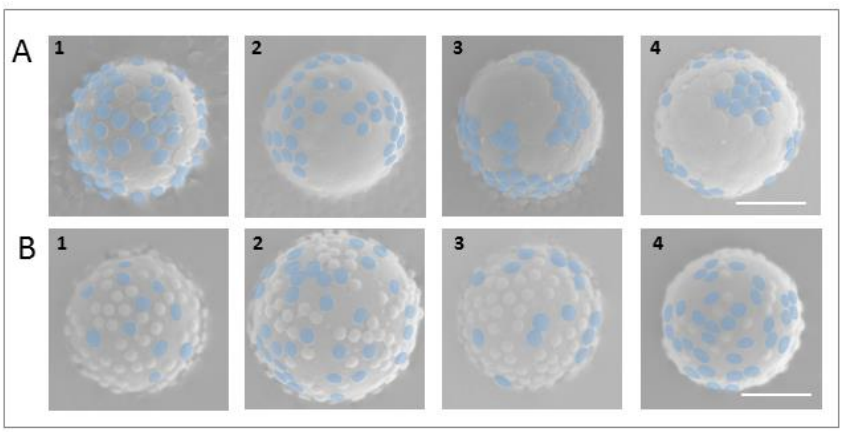

Figure 3.5. (A) SEM images of RLPs fabricated using binary microgel dispersions with varied ratios of 1 mol-% and 5 mol-% BIS cross-linked pNIPAm microgels deposited onto a functionalized coverslip. (B) SEM images of RLPs fabricated using binary microgel dispersions with varied ratios of pNIPAm or pNIPMAm microgels with 5 mol-% BIS deposited onto a functionalized coverslip. PNIPAm microgels with 5 mol-% BIS are false colored blue for clarity. False-coloring was assigned qualitatively through manual tracing and shading of microgels in magnified images. The original images are shown in **Figure 3.6**. Binary microgel dispersion compositions used for this investigation are listed in **Table 1**. Scale bars represent 2 μm.

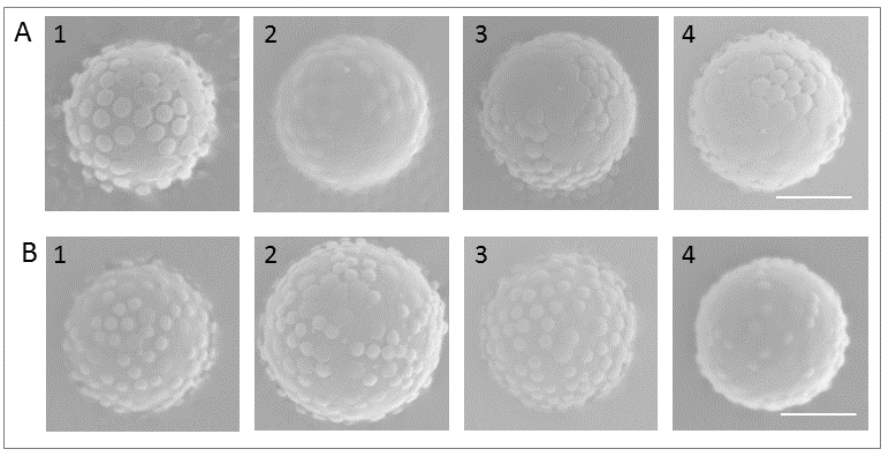

Figure 3.6. (A) SEM images of RLPs fabricated using binary microgel dispersions with varied ratios of 1 mol-% and 5 mol-% BIS cross-linked pNIPAm microgels deposited onto a functionalized coverslip. (B) SEM images of RLPs fabricated using binary microgel dispersions with varied ratios of pNIPAm or pNIPMAm microgels with 5 mol-% BIS deposited onto a functionalized coverslip. Scale bars represent 2 μm.

3.3.4. Development of a Two-Step Process to Fabricate Raspberry-Like Patchy Particles

For the pNIPAm/pNIPMAm dispersion, microgels do not appear to pack closely at either the planar or curved surfaces. Additionally, it is difficult to control the ratio of microgels at the interface based on the ratio of components in the colloidal mixture. In other words, the composition of the dispersion is not accurately reflected

in the composition of the coating. In order to enhance control over microgel coverage, a new two-step process was designed to coat a PS core particle with each microgel population separately for comparison. This two-step process requires an understanding of the microgel coating that occurs for each component at varied volume fractions in order to properly select synthesis conditions (**Figure 3.7**). After single-component RLP fabrication analysis was performed, the two-step process was analyzed. In this process, the PS core particles is immersed in a pNIPMAm microgel colloidal phase (φ_{eff} =0.3) to create a population of raspberry-like particles (RLPs) with a sparse microgel coating (**Figure 3.8A**). After purification and recovery of the RLPs, these particles are immersed in a pNIPAm colloidal phase to create RLPPs (**Figure 3.8B**). This method results in a population of RLPPs with a high packing density as visualized through SEM imaging. Although the RLPP population is well-coated as a whole, surface topography is not homogeneous throughout the entire RLPP population (**Figure 3.8C**). These results suggest that this method may offer enhanced control over microgel packing at a curved interface, but that challenges may still exist in terms of population uniformity. Optimization of volume fractions used in the two-step method could further enhance control over topographical features by creating an RLP population of evenly coated particles to template RLPP assembly.

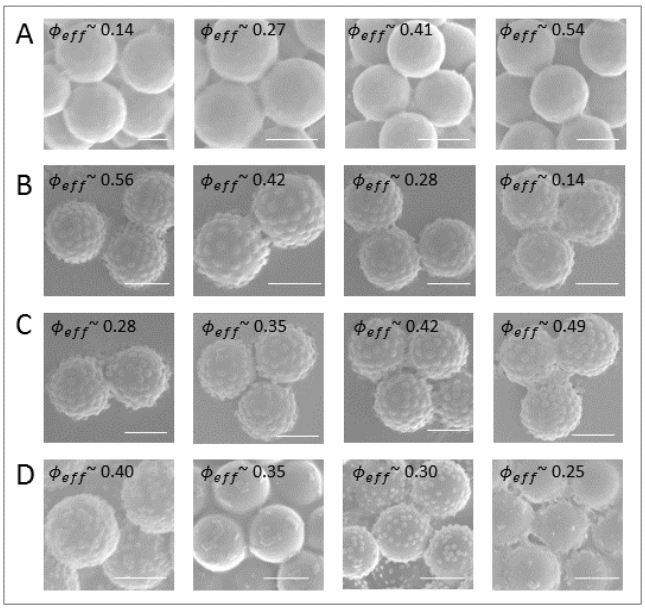

Figure 3.7. SEM imaging of single component RLPs for (A) pNIPAm:BIS (99:1), (B) pNIPAm:BIS (95:5), (C) pNIPMAm:BIS (99:1), and (D) pNIPMAm:BIS (95:5). All scale bars represent 2 μm.

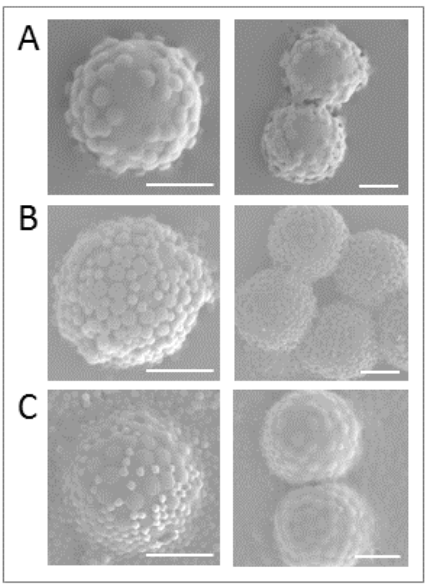

Figure 3.8. RLPPs fabricated using a two-step coating process where (A) a pNIPMAm microgel coating is first applied, (B & C) followed by a pNIPAm microgel coating resulting in particles with high microgel packing. All scale bars represent 2 μm.

3.4. Discussion

Architectural control over composite microparticles has become increasingly important for the development of functional materials. Hybrid colloids offer facile routes for unique functionality tailored through design of vehicles with complementary pairing of materials possessing multiple properties or characteristics.[38-40] For example, Park *et al.* developed magnetic hybrid colloids with silver nanoparticles localized on the surface for use as an antiviral.[41] Though silver nanoparticles have previously been demonstrated as an antiviral there are still concerns regarding the harmful effects of the uncontrolled release of these nanoparticles into a biological environment. Development of complex vehicles such as RLPPs are well-suited for encapsulation or delivery within sensitive biological systems where both spatial and temporal control over presentation of chemical and mechanical cues can have a large impact on cellular fate and function.[42-47] The use of microgels for encapsulation and delivery has been extensively characterized, demonstrating the high degree of synthetic control that influences molecular payload and release rates.[48-50] In such systems, one can envision a vehicle that is able to deliver multiple molecules at multiple rates, perhaps controlled by cross-linker content and/or charge. In contrast, one could also envision a thermoresponsive pNIPAm/pNIPMAm vehicle that is utilized to trigger release at multiple temperatures or even to sequester biomolecules from the surrounding environment. In addition, the Lyon Group is currently exploring the use of RLPs for development of tissue engineering scaffolds. Use of RLPPs for such applications could provide avenues for controlled functionalization of scaffolds with biomolecules using vehicles containing

one population of microgels that allows for facile bio-conjugation. Incorporation of such systems into three-dimensional microgel scaffolds also offers the potential for exploration of cellular responses to three-dimensional presentation of mechanical cues and/or topographical features.

3.5. Conclusions

A series of binary microgel coatings were constructed on planar and curved substrates in order to examine the relationship between binary microgel dispersions components and coating topography. Binary systems of pNIPAm microgels with varying BIS content exhibit robust, ordered coatings with apparent phase segregation at both planar and curved interfaces. In contrast, binary dispersions of microgels with constant BIS content composed of either pNIPAm or pNIPMAm exhibit poor, disordered coatings with little phase segregation at either planar or curved interfaces. Similarities in coating behavior at both planar and curved interfaces suggest that binary microgel dispersions do not exhibit interfacial reorganization at curved interfaces during colloidal-phase mediated heteroaggregation. The ability of the pNIPAm microgels containing 5 mol-% BIS to coat a substrate is influenced by the other microgel component in a binary microgel dispersion. While some binary microgel dispersions lead to coating compositions that are predictable based on the dispersion composition, others do not. To improve coating coverage and predictability, the use of a two-step coating process was established for enhanced control over microgel packing at a curved interface and reduced presence of bare PS. The RLPP constructs developed here serve as unique tri-heteroaggregate building

blocks that can function alone or be assembled for development of complex biomaterials.

3.6. References

1. Gan, T.; Guan, Y.; Zhang, Y., Thermogelable PNIPAM microgel dispersion as 3D cell scaffold: effect of syneresis. *J. Mater. Chem.* **2010**, *20* (28), 5937-5944.

2. Du, Y.; Lo, E.; Ali, S.; Khademhosseini, A., Directed assembly of cell-laden microgels for fabrication of 3D tissue constructs. *Proc. Natl. Acad. Sci. USA.* **2008**, *105* (28), 9522-9527.

3. Blackburn, W. H.; Dickerson, E. B.; Smith, M. H.; McDonald, J. F.; Lyon, L. A., Peptide-functionalized nanogels for targeted siRNA delivery. *Bioconjugate Chem.* **2009**, *20* (5), 960-968.

4. Bysell, H.; Mansson, R.; Hansson, P.; Malmsten, M., Microgels and microcapsules in peptides and protein drug delivery. *Adv. Drug Deliv. Rev.* **2011**, *63* (13), 1172-1185.

5. Chen, Z.; Xu, L.; Liang, Y.; Zhao, M., pH sensitive water-soluble nanospheric imprinted hydrogels prepared as horseradish perioxidase mimetic enzymes. *Adv. Mater.* **2010**, *22* (13), 1488-+.

6. Xia, Y.; Gu, Y.; Zhou, X.; Xu, H.; Zhao, X.; Yaseen, M.; Lu, J. R., Controllable stabilization of Poly(N-isopropylacrylamide)-based microgel films through biomimetic mineralization of calcium carbonate. *Biomacromolecules.* **2012**, *13* (8), 2299-2308.

7. Morris, G. E.; Vincent, B.; Snowden, M. J., Adsorption of led ions onto N-isopropylacrylamide and acrylic acid copolymer microgle.s *J. Colloid Interface Sci.* **1997**, *190* (1), 198-205.

8. Parasuraman, D.; Sarker, A. K.; Serpe, M. J., Poly(N-isopropylacrylamide)-based microgels and their assemblies for organic-molecule removal from water. *Chemphyschem.* **2012**, *13* (10), 2507-2515.

9. Lyon, L. A.; Meng, Z. Y.; Singh, N.; Sorrell, C. D.; John, A. S., Thermoresponsive microgel-based materials. *Chem. Soc. Rev.* **2009**, *38* (4), 865-874.

10. Senff, H.; Richtering, W., Temperature sensitive microgel suspensions: colloidal phase behavior and rheology of soft spheres. *J. Chem. Phys.* **1999**, *111* (4), 1705-1711.

11. Lyon, L. A.; Fernandez-Nieves, A.,The polymer/colloid duality of microgel suspensions. *Annu. Rev. Phys. Chem.* **2012**, *63*, 25-43.

12. Gasser, U.; Hyatt, J. S.; Lietor-Santos, J. J.; Herman, E. S.; Lyon, L. A.; Fernandez-Nieves, A.,. Form factor of pNIPAM microgels in overpacked states. *J. Chem. Phys.* **2014**, *141* (3), 9.

13. Meng, Z.; Cho, J. K.; Breedveld, V.; Lyon, L. A., Physical aging and phase behavior of multiresponsive microgel colloidal dispersions. *J. Phys. Chem. B.* **2009**, *113* (14), 4590-4599.

14. St. John, A. N.; Lyon, L. A., Local control over phase transitions in microgel assemblies. *J. Phys. Chem. B.* **2008**, *112* (36), 11258-11263.

15. Dijkstra, M.; van Roij, R.; Evans, R., Phase diagram of highly asymmetric binary hard-sphere mixtures. *Phys. Rev. E.* **1999**, *59* (5), 5744-5771.

16. Shevchenko, E. V.; Talapin, D. V.; Murray, C. B.; O'Brien, S., Structural characterization of self-assembled multifunctional binary nanoparticle superlattices. *J. Am. Chem. Soc.* **2006**, *128* (11), 3620-3637.

17. Bartlett, P.; Ottewill, R. H.; Pusey, P. N., Superlattic formation in binary-mixtures of hard-sphere colloids. *Phys. Rev. Lett.* **1992**, *68* (25), 3801-3804.

18. Linse, P.; Lobaskin, V., Electrostatic attraction and phase separation in solutions of like-charged colloidal particles. *Phys. Rev. Lett,* **1999**, *83* (20), 4208-4211.

19. Iyer, A. S. J.; Lyon, L. A., Self-healing colloidal crystals. *Angew. Chem. Int. Ed.* **2009**, *48* (25), 4562-4566.

20. Sorrell, C. D.; Lyon, L. A., Bimodal swelling responses in microgel thin films. *J. Phys. Chem. B.* **2007**, *111* (16), 4060-4066.

21. Desai, T. A., micro-and nanoscale structures for tissue engineering constructs. *Med. Eng. Phys.* **2000**, *22* (9), 595-606.

22. Cheng, C.-M.; Steward, R. L., Jr.; LeDuc, P. R., Probing cell structure by controlling the mechanical environment with cell-substrate interactions. *J. Biomech.* **2009**, *42* (2), 187-192.

23. Clause, K. C.; Liu, L. J.; Tobita, K., Directed stem cell differentiation: the role of physical forces. *Cell Commun. Adhes.* **2010**, *17* (2), 48-54.

24. Bao, G.; Suresh, S., Cell and molecular mechanics of biological materials. *Nature Mater.* **2003**, *2* (11), 715-725.

25. Flemming, R. G.; Murphy, C. J.; Abrams, G. A.; Goodman, S. L.; Nealey, P. F., Effects of synthetic micro- and nano-structured surfaces on cell behavior. *Biomaterials.* **1999**, *20* (6), 573-588.

26. Clark, P.; Connolly, P.; Curtis, A. S. G.; Dow, J. A. T.; Wilkinson, C. D. W., Topographical control of cell behavior. 1. Simple step cues. *Development.* **1987**, *99* (3), 439-448.

27. Engelmayr, G. C., Jr.; Papworth, G. D.; Watkins, S. C.; Mayer, J. E., Jr.; Sacks, M. S., *J.* Guidance of engineered tissue collagen orientation by large-scale scaffold microstructures. *Biomech.* **2006**, *39* (10), 1819-1831.

28. Ng, R.; Zang, R.; Yang, K. K.; Liu, N.; Yang, S.-T., Three-dimensional fibrous scaffolds with microstructures and nanotextures for tissue engineering. *RSC Adv.* **2012**, *2* (27), 10110-10124.

29. Carpenedo, R. L.; Bratt-Leal, A. M.; Marklein, R. A.; Seaman, S. A.; Bowen, N. J.; McDonald, J. F.; McDevitt, T. C., Homogeneous and organized differentiation within embryoid bodies induced by microsphere-mediated delivery of small molecules. *Biomaterials.* **2009**, *30* (13), 2507-2515.

30. Bratt-Leal, A. M.; Carpenedo, R. L.; Ungrin, M. D.; Zandstra, P. W.; McDevitt, T. C., Incorporation of biomaterials in multicellular aggregates modulates pluripotent stem cell differentiation. *Biomaterials.* **2011**, *32* (1), 48-56.

31. Hendrickson, G. R.; Smith, M. H.; South, A. B.; Lyon, L. A., Design of multiresponsive hydrogel particles and assemblies. *Adv. Funct. Mater.* **2010**, *20* (11), 1697-1712.

32. Saxena, S.; Lyon, L. A., Influence of microgel packing on raspberry-like heteroaggregate assembly. *J. Colloid Interface Sci.* **2015**, *442* (0), 39-48.

33. Gaulding, J. C.; Saxena, S.; Montanari, D. E.; Lyon, L. A., Packed Colloidal Phases Mediate the Synthesis of Raspberry-structured microgel heteroaggregates. *ACS Macro Lett.* **2013**, *2* (4), 337-340.

34. Smith, M. H.; Herman, E. S.; Lyon, L. A., Network deconstruction reveals network structure in responsive microgels. *J. Phys. Chem. B.* **2011**, *115* (14), 3761-3764.

35. Varga, I.; Gilanyi, T.; Meszaros, R.; Filipcsei, G.; Zrinyi, M., Effect of cross-link density on the internal structure of Poly(N-isopropylacrylamide) microgels. *J. Phys. Chem. B.* **2001**, *105* (38), 9071-9076.

36. Burmistrova, A.; Richter, M.; Uzum, C.; von Klitzing, R., Effect of cross-linker density of P(NIPAM-co-AAc) microgels at solid surfaces on the

swelling/shrinking behaviour and the Young's modulus. *Colloid Polym. Sci.* **2011**, *289* (5-6), 613-624.

37. Sierra-Martin, B.; Frederick, J. A.; Laporte, Y.; Markou, G.; Lietor-Santos, J. J.; Fernandez-Nieves, A., Determination of the bulk modulus of microgel particles. *Colloid Polym. Sci.* **2011**, *289* (5-6), 721-728.

38. Chen, M.; Zhou, S. X.; You, B.; Wu, L. M., A novel preparation method of raspberry-like pMMA/SiO2 hybrid microspheres. *Macromolecules* **2005**, *38* (15), 6411-6417.

39. Karg, M.; Lu, Y.; Carbo-Argibay, E.; Pastoriza-Santos, I.; Perez-Juste, J.; Liz-Marzan, L. M.; Hellweg, T., Multiresponsive hybrid colloids based on gold nanorods and poly(NIPAm-co-allylacetic acid) microgels. *Langmuir.* **2009**, *25* (5), 3163-3167.

40. Wu, W. T.; Mitra, N.; Yan, E. C. Y.; Zhou, S. Q., Multifunctional hybrid nanogel for integration of optical glucose sensing and self-regulated insulin release at physiolgical pH. *ACS Nano.* **2010**, *4* (8), 4831-4839.

41. Park, S.; Park, H. H.; Kim, S. Y.; Kim, S. J.; Woo, K.; Ko, G., Antiviral properties of silver nanoparticles on a magnetic hybrid colloid. *Appl. Environ. Microbiol.* **2014**, *80* (8), 2343-2350.

42. Lu, J.; Li, D. S.; Lu, K. H., Distribution and localization of fibroblast growth factor – 8 in rat brain and nerve cells during neural stem/progenitor cell differentiation. *Neural Regener. Res.* **2012**, *7* (19), 1455-1462.

43. Choi, K. C.; Yoo, D. S.; Cho, K. S.; Huh, P. W.; Kim, D. S.; Park, C. K., Effect of single growth factor and growth factor combinations on differentiation of neural stem cells. *J. Korean Neurosurg. Soc.* **2008**, *44* (6), 375-381.

44. Banerjee, A.; Arha, M.; Choudhary, S.; Ashton, R. S.; Bhatia, S. R.; Schaffer, D. V.; Kane, R. S., The influence of hydrogel modulus on the proliferation and differentiation of encapsulated neural stem cells. *Biomaterials.* **2009**, *30* (27), 4695-4699.

45. Her, G. J.; Wu, H. C.; Chen, M. H.; Chen, M. Y.; Chang, S. C.; Wang, T. W., Control of three-dimensional substrate stiffness to manipulate mesenchymal stem cell fate toward neuronal or glial lineages. *Acta Biomaterialia.* **2013**, *9* (2), 5170-5180.

46. Evans, N. D.; Minelli, C.; Gentleman, E.; LaPointe, V.; Patankar, S. N.; Kallivretaki, M.; Chen, X. Y.; Roberts, C. J.; Stevens, M. M., Substrate stiffness affects early differentiation events in embryonic stem cells. *Eur. Cell Mater.* **2009**, *18*, 1-14.

47. Engler, A. J.; Sen, S.; Sweeney, H. L.; Discher, D. E., Matrix elasticity directs stem cell lineage specification. *Cell.* **2006**, *126* (4), 677-689.

48. Eichenbaum, G. M.; Kiser, P. F.; Dobrynin, A. V.; Simon, S. A.; Needham, D.,Investigation of the swelling response and loading of ionic microgels with drugs and proteins: the dependence on cross-link density. *Macromolecules.* **1999**, *32* (15), 4867-4878.

49. Malmsten, M.; Bysell, H.; Hansson, P., Biomacromolules in microgels – opportunities and challenges for drug delivery. *Curr. Opin. Colloid Interface Sci.* **2010**, *15* (6), 435-444.

50. Oh, J. K.; Drumright, R.; Siegwart, D. J.; Matyjaszewski, K., The development of microgels/nanogels for drug delivery applications. *Prog. Polym. Sci.* **2008**, *33* (4), 448-477.

CHAPTER 4

COMPOSITE COLLOIDAL MICROGEL ASSEMBLIES FOR DELIVERY

4.1 Introduction

Embryonic stem cells (ESCs) represent a unique cell population that can differentiate into all three embryonic germ layers (endoderm, mesoderm, and ectoderm) (**Scheme 4.1**); ESCs are a promising cell source to develop tissues for tissue regeneration and drug screening.[1-3] Currently, there are many diseases that could potentially be treated with such cell therapeutics including myocardio infarction, spinal cord injury, cancer, and diabetes. However, before ESCs can be used as a source for therapeutic cell strategies, researchers must develop a robust, reproducible strategy to homogeneously differentiate stem cells. (**Scheme 4.2**).

For investigation and biomanufacturing, ESCs are often maintained in spheroidal aggregates, termed embryoid bodies (EB), which more closely mimic the biological environment than monolayer cell-culture. The spatial and temporal differentiation of ESCs within EBs is regulated by numerous coordinated interactions between soluble factors, cell-cell interactions, and extracellular matrix present, which help to define the biochemical and mechanical properties of the EB microenvironment that regulate cell fate.[4-7] Strategies to direct differentiation of ESC aggregates often employ an "outside-in" approach by addition of soluble factors to culture medium (**Scheme 4.3**). For example, soluble bone-morphogenetic protein-4 (BMP4) is often supplemented to direct mesoderm differentiation by inducing expression of transcription factor BrachyuryT.[8-9] However, a concentration gradient develops due to

the formation of a dense outer layer composed of ECM and cells, which may be partially responsible for nonhomogeneous cellular differentiation observed within EBs.[10-11]

Scheme 4.1. ESCs differentiate into a variety of cells (not all shown below).

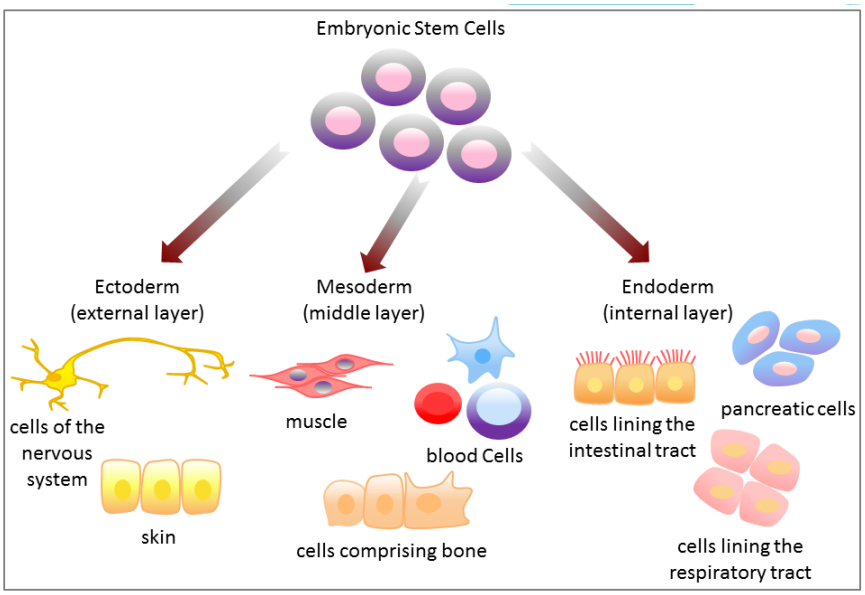

Scheme 4.2. Applications of embryonic stem cells and mesenchymal stem cells.

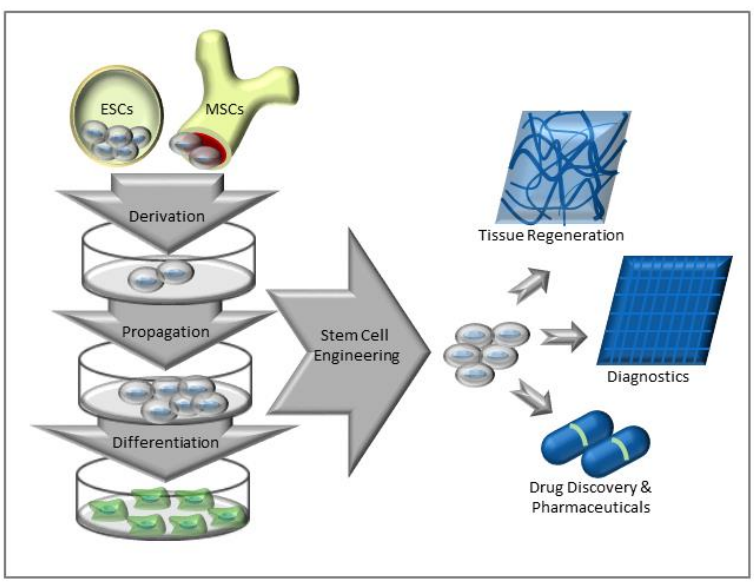

One method to potentially overcome diffusion limitations within three-dimensional multicellular aggregates and direct differentiation is incorporation of engineered microparticles to locally control molecular delivery; incorporation of microparticles has been demonstrated to induce organized, homogenous differentiation.[12-15] However, previous approaches are limited in terms of the materials used with respect to control over growth factor payload and release rates due to low synthetic control and high polydispersity.

Scheme 4.3. Strategies to direct embryoid body differentiation.

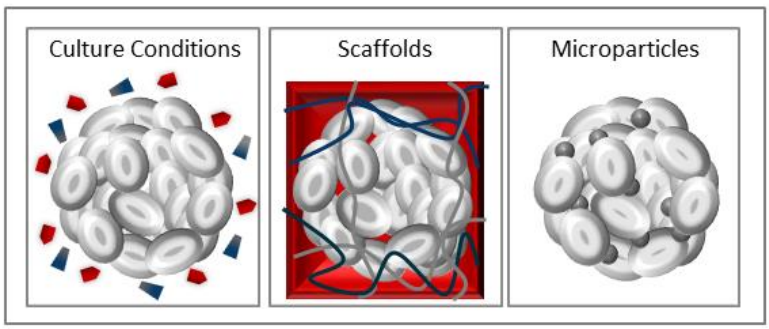

To develop a more effective microparticle construct that overcomes these limitations, we have approached this problem from a materials perspective, in collaboration with the McDevitt Stem Cell Engineering Lab. We believe the use of synthetic materials in a new hybrid construct could offer more spatio-temporal control over morphogen payloads and release rates, where alteration of the physical and chemical properties of the biomaterial enable customization of the spatial-temporal cues presented to stem cells.[4]

The microgels used in the Lyon Group are discrete hydrogel particles that have previously been used for drug delivery applications.[16-19] Microgel loading and release is highly dependent on network characteristics; the network mesh size, as determined by the cross-linking density and polymer-solvent interactions, are the most important parameters determining the mobility of embedded biomacromolecules and their diffusion rates within the swollen microgel.[20] Microgel charge can also influence the loading and release; electrostatic interactions can be tailored to enhance the loading ability or to increase retention time within the microgel. Due to their hydrophilic nature, microgels allow for the incorporation of peptides and proteins with few conformational changes and limited aggregation, maintaining the biological effectiveness of biomacromolecules.[21] Protein properties such as size, charge, polarity, and hydrophilicity play a critical role in their interactions with microgels during encapsulation and delivery. Previously in the Lyon Group, the "breathing in" method was developed to enable high loading of macromolecules within the microgels by adding a small, concentrated volume of macromolecules to a sample of lyophilized microgels.[22] Due to their high hydrophilicity, microgels immediately swell upon exposure to water and imbibe macromolecules in the process.

Unfortunately, we have discovered that microgels alone cannot be assembled with stem cells during formation of EBs due to their low density. Instead, we hypothesize that stem cell aggregates behave in a similar manner to particulate aggregates, and that the creation of a material that has similar properties to cells will enable successful incorporation. Herein we propose the use of a hybrid colloid that involves two distinct materials in a core-shell architecture that can be formed via

heteroaggregation. The present investigation explores the use of microparticles with the same architecture as those fabricated in **Chapter 2**: dense, hard 4.5 μm diameter polystyrene sphere surrounded by a shell of soft microgels. When considering the structure of these raspberry-like particles (RLPs), the polystyrene provides the correct size and density to assemble with the cells, while the microgels maintain the synthetic control over morphogen release that we desire (**Scheme 4.4**).

In the present investigation, we use a modified version of the process detailed in **Chapter 2**, colloidal-phase mediated heteroaggregation, to fabricate RLPs.[23] This unique heteroaggregation method enables production scale-up due to the specific parameters involved in the process, while minimizing compositional restraints. We perform critical materials characterization studies to assess particle morphology, payload, release, and compatibility with stem cells. We explore the use of these RLPs to load and release bone-morphogenetic protein-4 (BMP4) to EBs in order to induce controlled differentiation.

Scheme 4.4. Raspberry-like particles incorporated within embryoid bodies.

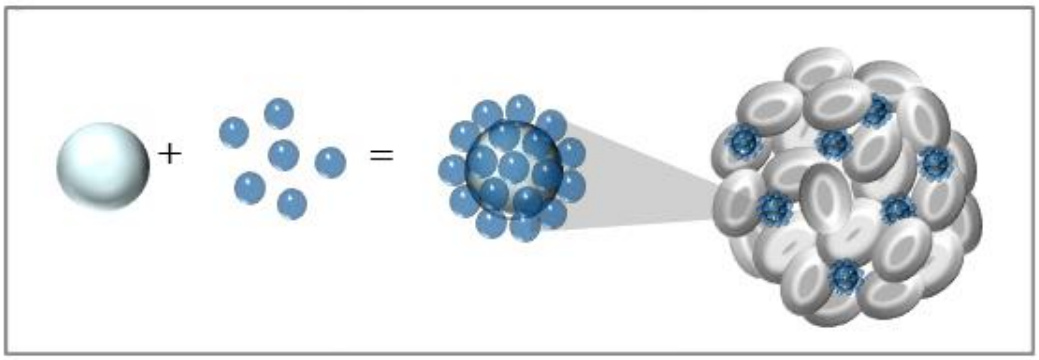

4.2. Experimental

4.2.1. Materials

Materials used in this investigation are described in section **2.2.1** with the following notable exception: methacryloxyethyl thiocarbamoyl rhodamine B (Rhodamine-B) was purchased from Polysciences, Inc. (Warrington, PA) and used as received. Carboxyl modified polystyrene spheres were purchased from Polysciences, Inc. (Warrington, PA) and Spherotech, Inc. (Lake Forest, IL).

4.2.2. Microgel Synthesis and Characterization

Microgels were synthesized as described in section **2.2.2** with the following modifications. PNIPMAm and BIS were dissolved in deionized water to a final total monomer concentration of 140 mM. After placing the solution in a 3-neck round-bottom flask and purging the solution with nitrogen for an hour while being heated in an oil bath at 70 °C, AAc was added. The solution was then purged with oxygen for an additional 10 min to purge the system of oxygen before adding the initiator APS using a syringe needle. Microgel hydrodynamic radius (R_H) values were determined using a DynaPro Dynamic Light Scattering (DLS) system (Wyatt, Technology, Santa Barbara, CA) in 10 mM MES (pH 5.5) buffer with 10 mM NaCl ionic strength.

4.2.3. Preparation of Raspberry-Like Particles

Raspberry-like particles were prepared using a modified version of the process described in sections **2.2.4** and **2.2.5** where the amounts of microgels and AB-functionalized PS cores have been scaled-up by more than an order of magnitude. 200 mg microgels were solvated in 2 mL deionized water overnight. AB-functionalized

core particles were re-suspended in 2 mL of EtOH (0.75 % w/v) and immersed in the microgel dispersion before the solution was UV coupled and then purified.

4.2.4. Characterization of Raspberry-Like Particles

RLP topography was assessed dry using SEM imaging as described in section **2.2.6**. In addition, RLPs were characterized in liquid using an LSM- 510 Zeiss Laser Scanning Confocal Microscope (Zeiss, Thornwood, NY). Samples were prepared by placing a drop of particles suspend in EtOH on a microscope slide, placing a coverslip on top, and sealing the sample with a polymer fixative to prevent evaporation.

4.2.5. Characterization Raspberry-Like Particle Loading and Release

RLP concentration was determined using a hemacytometer. Prior to growth factor loading, RLPs were re-suspended in EtOH, which was evaporated off overnight at room temperature to dehydrate the samples. Lyophilized BMP4 was re-suspended in 0.1% BSA in PBS prior to addition to dehydrated RLPs. The BMP4 binding capacity of RLPs was examined by addition of 1 ml of a low (10ng/mg RLP) and high (100 ng/mg RLP) dose of BMP4 in 0.1% BSA over 18 hours at either 4 °C to promote rehydration of RLPs with uptake of BMP4. Depletion of BMP4 from solution by RLP from the growth factor solution was quantified by analyzing the supernatant BMP4 concentration via an enzyme-linked immunosorbent assay (ELISA).

After addition of BMP4 solution, RLPs were centrifuged at 5,000 RPM for 5 min for removal of supernatant (or unbound BMP4). 1 ml of 0.1% BSA in PBS solution was added to pelleted RLPs. Passive release of BMP4 at 37 ° C was determined by removal of 300 µl of supernatant after centrifugation of BMP4-loaded RLPs every day for the first week of release and at 2 weeks.

4.2.6. Embryoid Body Formation and Culture

All cell studies were performed outside of the Lyon Group by Denise Sullivan, a member of the McDevitt Stem Cell Laboratory. Undifferentiated D3 ESCs were maintained in monolayer culture on 0.1% gelatin coated tissue culture dishes in Dulbecco's modified Eagle's medium (DMEM) media with high glucose supplemented with 15% fetal bovine serum (FBS) (HyClone Laboratories, Logan, UT), 2 mM L-glutamine (Invitrogen- Gibco, Calsbad, CA), non-essential amino acids (NEAA) (Invitrogen- Gibco, Calsbad, CA), penicillin and streptomycin (Invitrogen-Gibco, Calsbad, CA), 0.1mM β-mercaptoethanol (Invitrogen- Gibco, Calsbad, CA), and 10^3 U/ml leukemia inhibitory factor (LIF). D3 ESCs were cultured at 37 ℃ in a humidified 5% CO_2 atmosphere. Media exchange during ESC culture occurred every 2 days and cells were passaged every 3 days before reaching approximately 75% confluency. Monolayer cultures of undifferentiated BMP sentinel cells were maintained in the KO-N2B27 media composed of Knock-out DMEM (Invitrogen-Gibco, Calsbad, CA) supplemented with N2 (Invitrogen- Gibco, Calsbad, CA), B27 (Invitrogen- Gibco, Calsbad, CA), 100 U/ml penicillin, 100 U/ml streptomyocin, 0.25 mg/ml amphotericin, 2 mM L-glutamine, 10 ng/ml bone morphogenetic protein 4 (BMP4) and 10^3 U/ml LIF. Serum-free KO-N2B27 media was used for all suspension ESC aggregate cultures.

Prior to EB formation, cells were treated with trypsin to form a single-cell suspension culture. EBs were formed by forced aggregation of single cell ESCs in micro-well inserts composed of 3% agarose. Briefly, 1000-cell EBs were formed by addition of 1.2 million cells re-suspended in 0.5 ml of media and added to each insert,

containing approximately 1200 wells. Inserts containing cells were centrifuged at 200 x g for 5 min to aggregate cells within individual wells. After 18 h of culture, aggregated cells were removed from wells by gently pipetting with a wide bore pipette tip. Next, EBs were transferred in petri dishes at a concentration of 1200 EBs/ml and maintained in KO N2B27 media. EBs were maintained in suspension culture on rotary orbital shaker at 45 RPM to prevent agglomeration. EBs were re-fed every 3 days and 90% of spent media was exchanged with fresh media. In studies using BMP4 supplementation, 10 ng/ml of soluble BMP4 was added to culture media during initial centrifugation of ESCs in inserts, after transfer of EBs to suspension culture, and at all subsequent media exchanges. Prior to centrifugation, RLPs were re-suspended with ESCs in media and added to inserts. Quantification of RLP incorporation was determined following enzymatic dissociation of EBs via flow cytometry.

4.2.7. Quantification of Raspberry-Like Particle Incorporation

The presence of Rhodamine-B-labeled microgels on RLPs and CFP expressing sentinel cells within EBs was analyzed using an LSM 700-405 confocal microscope (Zeiss, Thornwood, NY). EBs were washed in PBS 3 times, fixed in 10% formalin for 30 min, and stained with either Hoescht (1:100) or ethidium homodimer (1:500) before imaging. For flow cytometry studies, EBs were washed with PBS and dissociated into single cell suspension with 0.25% trypsin-EDTA and trituration for 10 min. The single cell suspension was washed 3 times in PBS and fixed in 10% formalin with centrifugation at 200 x g for 5 min between each wash. Flow cytometry was performed with a BD LSRII flow cytometer (Becton Dickinson, East Rutherford,

NJ) with a minimum of 10,000 events per sample collected within the FSC/SSC gate for cell populations. RLPs and undifferentiated BMP sentinel cells were used to establish appropriate gates and controls. Polygonal gating was used on the FSC/AmCyan (405 nm excitation; 491± emission) plots to limit 1% of untreated embryoid body population ("No RLP" group) via FlowJo software (Tree Star, Inc., Ashland, OR).

Table 4.1. Primers and conditions used for PCR.

Gene	Forward Sequence	Reverse Sequence	Melt Temp. (°C)
18S	CTCTAGTGATCC CTGAGAAGTTCC	ACTCGCTCCACC TCATCCTC	58.0
Oct-4	CCG GTGAGGTGGAGT CTGGAG	GCGATGTGAGTG ATCTGCTGTAGG	58.0
Nanog	GAAATCCCTTCC CTCGCCATC	CTCAGTAGCAGA CCCTTGTAAGC	58.0
Brachyury T	CACACCACTGAC GCACAC	GAGGCTATGAGG AGGCTTTG	58.0
Flk-1	GGCGGTGGTGAC AGTATC	TGACAGAGGCG ATGAATGG	64.3
Pax-6	ACGGCATGTATG ATAAACTAAG	GCTGAAGTCGCA TCTGAG	58.0
AFP	CACACCCGCTTC CCTCATCC	TTCTTCTCCGTC ACGCACTGG	58.0

4.2.8. Gene Expression Analysis

Mesoderm differentiation of EBs treated with BMP4-loaded RLPs was assessed via quantitative PCR. RNA was extracted from undifferentiated ESCs and EBs at Day 2, 4, and 6 of differentiation using the RNeasy Mini Kit (Qiagen, Valencia, CA). Reverse transcription of RNA to complementary DNA was performed using the iScript cDNA synthesis kit (BioRad, Hercules, CA) and was analyzed using SyberGreen technology on the MyIQ cycler (BioRad, Hercules, CA). Forward and

reverse primer sequences for *Oct4*, *Nanog*, *BrachyuryT*, *Flk1*, *Pax6*, *AFP*, and *18S* were designed with Beacon Design software (PREMIER Biosoft, Palo Alto, CA) (**Table 4.1**). Gene expression was quantified with respect to levels of gene expression of undifferentiated ESCs and EBs without RLPs or BMP4 supplementation.

4.2.9. Statistical Analysis

All data are reported as mean ± standard error for a minimum of triplicate experimental samples. A Box-Cox power transformation was used to normalize data to a Gaussian distribution before statistical analysis. Statistical significance was assessed using a one-way ANOVA with Tukey's post hoc analysis. A *p*-value of less than 0.05 was considered statistically significant.

4.3 Results

4.3.1. Raspberry-Like Particle Characterization

DLS data indicate microgels have a low polydispersity with a hydrodynamic radius of approximately 222 ± 2 nm. RLPs were fabricated using a modified version of colloidal-phase mediated heteroaggregation in order to produce larger batches of microparticles to enable investigation of *in vitro* applications (**Figure 4.1**). RLPs exhibit a low polydispersity as seen via optical microscopy. SEM imaging reveals that the polystyrene core particle is fully covered by microgels, which would present a soft, biocompatible surface to the surrounding cells. Confocal microscopy imaging indicates that the microgels are fully swollen and cover the majority of the core particle in solution. Fabrication of RLPs produced approximately 18 million RLPs per mg of polymer with a narrow size distribution of 4.6 ± 1.0 μm in diameter.

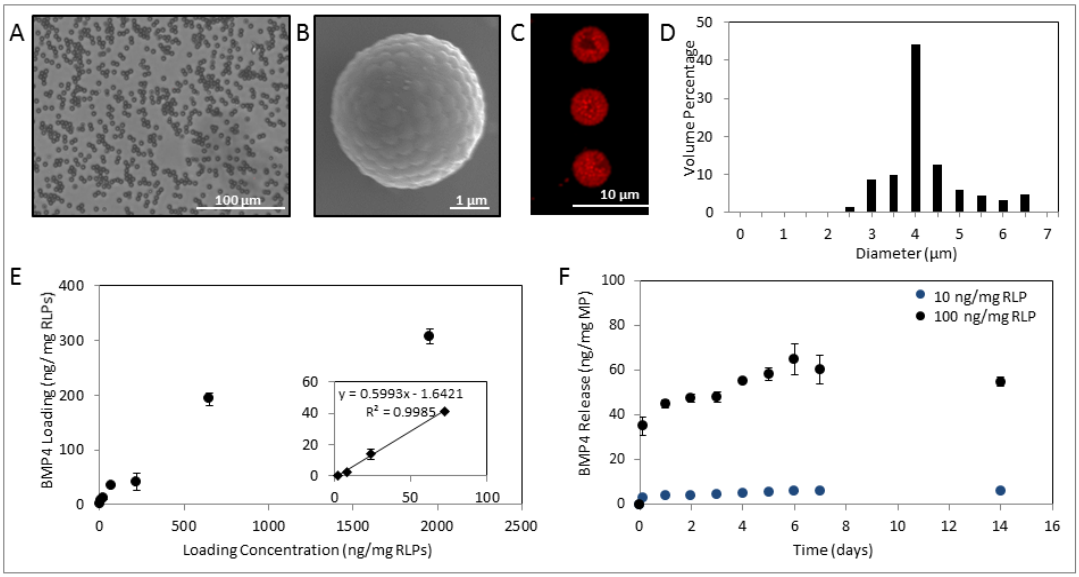

Figure 4.1. RLPs were fabricated using colloidal-phase mediated heteroaggregation. RLP morphology was characterized via (A) optical microscopy, (B) SEM, and (C) laser scanning confocal microscopy. (D) RLP size distribution was analyzed via coulter counter. (E) Binding and (F) release of the growth factor BMP4 to RLPs was determined through loading and depletion studies.

The microgels are negatively charged, due to their acrylic acid content, allowing for electrostatic interactions with positively charged BMP4 (pI = 8.97). The "breathing in" method was used to load RLPs with BMP4. The RLP binding capacity of BMP4 was examined by analyzing the depletion of BMP4 from solution using a fixed amount of RLPs (1 mg) and a range of BMP4 concentrations, ranging from 2-2,000 ng protein per mg RLPs (**Figure 4.1E**). Loading studies reveal that RLP binding capacity of BMP4 increases with increasing concentrations of BMP4. The relationship between RLP bound BMP4 and loading concentration of BMP4 is relatively linear (R^2 = 0.998) at BMP4 concentrations below 100 ng per mg RLPs with approximately 71.7% ± 16.9% of BMP4 binding to microparticles. However, at BMP4 concentrations above 100 ng per mg RLP, the efficiency of BMP4 binding

decreases to approximately 45.0% ± 14.9%. Average loading efficiency for BMP4 is 55.5 ± 6.2%.

Release of BMP4 from RLPs was assessed at a low (10 ng per mg of RLPs) and a high (100 ng per mg of RLPs) concentration of BMP4 at 37 °C (**Figure 4.1F**). RLPs loaded with the high concentration of BMP4 demonstrate a greater initial burst release within the first 3 hours (< 40%) and release a larger amount of BMP4 over 14 days than RLPs loaded with the low concentration of BMP4. RLPs loaded with low concentrations of BMP4 appear to exhibit a burst release followed by limited or no additional release taking place over time. Overall, total release of BMP4 after 14 days was approximately 60% of loaded protein, indicating that the majority of the protein is released by the RLPs.

4.3.2. Delivery of BMP4 to Embryoid Bodies via Raspberry-Like Particles

RLPs were incorporated within ESC aggregates using forced aggregation via centrifugation within agarose microwells at 1:10, 1:3, 1:1, and 3:1 (RLPs:cell) seeding ratios. Rhodamine B-labeled RLPs incorporated within aggregates were identified via confocal microscopy (**Figure 4.2**). Maximum RLP incorporation within aggregates was achieved with approximately 80 RLPs per ESC aggregate at a RLP to cell seeding ratio of 1:1, which was used for all subsequent studies. Incorporation efficiency of microparticles within aggregates decreases as the number of microparticles to cell ratio increases. Unfortunately, we see < 20% RLP incorporation for all ratios.

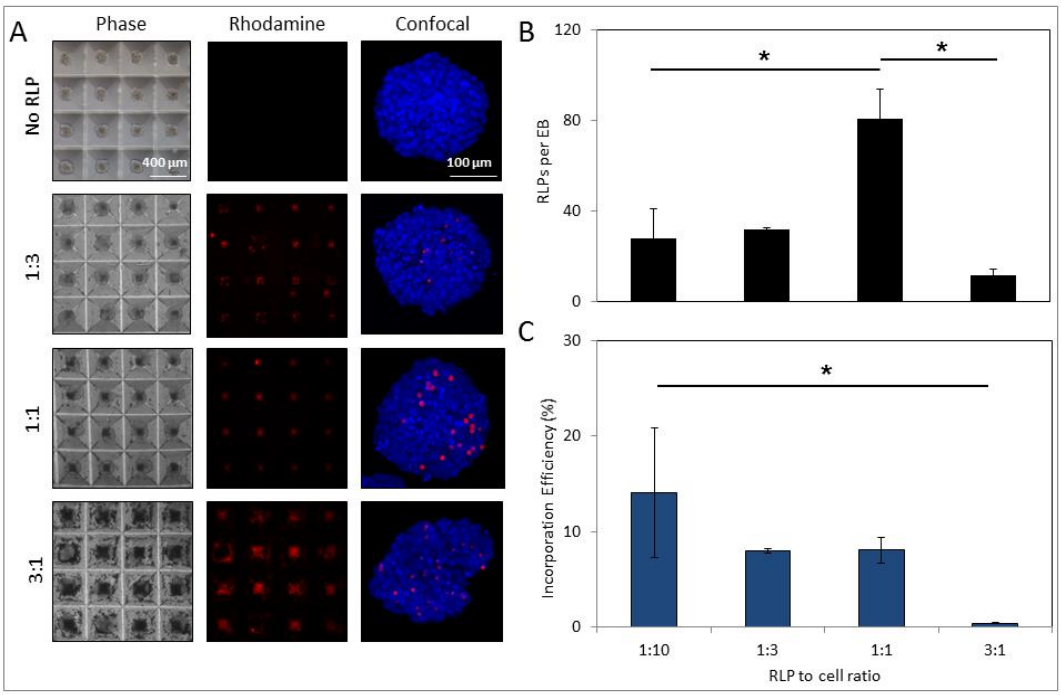

Figure 4.2. RLPs were incorporated within pluripotent stem cell aggregates. ESCs were centrifuged alone or with Rhodamine-B–labeled RLPs to form aggregates in µ-wells before transfer to a rotary orbital suspension culture. RLPs were incorporated in EBs at RLP:cell seeding ratios of 1:10, 1:3, 1:1 and 3:1. (A) Visualization of RLP incorporation was performed via laser scanning confocal microscopy. (B and C) Quantitative analysis of RLP incorporation was performed via flow cytometry (* $p < 0.05$). Images and flow cytometry data kindly collected by Ms. Denise Sullivan.

Scheme 4.5. Experimental design.

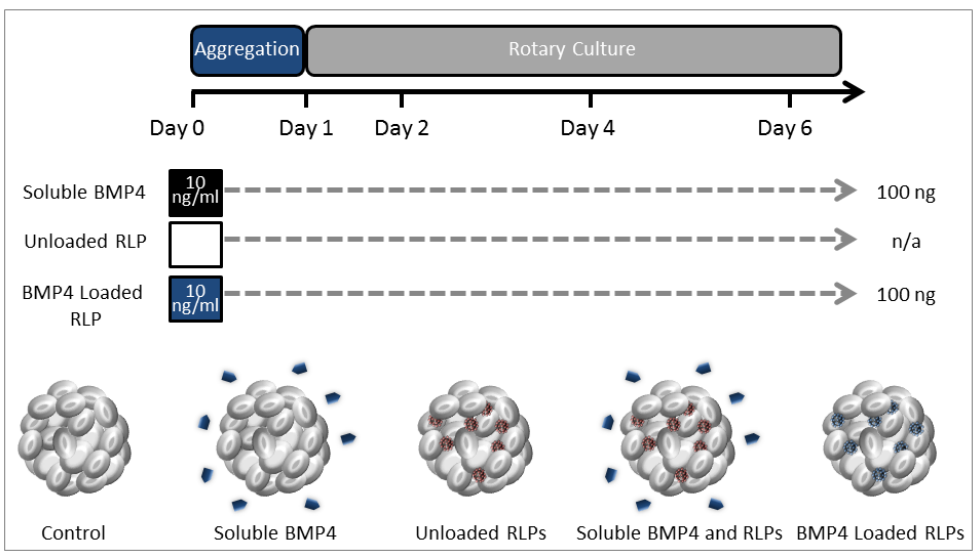

RLPs were used to deliver BMP4 within ESC aggregates to direct mesoderm differentiation under serum-free conditions. BMP4 delivery via RLPs to ESC aggregates was compared to unloaded RLPs and soluble BMP4 with or without incorporation of unloaded RLPs. BMP4 was delivered by RLPs at a loading concentration of 1500 ng of growth factor per mg of RLPs. The total corresponding amount of growth factor delivered via RLPs to 1200 EBs per culture plate was 10 ng of BMP4. Subsequently, growth factor delivery via RLPs was 10-fold less than the total amount of 100 ng of soluble BMP4 supplemented at the beginning of ESC aggregate culture (**Scheme 4.5**). After 6 days of culture, gene expression of pluripotency markers, Oct4 and Nanog, early lineage commitment markers, BrachyuryT, Flk1, Pax6, and AFP, were analyzed (**Figure 4.3**). As expected, all experimental groups demonstrate decreased expression of pluripotent transcription factors Oct4 and Nanog over the course of differentiation. No significant differences in the expression of the mesoderm marker BrachyuryT are observed between treatment groups. However, delivery of soluble BMP4 loaded RLPs results in increased expression of mesoderm marker Flk-1 and decreased expression of ectoderm marker Pax6. BMP4 loaded RLPs demonstrate similar expression of Flk1, Pax6, and AFP (endoderm marker) with no significant differences as compared to soluble delivery. Interestingly, only ESC aggregates treated with BMP4 loaded RLPs demonstrate significant differences in Pax6 expression as compared to all other treatment groups.

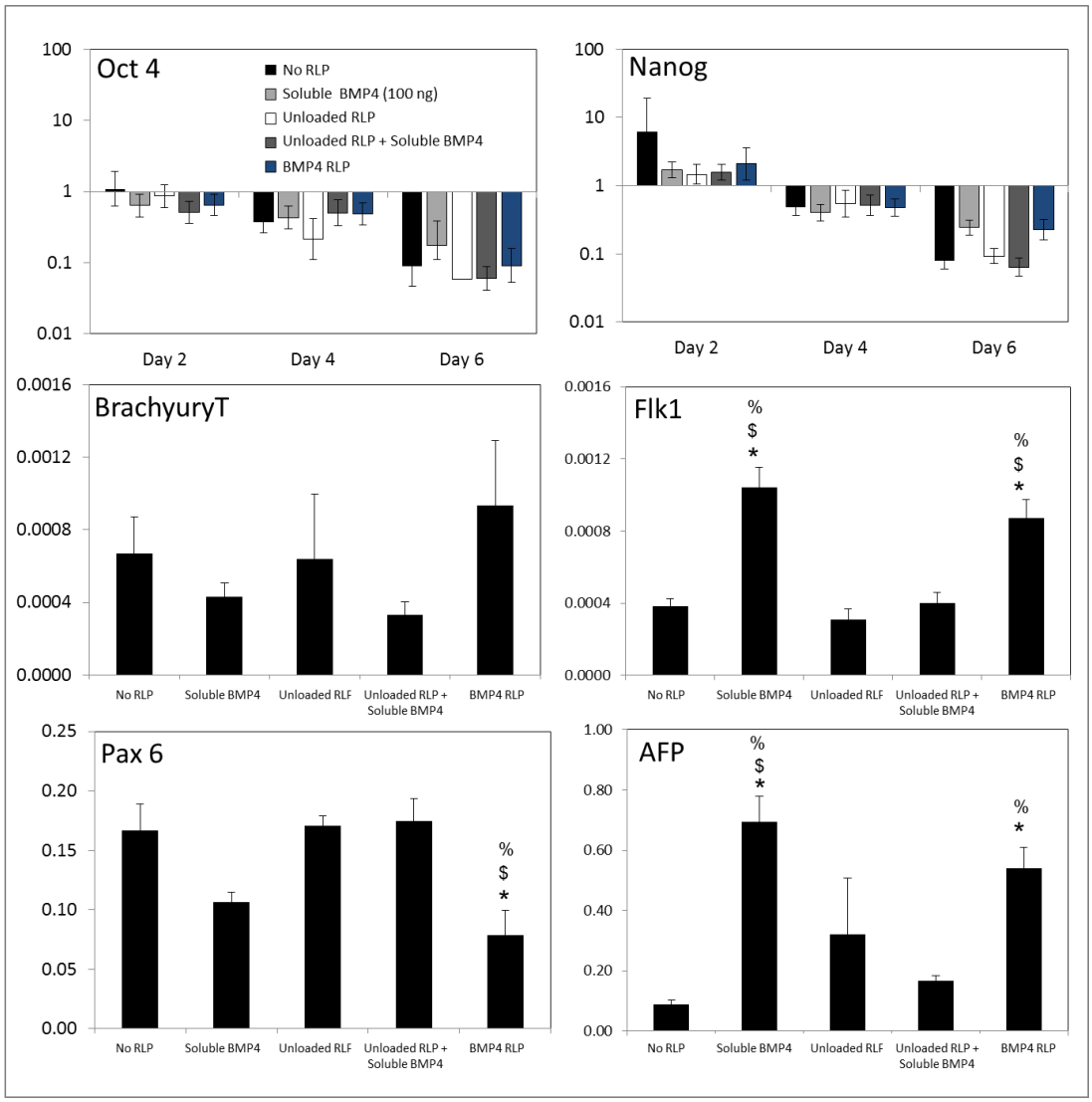

Figure 4.3. BMP4 loaded RLPs incorporated within pluripotent stem cell aggregates induce mesoderm differentiation. Changes in ESC gene expression of common markers associated with pluripotency and early lineage commitment was compared between soluble delivery and RLP delivery of BMP4 added during ESC aggregate formation over 6 days of culture (* = significantly from No RLP; $ = significantly from Unloaded RLP; % = significantly from Unloaded RLP + Soluble BMP4, $p < 0.05$). Gene expression analysis was performed by Ms. Denise Sullivan.

4.4. Discussion

In the present contribution, we demonstrate that raspberry-like microgel heteroaggregates mediate delivery of BMP4 within ESC aggregates and can be used

as a biomaterial based strategy to control the temporal release of growth factors to direct ESC differentiation. Exploration of this synthetic construct has demonstrated enhanced control over particle homogeneity. Microgel characterization indicates low polydispersity, an important feature of these synthetic constructs for controlled loading and release of morphogens in comparison to other naturally derived delivery vehicles. Characterization indicates that colloidal-phase mediated heteroaggregation produces a well-coated population of RLPs with low heterogeneity in terms of microgel coverage. Consistent microgel coverage is critical for presentation of a chemically and mechanically biocompatible synthetic material to the surrounding cells. RLPs also exhibit a low polydispersity (~1 μm) in comparison to previously explored natural constructs such as PLGA or heparin based microparticles that can have polydispersity values on the order of tens of microns.[24-26] The low polydispersity of both microgels and RLPs minimizes variations in payload and release rates of BMP4, a critical aim of this synthetic approach. The total amount of BMP4 released from RLPs is dependent on initial growth factor loading concentration; however more than 50% of BMP4 is released over a period of 14 days regardless of the initial amount of bound growth factor.

RLPs exhibit minimal aggregation at all stages of use, which is ideal for delivery and release vehicles that must be loaded in the dry state as many other constructs exhibit significant clumping and an inability to disperse loaded constructs. RLP incorporation studies also reveal minimal aggregation and clumping occur *in vitro*, which promote the development of a more even BMP4 concentration throughout the entire EB. The low incorporation efficiency of RLPs is most likely due

to lack of cell adhesive sites; previous studies demonstrated that incorporation efficiency of microparticles is directly dependent on the adhesive character of a material with more adhesive materials resulting in increased incorporation within ESC aggregates.[26] No significant differences are observed in the formation of ESC aggregates at RLP to cell seeding ratios of 1:10, 1:3, and 1:1. In contrast, ESC aggregate formation is hindered at higher RLP to cell seeding ratios resulting in smaller and less spherical shaped aggregates, suggesting that the presence of too many RLPs may affect the formation of necessary cell-to-cell contacts. Increased RLP incorporation could be promoted by the development of RLPs using microgels conjugated with the peptide sequence Arginine-Glycine-Asparagine (RGD) for enhanced cellular adhesion.

RLP delivery of BMP4 within ESC aggregates results in similar expression of mesoderm and ectoderm markers as compared to soluble delivery. While we observe no significant differences in expression of transient mesoderm marker BrachyuryT, expression of Flk1 is significantly increased in groups treated with either soluble BMP4 or BMP4 loaded RLPs. Furthermore, expression of Pax6 is significantly downregulated in ESCs treated with BMP4 loaded RLPs as compared to all other treatment groups. ESCs typically default to neural differentiation under basal conditions, suggesting that BMP4 loaded RLPs more efficiently direct ESCs away from a more neural fate and towards mesoderm as compared to conventional soluble delivery approaches. Overall, these results indicate that RLP delivery of BMP4 within ESC aggregates, even with 10-fold less protein delivered as compared to soluble

BMP4 supplementation, can be used to modulate ESC differentiation and induce comparable gene expression.

Further understanding of the influence of the delivery of BMP4 at later time points could be explored using RLPs with microgel compositions tailored to delayed and/or prolong BMP4 release as opposed to an initial burst release. Such constructs could demonstrate the long-term efficacy of RLP delivery of BMP4 as a means to induce synchronous organized ESC differentiation. RLPs can be used as a functional experimental tool by tailoring their composition for the loading and release of specific morphogens based on their size and charge. Using the modified synthesis method pioneered in this work, RLPs can be fabricated with a yield that is orders of magnitude larger than the previously established method, producing batches that are useful for further applications studies. This fabrication method allows for the facile development of a platform of RLPs uniquely tailored to release specific morphogens to induce controlled differentiation of stem cell aggregates down a number of phenotypic paths. Finally, due to the unique responsivity of microgels, more complex constructs can be envisioned for other stem cell engineering applications such as sequestration of extracellular factors using thermoresponsive, magnetic RLPs for facile separation.

4.5. Conclusion

Herein we demonstrate that the synthetic RLP microparticle construct is a competitive experimental tool for controlled loading and release of morphogens within stem cell aggregates. Loading and release studies demonstrate that RLPs can load and release BMP4 in a controlled manner. Incorporation studies reveal that RLPs

can be incorporated within an EB with minimal particle aggregation. Gene expression analysis reveals that RLP burst release profile of BMP4 significantly influences early time points in the differentiation process. Further studies will be targeted towards delaying BMP4 release to influence differentiation at later time points. Using a facile synthetic approach to mediate morphogen delivery enables the development of delivery vehicles for future investigation of EB differentiation. Future studies will be focused on tailoring RLP composition for controlled release of other morphogens such as VEGF and the use of RLPs for sequestration of secreted growth factors.

4.6. References

1. Thomson J.A.; Itskovitz-Eldor, J.; Shario, S.S.; Waknitz, M.A.; Swiergiel, J.J.; Marshall, V.S.; Jones, J.M., Embryonic stem cell lines derived from human blastocysts. *Science*. **1998**, *282* (5391), 1145–7.

2. Murry C.E.; Keller G., Differentiation of embryonic stem cells to clinically relevant populations: lessons from embryonic development. *Cell*. **2008**, *132* (4), 661–80.

3. Keller, G., Embryonic stem cell differentiation: emergence of a new era in biology and medicine. *Genes Dev.* **2005**, *19*, 1129-1155

4. Bratt-leal, M.; Carpenedo, R.L.; McDevitt, T.C., Engineering the embryoid body microenvironment to direct embryonic stem cell differentiation. *Biotechnol. Prog*. **2009**, *25* (1), 43–51.

5. Risau, W.; Sariola, H.; Zerwes, H.G.; Sasse, J.; Ekblom, P; Kemler, R.; Doetschman, T., Vasculogenesis and angiogenesis in embryonic-stem-cell-derived embryoid bodies. *Development*. **1988**, *478*, 471–8.

6. Wang, R.; Clark, R.; Bautch, V.L., Embryonic stem cell-derived cystic embryoid bodies form vascular channels : an in vitro model of blood vessel development. *Development*. **1992**, *114* (2), 303–16.

7. Kinney, M.A.; McDevitt, T.C., Emerging strategies for spatiotemporal control of stem cell fate and morphogenesis. *Trends biotechnol*. **2014**, *31* (2), 78–84.

8. Nostro, M.C.; Cheng, X.; Keller, G.M.; Gadue, P., Wnt, activin, and BMP signaling regulate distinct stages in the developmental pathway from embryonic stem cells to blood. *Cell Stem Cell*. **2008**, *2* (1), 60–71.

9. Purpura, K.A.; Morin, J.; Zandstra, P.W., Analysis of the temporal and concentration-dependent effects of BMP-4, VEGF, and TPO on development of embryonic stem cell-derived mesoderm and blood progenitors in a defined, serum-free media. *Experimental Hematol*. **2008**, *36* (9), 1186–98.

10. Sachlos, E.; Auguste, D.T., Embryoid body morphology influences diffusive transport of inductive biochemicals: a strategy for stem cell differentiation. *Biomaterials*. **2008**, *29* (34), 4471–80.

11. Van Winkle, A.P.; Gates, I.D.; Kallos, M.S., Mass transfer limitations in embryoid bodies during human embryonic stem cell differentiation. *Cells Tissues Organs.* **2012**, *196* (1), 34–47.

12. Carpenedo, R.L.; Bratt-Leal, A.M.; Marklein, R.A.; Seaman, S.A.; Bowen, N.J.; McDonald, J.F.; McDevitt, T.C., Homogeneous and organized differentiation within embryoid bodies induced by microsphere-mediated delivery of small molecules. *Biomaterials.* **2009**, *30* (13), 2507–15.

13. Bratt-Leal, A.M.; Nguyen, A.H.; Hammersmith, K.A.; Singh, A.; McDevitt, T.C., A microparticle approach to morphogen delivery within pluripotent stem cell aggregates. *Biomaterials*. **2013**, *34* (30), 7227–35.

14. Ferreira, L.; Squier, T.; Park, H.; Choe, H.; Kohane, D.S.; Langer, R., Human embryoid bodies containing nano- and microparticulate delivery vehicles. *Adv. Mater*. **2008,** *20* (12), 2285–91.

15. Purpura, K.A.; Bratt-Leal, A.M.; Hammersmith, K.A.; McDevitt, T.C.; Zandstra, P.W., Systematic engineering of 3D pluripotent stem cell niches to guide blood development. *Biomaterials*. **2011**, *33* (5), 1–10.

16. Oh, J.K,; Drumright, R.; Siegwart, D.J.; Matyjaszewski, K., The development of microgels/nanogels for drug delivery applications. *Prog. Polym. Sci.* **2008**, *33* (4), 448–77.

17. Gao, Y.; Zago, G.P.; Jia, Z.; Serpe, M.J., Controlled and triggered small molecule release from a confined polymer film. *ACS Appl. Mater. Interfaces.* **2013**, *5* (19), 9803–8.

18. Nolan, C.M.; Serpe, M.J.; Lyon, L.A., Thermally modulated insulin release from microgel thin films. *Biomacromolecules.* **2004**, *5* (5), 1940–6.

19. Smith MH, Lyon LA. Tunable encapsulation of proteins within charged microgels. *Macromolecules.* **2012**, *44* (20), 8154–60.

20. Klinger, D.; Landfester, K., Stimuli-responsive microgels for the loading and release of functional compounds: fundamental concepts and applications. *Polymer.* **2012**, *53* (23), 5209–31.

21. Zhang, Y.; Zhu, W.; Wang, B.; Ding, J., A novel microgel and associated post-fabrication encapsulation technique of proteins. *J. Control. Release.* **2005**, *105* (3), 260–8.

22. Jones, C.D.; Lyon, L.A., Synthesis and characterization of multiresponsive core - shell microgels. *Macromolecules.* **2000**, *33*, 8301–6.

23. Gaulding, J.C., Saxena, S.; Montanari, D.E.; Lyon, L.A., Packed colloidal phases mediate the synthesis of raspberry- structured microgel heteroaggregates. *ACS Macro Lett.* **2013**, *3*, 337–40.

24. Carpenedo, R.L.; Seaman, S.A.; McDevitt, T.C., Microsphere size effects on embryoid body incorporation and embryonic stem cell differentiation. *J. Biomed. Mater. Res. A.* **2010**, *94* (2), 466–75.

25. Bratt-Leal, A.M.; Carpenedo, R.L.; Ungrin, M.D.; Zandstra, P.W.; McDevitt; T.C., Incorporation of biomaterials in multicellular aggregates modulates pluripotent stem cell differentiation. *Biomaterials.* **2011**, *32* (1), 48–56.

26. Hettiaratchi, M.H.; Miller, T.; Temenoff, J.S.; Guldberg, R.E.; McDevitt, T.C.; Heparin microparticle effects on presentation and bioactivity of bone morphogenetic protein-2. *Biomaterials.* **2014**, *35* (25), 7228–38.

CHAPTER 5

TRADITIONAL PLANAR MICROGEL FILM ASSEMBLIES

Portions adapted from:
Saxena, S.; Spears, M.W.; Yoshida, H.; Gaulding, J.C.; Garcia, A.J.; Lyon, L.A. Microgel film dynamics modulate cell adhesion behavior. *Soft Matter*. **2014**, *10*, 1356-1364.
With kind permission from Royal Society of Chemistry.

5.1. Introduction

Cellular activity is known to be influenced by surrounding environmental factors.[1-3] In the past, researchers who have investigated biomaterials have focused on the influence of bulk properties on cellular behavior such as elastic modulus.[4-6] However, recently investigators have realized the impact that length-scale has on the properties being investigated and have shifted primary focus from the macro-environment to the micro- or even nano-scale environment.[7] This shift has been enabled by technological innovations that have emerged from the fields of nanomaterials and nanotechnology. Advancements in nano-fabrication techniques have allowed more precision and detail both in construction and investigation of the cellular environment. For instance, nano-pillar arrays made with precise control over pillar position and flexibility allowed for collection of previously immeasurable cell traction forces.[8-9] In another example, creation of a patterned elastomeric substrate allowed measurement of focal adhesion forces as the pattern was disrupted.[10] Other factors such as roughness[11] and chemical functionalization[12-13] have also been designed into systems to exert greater control over cell behavior.

Scheme 5.1. The physiological response to a biomaterial involves protein adhesion and cellular adhesion.

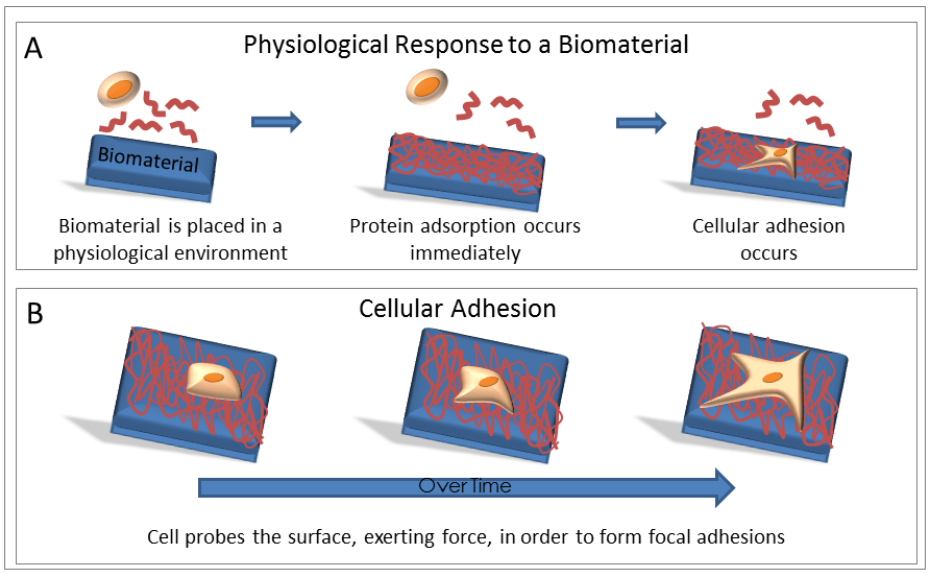

Biomaterials placed in physiological conditions immediately adsorb protein on the exposed surface soon followed by cell adherence (**Scheme 5.1A**).[14-15] Cellular adherence is often correlated with the amount of protein and the nature of specific interactions with surface receptors. For example, the amount of adsorbed fibronectin on bioactive glass correlates with the strength of osteoblast adhesion to the surface.[16] Cell adhesion to a synthetic surface or a natural matrix is a complex process that involves integrin receptors in the cell membrane binding to surface-localized proteins. These proteins, such as fibronectin, may be produced by the cells as they seek to strengthen their adherence, adsorbed from the medium, or even built directly into the material in the case of designed biointerfaces.[13] Since cellular adhesion is critical in cell functions, substrates are often functionalized with ECM proteins or related peptides such as RGD to improve cell attachment.[15] Following ligand binding, integrins cluster together and recruit cytoskeletal and signaling components to form

focal adhesions. These focal adhesion clusters are the primary way in which a cell interacts with its environment, providing feedback and mechanical cues about the surrounding material through the cell's cytoskeleton.[17]

Cells exert force on their surrounding environment as they attempt to probe the material properties through mechanosensing (**Scheme 5.1B**). Recent studies suggest that the primary mechanical property that controls cell adhesion and spreading is the elastic modulus, *E*.[18] Elasticity of the substrate can influence stem cell differentiation[19] and other cell functions such as movement[20] and nanoparticle uptake.[21] A cell can exert a significant amount of force on its surroundings. Munevar *et al.* measured the traction force of NIH3T3 fibroblasts on polyacrylamide substrates to be 3.03 nN/μm^2.[22] Galbraith and Sheetz measured the force exerted by an adhesive contact on a micro-machined silicon lever device to be approximately 3 nN.[23] Cells also have a characteristic appearance based on the modulus of the material that they are experiencing. "Hard" surfaces result in cell spreading and cytoskeletal organization, whereas "soft" surfaces result in rounded morphologies without the ability to form focal adhesions. In this context, "hard" surfaces are those having E > 10 kPa, because above this approximate threshold, cells adhere strongly and show little variation in adhesion characteristics regardless of elastic modulus. However, below this threshold (which we will consider "biologically soft"), cells have extraordinary sensitivity to the material modulus.[24]

The elastic component of biomaterials has been broadly studied, because the elastic modulus of a material can often be altered without great synthetic effort. However, not as much attention has been paid to the viscous component of

biomaterials. The questions of how biophysical forces are able to remodel a cell's surroundings or how movement of the surroundings is able to control cell behavior are largely unexplored. The difficulty in answering these questions lies primarily in selection and synthesis of a material with viscoelastic properties that respond to small forces on the time scale of cellular processes.

Scheme 5.2. Traditional Layer-by-Layer microgel film fabrication

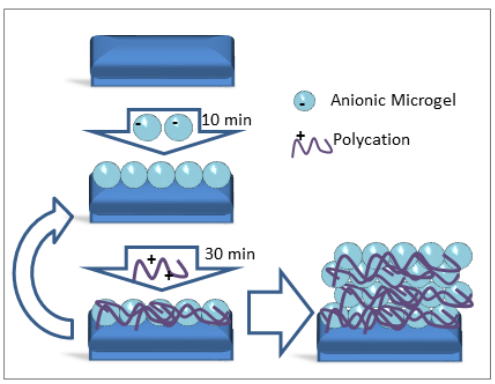

Microgels have been used extensively as building blocks in the fabrication of thin films as either monolayers or Layer-by-Layer (LbL) multilayer films as described in section **1.4.3.** (**Scheme 5.2**).[25-26] We have previously shown that microgel LbL films have the ability to heal mechanically induced damage when sufficiently hydrated.[27-28] This self-healing behavior is similar to other LbL polyelectrolyte systems that can recover from damage when exposed to water.[29] The self-healing process that microgel films exhibit suggests that they are dynamic materials that exhibit viscoelastic behavior on short time scales and small length scales.

Previous work in the Lyon Group demonstrated the non-fouling nature of

microgel films. The earliest studies assessed protein fouling and cell adhesion on a monolayer of poly(ethylene glycol diacrylate) (PEGDA) cross-linked microgels spin-coated onto glass. The amount of protein adsorption was low, with protein fouling decreasing as the length of the PEG cross-linker was increased. It was also found that microgel layers resisted cell attachment for several days, but surfaces not modified with PEGDA-containing microgels showed significant cell adhesion and proliferation.[30] A further study was conducted using the centrifugal deposition technique for building microgel films, which packs the particles tightly on the surface and ensures that no substrate is exposed. Four-layer microgel films strongly resisted cell attachment compared to glass or tissue culture polystyrene (TCP).[31] In addition, microgel-coated polyethylene terephthalate (PET) disks implanted in rats for 4 weeks resulted in a reduced inflammatory response relative to controls.[32] These successes prompted further study into the behavior of cells on microgel-modified substrates and exploration into the mechanism of adhesion resistance.

Given these previous studies, the growing knowledge of the dynamic nature of microgel multilayer films led the Lyon Group to investigate the properties of the film as a means of controlling cell adhesion. Salloum *et al.* demonstrated alteration of vascular smooth muscle cell behavior by manipulating surface charge and hydrophobicity of polyelectrolyte multilayers (PEM's).[33] PEM's can be manipulated to affect cell adhesion and spreading by varying cross-linker amounts within the film[34] or by tuning film compliance through assembly at varying pH conditions.[35] Responsive microgel films have also been used in the thermally-triggered detachment of cells, taking advantage of the changes in microgel softness during swelling.[36] In

principle, dynamic microgel multilayers also serve as intriguing substrates with which to study the effect of mechanical properties on cell behavior. For example, the rapid reorganization of the film components following perturbation (i.e. self-healing) could occur during cell attachment and spreading. This reorganization essentially represents a viscoelastic property of the film; the organization of the building blocks changes in response to an applied stress without a subsequent elastic recovery. Thus, we hypothesized that the viscoelasticity of microgel films could play a significant role in the process of cell attachment and spreading in a manner that differed from what might be predicted due to the film elasticity alone.

5.2. Experimental

5.2.1. Materials

Materials used in this investigation are described in section **2.2.1** with the following additions. Acrylic acid (AAc) and poly(ethylene glycol) diacrylate (PEGDA) (Mw = 575 Da) were used as received. Poly(diallyldimethylammonium chloride) (PDADMAC) (Mw = 400-500 kDa) and branched polyethyleneimine (PEI) (typical Mw = 750 kDa) 50% w/w solution in water were both prepared as 0.1 monoM and 0.1 monoM solutions in water, respectively.

5.2.2. Microgel Synthesis

Microgels were synthesized as previously described.[37] Microgels were synthesized using the procedure outlined in section **2.2.2** with a few modifications. The total monomer concentration was 100 mM with a molar composition of 66% NIPAm, 30% AAc, and either 4% PEGDA or 4% BIS. NIPAm, SDS, and either

PEGDA or BIS were dissolved in water. The solution was added to a 3-neck round bottom flask and heated to 70 °C while purging with nitrogen and stirring for 1 h. AAc was added 10 min prior to reaction initiation; 1 mL of APS solution in water was added and the reaction was allowed to proceed for 4 h.

5.2.3. Microgel Characterization

Diffusion coefficients were determined by dynamic light scattering (DLS) using a Protein Solutions DynaPro DLS (Wyatt Technology Corporation, Santa Barbara, CA) equipped with temperature control. Hydrodynamic radii (R_H) and polydispersity values were calculated using Dynamics software for each particle type used in these experiments. All DLS measurements were carried out at 25 °C in either 10 mM PBS at pH 7.4 and 100 mM NaCl ionic strength or 10 mM formate buffer at pH 3.0 with 100 mM NaCl ionic strength to confirm incorporation of acid groups and pH responsivity (**Table 5.1**).

5.2.4. Film Construction

Films for AFM force mapping and cell adhesion studies were assembled on amine-functionalized glass coverslips. To functionalize the surface, the substrates were shaken in 1% APTMS in absolute ethanol for 2 h. After rinsing, the film was equilibrated in 10 mM pH 7.4 PBS with 100 mM NaCl ionic strength control for 30 min. The functionalized substrate was centrifuged at 2250 x g for 10 min in a 0.1 mg/mL microgel solution to deposit the first layer. The first layer of each film was covalently attached to the surface through EDC coupling. The film was equilibrated in 10 mM pH 5.5 MES buffer with 100 mM NaCl ionic strength control for 30 min, then

transferred to a solution of 2 mM EDC / 5 mM NHS prepared in MES buffer and allowed to shake at room temperature for 2 h. Film buildup then proceeded by rinsing with water and shaking in 8.6 mg/mL PEI (750 kDa) or 0.1 monoM PDADMAC (400-500 kDa) solution for 30 min. This process was repeated to a total of 4 layers of microgels with microgels being the final layer. The following film types were created:

PEGDA-PDADMAC: PEGDA-containing microgels identical in composition to those used in our previously published work[31] deposited via PDADMAC LbL assembly up to four layers.

BIS-PDADMAC: BIS-containing microgels deposited via PDADMAC LbL assembly up to four layers.

BIS-PEI: BIS-containing microgels deposited via PEI LbL assembly up to four layers.

5.2.5. Film Cross-linking

In cases where the entire film was to be cross-linked, the coupling reaction was repeated after the film was completely assembled. The film was equilibrated in 10 mM pH 5.5 MES buffer with 100 mM NaCl ionic strength control for 30 min prior to cross-linking reaction. Films were then transferred to a solution of 8 mM EDC / 20 mM NHS prepared in MES buffer. The reaction was allowed to proceed for 2 h at room temperature while shaking. After the cross-linking reaction, the films were rinsed with water and immersed in a 40 mM glycine solution in MES buffer for 2 h to quench residual cross-linking reagents.

5.2.6. Atomic Force Microscopy

Atomic Force Microscopy (AFM) force mapping was used to determine the

elasticity of the microgel films. AFM has been used previously to probe the micro-environment elasticity of tissues and substrates in contact with cells, using a technique where the AFM tip is brought into contact with the surface to act as a nano-indenter.[38] Films were imaged and force mapped using an MFP-3D AFM from Asylum Research (Santa Barbara, CA). Images in air were collected in AC mode using silicon SPM probes with Al reflex coating, and a 42 N m^{-1} nominal force constant (Nanoworld, NCHR). Images in liquid were collected in contact mode using silicon nitride probes with Cr/Au reflex coating, and a 0.09 N m^{-1} nominal spring constant (Asylum, BL-TR400PB) mounted in the iDrive cantilever holder. All force curves were collected in contact mode. The samples were allowed to equilibrate in 10 mM, pH 7.4 PBS with 100 mM NaCl ionic strength control for approximately 30 min in the AFM chamber before analysis. Exact spring constants were determined on a clean glass coverslip by a combination of force curves and a thermal spectrum calibration using methods in the MFP-3D software. Force maps were collected as a 32 x 32 array of force curves with trigger point = 0.3 V. Elastic moduli were determined via the MFP-3D analysis tools using the Hertz model, assuming a Poisson ratio of 0.5 for the films, and assigning the appropriate tip geometry as a cone. Reported values were calculated by averaging all points from a force map on each of 3 separate samples and calculating a standard deviation for all points.

5.2.7. Protein Adsorption Assay

Human plasma fibronectin (FN, Mw: 400k - 500k, 500 μg/mL, Invitrogen, Calsbad, CA) was coupled with Alexa Fluor® 488 succinimidyl ester (1 mg/mL, Molecular Probes, Eugene, OR) in 0.1M $NaHCO_3$ (pH 9.0, 100 μL) for 2 h at room

temperature. Unreacted fluorescent label was removed by filtration and washing in PBS (pH 7.4) using Millipore (Billerica, MA) Amicon Ultra-15 centrifugal filtration units (3,000 MWCO). Fibronectin was recovered from the filter and the purified solution was diluted to approximately 2 ng/mL. The microgel films were immersed in 1 mL of the FN solution, kept for 24 hours at 37 °C, and washed with PBS three times. Fluorescence intensity of adsorbed FN was measured by a Biotek (Winooski, VT) Synergy H4 Multi-Mode Plate Reader. Films for stretching analysis after exposure to cell culture medium were treated according to the same procedure.

5.2.8. Cell Adhesion Assay

Microgel films were prepared in the same manner as above. The samples were washed with PBS 3 times and then immersed in 1 mL of Dulbecco's modified Eagle medium (DMEM) containing 10% fetal bovine serum (FBS). NIH3T3 fibroblast cells were seeded on the samples at the concentration of 2500 cells/cm^2 and cultured for 24 h in a CO_2 incubator (37 °C, 5% CO_2). Cells attached to the microgel films were stained by incubation in 1 mL of PBS containing 2 mM of calcein-AM and 4 mM of ethidium homodimer (EthD-1) (LIVE/DEAD Viability/Cytotoxicity Assay, L3224, Molecular Probes) for 30 min at room temperature and imaged with a Nikon (Tokyo, Japan) Eclipse E400 fluorescence microscope. 20 images were recorded and analyzed from each of 3 samples. The number of attached cells was counted, and cell adhesion area was calculated in ImageJ for at least 200 cells per sample. For focal adhesion staining, vinculin was immunostained according to the following procedure: cells were permeabilized in cytoskeleton buffer (CSK), once in CSK (-) and twice in CSK (+) buffer [CSK(-): 3.02 mg/mL PIPES, 2.92 mg/mL NaCl, 0.61 mg/mL $MgCl_2$-

$6H_2O$, and 51.3 mg/mL sucrose dissolved in water and adjusted to pH 6.8; CSK(+): same as CSK (-) plus 1 mM phenylmethylsulfonyl fluoride, 1 μg/mL leupeptin, 1 μg/mL aprotinin, 1 μg/mL pepstatin, and 0.5% Triton X-100] then fixed in 4% paraformaldehyde, and blocked in 1% goat serum. Finally, they were incubated with monoclonal anti-vinculin antibody produced in mouse (V4505, Sigma-Aldrich) against vinculin followed by Alexa Fluor® 488 goat anti-mouse IgG (A11001, Molecular Probes), and gelled overnight for approximately 14 hours with Prolong® Gold antifade reagent with DAPI (Invitrogen, Calsbad, CA).

5.3. Results and Discussion

5.3.1. Characterization of Microgel Films

The composition and tunable properties of these films allowed interrogation of the hypothesis that microgel film viscoelastic properties are a controlling factor in cell adhesion behavior. PDADMAC presents little opportunity for facile modification of covalent film connectivity, as it has no readily accessible reactive groups for conjugation. However, PEI is a highly branched polycation that similarly has many charged sites available for Coulombic interactions during the Layer-by-Layer buildup process. In addition, using PEI as the polycation introduces reactive amines into the film, enabling post-synthetic conjugation to the acid sites incorporated in the microgels. Films were either used as-prepared or the film mechanical properties were modulated by chemically cross-linking film components, thereby altering the elastic components as well as restricting the mobility of the components of the film (**Scheme 5.3**). The cross-linking reaction bound free amines on PEI to carboxylic acid groups

on the microgels using EDC/NHS carbodiimide coupling, a common bio-conjugation strategy (**Scheme 5.4**). However, since PDADMAC does not contain primary amines, there are no opportunities for cross-linking reactions between the microgels and the polycation.

Table 5.1. Microgel characterization.

Microgel	R_H, nm (pH 3.0)	R_H, nm (pH 7.4)
pNIPAm, BIS, AAc	239 ± 77	524 ± 104
pNIPAm, PEDGA, AAc	277 ± 25	510 ± 31

Scheme 5.3. EDC/NHS cross-linking may alter microgel film mobility

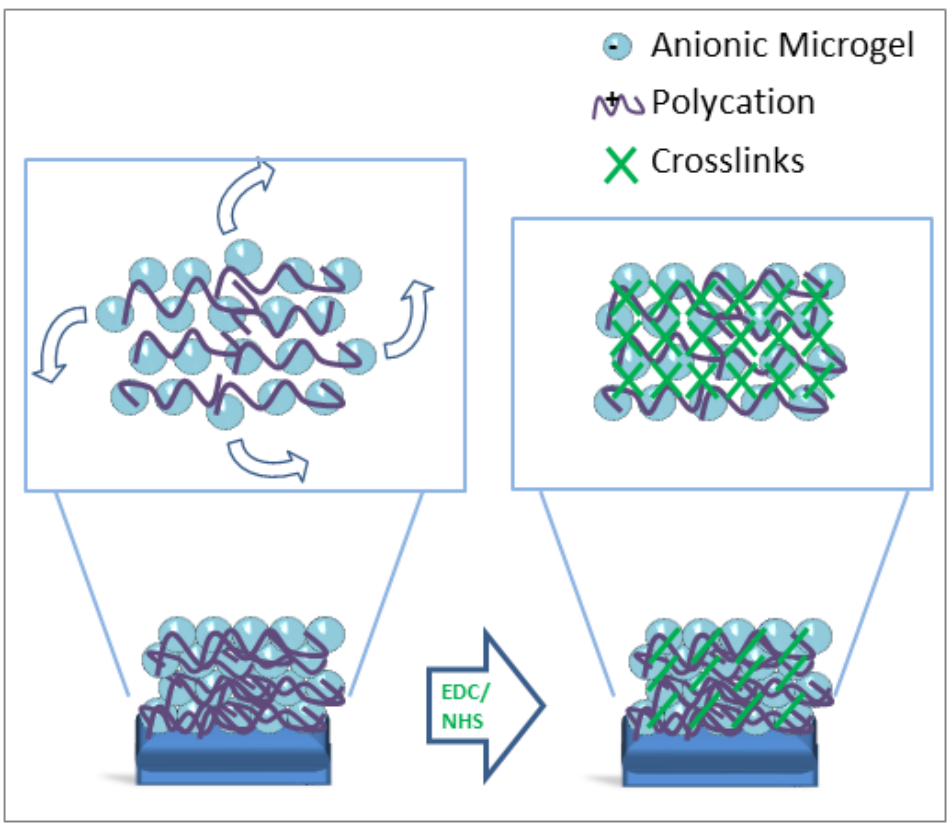

Scheme 5.4. Chemical structures of the polycations used for film assembly.

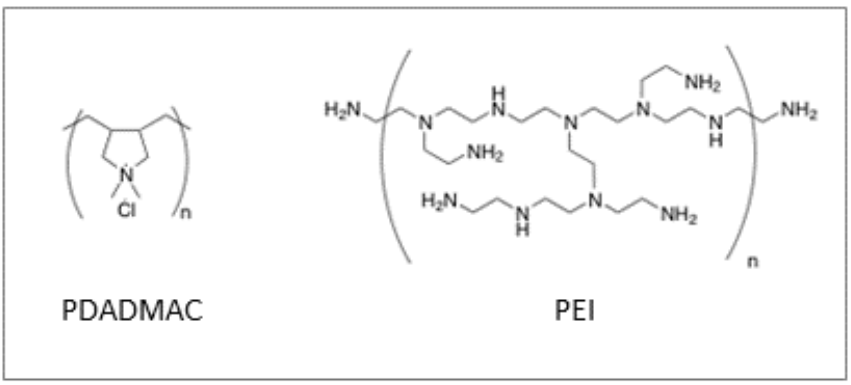

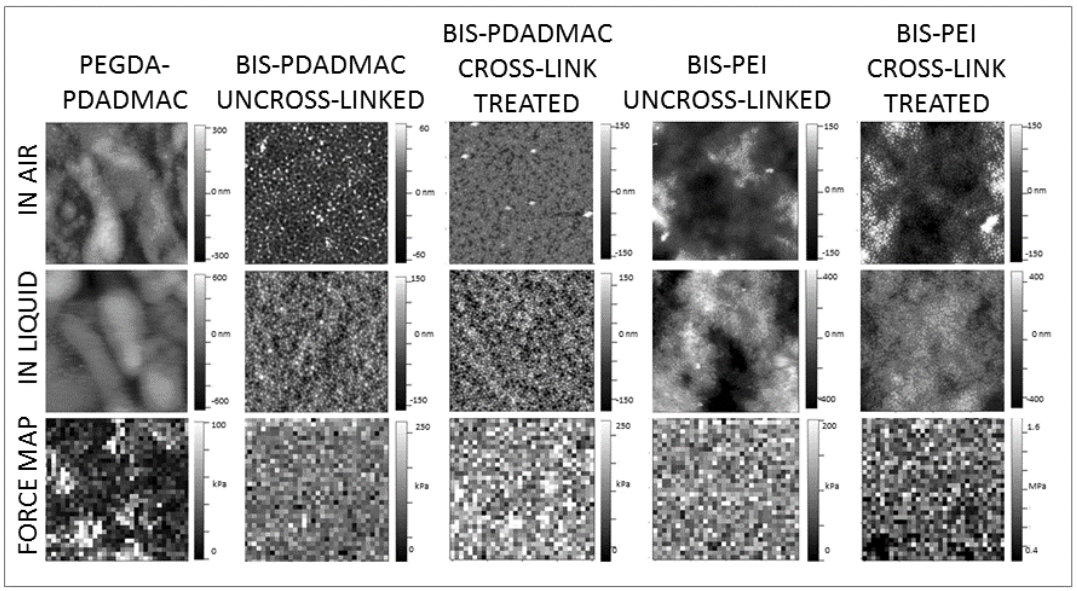

Figure 5.1. AFM height traces and force maps for films used in this study. All force maps were collected in PBS. Height scales and modulus scales are kept constant where appropriate. All images and force maps were collected at 20 °C. All images and force maps represent 20 x 20 μm scans.

The self-healing ability of BIS-PDADMAC and BIS-PEI films were assessed by applying a controlled strain to films assembled atop a PDMS substrate by Dr. Mark Spears. In these studies, films were dried, stretched to a specified strain,

relaxed, and then exposed to water to assess self-healing ability. These studies revealed that all BIS-PDADMAC films exhibited self-healing, regardless of cross-linking treatment. These findings suggest that the BIS-PDADMAC samples successfully served as a negative control for this cross-linking scheme. In contrast, with the BIS-PEI films, while uncross-linked BIS-PEI films exhibited self-healing properties, those that had been exposed to the cross-linking reaction no longer exhibited self-healing demonstrating the efficacy of the cross-linking.

Success of the cross-linking reaction and its effects on the film mechanics were also demonstrated by measuring the elastic properties of the films. AFM nanoindentation has been demonstrated as a powerful technique to determine the Young's modulus of a material. However, microgel films exhibit heterogeneity across the surface and, as they are composed of discrete building blocks, it is important to obtain an average modulus over a large area. Therefore, force mapping provides a mechanism to sample a large number of points within a film area in order to provide a high resolution picture of the film elasticity at the micro-scale. The heterogeneity of elasticity at this length scale may also be important in obtaining an understanding of cellular interactions with a substrate at the length scale of cells and their focal adhesions.

AFM images of each film type were collected both in-air and in-liquid. **Figure 5.1** shows height traces for all films including the cross-link-treated coatings. Importantly, four layers are sufficient to cover the surface and leave no exposed substrate. Even though identical BIS-containing microgels are used for BIS-PDADMAC and BIS-PEI films, the films have significant differences in appearance

attributable to the polycation. BIS-PDADMAC films tend to be flat with little undulation, but BIS-PEI films have raised areas as evidenced by the darker areas in the images and the larger height bar scale with each image. Individual microgels are difficult to discern in BIS-PEI films, whereas they are relatively simple to discern in the BIS-PDADMAC films.

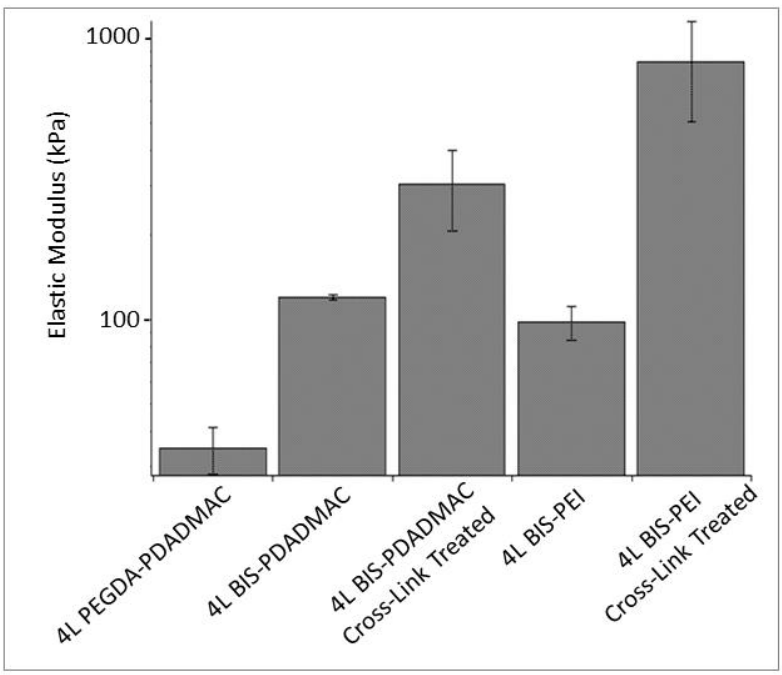

Figure 5.2 Graph of AFM force mapping results. Error bars are standard deviations; n = 3 for each film type. BIS-PDADMAC untreated vs. BIS-PDADMAC cross-link-treated, p = 0.012; BIS-PEI untreated vs. BIS-PEI cross-link-treated, p = 0.017.

An increase in the number of physical or chemical cross-links within an acrylamide gel increases the stiffness of a material as exhibited through an increase in the Young's modulus.[24] All AFM force maps were 32 x 32 arrays of force indentation curves as displayed alongside the corresponding height traces in **Figure 5.1**. The Young's modulus was determined for all film types as an average of all points within

the array, and the results are shown in **Figure 5.2**. Force mapping was conducted in pH 7.4 PBS buffer, thereby mimicking the pH & ionic strength conditions experienced during the cell adhesion studies. As mentioned previously, above the threshold of approximately 10 kPa cells are able to adhere and show little preference or discrimination to the material modulus.[24] The uncross-linked BIS and PEI films used in this study have a modulus of approximately 100 kPa, an order of magnitude higher than the threshold value. The PEGDA-PDADMAC films are also above the threshold with a modulus of approximately 35 kPa. Thus, even the uncross-linked films should be stiff enough for cell adhesion to be favorable. When cross-linked, the Young's modulus of PEI films increases an additional order of magnitude to approximately 1 MPa. A small increase in stiffness is noted for the negative (BIS-PDADMAC) control after exposure to cross-linking reagents, but as noted above, the change is not sufficient to restrict self-healing and therefore does not appear to restrict microgel or polycation mobility. For each film type, multiple samples and multiple spots on a single sample were tested; intra-sample and inter-sample variability was low (**Figure 5.3**).

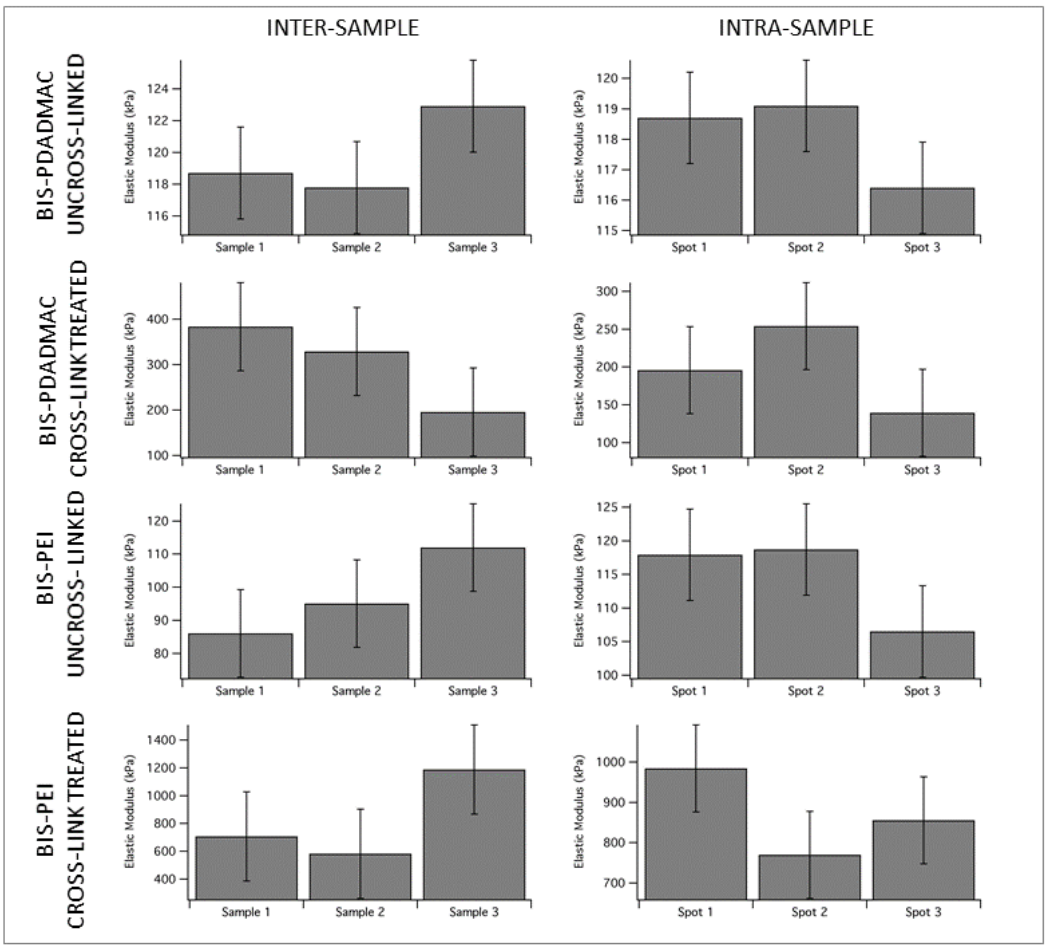

Figure 5.3. Intra- and inter-sample variability for AFM force maps for each type of film. Each column represents one force map with error bars representing the standard deviation of moduli within the map.

The modulus values reported may be thought of as "effective moduli." That is, the modulus value given may not be able to take microgel and polycation mobility into account, so the actual modulus of the film may be smaller than the measured value. The AFM tip used for force mapping has a diameter of 84 ± 24 nm and a height of 3.0 ± 0.5 μm. Thus, the tip samples a small portion of film surface area, but may be expected to sample a significant amount of film thickness. Film modulus and film dynamics are closely inter-related properties. Once films have been fabricated, one

property cannot be changed without influencing the other. In this investigation, the coupling reaction stiffens the film, causing both an increase in Young's modulus and reducing or eliminating the viscous component for the BIS-PEI films.

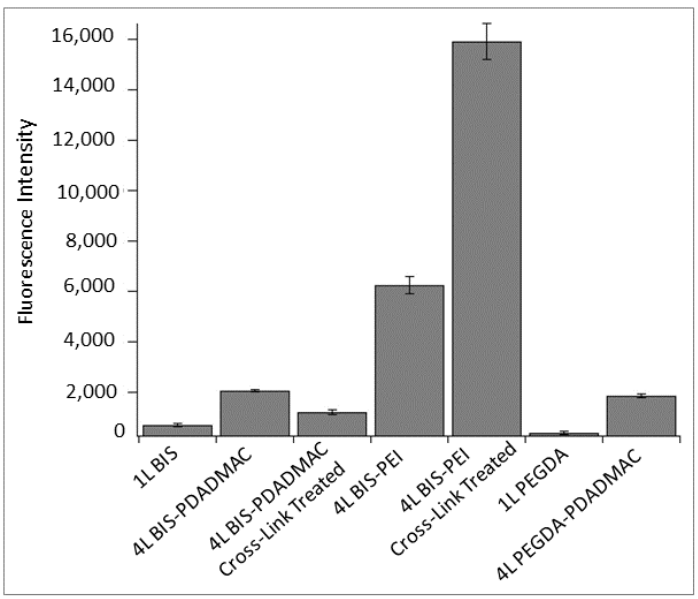

Figure 5.4 Fluorescence intensity values for fluorescent fibronectin adsorbed into microgel films at 37 °C. Error bars represent plus or minus one standard deviation. Results are statistically significant with all $p < 0.0045$ ($n = 3$).

5.3.2. Characterization of Protein Adhesion on Microgel Films

Monolayers of BIS particles compared to PEGDA particles had been shown to allow increased protein adsorption and increased cell adhesion.[30] To ascertain the influence of protein adsorption on these microgel films, we measured the amount of fluorescent fibronectin (a common protein associated with cell binding) adsorbed into both one and four layer films with results displayed in **Figure 5.4**. In agreement with the previous studies,[30, 31] both a single layer of PEGDA-containing microgels and a single layer of BIS-containing microgels have low fluorescence intensity,

corresponding to small amounts of adsorbed protein. Surprisingly, multilayer films have relatively high fluorescence intensity, indicating a high level of protein loading into the film. Even microgels incorporating PEGDA show very high protein loading when assembled into multilayers. BIS-PEI films, and the cross-link-treated BIS-PEI films in particular, adsorb a large amount of fibronectin, likely due to both the relatively large thickness of these films and the substantial excess charge within the film. When viewed independently of cell adhesion behavior, high protein loading into multilayer films is not a surprising result. Charged microgels adsorb large amounts of oppositely charged protein as demonstrated by loading of cytochrome c into AAc-containing microgels.[40] Also, in the film environment there are many excess charges on the polycation available for Coulombic interaction with proteins. We observe that multilayer films, which in previous studies displayed a strong resistance to cell attachment,[31] display the highest degree of protein ad/absorption. Thus, it appears that cell attachment does not correlate with protein fouling in the case of these particular films.

5.3.3. Characterization of Cellular Adhesion on Microgel Films

Since the levels of protein adsorption achieved by the films suggested that PEGDA was not the key factor in preventing cell attachment, we next investigated whether our previous observations regarding cell attachment to multilayers persisted in the novel film compositions of the present studies. Cell adhesion results and representative fluorescence images are displayed in **Figure 5.5**. Fibroblasts were stained with a LIVE/DEAD kit to assess cell viability after interaction with the film. Virtually all cells that adhered to the film remained alive. There is a degree of

heterogeneity in the film which may contribute to areas with more cells adhered than others. However, a sufficient number of images were counted and averaged to obtain meaningful data over a wide film area. Quantitative results in **Figure 5.5B** ponding four layer coatings have very few cells adhered. As noted above, cell adhesion is usually closely tied to the amount of protein on the surface, because cells interact with adsorbed proteins through specific receptors. Since the amount of protein adhered to four layer films is much higher than one layer films, it seems counterintuitive that the number of cells adhered follows the opposite trend. These data indicate that for uncross-linked microgel films, cell adhesion is not primarily controlled by the amount of protein on the surface, but is likely controlled by another film factor.

There is no statistical difference between the number of cells adhered on four layer BIS-PDADMAC and cross-link-treated BIS-PDADMAC films, indicating that the chemical change occurring during the cross-linking reaction is not affecting film properties or cell behavior. However, there is approximately a six-fold difference in the number of cells adhered to untreated and cross-link-treated BIS-PEI films, a change that we attribute both to the large change in Young's modulus and the restriction of microgel and polyelectrolyte mobility in these cross-linked films.

Further evidence for this hypothesis was obtained through examining cell morphology, and vinculin localization to focal adhesions. These two factors change dramatically on different film types and illustrate the cell interaction with the film. Representative images in **Figure 5.5C** show that cells are well spread on one layer films with recruitment of vinculin to focal adhesions at the cell periphery. One layer (that is covalently attached to the surface) films lack the mobile dynamics seen in

multilayer films, thus cells sense favorable mechanical cues and are able to form focal adhesions. When the same cells are cultured on four layer films, cells are always round and are not able to spread on the surface. This finding suggests that, while the apparent modulus of the film is high enough that cells should adhere strongly, the cells are unable to form focal adhesions, likely because they are applying traction forces to a dynamic, reconfigurable interface. Once the BIS-PEI film is cross-link-treated, the cells once again are able to spread on the surface and show evidence of high vinculin concentration at the membrane periphery.

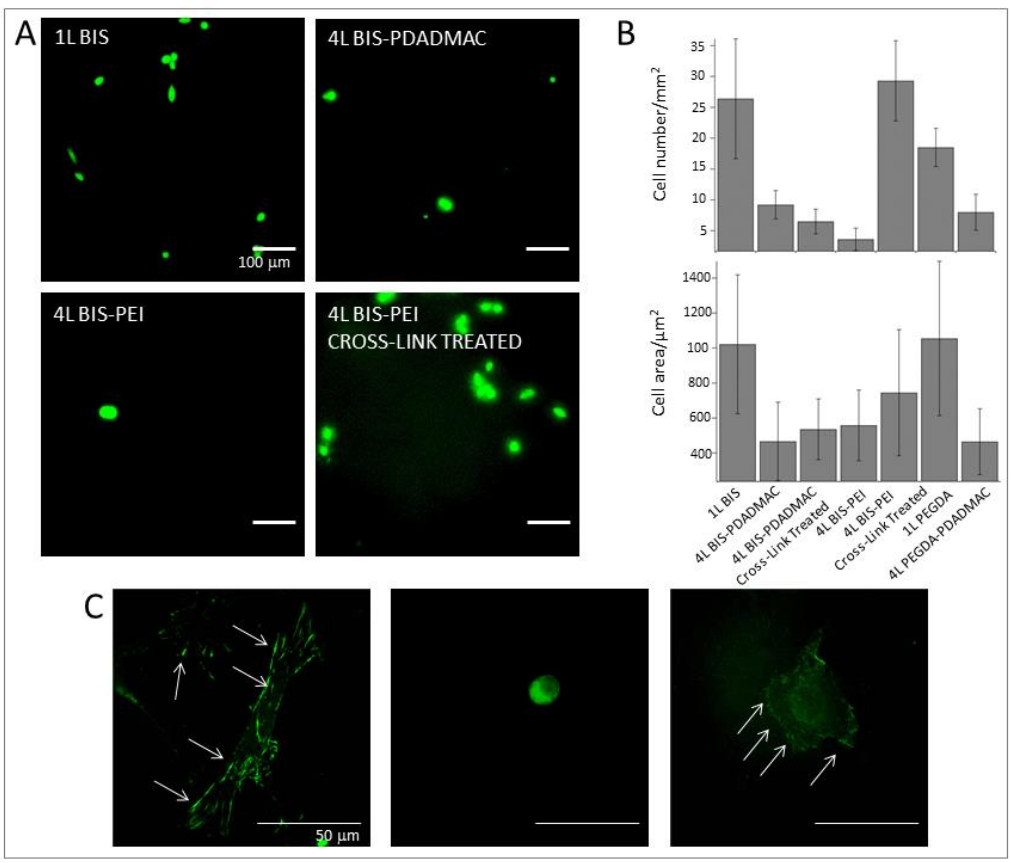

Figure 5.5. Fibroblast adhesion on microgel films after 24 h culture at 37 °C. (A) Representative images of LIVE/DEAD staining of cells on various films; scale bar = 100 µm (B) (upper panel) The number of cells adhered on the films analyzed from LIVE/DEAD images; 4L BIS-PDADMAC vs. 4L cross-link-treated BIS-PDADMAC,

p=0.206; all others p<0.04 (lower panel) Area of adhered cells analyzed from LIVE/DEAD images; all p>0.1 (C) Vinculin expression of fibroblasts cultured on various films; 1L BIS (left), 4L untreated BIS-PEI (middle), and 4L cross-link-treated BIS/PEI (right). Brightness increased in images to ensure facile visualization. Arrows in images indicate vinculin staining; scale bar = 50 μm. Cell studies kindly performed by Dr. Hiro Yoshida.

On the cross-linked films, a few cells were observed that were mostly rounded, indicating that the cross-linking treatment was not effective in that particular area of the surface or that there is some natural variation in fibroblast mechanosensing. This heterogeneity leads to no statistical difference in cell area on different substrates as seen in **Figure 5.5B** (bottom). The change in fibroblast morphology on uncross-linked and cross-link-treated films is striking, but it does not necessarily correlate with an equally stark difference in cell area.

5.4. Conclusions

A series of microgel films were constructed in order to examine the relationships between film mobility, protein adsorption, film mechanics, and fibroblast adhesion and spreading. Self-healing studies indicate that films wherein mobility of the microgels and polyelectrolyte is maintained are able to self-heal, while the cross-linked BIS-PEI films exhibit irreversible damage. AFM force mapping studies indicate that the Young's moduli of the films are all greater than 30 kPa, suggesting that all of them should appear physiologically stiff. The moduli increase with cross-linking, and cross-linked BIS-PEI films have the highest Young's modulus. Protein adsorption studies demonstrate that multilayer films adsorb large amounts of protein, regardless of incorporation of PEGDA. In contrast, fibroblast

adhesion is minimal in uncross-linked multilayers, while the cells only display a spread morphology on the films with lowest microgel and polyelectrolyte mobility, the cross-linked BIS-PEI films and monolayer films. Thus, cell adhesion, cell morphology, and vinculin localization results cannot be explained based only on the basis of elasticity and protein adsorption. At the microscale, these intriguing results can potentially be attributed to the dynamic nature of these films, which are able to self-heal, unless covalently cross-linked. At the nanoscale, this is due to the viscoelastic characteristics of the microgels and the intervening polycation in the film context as they interact with fibroblasts, shifting beneath the cells as they try to form focal adhesions. Control over cellular adhesion by shifting of the material underneath the cell due to traction forces is, to our knowledge, one of the first demonstrations of viscoelastic material properties influencing cell behaviour and attachment.

5.5. References

1. Boyan, B. D.; Hummert, T. W.; Dean, D. D.; Schwartz, Z., Role of material surfaces in regulating bone and cartilage cell response. *Biomaterials.* **1996**, *17* (2), 137-46.

2. Lutolf, M. P.; Hubbell, J. A., Synthetic biomaterials as instructive extracellular microenvironments for morphogenesis in tissue engineering. *Nature Biotechnol.* **2005**, *23* (1), 47-55.

3. Liu, W. F.; Chen, C. S., Engineering biomaterials to control cell function. *Mater. Today.* **2005**, *8* (12), 28-35.

4. Yeung, T.; Georges, P. C.; Flanagan, L. A.; Marg, B.; Ortiz, M.; Funaki, M.; Zahir, N.; Ming, W. Y.; Weaver, V.; Janmey, P. A., Effects of substrate stiffness on cell morphology, cytoskeletal structure, and adhesion. *Cell Motil. Cytoskeleton.* **2005**, *60* (1), 24-34.

5. Discher, D. E.; Janmey, P.; Wang, Y. L., Tissue cells feel and respond to the stiffness of their substrate. *Science.* **2005**, *310* (5751), 1139-1143.

6. Engler, A. J.; Sen, S.; Sweeney, H. L.; Discher, D. E., Matrix elasticity directs stem cell lineage specification. *Cell.* **2006**, *126* (4), 677-689.

7. Bechtle, S.; Ang, S. F.; Schneider, G. A., On the mechanical properties of hierarchically structured biological materials. *Biomaterials.* **2010**, *31* (25), 6378-6385.

8. Kuo, C. W.; Shiu, J. Y.; Chien, F. C.; Tsai, S. M.; Chueh, D. Y.; Chen, P. L., Polymeric nanopillar arrays for cell traction force measurements. *Electrophoresis.* **2010**, *31* (18), 3152-3158.

9. Kuo, C. W.; Chien, F. C.; Shiu, J. Y.; Tsai, S. M.; Chueh, D. Y.; Hsiao, Y. S.; Yang, Z. H.; Chen, P. L., Investigation of the growth of focal adhesions using protein nanoarrays fabricated by nanocontact printing using size tunable polymeric nanopillars. *Nanotechnology.* **2011**, *22* (26).

10. Balaban, N. Q.; Schwarz, U. S.; Riveline, D.; Goichberg, P.; Tzur, G.; Sabanay, I.; Mahalu, D.; Safran, S.; Bershadsky, A.; Addadi, L.; Geiger, B., Force and focal adhesion assembly: a close relationship studied using elastic micropatterned substrates. *Nature Cell Biology.* **2001**, *3* (5), 466-472.

11. Chung, T. W.; Liu, D. Z.; Wang, S. Y.; Wang, S. S., Enhancement of the growth of human endothelial cells by surface roughness at nanometer scale. *Biomaterials.* **2003**, *24* (25), 4655-4661.

12. Hersel, U.; Dahmen, C.; Kessler, H., RGD modified polymers: biomaterials for stimulated cell adhesion and beyond. *Biomaterials.* **2003**, *24* (24), 4385-4415.

13. Keselowsky, B. G.; Collard, D. M.; Garcia, A. J., Integrin binding specificity regulates biomaterial surface chemistry effects on cell differentiation. *Proc. Natl. Acad. Sci. USA.* **2005**, *102* (17), 5953-5957.

14. Schakenraad, J. M.; Busscher, H. J., Cell Polymer Interactions - The Influence of Protein Adsorption. *Colloid. Surf.* **1989**, *42* (3-4), 331-343.

15. Rahmany, M. B.; Van Dyke, M., Biomimetic approaches to modulate cellular adhesion in biomaterials: A review. *Acta Biomater.* **2013**, *9* (3), 5431-5437.

16. Garcia, A. J.; Ducheyne, P.; Boettiger, D., Effect of surface reaction stage on fibronectin-mediated adhesion of osteoblast-like cells to bioactive glass. *J. Biomed. Mater. Res.* **1998**, *40* (1), 48-56.

17. Geiger, B.; Spatz, J. P.; Bershadsky, A. D., Environmental sensing through focal adhesions. *Nat. Rev. Mol. Cell Bio.* **2009**, *10* (1), 21-33.

18. Michael, K. E.; Garcia, A. J., Cell adhesion strengthening: Measurement and analysis. *Methods Cell. Biol.* **2007**, *83*, 329-46.

19. Higuchi, A.; Ling, Q. D.; Chang, Y.; Hsu, S. T.; Umezawa, A., Physical Cues of Biomaterials Guide Stem Cell Differentiation Fate. *Chem. Rev.* **2013**, *113* (5), 3297-3328.

20. Lo, C. M.; Wang, H. B.; Dembo, M.; Wang, Y. L., Cell movement is guided by the rigidity of the substrate. *Biophys. J.* **2000**, *79* (1), 144-152.

21. Huang, C. J.; Butler, P. J.; Tong, S.; Muddana, H. S.; Bao, G.; Zhang, S. L., Substrate Stiffness Regulates Cellular Uptake of Nanoparticles. *Nano Lett.* **2013**, *13* (4), 1611-1615.

22. Munevar, S.; Wang, Y. L.; Dembo, M., Traction force Microscopy of migrating normal and H-ras transformed 3T3 fibroblasts. *Biophys. J.* **2001**, *80* (4), 1744-1757.

23. Galbraith, C. G.; Sheetz, M. P., A micromachined device provides a new bend on fibroblast traction forces. *Proc. Natl. Acad. Sci. USA.* **1997**, *94* (17), 9114-9118.

24. Rehfeldt, F.; Engler, A. J.; Eckhardt, A.; Ahmed, F.; Discher, D. E., Cell responses to the mechanochemical microenvironment - Implications for regenerative medicine and drug delivery. *Adv. Drug Deliv. Rev.* **2007**, *59* (13), 1329-1339.

25. Guan, Y.; Zhang, Y., PNIPAM microgels for biomedical applications: from dispersed particles to 3D assemblies. *Soft Matter.* **2011**, *7* (14), 6375-6384.

26. Wong, J. E.; Gaharwar, A. K.; Mueller-Schulte, D.; Bahadur, D.; Richtering, W., Layer-by-layer assembly of a magnetic nanoparticle shell on a thermoresponsive microgel core. *J. Magn. Magn. Mater.* **2007**, *311* (1), 219-223.

27. South, A. B.; Lyon, L. A., Autonomic Self-Healing of Hydrogel Thin Films. *Angew. Chem. Int. Ed.* **2010**, *49* (4), 767-771.

28. Gaulding, J. C.; Spears, M. W.; Lyon, L. A., Plastic deformation, wrinkling, and recovery in microgel multilayers. *Polym. Chem.* **2013**, *4*, 4890-4896.

29. Li, Y.; Wang, X.; Sun, J. Q., Layer-by-layer assembly for rapid fabrication of thick polymeric films. *Chem. Soc. Rev.* **2012**, *41* (18), 5998-6009.

30. Nolan, C. M.; Reyes, C. D.; Debord, J. D.; Garcia, A. J.; Lyon, L. A., Phase transition behavior, protein adsorption, and cell adhesion resistance of poly(ethylene glycol) cross-linked microgel particles. *Biomacromolecules.* **2005**, *6* (4), 2032-2039.

31. South, A. B.; Whitmire, R. E.; Garcia, A. J.; Lyon, L. A., Centrifugal Deposition of Microgels for the Rapid Assembly of Nonfouling Thin Films. *ACS Appl. Mater. Interfaces.* **2009**, *1* (12), 2747-2754.

32. Bridges, A. W.; Singh, N.; Burns, K. L.; Babensee, J. E.; Lyon, L. A.; Garcia, A. J., Reduced acute inflammatory responses to microgel conformal coatings. *Biomaterials.* **2008**, *29* (35), 4605-4615.

33. Salloum, D. S.; Olenych, S. G.; Keller, T. C. S.; Schlenoff, J. B., Vascular smooth muscle cells on polyelectrolyte multilayers: Hydrophobicity-directed adhesion and growth. *Biomacromolecules.* **2005**, *6* (1), 161-167.

34. Schneider, A.; Francius, G.; Obeid, R.; Schwinte, P.; Hemmerle, J.; Frisch, B.; Schaaf, P.; Voegel, J. C.; Senger, B.; Picart, C., Polyelectrolyte multilayers with a tunable Young's modulus: Influence of film stiffness on cell adhesion. *Langmuir.* **2006**, *22* (3), 1193-1200.

35. Thompson, M. T.; Berg, M. C.; Tobias, I. S.; Rubner, M. F.; Van Vliet, K. J., Tuning compliance of nanoscale polyelectrolyte multilayers to modulate cell adhesion. *Biomaterials.* **2005**, *26* (34), 6836-6845.

CHAPTER 6
FABRICATION TECHNIQUE ENABLING THE DESIGN OF MODULAR BIOMATERIALS

6.1. Introduction

Development of two-dimensional films with fine spatial control over mechanical properties and chemical functionalities has become increasingly important for a variety of applications including membranes, sensors, tissue engineering scaffolds, and biomedical devices. Previously, development of films with detailed patterns or hierarchical ordering have been achieved via either a "bottom-up" approach, where patterns are self-assembled,[1,2] or a "top-down" approach where a monolith of material is deposited followed by removal of certain areas. Well-established, versatile nanolithography approaches include soft lithography,[3] dip-pen nanolithography,[4] electron-beam direct-write lithography,[5] scanning-probe lithography,[6] nanoimprint lithography,[7] and photolithography;[8] these techniques have been demonstrated to produce nanoscale patterns for a variety of materials including inorganic materials and organic materials.

In the field of biomaterials in particular, hydrogels represent a class of materials under heavy investigation as a potential system for biomedical applications including drug delivery,[9] tissue engineering scaffolds,[10] and biosensing.[11] A variety of two-dimensionally and three-dimensionally patterned hydrogel systems have been explored for use in tissue engineering applications[12-16] and biosensing.[17-19] For example, Hu *et al.* demonstrated the ability to produce stimuli-responsive surface patterns on bulk hydrogels by selectively depositing a gold film via sputtering over a mask.[20] However, these studies specifically used two-component systems and lacked the ability to create surface patterns

with a single material. Later, Hahn *et al.* demonstrated the ability to pattern hydrogel surfaces with bound peptides using photolithography, which requires specific chemistries in order to successfully pattern a substrate.[21] In terms of three-dimensional patterning, researchers have successfully developed patterned constructs with control over chemical and mechanical properties. For example, Wylie *et al*. demonstrated the ability to pattern protein in hydrogel scaffolds to provide a biomimetic environment for cell culture.[22] However, this method requires the specific chemistry of coumarin caged thiols and a transparent material for success of the coupling method. This method also requires an excess of proteins in order to ensure coupling to the immobilized bioactive factors, streptavidin and barnase, which could be cost prohibitive. Click-chemistry has also been demonstrated to be a useful route to create three-dimensional patterns of biological functionalities in hydrogels, but again relies on strict chemistries to enable photopatterning.[23] In terms of patterning of mechanical properties there are even fewer options available. For example, Mosiewicz *et al*. demonstrated that photopatterning of hydrogels containing caged thiols successfully altered hydrogel cross-linking density, and thus hydrogel stiffness.[24] Again, we see that this method is limited by strict chemistries. Thus, the development of a facile method to pattern hydrogel materials with spatial control over chemical functionality and/or mechanical properties without the need for complex chemistries could be greatly beneficial for the advancement of patterned biomaterials in biomedical research.

Hydrogel nanoparticles, also known as microgels, are discrete hydrogel particles that can be used as modular building block to fabricate tunable two-dimensional films and three-dimensional scaffolds with enhanced control over material properties, making

these materials extremely promising for a range of biomaterial applications.[25-27] Investigators have demonstrated the ability to synthesize hydrogel nanoparticles at various sizes with low polydispersity using precipitation polymerization, which can be difficult to achieve with both natural and synthetic polymers, as well as other polymerization techniques. Moreover, researchers have previously demonstrated the ability to synthesize microgels with complex architectures including core-shell microgels and hallow microgels, for added functionality.[28-31]

Microgel assemblies have previously been investigated for a variety of applications including drug delivery,[32-33] non-fouling coatings,[34] and sensing.[35-36] As a hydrogel material, microgel assemblies have the added benefit of enabling development of materials with finely tuned properties or characteristics through careful selection of the hydrogel nanoparticle types used as modular building blocks. As discussed in **Chapter 5**, the Layer-by-Layer (LbL) technique is the established method for fabricating polyelectrolyte microgel films.[37] Though the LbL method has been well-established and widely used throughout the microgel research field, it can be a limiting factor for the development of films, particularly those with more complex architectures. Development of patterned microgel films, for example, presents a problem to the current fabrication strategy. Few investigators have successfully developed patterned microgel assemblies. Most notably, Peng *et al.* demonstrated the ability to pattern microgel monolayers via cool microcontact printing.[38] Additionally, Lord *et al.* demonstrated the ability to cast solution of carbon disulfide and microgels prepared from RAFT derived polystyrene in order to produce films with a porous honeycomb structure.[39] Though researchers have demonstrated the ability to pattern microgel monolayers, there has been little success in

patterning microgel multilayers. Moreover, the existing methods are limiting in the film compositions as well as the patterning architecture that can be achieved.

Scheme 6.1. This simple fabrication process can be used to develop an array of material systems using a few basic building blocks.

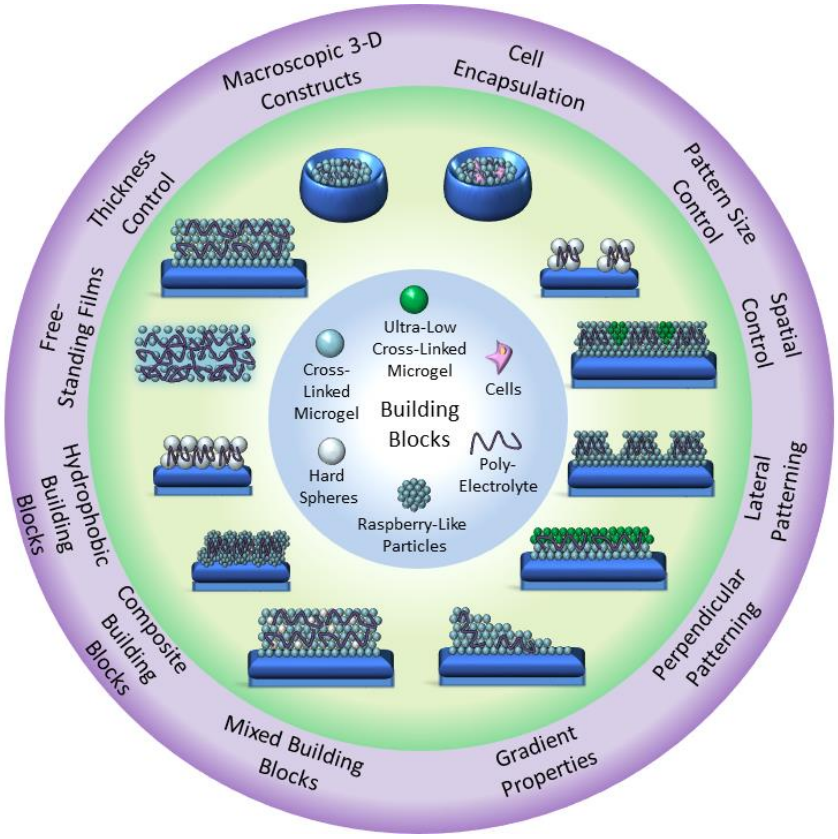

In the present contribution, an enabling film fabrication technique is investigated wherein polyanionic components and polycation are mixed, forming a polyelectrolyte complex, and immediately deposited via centrifugation. This film fabrication technique is compared to the traditional LbL approach; the versatility of this technique is also demonstrated through the development of several constructs not previously feasible using the LbL technique including laterally and perpendicularly patterned polyelectrolyte

microgel constructs (**Scheme 6.1**). Finally, it is demonstrated that these constructs can be used as biological interfaces to interrogate cellular behavior. Together, these studies demonstrate that this method can be a facile route to fabricate a variety of constructs that can be used as model experimental systems to interrogate fundamental film properties, elicit basic cellular responses, and develop biomaterials/biomedical devices.

6.2. Experimental

6.2.1. Materials

Materials used in this investigation are described in section **2.2.1** with the following additions. Acrylic acid (AAc) was used as received. Branched polyethyleneimine (PEI) (typical Mw = 750 kDa) 50% w/w solution in water were prepared as either a 0.086 g/mL or 8.6 mg/mL solution in PBS. Methacryloxyethyl thiocarbamoyl rhodamine B (Rhodamine B) and 4-acrylamidofluorescein (AFA) were used as fluorophores.

6.2.2. Microgel Synthesis

Microgels were synthesized using the procedure outlined in section **2.2.2** with a few modifications. For all microgels, the total monomer concentration was 100 mM with molar compositions of 66 mol-% pNIPAm, 4 mol-% BIS, and 30 mol-% AAc. Monomer, cross-linker, and surfactant SDS were dissolved in water. For fluorescent microgels, the fluorophore Rhodamine B was also added at this time. For ultra-low cross-linked microgels, no cross-linker was added to the solution. The solution was placed in a 3-neck round bottom flask equipped with a condenser, heated to 70 °C while mixing with a magnetic stir bar (stir speed 450 RPM) while being purged with N_2 for approximately 1 h. AAc was added 10 min prior to reaction initiation; 1 mL of APS solution in water was added and the reaction was allowed to proceed for 4 h. Microgel compositions used in

these studies are listed in **Table 6.1**. Microgel hydrodynamic radius (R_H) values were determined using a DynaPro Dynamic Light Scattering (DLS) instrument (Wyatt, Technology, Santa Barbara, CA).

6.2.3. Preparation of Buffers

A 10 mM phosphate buffer solution (PBS) was prepared with 150 mM ionic strength of NaCl and a pH of 7.4. 10 mM formate buffers (pH 3.3) were prepared with either 25 mM, 100 mM, or 150 mM NaCl. 10 mM MES buffers (pH 5.5) were prepared with wither 25 or 150 mM NaCl.

Table 6.1. Microgel composition.

Sample	pNIPAm (mol-%)	BIS (mol-%)	Acc (mol-%)	Other
1	66	4	30	N/A
2	66	4	30	<1% Rhodamine B derivative
3	70	0	30	<1% AFA

6.2.4. Preparation of Microgel Polyelectrolyte Films using the Single-Step Method

Microgel solutions were suspended on a shaker over night before each experiment was performed. Glass coverslips were functionalized in a solution of 1% APTMS in absolute EtOH on a shaker for 2 h. Coverslips were rinsed with deionized water and placed in the bottom of a well-plate. A 0.086 g/mL stock solution of branched PEI was prepared in PBS. For best results, PEI stock solution should be made 2-12 h prior to fabrication to ensure that the PEI solution is well-mixed. Use of PEI stock solutions prepared >12-24 h prior to film fabrication, can result in unstable polyelectrolyte solutions when combined with microgels. Microgels solutions were also prepared in PBS for a stock solution concentration of 10 mg/mL. Within each well a solution was prepared

containing PBS, PEI, and microgels that was immediately mixed. Various amounts of microgel dispersions and PEI were used to prepare the constructs, but all components had a consistent ratio of PBS:PEI:Microgel 2:1:1. Samples were centrifuged at 2250 x g for 20 min. Liquid was removed using a transfer pipette. Samples were removed and dipped in DI water to rinse excess film transferred from the surrounding area of the well-plate, if necessary. Samples were allowed to air dry.

6.2.5. Preparation of Microgel Polyelectrolyte Layer-by-Layer (LbL) Films

Microgel solutions were suspended on a shaker over night before each experiment was performed. Glass coverslips were functionalized in a solution of 1% APTMS in absolute EtOH on a shaker for 2 h. Films were equilibrated in PBS for 30 min. Film buildup occurred by depositing 1 mL of a 0.1 mg/mL solution of microgels suspended in PBS. Films were then washed. Next, films were placed in a solution of PEI (8.6 mg/mL) in PBS for 30 min on a shaker. Films were again washed. This process was repeated until four layers of microgels and three layers of polycation were added.

6.2.6. Characterization of Microgel Film Topography and Thickness

Film topography was characterized for a four layer (4L) LbL film and for single-step films prepared with either 1 mg, 2 mg, or 4 mg of microgels via an MFP-3D AFM (Asylum Research, Santa Barbara, CA). Images in air were collected in AC mode using silicon SPM probes with AL reflex coating, and a 42 N/m nominal force constant (Nanoworld, NCHR). Dry film thickness was characterized using a NOVA 200 Focused Ion Beam/Scanning Electron Microscope system (FEI, Hillsboro, OR). Samples were adhered to vertical metal stubs using copper tape and were coated with gold/palladium using a Hummer V Sputterer (Anatech, USA, Union City, CA) for 2-3 min.

6.2.7. Characterization of Microgel Film Mechanical Properties

AFM nanoindentation was performed to determine the elastic Young's modulus of films. AFM has been used previously to probe the micro-environment mechanical properties of a substrate, using a technique where the AFM tip is brought into contact with the surface to act as a nano-indenter.[40] AFM nanoindentation was performed using an MFP-3D AFM (Asylum, Santa Barbara, CA). These studies were performed in liquid using silicon nitride probes with Cr/Au reflex coating, and a 0.09 N/m nominal spring constant (Asylum, BL-TR400PB) mounted in the iDrive cantilever holder. For extremely soft samples E < 10 kPa, a surface probe was used that had a 3.5 µm diameter SiO_2 bead attached to a 200 µm length triangular cantilever with a 0.08 N/m force constant (Surface Science Support). All force curves were collected in contact mode. The samples were allowed to equilibrate in 10 mM, pH 7.4 PBS with 100 mM NaCl ionic strength for a minimum of 30 min. For samples where silicon nitride probes were used, exact spring constants were determined using the GetReal Probe program provided by Asylum. For samples where surface probe microscopy was required, exact spring constants were determined on a clean glass coverslip by a combination of force curves and thermal spectrum calibration using methods in the MFP-3D software. Force maps were collected as 32 x 32 arrays of force curves with trigger point = 0.3 V except for samples with an E < 10 kPa, which were collected as a 10 x 10 array. Elastic moduli were determined via the MFP-3D analysis tools using the Hertz model, assuming a Poisson ratio of 0.5 for the films, and assigning the appropriate tip geometry as a cone or a sphere for the silicon nitride probes and polystyrene probes, respectively. Reported values were calculated by

averaging 108 data points collected from three samples with 36 points taken from 2-3 spots on each individual sample and calculating a standard deviation for all points.

6.2.8. Microgel Film Swelling

Polyelectrolyte microgel films were prepared in a 24-well-plate using 12 mm diameter glass coverslips functionalized with APTMS. 150 µL of microgels (10 mg/mL), 150 µL PEI (0.086 g/mL), and 300 µL PBS were mixed and deposited via centrifugation. Films were air dried overnight. A razorblade was used to score the edge of the glass coverslip to detach the film prepared on the top of the coverslip from remnant film on the bottom of the coverslip. Films were then placed in 6-well-plate with either formate buffer (10 mM formate, pH 3), MES buffer (10 mM MES, pH 5) or PBS (10 mM phosphate, pH 7.4) with either 150 mM NaCl or 25 mM NaCl and left on a shaker for 1.5 hours. After that time, films were left standing in buffer for several months. Polyelectrolyte microgel films that were able to detach from glass coverslips were imaged using a camera. The increase in diameter was determined via Image J analysis of three films. To characterize how film thickness and film area influence film swelling, films were prepared on either 12 mm or 22 mm diameter coverslips that had been functionalized with APTMS. Either 1.5, 3, or 6 mg of microgel (using the 10 mg/mL stock solution) were mixed with an equal amount of the polycation and deposited via centrifugation. Film swelling was then characterized by placing all samples in formate buffer with 100 mM NaCl concentration. Films were placed on a shaker for 24 h; after that time, films were removed and left on an immobile surface.

6.2.9. Preparation and Characterization of Laterally Patterned Microgel Polyelectrolyte Films

Square 9 mm x 9 mm glass coverslips were functionalized with a solution of 1% APTMS. Excess solution was washed away with deionized water and coverslips were then placed in a 24-well-plate. 1 mL of 0.1 mg/mL microgels (either microgel 1 or microgel 2, see **Table 6.1**) was added to each well and deposited via centrifugation at 2250 x g for 10 min. Samples were washed with deionized water to remove excess microgel solution. Microgel monolayers were cross-linked to the APTMS functionalized surface via carbodiimide coupling. Films were cross-linked overnight in 1 mL of MES buffer containing 2 mM EDC and 5 mM NHS. Films were washed with deionized water. 1 mL of PBS was then added to each well followed by the addition of 0.5 mL of PEI (8.6 mg/mL) to each well that was mixed with the PBS. A TEM grid was then immersed in the solution and applied to the surface of the coverslip. Finally, 0.5 mL of a 1 mg/mL microgel solution was added and quickly mixed with the existing solution. Microgels and PEI were deposited via centrifugation at 2250 x g for 20 min. Samples were carefully removed and dipped in deionized water to remove excess film detached during the transfer process. Patterned microgel films were imaged using an Olympus IX-70 inverted microscope (Olympus, Center Valley, PA) equipped with a PixelFly black and white CCD camera (Andor, South Windsor, UK).

6.2.10. Preparation and Characterization of Perpendicularly Patterned Polyelectrolyte Microgel Films

Microgel films exhibiting patterns normal to the substrate were created using microgels 1, 2, and 3 as listed in **Table 6.1**. Square 9 x 9 mm glass coverslips were functionalized with a solution of 1% APTMS. Excess solution was washed away with deionized water. Each layer was added using the single-step film fabrication process

detailed previously in this section. For films containing microgels 1 and 2, the construct was patterned as follows: 2:1:2:1:2. For films containing microgels 2 and 3, the construct was patterned as follows: 2:3:2. For all films, 0.5 mL of a 0.1 mg/mL solution of microgels was mixed with 0.5 mL of PEI (8.6 mg/mL).

6.2.11. Preparation of Polyelectrolyte Raspberry-Like Particle Films

Raspberry-like particles (RLPs) were prepared by immersing aminobenzophenone (ABP)-functionalized PS cores into a concentrated microgel dispersion by scaling up a previously described method.[41] Glass coverslips were functionalized in 1% v/v APTMS in 95% v/v EtOH for 2 h on a shaker. Coverslips were rinsed with deionized water and then placed at the bottom of a well-plate. 1.25 mL PBS was added to the well, followed by 0.5 mL of PEI (8.6 mg/mL), and the solution was mixed. Finally, 0.250 mL of RLPs suspended in PBS was added and gently mixed with a pipette. This solution was then deposited via centrifugation at 2250 x g for 30 min. Samples were gently rinsed with deionized water and left on a benchtop to dry overnight. Allow films to air dry overnight. Films were imaged using an Olympus IX-70 inverted microscope (Olympus, Center Valley, PA) equipped with a PixelFly black and white CCD camera (Andor, South Windsor, UK).

6.2.12. Preparation of Polyelectrolyte Carboxyl-Functionalized PS Films

Glass coverslips were functionalized in 1% v/v APTMS in 95% v/v EtOH for 2 h on a shaker. Coverslips were rinsed with deionized water and then placed at the bottom of a well-plate. 1.25 mL PBS was added to the well, followed by 0.5 mL of PEI (8.6 mg/mL)), and the solution was then mixed. Finally, 0.250 mL of carboxyl-functionalized PS (0.25% w/v) was suspended in PBS and gently mixed with a pipette. This solution

was then deposited via centrifugation at 2250 x g for 30 min. Films were gently rinsed with deionized water and left on a benchtop to dry overnight. Films were imaged using an Olympus IX-70 inverted microscope (Olympus, Center Valley, PA) equipped with a PixelFly black and white CCD camera (Andor, South Windsor, UK).

6.2.13. Preparation of Laterally Patterned Polystyrene Films

Glass coverslips were functionalized in 1% v/v APTMS in 95% v/v EtOH for 2 h on a shaker. Coverslips were then rinsed with deionized water and placed at the bottom of a well-plate. A monolayer of microgels was deposited by centrifuging 1 mL of 0.1 mg/mL microgels for 10 min at 2250 x g. PEI was added first, followed by addition of PBS, a TEM grid was then applied, and finally a solution of carboxyl-functionalized PS beads (0.25% w/v) were added before centrifugation for 30 min at 2250 x g. Samples were removed from the well, gently rinsed with deionized water to remove grids, and air dried overnight. For initial characterization, film composition was the same of the PS monolayers. Samples prepared for cell studies were fabricated using 0.5 mL PEI (8.6 mg/mL), 0.2 mL PS, and 0.3 mL PBS. Films were imaged using an Olympus IX-70 inverted microscope (Olympus, Center Valley, PA) equipped with a PixelFly black and white CCD camera (Andor, South Windsor, UK).

6.2.14. Preparation and Characterization of Bulk Polyelectrolyte Gels

To prepare bulk polyelectrolyte gels, 0.5 mL of 10 mg/mL of microgels were mixed with 0.5 mL of PEI (0.086 g/mL), and 1 mL of PBS in a microcentrifuge tube. This solution was mixed and centrifuged at 2250 x g for 20 min. Excess liquid was removed using a transfer pipette. Samples were cross-linked with EDC/NHS concentrations of 0.2/0.5 mM, 2/5 mM, and 20/50 mM. Bulk gel mechanical properties

were investigated using an Anton Parr plate-and-cone rheometer. Samples were subjected to a pre-shearing protocol to eliminate material memory. Samples were next subjected to a strain sweep to determine an optimal strain. Finally, rheology studies were undertaken at a single strain (0.8) by varying the oscillatory frequency.

6.2.15. Analysis of Cell Attachment and Spreading on Microgel Films

NIH-3T3 fibroblasts were purchased from ATCC and were maintained in DMEM media supplemented with 10% Bovine Calf Serum (BCS) and 1% Penicillin/streptomycin. Cells were cultured to 70-80% confluency prior to experiments. Cells were trypsinized and then membranes were stained with either CellTracker Green CMFDA or Deep Red Dye (Life Technologies). NIH-3T3 cells stably transfected with an m-Emerald Actin construct were utilized for analysis of actin distribution and alignment on microgel films. Cells were plated at a density of 5,000 cells/cm^2, and following 24 h in culture, samples were fixed and mounted. Samples were imaged using a 700-405 Zeiss Laser Scanning Confocal Microscope (Zeiss, Thornwood, NY). Cell attachment, circularity, aspect ratio and area were determined through Image J (NIH freeware). All statistical analyses were performed with Prism software program (GraphPad, San Diego CA). Data were analyzed using a Kruskal-Wallis test with Dunn posthoc test; cells were not expected to exhibit a Gaussian distribution in response to the film patterns.

6.2.16. Preparation of Bulk Gels and Rheological Characterization

Bulk gels were prepared by mixing 0.5 mL of 10 mg/mL microgels, 0.5 mL of PEI (8.6 mg/mL), and 1 mL of PBS in a microcentrifuge tube. Samples were vortexed and centrifuged for 20 min at 2250 x g for 20 min. For cross-linked samples, 0.2/0.5 mM,

2/5 mM, or 20/50 mM EDC/NHS was used. For bulk gels containing a 1:1 ratio of 4% BIS non-fluorescent microgels and AFA containing ULC microgels, 0.25 mL of non-fluorescent microgels and 0.25 mL of ULC microgels were used in each sample. The viscoelastic properties of these gels were studied under oscillatory shear conditions using a stress-controlled rheometer (Anton Paar, Physica MCR 501). Material history was erased via a preshearing process. The transition from the linear to nonlinear regime was first detected by conducting strain sweeps at constant frequency. The viscoelastic mechanical properties of the elastic storage modulus (G') and the viscous loss modulus (G') were determined as a function of the angular frequency at a constant strain of 0.8.

6.2.17. Preparation of Bulk Gels with Embedded Cells

Bulk gels were prepared by adding 0.3 mL of a 10 mg/mL solution of microgels, 0.3 mL of a PEI solution (0.086 g/mL), and 0.6 mL of PBS to a 2 mL microcentrifuge tube. The solution was then mixed and immediately centrifuged at 2250 x g for 20 min. Excess solution was removed from the tube. NIH-3T3 fibroblasts cells were labeled with the membrane dye CellTracker Green CMFDA and then washed with PBS to remove excess dye. 25 μL of stained NIH-3T3 fibroblasts at roughly 1.9 x 10^6 cells/mL were added to each microgel-containing tube. Samples were then centrifuged for either 500 RPM for 1 min or 1000 RPM for 30 sec. Samples were fixed overnight in a solution of 5% glutaraldehyde in PBS. Samples were imaged using a 700-405 Zeiss Laser Scanning Confocal Microscope (Zeiss, Thornwood, NY).

6.3. Results and Discussion

6.3.1. Investigation of Planar Films

Microgel film fabrication was investigated using two soft polymeric building blocks: pNIPAm microgels containing 30 mol-% acrylic acid (AAc) that are either cross-linked with 4 mol-% BIS or self-cross-linked, termed ultra-low-cross-linked (ULC) microgels. Even though both the BIS and ULC microgels are soft, they exhibit significantly different mechanical properties. The Lyon Group has previously demonstrated that ULC microgels have a Young's modulus <10 kPa and are an order of magnitude softer than typical BIS-containing microgel constructs, which have a Young's modulus closer to ~100 kPa.[34,42] To complete these studies, three microgel populations were fabricated and characterized (**Table 6.2)**.

T**able 6.2.** Microgel Characterization.

Sample	**Chemical Composition**					**R_H (nm)**
	pNIPAm (mol-%)	AAc (mol-%)	BIS (mol-%)	Rhodamine-B (mol-%)	AFA (mol-%)	
Unlabeled Microgels	66	30	4%	0%	0%	509 ± 10
Rhodamine/ Red Microgels	66	30	4%	<1%	0%	288 ± 53
AFA/ Green Microgels	70	30	0%	0%	<1%	620 ± 10

Films were prepared by combining well-mixed solutions of an anionic polymer building block and the polyelectrolyte branched PEI in a well-plate before centrifugation onto a functionalized glass coverslip using the "single-step" fabrication technique (**Scheme 6.2**). The development of microgel films was first explored using two distinct microgel components: a pNIPAm microgel containing AAc (30 mol-%) and BIS (4 mol-%) and an ultra-low cross-linked microgel sample that contained only pNIPAm and AAc

(30 mol-%). Films were prepared with either 0.5 mg, 1 mg, 2 mg, or 4 mg of microgels, while maintaining a constant ratio of PEI.

Scheme 6.2. Depiction of the single-step fabrication technique. This method requires that (1) the polycation and anionic building blocks are mixed and (2) immediately deposited via centrifugation onto a functionalized substrate. To make free-standing microgel films, the films are then (3) solvated in acidic buffer.

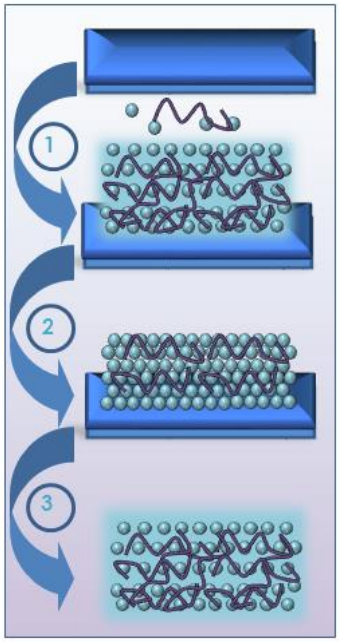

In order to investigate film buildup, SEM imaging of film cross-sections was performed (**Figure 6.1**). Single-step films prepared using 0.1, 0.5, 1, 2, and 4 mg of microgel exhibit film thicknesses of 1.4 µm ± 390 nm, 4.1 µm ± 640 nm, 9.3 µm ± 2.0 µm, 19.5 µm ± 3.1 µm and 55.6 µm ± 12.2 µm, respectively. In contrast, LbL films prepared with 0.4 mg of microgel in total exhibit a thickness of 630 nm ± 130 nm. These experiments demonstrate that the single-step method enables the fabrication of ultra-thick microgel films not typically feasible using an LbL approach. The single-step film fabrication technique also uses material more efficiently than the LbL method. These

studies reveal that single-step films containing only 0.1 mg of microgels, one-fourth the amount used for a typical 4L LbL film, are almost twice as thick as a typical 4L LbL film. Quantitative analysis of SEM images reveals that film buildup does not occur in a linear fashion, regardless of microgel composition, when using the single-step method, and that film buildup of ULC microgels differs from 4% BIS microgels when large amounts of microgels are used.

To explore how the single-step fabrication technique influences film topography, microgel films were imaged via AFM (**Figure 6.2**). In these studies, films were prepared from the microgels containing 4 mol-% BIS. AFM images reveal that microgels are highly packed and exhibit uniformity at the surface of the film. The degree of microgel packing appears consistent regardless of the amount of polymer used. However, films prepared with increasing amounts of microgels exhibit greater uniformity. Films prepared with the lowest amount of microgels likely exhibit increased heterogeneity due to the small volume used during fabrication (400 µL), which may limit the ability to mix the solution. In contrast, AFM images of films prepared using the established LbL method reveal a higher degree of heterogeneity. Films appear to contain a microgel layer with partial coverage at the surface; individual microgels do not appear integrated into a single layer, appearing less packed overall compared to single-step films. Because of these partial microgel layers, more peaks and valleys at the 1-5 micron level are evident at the film surface.

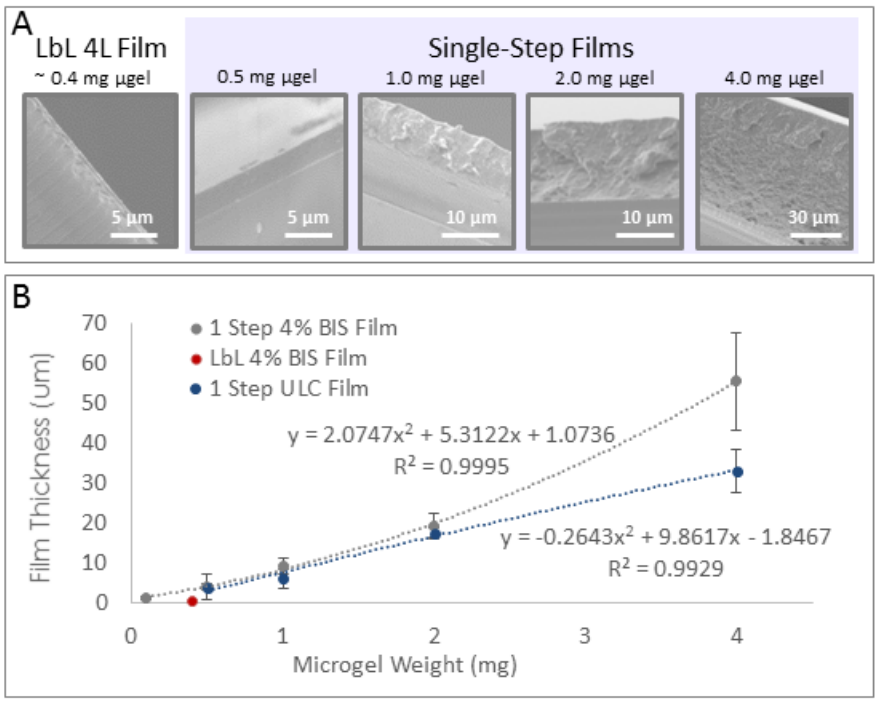

Figure 6.1. Characterization of film buildup. (A) Cross-sections of microgel films prepared with varied weights of microgels and PEI were imaged via SEM. Films were adhered to vertical stubs using copper tape. (B) Thickness was determined using Image J. Error bars represent plus or minus one standard deviation value about the average value of 9 measurements taken in distinct spots on each film.

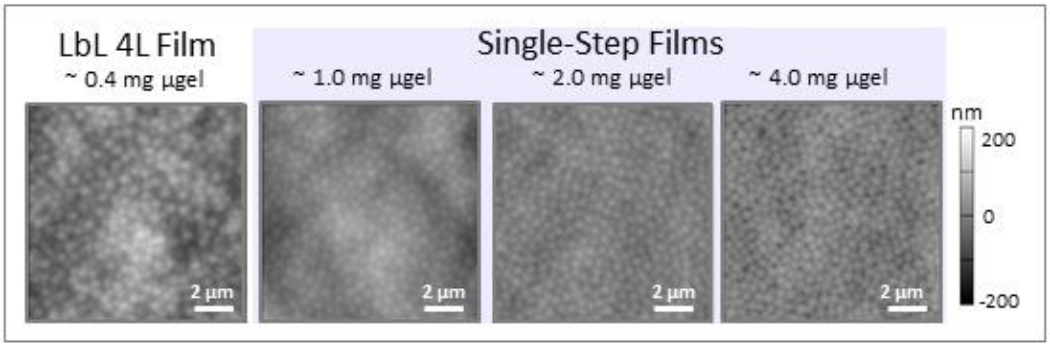

Figure 6.2. Characterization of microgel film topography. Dry films were imaged via AFM. Contrast indicates topographical height distribution.

Next, AFM nanoindentation studies were performed on films prepared using 4 mol-% BIS microgels to characterize the micro-mechanical properties (**Figure 6.3**). Films prepared using the single-step method were fabricated to be roughly 500 nm, 5 µm,

or 50 μm in thickness; these films exhibit a Young's moduli of 101 kPa ± 37 kPa, 72 kPa ± 12 kPa, and 5 kPa ± 3 kPa, respectively. Films prepared with a dry thickness of approximately 50 μm and subsequently subjected to EDC/NHS cross-linking exhibit an increased Young's modulus of 44 kPa μm ± 34 kPa. In comparison, a typically 4L LbL film has a Young's modulus of 111 kPa ± 46 kPa. These AFM nanoindentation studies demonstrate that films fabricated using the single-step method exhibit more uniform mechanical properties compared to films fabricated via the LbL method. These studies also reveal that for single-step films, stiffness is inversely proportional to film thickness. Ultra-thick microgel films (~55 μm in thickness) exhibited a Young's modulus of ~5 kPa, which is significantly lower than 4 layer LbL films previously prepared and characterized in the Lyon Group. As such, the single-step fabrication technique enables the development of biomaterial constructs that have mechanical properties in the range of cell sensitivity (<10 kPa). The large influence that film thickness has on mechanical properties can likely be attributed to film swelling characteristics. Upon visual inspection, it is apparent that thicker films are swollen to a larger degree and exhibit lateral movement when they are disturbed; additionally, thicker samples are more likely to minimize sampling of the underlying substrate. Carbodiimide coupling is also demonstrated to be a facile method to tune the mechanical properties of these films. Upon EDC/NHS cross-linking of the thickest films, Young's modulus increases, demonstrating the efficacy of this cross-linking scheme.

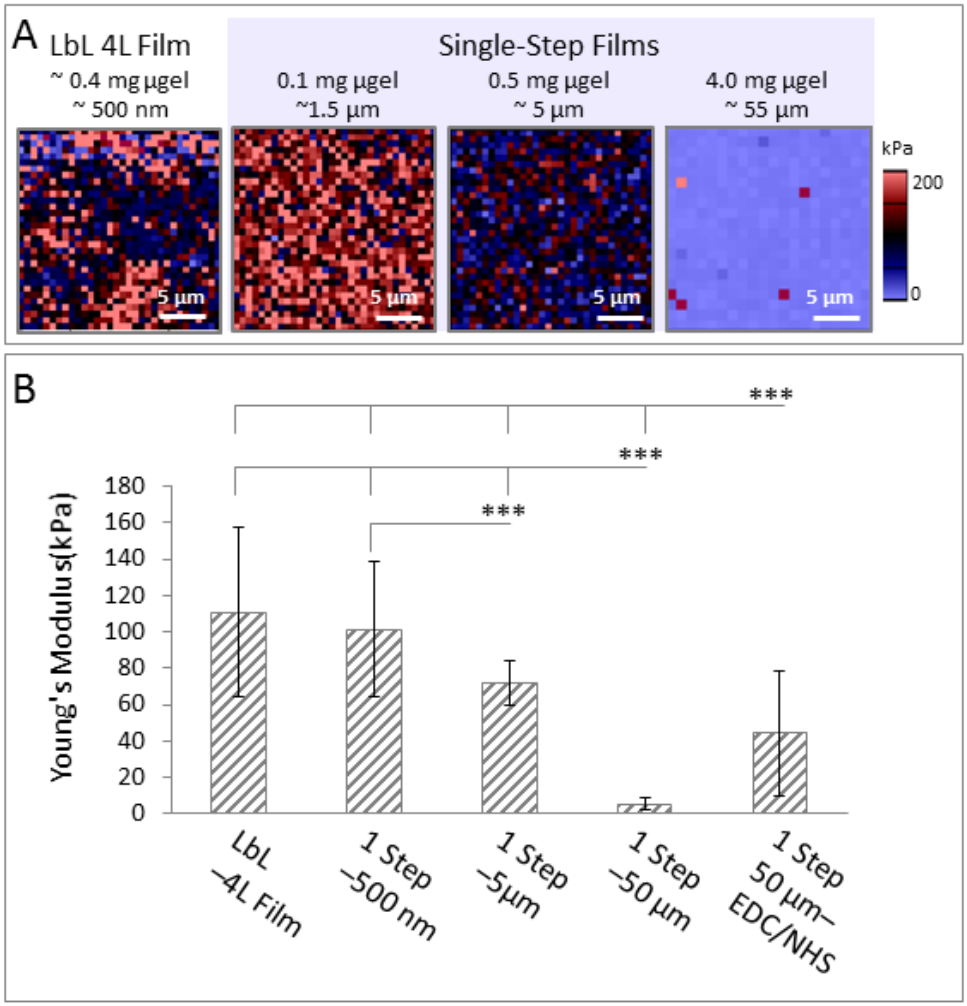

Figure 6.3. Characterization of microgel mechanical properties via AFM nanoindentation. (A) Representative AFM nanoindentation force maps are displayed. (B) Young's modulus was quantified. Error bars represent plus or minus the standard deviation of the average values from three independent samples. All comparisons of samples to either the single-step (1 Step) 50 µm or single-step 50 µm EDC/NHS samples are statistically significant ($p<0.001$). Comparison between the single-step 500 nm and single-step 5 µm films is also statistically significant ($p<0.01$). Statistical analysis was performed using the Kruskal-Wallis test with Dunn post-test analysis due to the significant differences between sample variations; all sample points were pooled together for statistical analysis.

Next, controlled swelling studies were performed where films were placed in either 10 mM formate buffer (pH 3.3), 10 mM MES buffer (pH 5.5) or 10 mM PBS (pH 7.4) with either 25 mM or 150 mM NaCl. Swelling studies reveal that films prepared on

12 mm diameter glass coverslips detach from the glass substrate when placed in acidic buffer conditions; specifically, films detach in 10 mM formate buffer (pH 3.3) or 10 mM MES buffer (pH 5.5) both with 150 mM NaCl, forming stable free-standing films (**Figure 6.4**). This detachment process is likely influenced by a strong force caused by the swelling of the film that is further promoted by changes in protonation of the acid groups on the microgels, which would be protonated below pH 4.6.

Further swelling studies were preformed to investigate the influence of film thickness and film area on the detachment process. In one of the studies, films were prepared on 22 mm diameter coverslips with either 1.5 mg, 3 mg, or 6 mg microgel; films `were then solvated in optimal buffer conditions (10 mM formate, pH 3.3, 100 mm NaCl) on a shaker for 24 h (**Figure 6.5**). All films prepared at the smallest thickness detach from the glass, tearing into pieces in the process. All films prepared with 3 mg of microgels also detach, but they do not exhibit appreciable tearing. Finally, approximately 33% of films prepared using 6 mg of microgels detach completely. In this case, the film exhibits rolling because the film has swollen to a size that is physically confined by walls of the 6-well-plate. A swelling study was also performed using 12 mm diameter coverslips (**Figure 6.6**), and in these studies, films prepared with 3 mg or 6 mg of microgels did not completely detach during the 24 h period of solvation in 10 mM formate (pH 3.3) buffer with 100 mM NaCl. Lack of film detachment may have occurred for several reasons. The thickness of the microgel films may inhibit the rate of swelling to an appreciable degree; an insufficient lateral swelling force could be responsible for the lack of film detachment. Stability studies reveal that if a film remains intact during the detachment process, the film will exhibit minimal degradation when left standing in

buffer for more than 3 months; films in neutral buffer slowly begin to detach from the glass (**Figure 6.7**). Overall, these studies demonstrate that preparation of microgel films using the single-step method followed by solvation in an acidic buffer is a simple route to obtain free-standing microgel films.

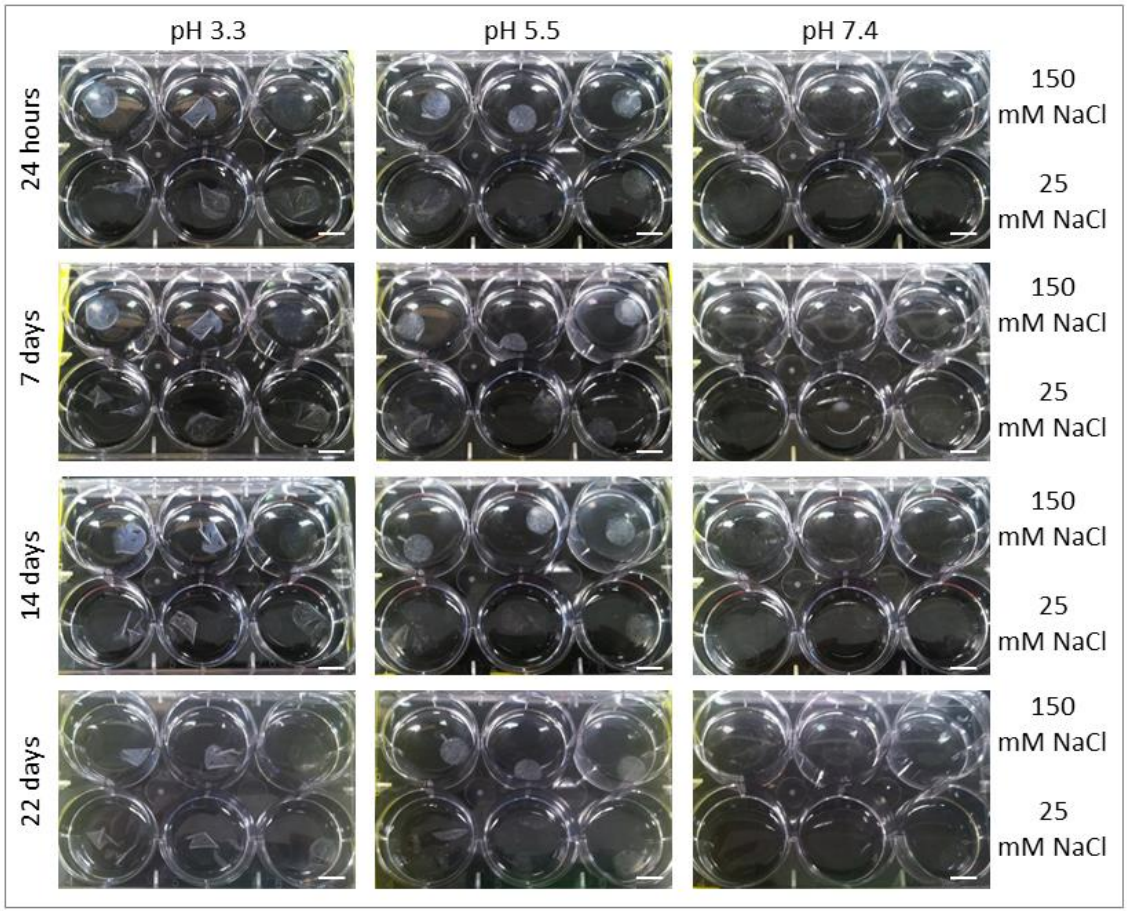

Figure 6.4. Characterization of microgel film swelling. Microgel films were prepared using the single-step method and left until dry. Films were then solvated in six buffers for several weeks to observe detachment. Buffer conditions included a high salt concentration (25 mM NaCl) and a low salt concentration (150 mM NaCl) for formate buffer (pH 3.3), MES buffer (pH 5.5), and PBS (pH 7.4). Scale bars represent 10 mm.

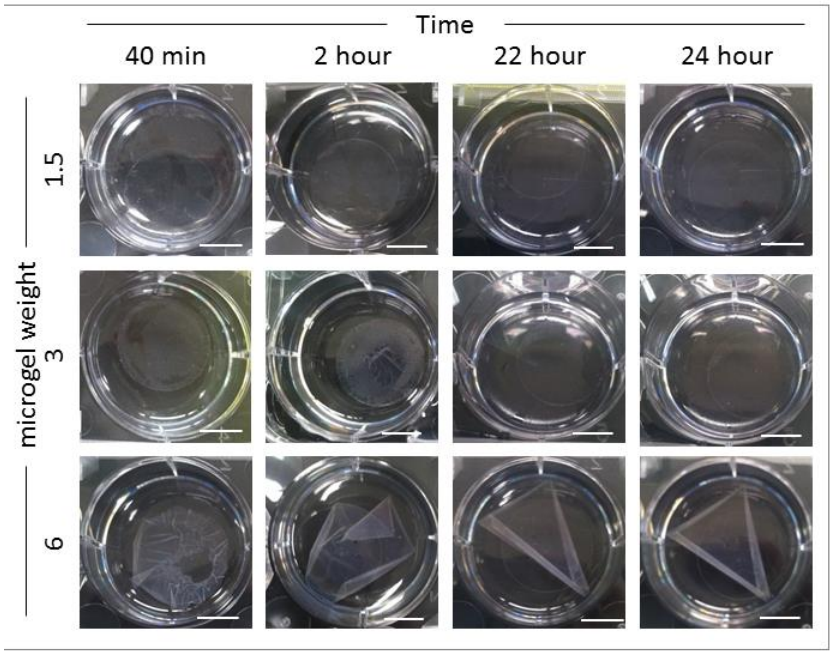

Figure 6.5. Characterization of film swelling dependence on size. Microgel films of varied thickness were prepared on functionalized glass coverslips (22 mm diameter) by modulating the weight of polymer used during fabrication. Films were dried and then hydrated in 10 mM formate (pH 3.3) with 100 mM NaCl. Films were left on a shaker for 24 h to assess detachment. Scale bars represent 10 mm.

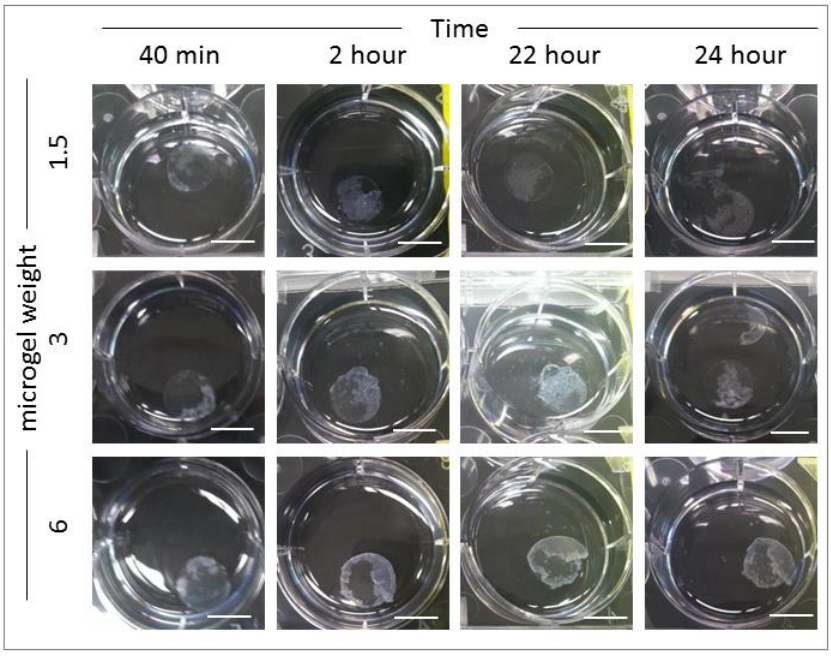

Figure 6.6. Characterization of film swelling dependency on size. Microgel films of varied thickness were prepared on functionalized glass coverslips (12 mm diameter) by

modulating the weight of polymer used during fabrication. Films were dried and then hydrated in 10 mM formate (pH 3.3) with 100 mM NaCl. Films were left on a shaker for 24 h after which detachment was assessed. Scale bars represent 10 mm.

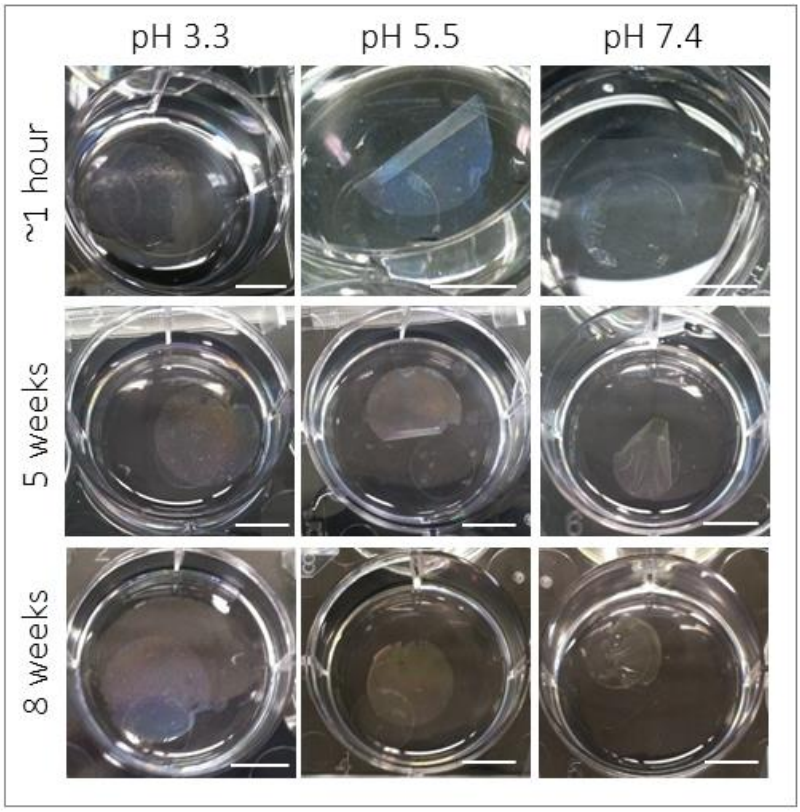

Figure 6.7. Characterization of film degradation over several weeks. Films that remain intact after detachment process remain stable in solution for several weeks. Scale bars represent 10 mm.

In addition, the single-step technique was demonstrated to enable the fabrication of an array of constructs with unique characteristics (**Figure 6.8**). First, films with a gradient of mechanical properties were fabricated simply based upon placement of coverslip and polyelectrolyte mixture in an outer well of a well-plate during centrifugation; this results in fabrication of a film that is thickest on the outside due to pooling of the material, which then exhibits gradual thinning. Such gradient films were

not extensively characterized, however, because the non-level surface of these films led to difficulties with AFM nanoindentation.

The use of hard sphere carboxyl-functionalized polystyrene (PS) beads and composite PS-microgel microparticles were also explored as alternative building blocks. Fabrication of monolayers of carboxyl-functionalized PS and composite raspberry-like particles was demonstrated using the single-step method. Finally, fabrication of films composed of microgels with polystyrene beads distributed throughout was demonstrated using the same approach. Hard spheres do not exhibit the same compressibility as microgels, providing another dimension of information regarding how building block characteristics influence the fabrication technique.

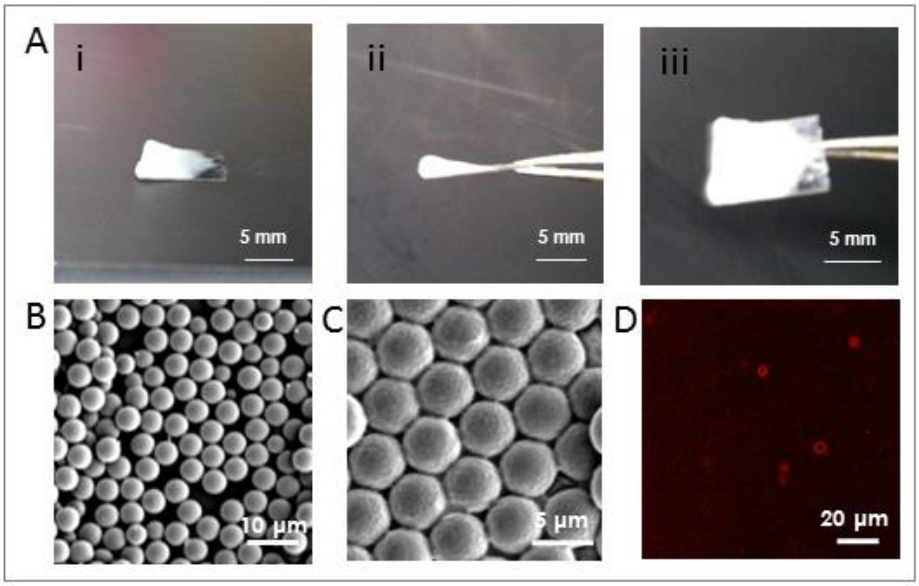

Figure 6.8. Visual characterization of various films fabricated using the single-step fabrication technique. (A) Gradient microgel films were prepared using the single-step fabrication technique by placing polymer components in a well located in either the first or last column of a 24-well-plate during centrifugation. The single-step fabrication can also be used to fabricate monolayers of (A) polystyrene beads and (B) raspberry-like particles (imaged via brightfield microscopy).

6.3.2. Investigation of Laterally and Perpendicularly Patterned Films

Next, the development of both laterally and perpendicularly patterned constructs was explored using modified versions of the single-step technique. In the "grid method," laterally patterned constructs were fabricated by depositing a monolayer of microgels onto a glass substrate, applying a TEM grid on top of the monolayer, depositing a solution of the polymer building blocks mixed with the polycation via centrifugation, and finally removing the TEM grid via gentle rinsing (and in some cases using tweezers). Fabrication of microgel films with micron-scale patterns was demonstrated. To fabricate perpendicularly patterned microgel constructs (**Scheme 6.3B**), microgels mixed with a polycation are deposited onto a glass coverslip to build the first layer. This step is then repeated with alternating microgel building blocks to build a vertical pattern. Because film thickness is controlled by the amount of microgels deposited, this technique can be used to create patterns with varied layer thicknesses if required. Using the grid method, fabrication of patterned microgel films with multiple micron-scale square sizes was also demonstrated (**Figure 6.9A**). Additionally, fabrication of patterned PS films with multiple pattern features including squares and channels was demonstrated (**Figure 6.9B**). Films prepared using both soft and hard building blocks exhibit well-defined pattern edges.

Scheme 6.3. Depiction of method to fabricate fabrication laterally and perpendicularly patterned films. (A) Laterally patterned films can be fabricated by deposition of a microgel monolayer followed by deposition of a mixture of microgels and polycation over a TEM grid, which is used as a deposition mask. (B) Fabrication of perpendicularly patterned films can be achieved by sequentially depositing a mixture of microgels and polycation.

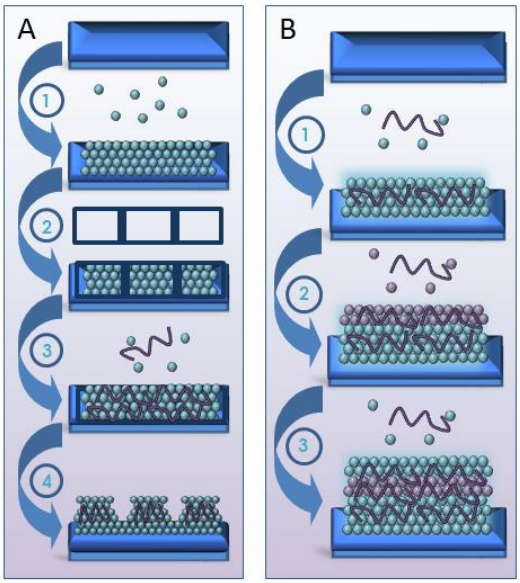

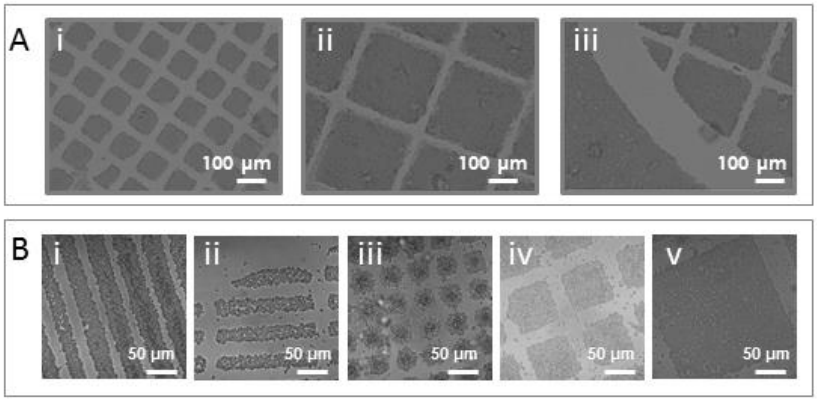

Figure 6.9. Characterization of laterally patterned microgel films. (A) Laterally patterned microgel films characterized via brightfield microscopy. (B) Laterally patterned PS films characterized via laser scanning confocal microscopy.

In terms of perpendicularly patterned films, constructs with two architectures were explored (**Figure 6.10**). First, the development of perpendicularly patterned

microgel constructs using two similar microgels was explored to demonstrate the ability to create distinct microgel layers. The two populations of microgels that were used were composed of pNIPAm (66 mol-%), AAc (30 mol-%), and BIS (4 mol-%); one population was unlabeled while the other was labeled red using Rhodamine-B. These films exhibit a perpendicular pattern containing five layers, three red layers and two non-fluorescent layers, establishing the efficacy of this patterning method. Next, the fabrication of perpendicularly patterned microgel films was explored using microgels with distinct compositions and, thus, mechanical properties and density. In these studies, development of patterned constructs was explored using the Rhodamine-B labeled microgels and ultra-low-cross-linked pNIPAm microgels containing 30 mol-% AAc labeled with AFA. In this case, three layers were deposited, yet only two layers are observed in the resulting construct. The absence of three layers suggests that the denser 4 mol-% BIS microgels penetrate the weaker ULC microgel layer, resulting in a single layer of each particle. Thus, use of building blocks with highly dissimilar mechanical properties and densities is possible, but may be limited by the number of layers formed.

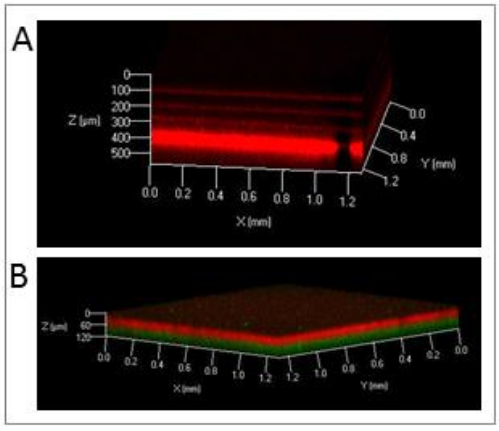

Figure 6.10. Perpendicularly patterned microgel films characterized via laser scanning confocal microscopy. (A) Films were fabricated using alternating layers of pNIPAm

microgels containing 30 mol-% AAc and 4 mol-% BIS. Five distinct layers are visible; the bottom red layer is an imaging artifact created by the glass substrate. (B) Films were fabricated using alternating layers of the ULC microgels and the 4 mol-% BIS microgels.

6.3.3. Investigation of Patterned Films as a Biological Interface

Previously the Lyon Group has assessed how fibroblast cells adhere and spread on microgel multilayers.[34] These studies demonstrated that fibroblasts exhibit less adhesion and spreading on microgel multilayers compared to microgel monolayers. These studies also demonstrated that this non-adherent behavior was not caused by a typical protein non-fouling mechanism. Instead, the non-adherent properties of these films were attributed to the mobility of components within the microgel polyelectrolyte network, which results in viscoelastic behavior of the films. Building upon these studies, the laterally patterned microgel films were explored as an intriguing construct to interrogate how fibroblast adhesion and spreading is influenced by microenvironments containing both microgel multilayers and monolayers. Laterally patterned microgel films were prepared using the grid method to assess fibroblast adhesion over a 24 h period (**Figure 6.11**). These studies reveal that pattern size influences fibroblast behavior (**Figure 6.12**). Overall, fibroblasts preferentially adhere on the monolayer section of these patterned films in between the microgel multilayer pillars. When fibroblasts are seeded onto films with smaller pattern sizes (80 µm x 80 µm), more cells are able to adhere. In fact, for these films, cells interacting with the microgel monolayers exhibit a high degree of spreading in between the multilayers. In contrast, for large microgel patterns where multilayer pillars are 283 µm x 283 µm, fibroblasts are unable to spread on the monolayer and exhibit a round morphology overall. In these studies, cell numbers were

low; five cells or less are present in all the images, revealing that these films inhibit cellular adhesion and proliferation. These findings suggest that patterned microgel films with smaller feature sizes can be used to obtain greater cellular adhesion and spreading; these films may also be used to direct cellular spreading. In contrast, the patterned microgel films containing larger features may exhibit a higher degree of film swelling due to the larger film area, which could contribute to the low cell attachment numbers and lack of cell spreading. Overall, these studies demonstrate that patterned microgel films present a unique experimental tool to assess cellular responses to a microenvironment for further development of platforms that either promote or inhibit cellular adhesion and proliferation.

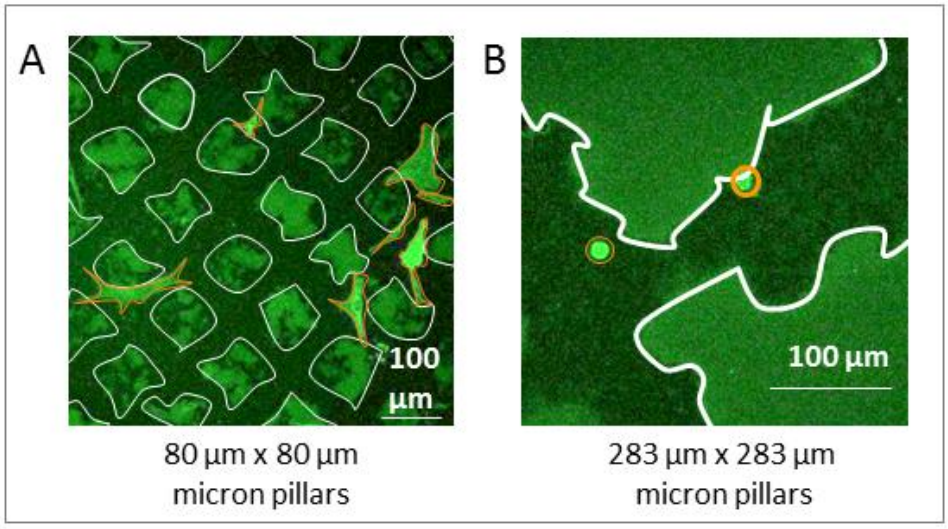

Figure 6.11. Fibroblast behavior is influenced by film patterns. NIH-3T3 cells were stained with either CellTracker Green CMFDA or Deep Red Dye (Life Technologies) to visualize the cell membrane. NIH-3T3 cells stably transfected with an m-Emerald Actin construct were utilized for analysis of actin distribution and alignment on microgel films. Cells were plated at a density of 5,000 cells/cm^2 on laterally patterned microgel films with either (A) 80 µm x 80 µm squares or (B) 283 µm x 283 µm. Cellular adhesion studies kindly performed by Dr. Ashley Brown.

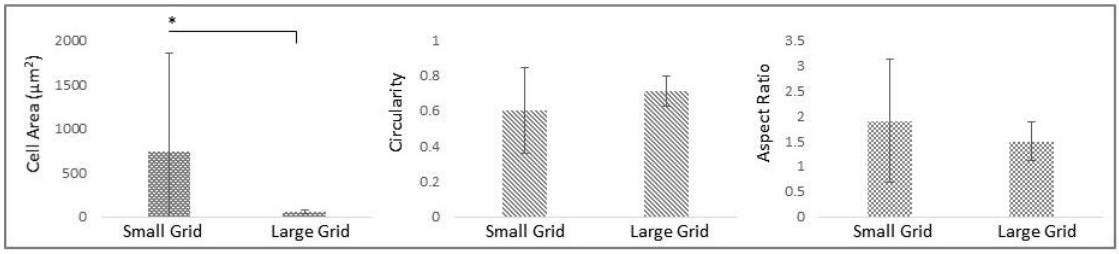

Figure 6.12. Fibroblast studies on laterally patterned microgel films. A two-tailed unpaired p-test was performed to assess statistical significances (*= $p<0.01$).

The response of fibroblasts to laterally patterned polystyrene films was also explored (**Figure 6.13**). Quantitative analysis of cell area, cell circularity, and cell aspect ratio reveal that fibroblast spreading is influenced by pattern features, pattern sizes, and building block sizes (**Figure 6.14** and **Figure 6.15**). When fibroblasts were seeded on films with polystyrene channels, fibroblasts adhere preferentially to the polystyrene beads and elongate along the polystyrene channels. For the polystyrene square patterned films, fibroblasts adhere preferentially to the polystyrene squares for larger pattern features. However, when pattern features approach the length scale of cells (30 μm x 30 μm PS square sizes), fibroblasts are more likely to bridge multiple PS squares (**Figure 6.13**). These responses suggest that this construct could be a strong platform to direct cellular adhesion and spreading, and could be useful for directing such responses for a variety of applications, such as enhanced wound healing.

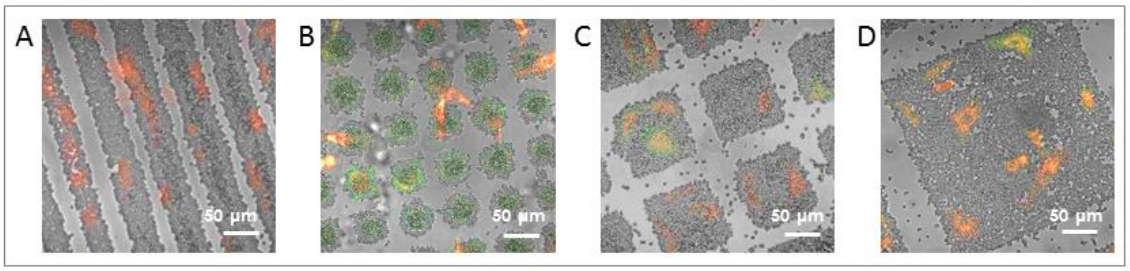

Figure 6.13. Fibroblast behavior is influenced by film patterns. NIH-3T3 cell were stained with either CellTracker Green CMFDA or Deep Red Dye (Life Technologies) to visualize the cell membrane. NIH-3T3 cells stably transfected with an m-Emerald Actin construct were utilized for analysis of actin distribution and alignment on microgel films. Cells were plated at a density of 5,000 cells/cm^2 on horizontally patterned PS films. Following 24 h in culture, samples were fixed and mounted. Image saturation was enhanced to allow visualization of the cells.

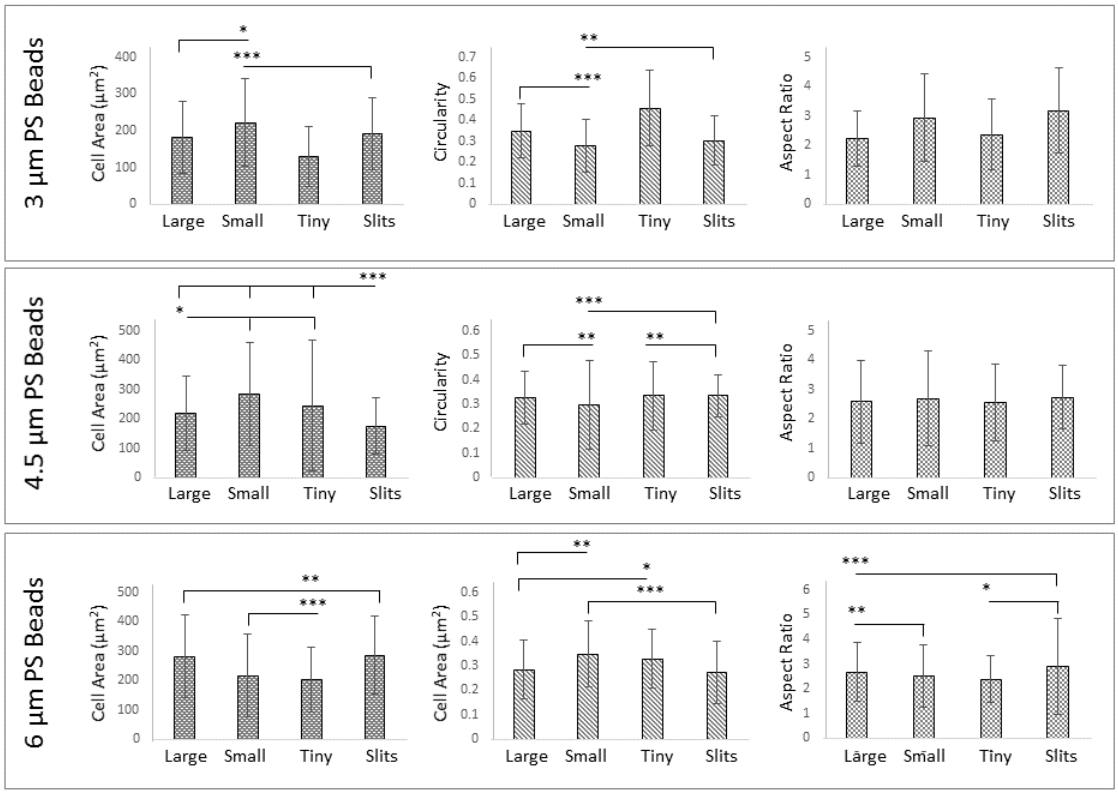

Figure 6.14. Fibroblasts on PS films. Comparison between fibroblast responses grid patterns with varied PS bead sizes. Statistical analysis was performed using the Kruskal-Wallis test with Dunn post-test analysis because the cells were not expected to exhibit a Gaussian distribution in response to these conditions; all sample points were pooled together for statistical analysis (***= $p<0.001$, **= $p<0.01$, *= $p<0.05$).

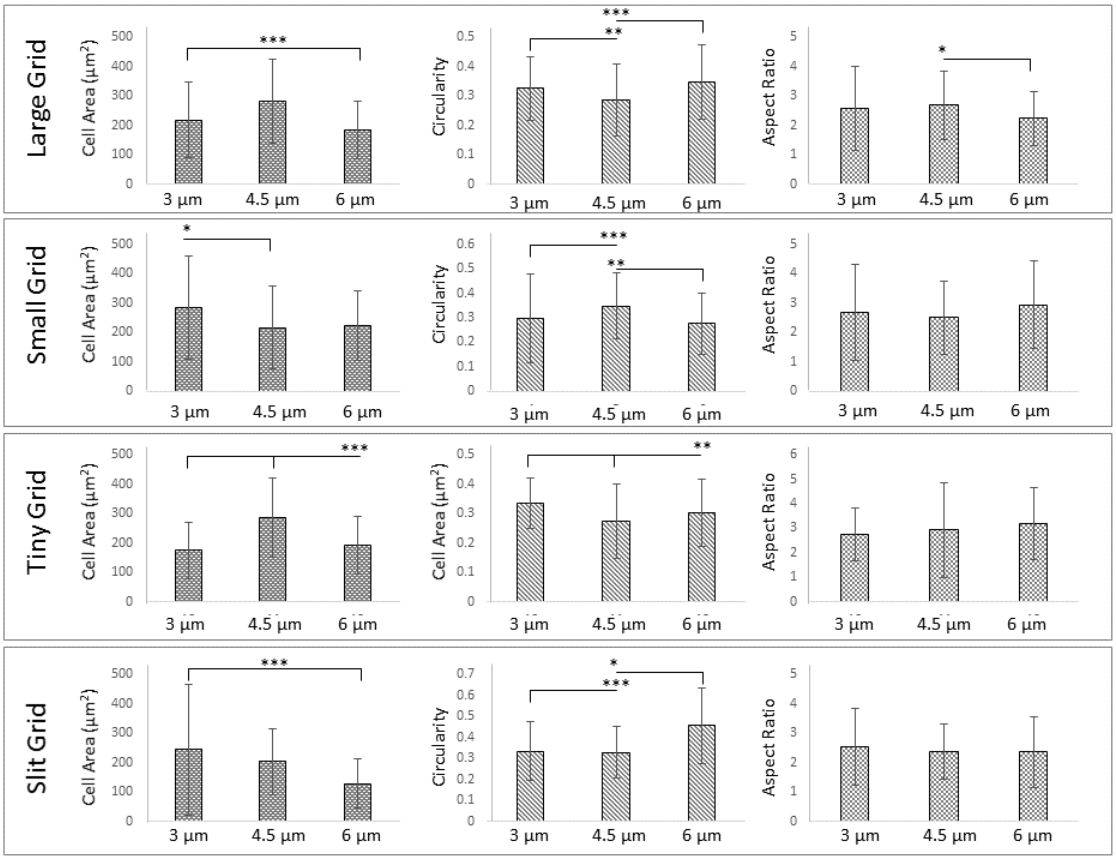

Figure 6.15. Fibroblasts on PS films. Comparison between fibroblast responses to different grid patterns at the same PS bead sizes. Statistical analysis was performed using the Kruskal-Wallis test with Dunn post-test analysis because the cells were not expected to exhibit a Gaussian distribution in response to these conditions; all sample points were pooled together for statistical analysis (***= $p<0.001$, **= $p<0.01$, *= $p<0.05$).

6.3.4. Investigation of Bulk Polyelectrolyte Microgel Gels

Finally, the development of bulk polyelectrolyte constructs was explored (**Scheme 6.4**). A simple modification of the single-step method allowed the fabrication of bulk gels; a microgel solution was mixed with a polycation solution, centrifuged in a microcentrifuge tube, and the supernatant was subsequently removed. This procedure can be further modified to enable cell encapsulation. In this case, a solution of cells was then added to the sample before centrifuging the sample for a short time (1 min or less) to distribute cells throughout the gels.

Scheme 6.4. Development of bulk polyelectrolyte gels. (A) Bulk gels are created by (1) centrifuging a mixture of polyelectrolyte and microgels within a microcentrifuge tube. Gels with encapsulated cells are then prepared by (2) centrifuging a solution of suspended cells into a fabricated gel.

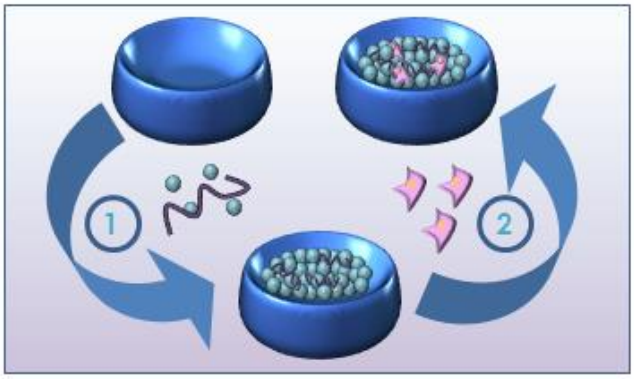

First, bulk gels were fabricated from typical pNIPAm-co-AAc microgels containing 4 mol-% BIS. Next, EDC/NHS cross-linking is demonstrated to be an effective route to tune the mechanical properties of the bulk gel by chemically cross-linking the polycation to the microgels (**Figure 6.16**). Composite bulk gels were also fabricated from two separate microgel components, including a typical microgels containing 4 mol-% BIS cross-linker as well as the ULC microgels. Oscillatory rheology was performed to investigate the mechanical properties of these gels (**Figures 6.17**, **6.18**, **6.19)**. In all cases, mechanical properties are similar and reminiscent to an elastic system on the region where experiments were performed. Finally, cell encapsulation within the bulk gels is demonstrated (**Figure 6.20**).

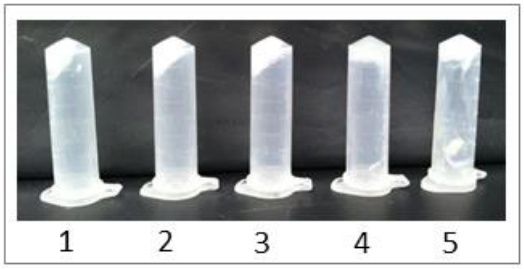

Figure 6.16. Development of bulk polyelectrolyte gels. Images of bulk gels. Samples 1-3 have been cross-linked with EDC/NHS at 20/50 mM, 2/5 mM, and 0.2/0.5 mM concentrations, respectively. Sample 4 contains a ULC gel and sample 5 is a mixture of 4 mol-% BIS microgels and ULC microgels.

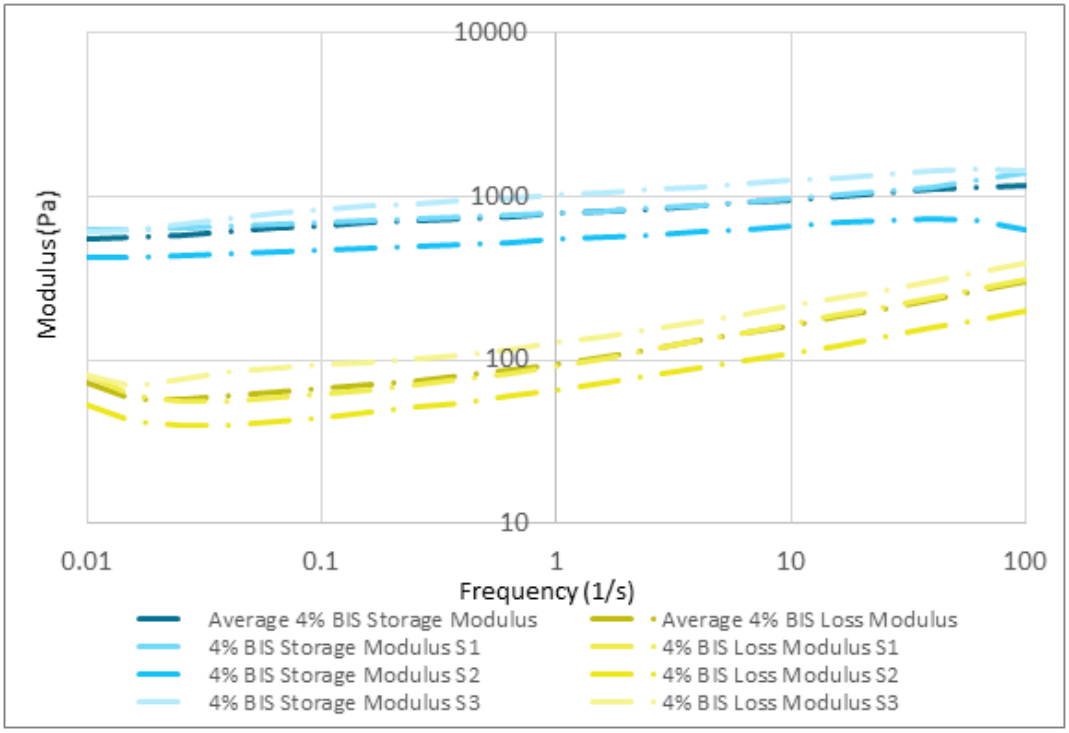

Figure 6.17. Rheological characterization of 4 mol-% BIS microgel bulk polyelectrolyte gel sample. The viscoelastic properties of these gels were studied under oscillatory shear conditions using a stress-controlled rheometer (Anton Paar, Physica MCR 501). Preshearing was performed to erase any history dependence of the result. The transition from the linear to nonlinear regime was first detected by conducting strain sweeps at constant frequency. The storage modulus, G', and loss modulus, G', were determined as a function of the angular frequency at a constant strain of 0.8. Rheology studies kindly performed by Dr. Miguel Fernandez.

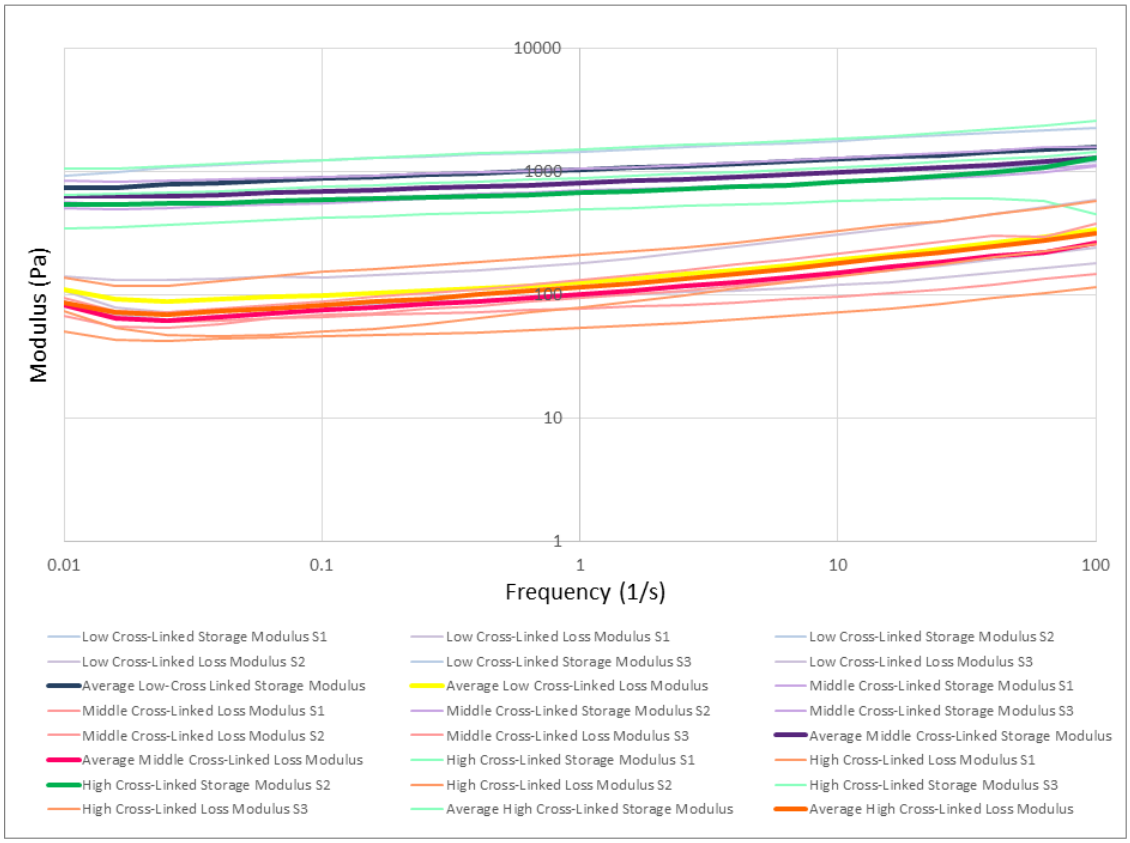

Figure 6.18. Rheological characterization bulk polyelectrolyte gels composed of 4 mol-% BIS microgels that have been cross-linked with either 0.2/0.5 (low), 2/5 (middle), or 20/50 (high) mM EDC NHS. The viscoelastic properties of these gels were studied under oscillatory shear conditions using a stress-controlled rheometer (Anton Paar, Physica MCR 501). Preshearing was performed to erase any history dependence of the result. The transition from the linear to nonlinear regime was first detected by conducting strain sweeps at constant frequency. The storage modulus, G', and loss moduls, G', were determined as a function of the angular frequency at a constant strain of 0.8.

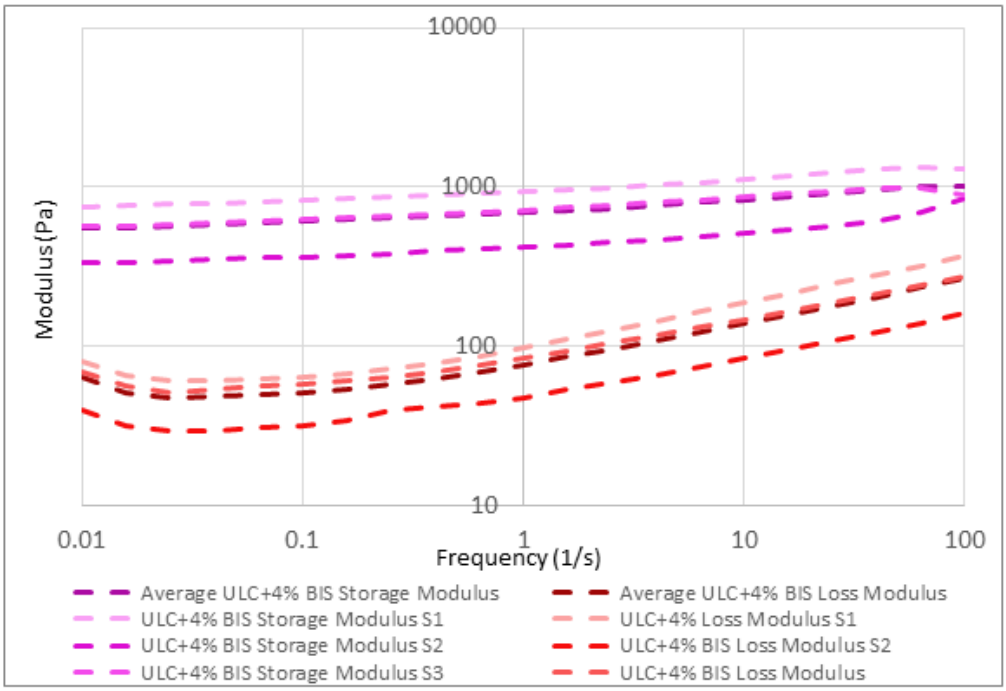

Figure 6.19. Rheological characterization of 50/50 mixture of ULC microgels and 4% BIS microgels in a bulk polyelectrolyte gel sample. The viscoelastic properties of these gels were studied under oscillatory shear conditions using a stress-controlled rheometer (Anton Paar, Physica MCR 501). Preshearing was performed to erase any history dependence of the result. The transition from the linear to nonlinear regime was first detected by conducting strain sweeps at constant frequency. The storage modulus, G', and loss modulus, G', were determined as a function of the angular frequency at a constant strain of 0.8.

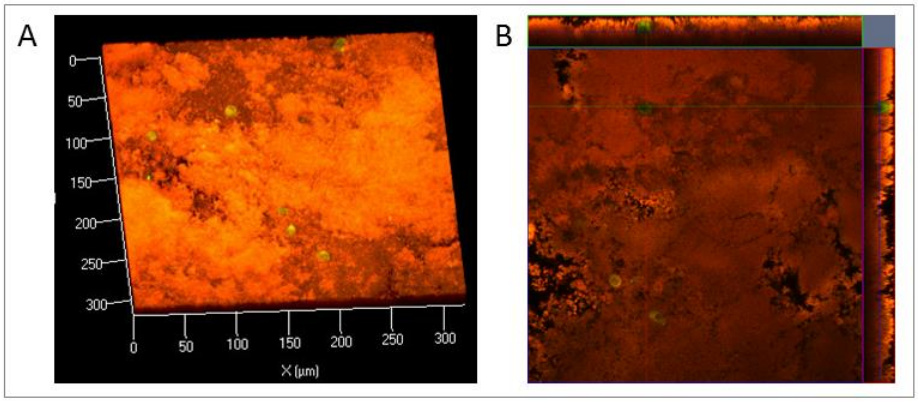

Figure 6.20. Cells encapsulated in bulk gels. Laser scanning confocal microscopy was used to image a (A) z-stack of a gel and (B) an orthogonal view on another gel that demonstrate cells are distributed within the gel.

6.4. Conclusions

This investigation details the versatility of a facile method to rapidly fabricate an array of polyelectrolyte constructs with varying levels of hierarchical structure. Specifically, the utility of this method to fabricate both two-dimensionally and three-dimensionally patterned microgel and PS constructs was established. Microgel films were fabricated using both the established LbL technique and the new "single-step" fabrication technique. Comparison between microgel films indicates that single-step films exhibit less heterogeneity in topographical features and mechanical properties than 4L LbL films. Investigation of single-step film swelling and degradation reveals that single-step films exhibit a high degrees of swelling; depending on film thickness, single-step microgel films solvated in acidic conditions are able to form stable free-standing microgel films. The "grid method" was established to fabricate laterally patterned microgel multilayer films and laterally patterned PS films. Laterally patterned films exhibit a variety of micron-scale features. The single-step method was used in a repetitive manner to successfully fabricate perpendicularly patterned microgel films using microgels of varied chemical and mechanical properties. Bulk polyelectrolyte gels were also fabricated and characterized; oscillatory rheology studies indicate that these systems are weakly elastic. Encapsulation of cells within bulk polyelectrolyte gels was demonstrated, as well. Overall, this method is fast, inexpensive and enabling, eliminating many of the constraints of previous techniques.

Laterally patterned microgel films and patterned PS films were used to interrogate cellular responses to patterned materials with varied mechanical properties. For patterned microgel films, cellular adhesion and spreading are influenced by feature size. Laterally

patterned PS films influence cell adhesion and spreading as well. Cellular adhesion studies demonstrate the utility of these constructs as competitive experimental tools to interrogate fundamental responses of cells to varied chemical, mechanical, or topographical features. Polyelectrolyte materials fabricated using this method can be used for a variety of applications including hemostatic materials, environmental sensing coatings, self-healing coatings, non-adherent coatings, drug delivery scaffolds, tissue engineering scaffolds, cell encapsulation scaffolds, underwater adhesives, medical adhesives, and further experimental tools.

6.5. References

1. Krishnamoorthy, S.; Hinderling, C.; Heinzelmann, H. Nanoscale patterning with block copolymers. *Mater. Today.* **2006**, *9* (9), 40-47.

2. Whitesides, G. M.; Grzybowski, B. Self-assembly at all scales. *Science.* **2002**, *295* (5564), 2418-2421.

3. Whitesides, G. M.; Ostuni, E.; Takayama, S.; Jiang, X. Y.; Ingber, D. E. Soft lithography in biology and biochemistry. *Annu. Rev. Biomed. Eng.* **2001**, *3*, 335-373.

4 Piner, R. D.; Zhu, J.; Xu, F.; Hong, S. H.; Mirkin, C. A. "Dip-pen" nanolithography. *Science.* **1999**, *283* (5402), 661-663.

5. Randolph, S. J.; Fowlkes, J. D.; Rack, P. D. Focused, nanoscale electron-beam-induced deposition and etching. *Crit. Rev. Solid State Mater. Sci.* **2006**, *31* (3), 55-89.

6. Kramer, S.; Fuierer, R. R.; Gorman, C. B. Scanning probe lithography using self-assembled monolayers. *Chem. Rev.* **2003**, *103*, 4367-4418.

7. Hoff, J. D.; Cheng, L. J.; Meyhofer, E.; Guo, L. J.; Hunt, A. J. Nanoscale protein patterning by imprint lithography. *Nano Lett.* **2004**, *4* (5), 853-857.

8. Levenson, M. D.; Viswanathan, N. S.; Simpson, R. A. Improving resolution in photolithography with a phase-shifting mask. *IEE Trans. Electron Devices.* **1982**, *29* (12), 1828-1836.

9. Qiu, Y.; Park, K. Environment-sensitive hydrogels for drug delivery. *Adv. Drug Deliv. Rev.* **2001**, *53* (3), 321-339.

10. Rana, D.; Kumar, T. S. S.; Ramalingam, M. Cell-Laden Hydrogels for Tissue Engineering. *J. Biomater. Tiss. Eng.* **2014**, *4* (7), 507-535.

11. Gawel, K.; Barriet, D.; Sletmoen, M.; Stokke, B. T. Responsive Hydrogels for Label-Free Signal Transduction within Biosensors. *Sensors.* **2010**, *10* (5), 4381-4409.

12. Tsutsui, H.; Yu, E.; Marquina, S.; Valamehr, B.; Wong, I.; Wu, H.; Ho, C.M. Efficient Dielectrophoretic Patterning of Embryonic Stem Cells in Energy Landscapes Defined by Hydrogel Geometries. *Ann. Biomed. Eng.* **2010**, *38* (12), 3777-3788.

13. Lee, Y.; Park, S.; Han, S. W.; Lim, T. G.; Koh, W.-G. Preparation of photolithographically patterned inverse opal hydrogel microstructures and its application to protein patterning. *Biosens. Bioelectron.* **2012**, *35* (1), 243-250.

14. Greiner, A. M.; Hoffmann, P.; Bruellhoff, K.; Jungbauer, S.; Spatz, J. P.; Moeller, M.; Kemkemer, R.; Groll, J. Stable Biochemically Micro-patterned Hydrogel Layers Control Specific Cell Adhesion and Allow Long Term Cyclic Tensile Strain Experiments. *Macromol. Biosci.* **2014**, *14*, 1547-1555.

15. Hsiao, T. W.; Tresco, P. A.; Hlady, V. Astrocytes alignment and reactivity on collagen hydrogels patterned with ECM proteins. *Biomaterials.* **2015**, *39*, 124-130.

16. McMurtrey, R. J. Patterned and functionalized nanofiber scaffolds in three-dimensional hydrogel constructs enhance neurite outgrowth and directional control. *J. Neural Eng.* **2014**, *11* (6), 066009. doi: 10.1088/1741-2560/11/066009.

17. Koh, W.-G.: Cell Microarrays Based on Hydrogel Microstructures for the Application to Cell-Based Biosensor. *Methods Mol. Biol.* **2011**, *671*, 133-145.

18. Meiring, J. E.; Lee, S.; Costner, E. A.; Schmid, M. J.; Michaelson, T. B.; Willson, C. G.; Grayson, S. M. Pattern recognition of shape-encoded hydrogel biosensor arrays. *Opt. Eng.* **2009**, *48* (3), 037201. doi: 10.1117/1.3099722

19. Pedrosa, V. A.; Yan, J.; Simonian, A. L.; Revzin, A. Micropatterned Nanocomposite Hydrogels for Biosensing Applications. *Electroanalysis.* **2011**, *23* (5), 1142-1149.

20. Hu, Z. B.; Chen, Y. Y.; Wang, C. J.; Zheng, Y. D.; Li, Y. Polymer gels with engineered environmentally responsive surface patterns. *Nature.* **1998**, *393*, 149-152.

21. Hahn, M. S.; Taite, L. J.; Moon, J. J.; Rowland, M. C.; Ruffino, K. A.; West, J. L. Photolithographic patterning of polyethylene glycol hydrogels. *Biomaterials.* **2006**, *27* (12), 2519-2524.

22. Wylie, R. G.; Ahsan, S.; Aizawa, Y.; Maxwell, K. L.; Morshead, C. M.; Shoichet, M. S. Spatially controlled simultaneous patterning of multiple growth factors in three-dimensional hydrogels. *Nature Mater.* **2011**, *10* (10), 799-806.

23. DeForest, C. A.; Polizzotti, B. D.; Anseth, K. S. Sequential click reactions for synthesizing and patterning three-dimensional cell microenvironments. *Nature Mater.* **2009**, *8* (8), 659-664.

24. Mosiewicz, K. A.; Kolb, L.; van der Vlies, A. J.; Lutolf, M. P. Microscale patterning of hydrogel stiffness through light-triggered uncaging of thiols. *Biomater. Sci.* **2014**, *2* (11), 1640-1651.

25. Clarke, K. C.; Douglas, A. M.; Brown, A. C.; Barker, T. H.; Lyon, L. A. Colloid-matrix assemblies in regenerative medicine. *Curr. Opin. Colloid Interface Sci.* **2013**, *18* (5), 393-405.

26. Guan, Y.; Zhang, Y. PNIPAM microgels for biomedical applications: from dispersed particles to 3D assemblies. *Soft Matter.* **2011**, *7* (14), 6375-6384.

27. Lyon, L. A.; Meng, Z. Y.; Singh, N.; Sorrell, C. D.; John, A. S. Thermoresponsive microgel-based materials. *Chem. Soc. Rev.* **2009**, *38* (4), 865-874.

28. Hu, X. B.; Tong, Z.; Lyon, L. A. One-Pot Synthesis of Microcapsules with Nanoscale Inclusions. *Macromol. Rapid Comm.* **2011**, *32* (18), 1461-1466.

29. Berndt, I.; Richtering, W. Doubly temperature sensitive core-shell microgels. *Macromolecules.* **2003**, *36* (23), 8780-8785.

30. Tripathi, B. P.; Dubey, N. C.; Stamm, M. Hollow Microgel Based Ultrathin Thermoresponsive Membranes for Separation, Synthesis, and Catalytic Applications. *ACS Appl. Mater. Inter.* **2014**, *6* (20), 17702-17712.

31. Lee, S. M.; Bae, Y. C. Swelling Behaviors of Doubly Thermosensitive Core-Shell Nanoparticle Gels. *Macromolecules.* **2014**, *47* (23), 8394-8403.

32. Serpe, M. J.; Yarmey, K. A.; Nolan, C. M.; Lyon, L. A. Doxorubicin uptake and release from microgel thin films. *Biomacromolecules.* **2005**, *6* (1), 408-413.

33. Nolan, C. M.; Serpe, M. J.; Lyon, L. A. Pulsatile release of insulin from Layer-by-Layer assembled microgel thin films. *Macromol. Symp.* **2005**, *227* (1), 285-294.

34. Saxena, S.; Spears, M. W., Jr.; Yoshida, H.; Gaulding, J. C.; Garcia, A. J.; Lyon, L. A. Microgel film dynamics modulate cell adhesion behavior. *Soft Matter.* **2014**, *10* (9), 1356-1364.

35. Hu, L.; Serpe, M. J. Color-Tunable Etalons Assembled from Poly (N-Isopropylacrylamide) Based Microgels. *Polymers.* **2012**, *4* (1), 134-149.

36. Sorrell, C. D.; Carter, M. C. D.; Serpe, M. J. Color Tunable Poly (N-Isopropylacrylamide)-co-Acrylic Acid Microgel-Au Hybrid Assemblies. *Adv. Funct. Mater.* **2011**, *21* (3), 425-433.

37. Decher, G. Fuzzy nanoassemblies: Toward layered polymeric multicomposites. *Science.* **1997**, *277* (5330), 1232-1237.

38. Peng, J.; Zhao, D.; Tang, X.; Tong, F.; Guan, L.; Wang, Y.; Zhang, M.; Cao, T., Cool microcontact printing to fabricate thermosensitive microgel patterns. *Langmuir.* **2013**, *29* (38), 11809-11814.

39. Lord, H. T.; Quinn, J. F.; Angus, S. D.; Whittaker, M. R.; Stenzel, M. H.; Davis, T. P. Microgel stars via Reversible Addition Fragmentation Chain Transfer (RAFT) polymerisation - a facile route to macroporous membranes, honeycomb patterned thin films and inverse opal substrates. *J. Mater. Chem.* **2003**, *13* (11), 2819-2824.

40. Domke, J.; Radmacher, M. Measuring the elastic properties of thin polymer films with the atomic force microscope. *Langmuir.* **1998**, *14* (12), 3320-3325.

41. Saxena, S.; Lyon, L. A. Influence of microgel packing on raspberry-like heteroaggregate assembly. *J. Colloid Interface Sci.* **2015**, *442*, 39-48.

42. Bachman, H.; Brown, A. C.; Clarke, K. C.; Dhada, K. S.; Douglas, A.; Hansen, C. E.; Herman, E.; Hyatt, J. S.; Kodlekere, P.; Meng, Z. Y.; Saxena, S.; Spears, M. W.; Welsch, N.; Lyon, L. A. Ultrasoft, highly deformable microgels. *Soft Matter.* **2015**, *11* (10), 2018-2028.

CHAPTER 7

MICROGEL FILMS AUGMENT HEMOSTASIS IN NEONATES

7.1 Introduction

Hemostasis is the first stage of wound healing during which liquid blood undergoes gelation, forming a blood clot, via the coagulation cascade (**Scheme 7.1**).[1] This process results in clotting that is localized at a vascular injury site, minimizing disturbance of blood flow elsewhere. In both the intrinsic and extrinsic pathway, the proteolytic enzyme thrombin mediates the proteolytic cleavage of fibrinogen into fibrin, initiating the final common pathway of the clotting cascade.[2-3] After this activation step, fibrin monomers polymerize into a robust fibrin network (**Scheme 7.2**). The fibrin network is strengthened through cross-links that are introduced by factor XIII ($fXIII_a$), which is also activated by thrombin.

Scheme 7.1. Coagulation cascade contains an intrinsic and extrinsic pathway.

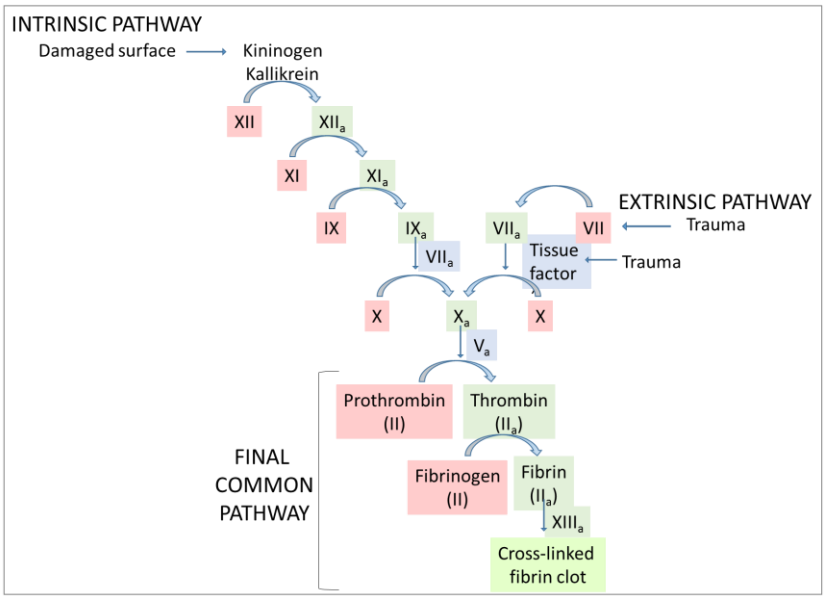

Scheme 7.2. Fibrin polymerization. Thrombin activates fibrinogen through cleavage of fibrinopeptides exposing Glycine-Histidine-Arginine sequences that enable polymerization.

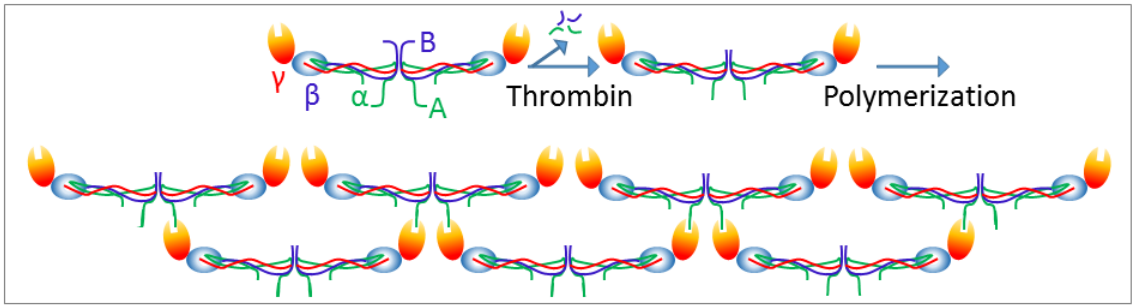

Neonates (children less than 30 days of age) are known to have underdeveloped coagulation systems. Although all key components of the hemostatic system are present at birth, many quantitative and qualitative differences exist. For example, the levels of FII, FVII, FIX, FX, FXI, Protein S, Protein C, Antithrombin, Heparin Cofactor II, Plasminogen, Prekallikrein, and High-Molecular Weight Kininogen are all half the level of adult concentrations in normal neonates; however, neonates maintain levels of FV, FVIII, FXIII, and fibrinogen that are closer to adult values.[4-6] A growing body of literature also suggests that neonatal fibrinogen, which exists until approximately one year of age, is qualitatively dysfunctional in comparison to adult fibrinogen. The first evidence of dysfunction in human fetal fibrinogen was the observance of delayed clotting times.[7] Soon after the idea emerged, scientists investigated differences in clotting of cord blood plasma and adult plasma.[8] Key findings indicated that fibrin polymerization time was longer for cord fibrinogen than for adult fibrinogen, which suggested that a polymerization defect may exist in fetal fibrinogen. This polymerization defect may be a result of several structural differences that exist between fetal fibrinogen and adult fibrinogen. Witt and Hasler previously investigated the differences in the amount of

organically bound phosphorous in fetal and adult fibrinogen.[9] They found that fetal fibrinogen contains twice as much organically bound phosphorous as adult fibrinogen. Further investigation has revealed that fetal fibrinogen contains increased concentrations of sialic acid, leading to charge differences.[10]

Past investigations have yielded conflicting information regarding the efficacy of the neonatal coagulation system, leading scientists to believe that there exists a delicate balance in the neonatal coagulation system when it is functioning properly that can be easily disrupted.[11,12] As an example patient population, neonates that have congenital heart defects must undergo reparative surgeries and often exhibit uncontrolled bleeding at suture sites post-operation. The current strategy to treat uncontrollable bleeding is to administer multiple transfusions of adult blood products. The necessity for numerous rounds of adult blood transfusions suggests that fundamental differences between neonatal and adult fibrinogen may inhibit robust clot formation. In addition to varied polymerization rates, the known biochemical differences between fetal fibrinogen and adult fibrinogen may result in (fibrin) polymer mixing issues during fibrin polymerization, contributing to the low efficacy of this treatment strategy. In addition, these biochemical differences may lead to ideal neonatal clotting conditions that are not typical of a physiological environment (i.e. varied pH and salt concentration).

In general, the field of hemostatic materials research has lagged behind the other fields of biomedical devices and medicine, resulting in few major clinical developments.[13] While hemostatic devices already exist, many do not meet the requirements of safety, efficacy, cost, and storage necessary for practical use. Among the materials being researched to develop improved hemostatic devices, hydrogels are of

interest because they are typically inexpensive, easy to handle, and often biocompatible. In addition, hydrogels enable the development hemostatic biomedical devices that take on many forms and can, thus, be explored for a variety of bleeding complications. For example, Behrens *et al.* demonstrated that hydrogel particles composed of N-(3-aminopropyl)methacrylamide can be used as a hemostatic agent, forming blood aggregates and promoting bulk blood coagulation.[14] Chen *et al.* demonstrated that reinforced poly(ethylene glycol)-chitosan hydrogels function effectively as a wound dressing and promote wound healing.[15] Ishihari *et al.* demonstrated that chitosan based hydrogels could be used to augment blood coagulation and subsequent wound healing.[16]

In the present investigation, microgel building blocks are used to fabricate bulk hydrogels, in the form of polyelectrolyte microgel films and gels, for use as hemostatic materials. Use of microgels to build bulk hydrogels is of particular interest because microgels can be easily tuned during synthesis or even post-synthesis, which can be leveraged for further development of more complex constructs. PNIPAm microgels, like those used in the Lyon Group, have previously been modified with a small peptide to augment blood clotting; these peptide-modified ultra-low cross-linked microgels exhibit platelet-like behaviors.[17] This investigation specifically explores the use of thick (>1 μm) microgel films for this application because they are less fragile than thin films (< 1 μm). These films were fabricated using the single-step fabrication technique described in **Chapter 6**. This method is faster than the established LbL approach and reduces microgel waste, which is beneficial for potential commercialization. Additionally, previous characterization, detailed in **Chapter 6**, demonstrates that these films can detach from the glass coverslip as stable, free-standing films, which could also be leveraged for

future device development. Due to the known differences between fetal fibrinogen and adult fibrinogen, we believe microgel films soaked in buffers can be used as a surgical dressing to tune the local pH and salt concentration at a wound site in order to promote the polymerization of fetal fibrinogens; success of this strategy will help reduce the number of adult blood transfusions required of neonates.

In the present investigation, the influence of pH and salt concentration on neonatal and adult clotting is explored using plasma and whole blood where low levels of thrombin are doped in to activate the clotting cascade. Through real-time imaging of clotting *in situ*, structural features are assessed at varied pH and salt conditions. Next, clotting is assessed on microgel films soaked in the same electrolyte solutions. Using real-time imaging of clotting *in situ*, the influence of microgel films on both neonatal and adult clotting was observed. Finally, clotting on microgel films is assessed using re-calcified whole blood in order to compare clotting of platelet-poor-plasma to clotting of whole blood on microgel films.

7.2. Experimental

7.2.1. Materials

Materials used in this investigation are described in section **2.2.1** with the following additions. Acrylic acid (AAc)) was used as received. Branched polyethyleneimine (PEI) (typical Mw = 750 kDa) 50% w/w solution in water was prepared as 0.086 g/mL in PBS. All in vitro fibrin polymerization assays were conducted with materials purchased from Enzyme Research Laboratory unless stated otherwise.

7.2.2. Collection of Neonatal Plasma Samples and Isolation of Neonatal Platelet-Poor Plasma

In accordance with our Emory University IRB approval, neonatal blood was collected from patients prior to undergoing a non-emergent cardiac surgery. After placement into an appropriate citrated tube, samples were centrifuged for 20 min to yield platelet poor plasma (PPP) and stored at -80 ˚C. We obtained a single baseline sample of blood in six patients. After isolation of PPP, samples were pooled in order to isolate purified neonatal fibrinogen through affinity chromatography using GPRP-sepharose beads.[18] Sodium Borate (pH 5.4) was used to dissociate fibrinogen from beads after a one hour incubation period. The isolated fibrinogen was then transferred into HEPES buffer (25 mM HEPES, 150 mM NaCl, ph7.4) and stored at -80 ˚C. Highly pure fibrinogen (>90%) was isolated.

7.2.3. Collection of Adult Plasma and Isolation of Adult Platelet-Poor Plasma

Whole blood was obtained from healthy adults in citrated tubes. Samples were centrifuged at 150 x g for 15 min to obtain platelet rich plasma (PRP). PRP was centrifuged a second time at 900 x g for 5 min to obtain PPP and stored at -80 ◦C.

7.2.4. Collection of Adult Whole Blood

Whole blood was obtained from an adult donor and treated with citrate to inhibit coagulation until the experiment began.

7.2.5. Microgel Synthesis

Microgels were synthesized using the procedure outlined in section **2.2.2** with a few modifications. The total monomer concentration was 100 mM with a molar composition of 66% NIPAm, 30% AAc, and 4% BIS. NIPAm, SDS, and BIS were dissolved in water. The solution was added to a 3-neck round bottom flask and heated to 70 ℃ while purging with nitrogen and stirring for 1 h. AAc was added 10 min prior to

reaction initiation; 1 mL of APS solution in water was added and the reaction was allowed to proceed for 4 h.

7.2.6 Microgel Characterization

Diffusion coefficients were determined by dynamic light scattering (DLS) using a DynaPro DLS (Wyatt Technology Corporation, Santa Barbara, CA) equipped with temperature control. Hydrodynamic radii (R_H) and polydispersity values were calculated using Dynamics software for each particle type used in these experiments. DLS data can be found in **Chapter 6**.

7.2.7 Microgel Film Fabrication

Microgel films were fabricated as previously described in section **6.2.4.** Films were prepared by centrifuging a mixture of 150 µL of microgel (10 mg/mL) and 150 µL of PEI (0.086 g/mL), and 300 µL of PBS on either 9 x 9 mm glass coverslips or 12 mm diameter glass coverslips that were previously functionalized with APTMS.

7.2.8 Clot Formation and Characterization *In Vitro*

30 µL clots were formed from purified human fibrinogen (2.5 mg/mL), NaCl (25, 150, or 300 mM), $CaCl_2$ (5 mM), HEPES buffer (25 mM) and the addition of human alpha-thrombin (5 U/mL). Fluorescently labeled purified adult fibrinogen (10%) was included to allow for visualization of fibrin network. Clots were polymerized between a glass slide and a cover glass, allowed to polymerize for 2 h, and then imaged via a Zeiss Laser Scanning Confocal Microscope (LSM 510 VIS, Zeiss Inc., Thornwood, NY).

7.2.9 Clot Formation and Characterization on Microgel Films *In Vitro*

Clots were formed from adult PPP, neonatal PPP, and adult whole blood that was re-calcified. Films were solvated in 1 mL of HEPES for a minimum of 30 min on a

shaker prior to use. Films were removed from HEPES 5-10 min before each sample to decrease the interference of an excess of HEPES on the studies. For adult PPP samples, a 25 µL sample of PPP containing Alexa-Flour 555 labeled fibrinogen (0.1 mg/mL)) and human alpha-thrombin (0.1 U/mL) was added to each film. For neonatal PPP samples, a 30 µL sample of PPP containing Alexa-Flour 555 labeled fibrinogen (0.1 mg/mL)) and human alpha-thrombin (0.25 U/mL) was added to each film. For whole blood samples, 50 µL whole blood, 5 µL Alexa-Flour 488 labeled fibrinogen (5% v/v), and 5 µL $CaCl_2$ (0.1 M) were combined and mixed. Using this stock, 25 µL clots were deposited on top of a microgel film for whole blood experiments. Films were imaged in 5 min intervals over a 20 min period to monitor clot formation via a Zeiss Laser Scanning Confocal Microscope (LSM 510 VIS, Zeiss Inc., Thornwood, NY).

7.3. Results and Discussion

7.3.1. Influence of pH and Ionic Strength on Fibrin Polymerization *In Vitro*

First, we explored formation of neonatal and adult clots at varied pH and salt concentrations to determine the influence of these factors on clotting in the absence of a microgel film (**Figure 7.1**). We explored a large range of pH and salt concentrations, which enabled us to later target pH and salt concentration ranges that enhance blood clotting for further studies. Purified neonatal fibrinogen clots formed at physiological condition and pH 5 with 300 mM NaCl result in poorly developed clots with little fibrous structure apparent. In contrast, neonatal clots formed at pH 9 and pH 7.4 with either 25 mM or 125 mM NaCl have a distinctly aligned fiber structure. Notably, clots formed at pH 7.4 with 25 mM NaCl have the densest and most branched fibrin network. When looking at the adult blood clots, those formed from purified adult fibrinogen polymerized

at low pH (pH 5) and/or low salt concentration (NaCl), highly branched three-dimensional fibrin networks form. All other conditions exhibit limited clotting with the formation of aligned wispy fibers in some cases. These findings demonstrate that pH and salt concentration influence both neonatal and adult clotting. However, this simple alteration of pH and salt concentration does not lead to the formation of a robust neonatal fibrin network. Because clots formed at pH 9 and 300 mM NaCl do not appear to have a more robust clot structure as determined by fibrin branching, we chose not to include these conditions in later studies.

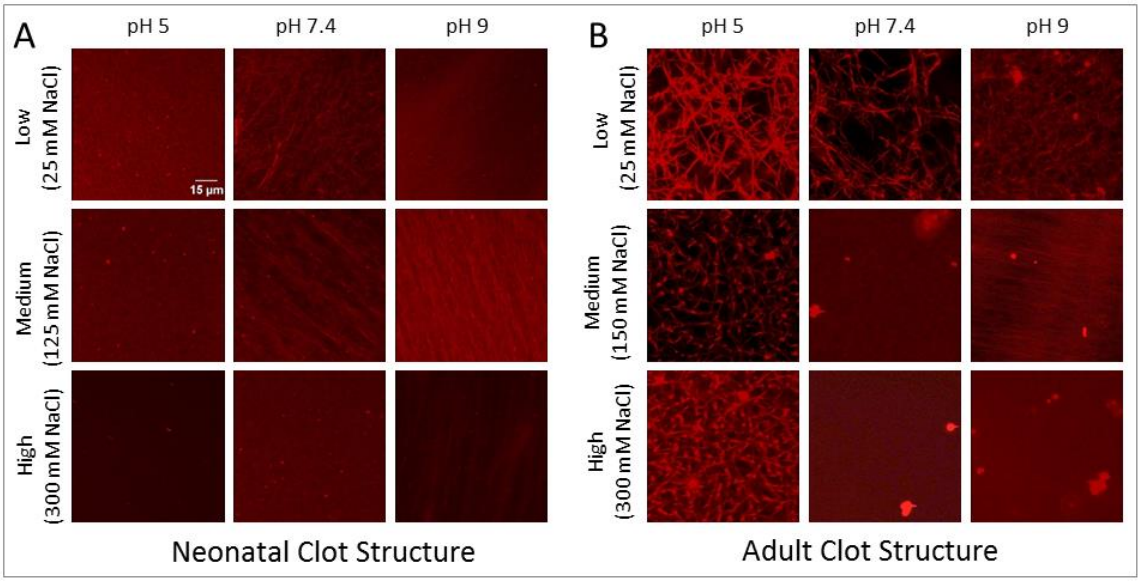

Figure 7.1. Neonatal blood clots that form have wispy aligned fibers. Low pH and low salt concentration promote the development of a three-dimensional adult fibrin network. (A) Neonatal and (B) adult clots were formed at three pH conditions and three salt concentrations between glass coverslips. Samples were polymerized for 2 h and then imaged via laser scanning confocal microscopy. 3D projections are shown. Scale bar indicates 15 µm.

7.3.2. Influence of Solvent-Swollen Microgel Film on Fibrin Polymerization *In Vitro*

We next explored the formation of adult and neonatal clots on microgel films swollen in varied electrolyte solutions. Overall, adult blood clots formed on microgel films are dense and branched at the end of a 20 min monitoring period (**Figure 7.2**). Blood clots appear to be more highly branched at pH 7.4 than at pH 5. These results demonstrate that the presence of swollen microgel films influences the fibrin network structure. The polymerization studies performed on microgel films resulted in fibrin network structures that are more similar to one another at all solution conditions as compared to clots formed in the absence of microgel films. These results suggest that the microgel film itself is also contributing to the augmentation of blood clotting, likely through swelling of the film and local buffering.

Neonatal blood clots were next formed on microgel films and monitored over a 20 min period (**Figure 7.3**). Polymerization studies indicate that fibrin network formation is influenced by solution conditions. At pH 5, clots have small, branched fibrin fibers forming a network structure with a small mesh size. While salt concentration does not appear to have an appreciable effect on clots formed at pH 5, salt concentration appears to influence the structure of clots formed at pH 7.4. For both salt concentrations at pH 7.4, fibrin networks appear less dense and exhibit a larger mesh size and longer fibers as compared to clots formed at pH 5. In comparison to clots formed at pH 7.4 and 150 mM NaCl, clots formed at pH 7.4 and 25 mM NaCl exhibit a smaller mesh size and appear to be less branched.

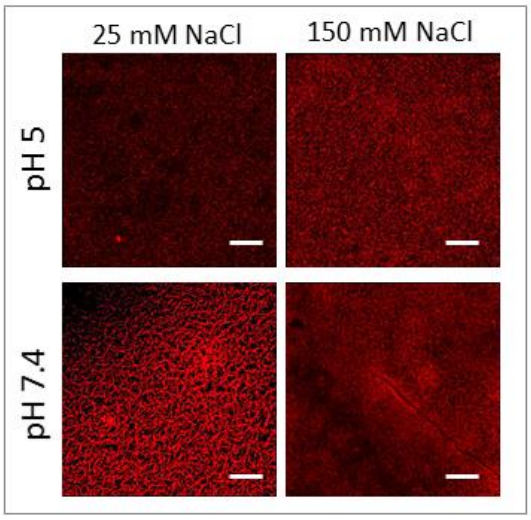

Figure 7.2. Adult blood clots that form exhibit robust three-dimensional fibrin networks on microgel films regardless of pH or salt concentration. Clots were formed from adult PPP with labeled fibrinogen and a low concentration of human alpha-thrombin (0.1 U/mL) on microgel films. Clots were monitored over a 20 min period using laser scanning confocal microscopy. 3D projections are shown. All scale bars represent 50 µm.

Neonatal clot structure is strongly influenced by the presence of microgel films as can be seen clearly by comparison of pH and ionic strength conditions of clots prepared in the absence or presence of microgel films (**Figures 7.1A** and **Figure 7.3**). Clots polymerized in the absence of microgel films exhibit wispy fibers that are aligned in most cases. A robust three-dimensional fibrin network is not apparent for clots formed at any polymerization condition in the absence of the microgel film. These differences suggest that microgel films promote the formation of a three-dimensional fibrin network through a swelling mechanism. The presence of the swollen microgel film both maintains the pH and salt concentration where the clot is localized, while providing a soft scaffold for the fibrin network to polymerize through. Differences in clot structures, such as porosity and fiber length, which are seen when using microgel films solvated in different solutions, are a result of both the varied pH and ionic strength conditions as well as the varied degree of swelling of the film network. When comparing neonatal fibrin network structures formed

in pH 5 conditions versus pH 7.4 conditions, the differences seen are likely due to pH; as clots prepared using these solution conditions in the absence of microgel films also have unique fibrin network structures. However, solution conditions will alter both the swelling of the individual microgels and the network as a whole, leading to differences in microgel microstructure that may contribute to the varied porosity seen in neonatal clots formed at pH 7.4 at varied salt concentration.

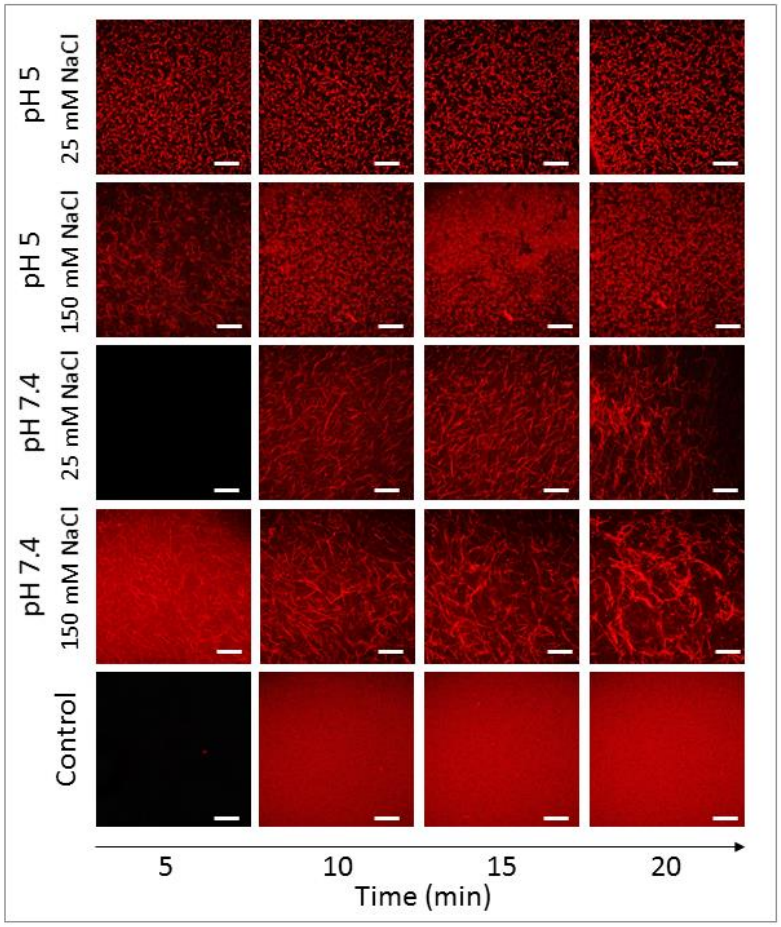

Figure 7.3. Neonatal clots that form exhibit enhanced three-dimensional fibrin network formation when placed on solvated microgel films. Clot structure is influenced by pH and salt concentration. Clots were formed from neonatal PPP with labeled fibrinogen and a low concentration of human alpha-thrombin (0.25 u/mL) on thick microgel films. Clots were monitored over a 20 min period using laser scanning confocal microscopy. Contrast and brightness of the images were enhanced for visualization. All scale bars represent 50 µm. Images kindly collected by Dr. Ashley Brown.

7.3.3. Influence of Solvated Microgel Film on Clot Formation *In Vitro* Using Whole Blood

Finally, we explored the polymerization of clots on microgel films using re-calcified adult whole blood at the same pH and salt conditions as before, but with either a highly concentrated (5x) solution or the standard solution (1x) (**Figure 7.4**). These polymerization studies were conducted to provide a more physiologically-relevant biological system for further validation. In addition, these studies provide critical information for comparison to future microfluidic studies in order to deduce the influence of dilution during clotting in a vasculature setting. These polymerization studies demonstrate that in all conditions, robust three-dimensional fibrin networks form; however, results indicate a preference for clot formation in standard conditions versus concentrated conditions when viewing experimental repetitions. These clotting studies also reveal that the fibrin clots are not homogeneous, displaying heterogeneity at the 100-200 micron level that is not present when PPP is used.

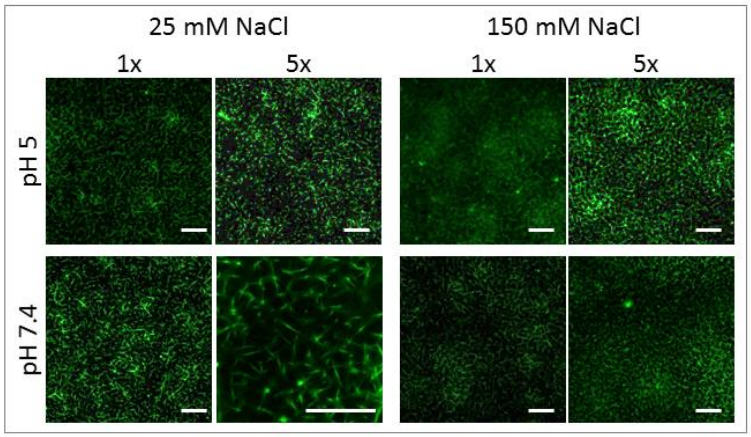

Figure 7.4. Clots formed from re-calcified adult whole blood with labeled fibrinogen on thick microgel films solvated in HEPES solutions (1x and 5x concentrations). Clots were

monitored over a 20 min period using laser scanning confocal microscopy. Contrast and brightness of the images were enhanced for visualization. All scale bars represent 50 μm.

These studies reveal critical information regarding the preparation of microgel films for use as a hemostatic dressing. Experimental observations seen throughout the investigation suggest that microgel films should be fully dried before hydration for highest efficacy in augmentation of blood clotting. These studies also reveal that films applied immediately after solvation without a few minutes to allow "drying" exhibit limited augmentation of blood clotting. These findings suggest that if too much solution is present the clotting factors may be diluted, inhibiting the formation of a robust fibrin clot.

7.4. Conclusions

Fibrin clotting studies were performed to explore the influence of pH and ionic strength on both adult and neonatal clotting. Clotting studies reveal that pH and ionic strength highly influence the fibrin network structure in an adult clot. In contrast, pH and ionic strength appear to have a modest influence on the formation of neonatal clot structure. In addition, we demonstrated the ability to modulate and augment blood clotting using microgel films soaked in electrolyte solutions. In particular, use of swollen microgel films enables the formation of robust, three-dimensional neonatal fibrin networks not seen through simple alteration of pH and ionic strength conditions. Future studies will explore the influence of flow on the time required for clotting to occur on microgel films. In addition, *in vivo* studies will be performed to further assess the efficacy of this system for potential commercialization.

7.5. References

1. Davie, E. W.; Fujikawa, K.; Kisiel, W. The coagulation cascade - initiation, maintenance, and regulation. *Biochemistry.* **1991**, *30* (43), 10363-10370.

2. Crawley, J. T. B.; Zanardelli, S.; Chion, C.; Lane, D. A. The central role of thrombin in hemostasis. *J. Thromb. Haemost.* **2007**, *5*, 95-101.

3. Tanaka, K. A.; Key, N. S.; Levy, J. H. Blood Coagulation: Hemostasis and Thrombin Regulation. *Anesth. Analg.* **2009**, *108* (5), 1433-1446.

4. Andrew, M.; Paes, B.; Milner, R.; Johnston, M.; Mitchell, L.; Tollefsen, D. M.; Powers, P. Development of the human coagulation system in the full-term infant. *Blood* **1987**, *70* (1), 165-172.

5. Andrew, M.; Paes, B.; Milner, R.; Johnston, M.; Mitchell, L.; Tollefsen, D. M.; Castle, V.; Powers, P. Development of the human coagulation system in the healthy premature-infant. *Blood.* **1988**, *72* (5), 1651-1657.

6. Andrew, M.; Paes, B.; Johnston, M. Development of the hemostatic system in the neonate and young infant. *Am. J. Pediat. Hematol.* **1990**, *12* (1), 95-104.

7. Witt, I.; Muller, H.; Kunzer, W. Evidence for existence of foetal fibrinogen. *Thromb. Diath. Haemorrh.* **1969**, *22* (1), 101

8. Tegernil.Ac; Ekelund, H. Fibrinogen to fibrin transformation in umbilical-cord blood and purified neonatal fibrinogen. *Thromb. Res.* **1974**, *5* (5), 601-612.

9. Witt, I.; Hasler, K. Influence of organically bound phosphorus in fetal and adult fibrinogen on kinetics of interaction between thrombin and fibrinogen. *Biochim. Biophys. Acta.* **1972**, *271* (2), 357-362.

10. Galanakis, D. K.; Martinez, J.; McDevitt, C.; Miller, F. Human-fetal fibrinogen -- its characteristics of delayed fibrin formation, high sialic-acid and ap peptide content are more marked in preterm than in term samples. *Ann. NY. Acad. Sci.* **1983**, *408*, 640-643.

11. Saxonhouse, M. A.; Manco-Johnson, M. J. The Evaluation and Management of Neonatal Coagulation Disorders. *Semin. Perinatol.* **2009**, *33* (1), 52-65.

12. Saracco, P.; Parodi, E.; Fabris, C.; Cecinati, V.; Molinari, A. C.; Giordano, P. Management and investigation of neonatal thromboembolic events: Genetic and acquired risk factors. *Thromb. Res.* **2009**, *123* (6), 805-809.

13. Behrens, A. M.; Sikorski, M. J.; Kofinas, P. Hemostatic strategies for traumatic and surgical bleeding. *J. Biomed. Mater. Res. A.* **2014**, *102* (11), 4182-4194.

14. Behrens, A. M.; Sikorski, M. J.; Li, T. L.; Wu, Z. J. J.; Griffith, B. P.; Kofinas, P. Blood-aggregating hydrogel particles for use as a hemostatic agent. *Acta Biomater.* **2014**, *10* (2), 701-708.

15. Chen, S. H.; Tsao, C. T.; Chang, C. H.; Lai, Y. T.; Wu, M. F.; Chuang, C. N.; Chou, H. C.; Wang, C. K.; Hsieh, K. H. Assessment of reinforced poly(ethylene glycol) chitosan hydrogels as dressings in a mouse skin wound defect model. *Mater. Sci. Eng. C Mater. Biol. Appl.* **2013**, *33* (5), 2584-2594.

16. Ishihara, M.; Nakanishi, K.; Ono, K.; Sato, M.; Kikuchi, M.; Saito, Y.; Yura, H.; Matsui, T.; Hattori, H.; Uenoyama, M.; Kurita, A. Photocrosslinkable chitosan as a dressing for wound occlusion and accelerator in healing process. *Biomaterials.* **2002**, *23* (3), 833-840.

17. Brown, A. C.; Stabenfeldt, S. E.; Ahn, B.; Hannan, R. T.; Dhada, K. S.; Herman, E. S.; Stefanelli, V.; Guzzetta, N.; Alexeev, A.; Lam, W. A.; Lyon, L. A.; Barker, T. H. Ultrasoft microgels displaying emergent platelet-like behaviours. *Nature Mater.* **2014**, *13* (12), 1108-1114.

18. Stabenfeldt, S. E.; Gossett, J. J.; Barker, T. H. Building better fibrin knob mimics: an investigation of synthetic fibrin knob peptide structures in solution and their dynamic binding with fibrinogen/fibrin holes. *Blood.* **2010**, *116* (8), 1352-1359.

CHAPTER 8

CONCLUSIONS AND FUTURE DIRECTIONS

8.1. Introduction

In this dissertation, development of several tunable microgel assemblies was investigated for fabrication of drug delivery systems and biointerfaces. However, a number of obstacles remain before the true potential of these constructs can be realized in an experimental or clinical setting. This chapter will discuss the future use of these constructs as valuable investigatory tools and in biomedical devices.

8.2. Development and Applications of Raspberry-Structured Microgel Heteroaggregates

8.2.1. Development of Raspberry-Like Particles

Raspberry-like particles (RLPs) have been explored extensively for years via ion-pair based self-assembly. Ion-pairing based self-assembly methods have many disadvantages as they limit the possible material compositions of heteroaggregates. Moreover, it has been shown that the success of this method is highly dependent on the solution conditions, in particular pH and ionic strength due to the charge of the particles.[1] Development of RLPs via ion-pair driven heteroaggregation is also influenced by the size ratio of the two components; core particles that are much larger than the shell particles are often more successful.[2-1] Instead, the use of colloidal-phase mediated heteroaggregation, explored within this dissertation, could promote the development of tailored RLPs for a variety of applications. The ease of this process, compositional versatility of core and shell particles utilized, and scalability of this method make

colloidal-phase mediated heteroaggregation a promising new avenue for the development of tunable RLPs.

Chapter 2 of this dissertation provides critical information regarding the influence of microgel structure and stiffness on the efficiency of colloidal-phase mediated heteroaggregation. In addition, **Chapter 2** reveals that pH and ionic strength of the solution have limited influence on the success of colloidal-phase mediated heteroaggregation for microgels containing no acid content. Future understanding of compositional advantages and limitations can be gained through exploration of the influence of acid content of microgels on the process.

Similar stimulus-responsive materials have been investigated for the production of heteroaggregates using ion-pair driven heteroaggregation. Triggered heteroaggregation has been investigated to control the aggregation rate by use of hydrogen bonding, temperature, pH, and light in conjunction with stimuli-responsive materials.[3] Such variables have even been used to produce reversible heteroaggregation. Future studies aimed at understanding the advantages and limitations of colloidal-phase mediated heteroaggregation could be directed toward investigation of triggered and/or reversible heteroaggregation because of the responsivity of microgels.

8.2.2. Development of Raspberry-Like Patchy Particles

The use of colloidal-phase mediated heteroaggregation to produce tri-heteroaggregate, Raspberry-Like Patchy Particles (RLPPs) is explored in **Chapter 3**. These investigations demonstrate that colloidal-phase mediated heteroaggregation could successfully be used to develop RLPPs where both monomer and cross-linker content are varied. These studies also reveal a great deal of information regarding coating behavior of

binary microgel dispersions. These studies suggest that the coating ability of microgels in a binary microgel dispersion is influenced by surrounding microgels. In addition, comparison of microgel coverage at planar and curved interfaces suggests that rearrangement of the colloidal-phase does not occur during colloidal-phase mediated heteroaggregation. This realization indicates that studies of microgel dispersion behavior at a planar interface could be used as a high-throughput method to analyze coating ability and resulting topography of a variety of binary microgel dispersions.

These studies also suggest that microgel mechanical properties may influence the behavior of binary microgel phases at an interface. Use of laser scanning confocal microscopy to investigate the phase behavior of labeled binary mixtures of microgels with varied mechanical properties could shed light on similarities and differences between phase behaviors in the bulk to that at an interface. Such studies would provide a greater understanding of the influence of the binary phase on resulting coatings. The influence of microgel acid content on the success of colloidal-phase mediated heteroaggregation when using binary microgel dispersions should also be explored. In addition, influence of microgel size using mis-matched binary mixtures in both planar and curved interface experiments is worth investigating. Finally, a systematic approach comparing the influence of a wide variety of binary microgel mixtures on success of colloidal-phase mediated heteroaggregation as compared to the two-step fabrication technique should be performed to gain an understanding of the versatility of this technique to produce such tri-heteroaggregates.

8.2.3. Use of Raspberry-Like Particles and Raspberry-Like Patchy Particles for Delivery

Microgel-heteroaggregates can be used in a variety of applications. In **Chapter 4**, the biological system we tailored our microparticles to was the embryoid body (EB), a spherical aggregate of embryonic stem cells (ESCs). Previously, efforts to control differentiation of EBs have focused on the manipulation of culture conditions or the use of scaffold materials.[4-6] However, concentration gradients develop within the EBs due to molecular transport limitations, causing heterogeneous differentiation. Recently, the McDevitt Stem Cell Engineering Lab successfully directed homogeneous, synchronous, and organized differentiation by the release of small molecules using poly(lactic-co-glycolic acid) (PLGA) microparticles incorporated in EBs.[6] This method provides the ability to distribute growth factors in a more uniform manner through the EB. However, these approaches are still limited with respect to control over growth factor payload and release rates. Through a collaboration with the McDevitt Stem Cell Engineering Lab, we demonstrate the ability to use RLPs as a synthetic construct to deliver growth factors to stem cell aggregates in order to influence cell fate, as detailed in **Chapter 4**.

The ability of RLPs to efficiently encapsulate and deliver macromolecules is highly dependent on the microgels, which act as the primary component utilized for macromolecule loading and release. Because of their hydrophilic nature, microgels allow for the incorporation of peptides and proteins with few conformational changes and limited aggregation, maintaining the biological effectiveness of biomacromolecules.[7] Microgel loading and release is highly dependent on network characteristics; the network mesh size, as determined by the cross-linking density and polymer-solvent interactions, are the most important parameter determining the mobility of embedded biomacromolecules and their diffusion rates within the swollen microgel.[8] Microgel

charge can also influence the loading and release; electrostatic interactions can be tailored to enhance the loading ability or to increase retention time within the microgel. Protein properties such as size, charge, polarity, and hydrophilicity play a critical role in their interactions with microgels during encapsulation and delivery.

Taken together, all of these factors suggest that a platform of RLPs can be designed using microgels of varied compositions tailored to deliver a range of macromolecules based on specific characteristics. **Chapter 4** details the proof-of-principle studies we conducted with a model RLP construct. Further studies should be performed characterizing a variety of RLPs to develop a platform of constructs to facilitate direction of differentiation down a variety of lineages. RLPs can also be used as a tool to gather more information about how ESCs develop and differentiate within an EB. Researchers recently begun to investigate materials that are able to sequester macromolecules, such as heparin, from the surrounding environment.[9] The concept of "sequestering" can be translated to studies of EBs through the use of microparticles. The ability to "sequester" macromolecules from within EBs is an unexplored area that would provide a means to gain a better understanding of the processes occurring. We performed preliminary studies that suggest that pNIPAm RLPs are a good candidate for thermally triggered sequestration and release of macromolecules; however, further investigation is needed.

8.3. Development of Tunable Biointerfaces from Microgel Assemblies

8.3.1. Modulation of Mechanical Properties

This dissertation explores a variety of tunable biointerfaces for use as experimental tools and for applications. **Chapter 5** explores the traditional development

of microgel thin films via the Layer-by-Layer (LbL) technique and the modulation of mechanical properties through chemical cross-linking of the microgels to the polyelectrolyte (via EDC/NHS chemistry). Investigation of cell spreading on uncross-linked and cross-linked films was also performed. This study suggests that microgel thin films inhibit cellular adhesion through a mechanism other than traditional non-fouling. Instead, we believe that cellular adhesion is inhibited due to the mobility exhibited in the films, manifesting in viscoelastic properties. Building upon this study, Dr. Mark Spears explored the fine tuning of the mechanical properties of these films by varying the degree of chemical cross-linking. These studies demonstrated that cell spreading can be optimized using this cross-linking method.

We believe that microgel thin films may be a model system to evaluate the influence of viscoelastic mechanical properties of a substrate on cellular adhesion. Though the influence of substrate mechanical properties on cell behavior has been explored in detail, most studies focus on the elasticity and few studies are able to target the influence of the viscous component. In order to validate the hypothesis that the viscoelasticity of these films influences cellular adhesion, further studies must be performed. Specifically, studies aimed at characterizing the viscoelastic properties of these films must be performed. These studies have not been performed previously because the microgel films are too thin for typical cone-and-plate rheology studies.

8.3.2. Versatile Polyelectrolyte Construct Fabrication Technique

This dissertation also explores the development of polyelectrolyte films and gels using a novel fabrication technique wherein the polycation and polyanionic building block are mixed and immediately deposited via centrifugation in **Chapter 6**. Typically,

LbL film fabrication relies on building layers using an excess of the materials necessary to ensure a full layer is built. In addition, this process requires many steps (typically 10+) to build robust thin films. For example, in the LbL technique employed by our lab and many others, microgels are typically deposited via centrifugation for 10 min and then the polycation is incorporated through passive adsorption for a 30 minute period.[2] Thus, fabrication of each layer requires a minimum of 40 min. A typical four layer film (four layers of microgels with three layers of polycation) is roughly 500 nm in dry thickness as determined via SEM imaging. Thus, building thick films is impractical using this method. In contrast, using the novel process we have developed, thick microgel films (>50 μm dry thickness via SEM) can be fabricated in less than a half hour. Additionally, the thickness of films can be increased without an exponential increase in wasted materials. The ability to fabricate thicker films not only leads to unique properties, but also increases the potential for commercialization, due to an immense saving of resources.

Moreover, this method can be used to create films composed of a variety of polymer building blocks with varied chemical and mechanical properties. This method is successful for both soft materials, such as microgels, and hard materials, including latex beads. Similarly, this method is compatible with both hydrophilic and hydrophobic polymer components. As such, this is a much more versatile fabrication technique than those previously established in the literature. This method can also be used to create patterned microgel films when a mask is applied to the substrate prior to microgel deposition via centrifugation. Brightfield imaging reveals patterns have relatively clean edges using this method for both microgels and latex beads. Currently, few methods exist for preparing patterned microgel films. One such method enables the development of

porous honeycomb patterned films by casting samples from carbon disulfide solutions of polymers.[5] Two-dimensional arrays of single core-shell microgel heteroaggregates have been developed via self-assembly of a dilute solution of particles.[7] However, these methods are limited in the patterns they are able to produce. This method enables the use of templates with feature sizes ranging from tens of microns to several hundred microns.

A variety of constructs were explored including films of various thickness and various hierarchical ordering. Studies investigating cell spreading on these substrates suggest that these patterned films may be model tools to explore cellular responses to mechanics and topography. Microgel film fabrication studies demonstrate that this method can be used to create very soft microgel assemblies (Young's modulus ~5 kPa). In addition, these studies demonstrate that microgel film properties are more uniform than those fabricated using the traditional LbL technique. Swelling studies reveal that thick microgel films form robust free-standing films that are stable for several months. Typically, development of stable free-standing microgel films is difficult to achieve. Thus, this method also shows a more effective path to fabricate such films. Because of their robust nature, these free-standing films can be used for a variety of applications that typical microgel thin films may not be suitable for. In particular, exploration of thick microgel films for hemostatic surgical dressings and medical adhesives should be explored in more detail. Finally, bulk polyelectrolyte microgel gels are fabricated and characterized via cone-and-plate rheology; these gels also have the potential for use as a hemostatic agent.

In regards to the microgel films, further comparison between film fabricated via the novel method and the traditional LbL method should be conducted. First, detailed

comparison of film buildup using additional polycations such as PDADMAC would provide useful information on the versatility of this method with regards to polycation use. In addition, further investigation should be conducted in order to fully characterize film microstructure. Although investigations characterizing the microstructure were performed using laser scanning confocal microscopy of films with fluorescent microgels, it would be worthwhile to fabricate films with both fluorescent microgels and polycation. Preliminary studies also demonstrate that microgel films can be fabricated using multiple microgel components or multiple building block components. Further characterization of finely tuned constructs based on the ratio of components and resulting film architecture and microstructure should be investigated.

In addition, studies should be conducted comparing cell spreading on microgel films, polystyrene bead films, and RLP films. Preliminary studies have suggested that cell phenotype varies on these constructs. Further studies could shed light on the use of composite microparticles as a modular building block to control cellular phenotype. However, these studies would need to control for chemical differences between the systems and varied topography in order to fully understand what is causing these differences in cell phenotype.

8.3.3 Polyelectrolyte Microgel Films for Hemostasis

Finally, in **Chapter 7** this dissertation explores the use of polyelectrolyte microgel films (fabricated via the new single-step film fabrication technique described in **Chapter 6**) for use as a hemostatic surgical dressing. Studies were performed characterizing the formation of fibrin networks on thick microgel films hydrated in various buffers. Clot formation on films using both platelet poor plasma and re-calcified

whole blood were are explored *in vitro*. Studies reveal that thick, polyelectrolyte films solvated in HEPES solutions of varied pH and salt concentration augment blood clotting. In particular, films solvated in pH 7.4 buffer are effective at augmenting adult blood clotting. Additionally, we demonstrate that microgel films significantly alter neonatal clot structure, promoting the formation of robust, three-dimensional fibrin networks that are not seen in the absence of the microgel film. These studies reveal that robust clots form in 20 min and that clot formation begins quickly. These films have a strong potential for commercialization due to their high efficacy at augmenting blood clotting in a patient group that has unmet hemostatic device needs. However, future studies must be performed to validate the clinical relevance of these studies. Microfluidic studies should be conducted to determine the influence of blood flow on the efficacy of these films as a hemostatic platform *in vitro*. Finally, *in vivo* studies using rat femoral vessel injury model should be conducted to further characterize their clinical efficacy.

8.4. Conclusions

In this chapter, several new research directions were proposed to further understanding of the fabrication processes explored and applications of the materials developed within this dissertation. For example, further studies aimed at exploring how more complex microgel compositions (such as those containing acid) influence colloidal-phase mediated heteroaggregation using both single and binary microgel dispersions can provide a more complete understanding of how microgel dispersion phase and particle architecture influence success of this technique in the development of complex encapsulation and delivery vehicles (**Sections 8.1**). In terms of film work, more detailed studies understanding how to modulate material properties of microgel thin films to elicit

specific cellular responses in terms of spreading and adhesion would be beneficial for development of coatings for particular applications targeted at either enhancing or inhibiting cell proliferation (i.e. tissue engineering scaffolds versus implant coatings) (**Section 8.2**). Such studies should also be performed using the films with novel architectures explored in **Chapter 6**, as well. In addition, further characterization of this new film and gel fabrication technique should be conducted in order to fully realize the potential versatility of this technique (**Section 8.2**). And finally, use of these constructs for specific applications, such as microgel films for hemostatic surgical dressings, should be explored to demonstrate the real-world applicability of using the tunable hydrogel nanoparticle constructs explored within this dissertation.

8.4. References

1. Furusawa, K.; Anzai, C., Heterocoagulation behavior of polymer lattices with spherical silica. *Colloid. Surf.* **1992,** *63* (1-2), 103-111.

2. Harley, S.; Thompson, D. W.; Vincent, B., The adsorption of small particles onto larger particles of opposite charge - direct electron-microscope studies. *Colloid. Surf.* **1992,** *62* (1-2), 163-176.

3. Bradley, M.; Lazim, A. M.; Eastoe, J., Stimulus-responsive heteroaggregation of colloidal dispersions: reversible systems and composite materials. *Polymers.* **2011,** *3* (3), 1036-1050.

4. Battista, S.; Guarnieri, D.; Borselli, C.; Zeppetelli, S.; Borzacchiello, A.; Mayol, L.; Gerbasio, D.; Keene, D. R.; Ambrosio, L.; Netti, P. A., The effect of matrix composition of 3D constructs on embryonic stem cell differentiation. *Biomaterials.* **2005,** *26* (31), 6194-6207.

5. Schukur, L.; Zorlutuna, P.; Cha, J. M.; Bae, H.; Khademhosseini, A., Directed differentiation of size-controlled embryoid bodies towards endothelial and cardiac lineages in RGD-modified poly(ethylene glycol) hydrogels. *Adv. Healthc. Mater.* **2013,** *2* (1), 195-205.

6. Carpenedo, R. L.; Bratt-Leal, A. M.; Marklein, R. A.; Seaman, S. A.; Bowen, N. J.; McDonald, J. F.; McDevitt, T. C., Homogeneous and organized differentiation within

embryoid bodies induced by microsphere-mediated delivery of small molecules. *Biomaterials.* **2009,** *30* (13), 2507-2515.

7. Zhang, Y.; Zhu, W.; Wang, B. B.; Ding, J. D., A novel microgel and associated post-fabrication encapsulation technique of proteins. *J. Control. Release.* **2005,** *105* (3), 260-268.

8. Klinger, D.; Landfester, K., Stimuli-responsive microgels for the loading and release of functional compounds: Fundamental concepts and applications. *Polymer.* **2012,** *53* (23), 5209-5231.

9. Hudalla, G. A.; Murphy, W. L., Biomaterials that regulate growth factor activity via bioinspired interactions. *Adv. Funct. Mater.* **2011,** *21* (10), 1754-1768.

VITA

SHALINI SAXENA

Shalini Saxena was born in Silver Spring, Maryland and was raised in Bethesda, Maryland. As a child, Shalini was often found creating inventive artworks and objects. For her elementary and middle school education, she attended Norwood School in where she was exposed to an education rich in science, art, and culture. She attended the APEX Program at Walter Johnson High School and graduated as an APEX Scholar in 2008. Shalini then moved across the country to Terre Haute, Indiana where she earned a B.S. in Chemical Engineering from Rose-Hulman Institute of Technology in 2011.

Before coming to the Georgia Institute of Technology Shalini researched at the National Institutes of Health as an ORWH-FAES Research Fellow where she investigated the influence of several chemicals on cancer growth and on neutrophil chemotaxis. In addition, Shalini attended a research program for undergraduates at Pennsylvania State University where she investigated the growth of algae for use in biofuel production. Shalini also interned as a manufacturing engineer at a major biomedical company.

While at the Georgia Institute of Technology, Shalini was a Stem Cell Biomanufacturing NSF IGERT Trainee. As a trainee, Shalini was educated about current concerns regarding stem cell engineering practices. In addition, Shalini was a GT Leadership Fellow and gained valuable experience coaching undergraduates as they developed their leadership skills. During her final year, Shalini was also the leader of the MSE Women's Group and invested a great deal of her time developing professional and

education seminars to empower female graduate students. During this time, Shalini also began her career as a science writer at a popular online media source.

When Shalini is not off investigating process engineering or developing new material systems, she continues to develop her creative portfolio. She is an avid artist who pursues drawing, painting, photography, and jewelry-making.